Resilience modeling of urban multimodal transport networks

Elise Henry

N°d'ordre NNT : 2021LYSET012

THÈSE de DOCTORAT DE L'UNIVERSITÉ DE LYON
opérée au sein de
École de l'aménagement durable des territoires (ENTPE)

École Doctorale N° 162
Mécanique, Énergétique, Génie civil, Acoustique (MEGA)
Spécialité : Génie Civil

Laboratoire d'Ingénierie Circulation Transports (LICIT)

Soutenue publiquement le 17 Décembre 2021, par :
Élise Henry

Modélisation de la résilience multimodale des réseaux de transports urbains

---

Devant le jury composé de :

Pr. Laure Tougne	Université Lyon 2	Présidente
Dr. Bidisha Ghosh	Trinity College of Dublin	Rapporteure
Pr. El Houssaine Aghezzaf	Ghent University	Rapporteur
Dr. David Rey	Skema Business School	Examinateur
Pr. Nour-Eddin El Faouzi	Université Gustave Eiffel – ENTPE	Directeur de thèse
Dr. Angelo Furno	Université Gustave Eiffel – ENTPE	Co-directeur de thèse

Traffic and Transport Engineering Laboratory (LICIT)
Joint Research Unit (UMR T9401)

University Gustave Eiffel (UGE) and School of Civil, Environmental & Urban Engineering (ENTPE)

Resilience Modelling of Urban Multimodal Transport Networks

Elise Henry

DOCTORAL THESIS
Doctoral School **MEGA** (ED 162) – Mechanics, Energy, Civil Engineering, Acoustics

---

Examining committee:

Prof. **El-Houssaine Aghezzaf** , Ghent University, Belgium	Rapporteur
Prof. **Nour-Eddin El Faouzi**, UGE - ENTPE, France	Thesis Director
Dr. **Angelo Furno**, UGE - ENTPE, France	Thesis Co-Director
Dr. **Bidisha Ghosh**, Trinity College Dublin, Ireland	Rapporteur
Dr. **David Rey**, SKEMA Business School, France	Examiner
Prof. **Laure Tougne**, University Lyon 2, France	Examiner

Manuscript submitted on October 20, 2021

The thesis has been supported by the French ANR research project PROMENADE, grant number ANR-18-CE22-0008, and the French government: Ministère de la Transition Ecologique (MTE).

DATA-DRIVEN
RESILIENT MOBILITY

Abstract

In addition to operating close to their maximum capacity, transport networks, and especially the urban ones, are subject to various disruptions induced by human, technical or natural factors, which often generate loss of performance, damages and high maintenance costs. Introduced in the 70's, the notion of resilience represents the ability of a system to maintain an acceptable level of performance in presence of a disruption. Modeling and quantifying the resilience of multimodal, large-scale, urban transport networks is expected to allow cities guaranteeing higher-quality of service and seamless mobility, even in the presence of disruptions and major, predictable events. The research presented in this dissertation is motivated by the need of proper defining the resilience of the transport network in order to understand their vulnerabilities. Such indication aims at improving the functioning of the network under disruption and anticipating the loss of performance by means of a resilient-oriented transport network design. In the literature, two major approaches aim at quantifying the network resilience. On the one hand, the topological approach, based on graph theory, which characterizes the static components of transport resilience, as issued from the redundancy of the network and its connectivity. On the other hand, the dynamic approach, which takes into account the traffic dynamics and leverages traffic theory for quantifying resilience induced by the network users behaviors and the transport network performances. The combination of the static and the dynamic approaches for resilience characterization is promising and provides deeper insights in the properties of a network, both in terms of its topology and performance. Centrality measures, aiming at ranking the importance of the graph components and issued from graph theory, are mainly analyzed to characterize the transport networks in static settings. By computing them on dynamic weighted graphs that capture traffic conditions and by adapting their formulation to consider the users' demand, we are able to jointly consider network topology and traffic dynamics in resilience characterization. To emulate the impact of disruptions, both simulated and real data are considered. A stress test methodology, mostly used in the bank and nuclear sectors, which aims at simulating the worst scenarios in order to analyze the impact and the reaction of the network, is developed to observe the transport network behavior. Finally, we develop a methodology, quick-to-compute, which aims at prioritizing the construction of some new transport mode lines, by maximizing the performance improvement in a resilience context. We also propose an algorithm for the optimal deployment of a disruption-adapted park-and-ride system.

Keywords: Transport network Resilience, Complex networks, Disruptions, Stress test, Network design

Résumé

Les réseaux de transports urbains sont essentiels pour nos sociétés et en effet, la demande de mobilité, qu'elle soit urbaine ou interurbaine, continue à croître régulièrement en Europe Comme dans le reste du monde, le transport de marchandises devrait avoir augmenté d'environ 80% en 2050 par rapport à 2005, tandis que le trafic passager devrait croître de 51%. Pour autant, les réseaux de toutes natures se trouvent déjà saturés dans actuelle l'état actuel des systèmes de transport et c'est pourquoi il convient d'imaginer de nouvelles formes d'optimisation et de gestion innovante. A cela s'ajoute le fait que les infrastructures des réseaux urbains, indispensables en cas de gestion de crise pour l'intervention des secours ou l'évacuation des villes, sont exposées à des risques. Cette vulnérabilité a été mise en évidence à de nombreuses reprises comme le prouvent de nombreux événements récents : le tempête Alex du 2 Octobre 2020 qui a coupé l'accès à la vallée de la Roya ; la vague de chaleur au Canada et dans l'ouest des États-Unis en Juin et Juillet 2021 qui a induit la fermeture de plusieurs routes à cause de la fonte de l'asphalte ; les inondations du 14 Juillet 2021 à l'ouest de l'Allemagne qui ont empêchées l'accès à de nombreuses routes ; l'incendie du 17 Août 2021 au sud de la France qui a conduit à isoler toute une portion du réseau routier dont une autoroute; ... Les perturbations auxquelles ces réseaux de transports notamment urbains sont soumis, peuvent être d'origine humaine, technique ou naturelle et impliquent régulièrement des pertes de performances, des dommages et des coûts de maintenance élevés.

Il est donc important de limiter leur exposition aux risques. Il est aussi nécessaire de les rendre plus résistants afin de conserver un niveau de performances acceptable en toutes circonstances. L'ingénierie de la résilience agit en ce sens puisqu'elle représente un moyen innovant pour la compréhension du fonctionnement des réseaux de transports. Introduite dans les années 70, la résilience est de plus en plus prégnante dans la gestion et l'exploitation des infrastructures. Elle est définie comme la capacité d'un système à fournir et maintenir un niveau de service acceptable face à des situations anormales. La résilience peut être abordée selon différents angles : robustesse, aptitude à rebondir à la suite d'un traumatisme pour retrouver l'équilibre, redondance, capacité de maintenir son trajet via un autre itinéraire, ... Modéliser puis quantifier la résilience multimodale de larges réseaux de transports urbains permettrait de garantir un service de mobilité de qualité aux villes, même en présence de perturbations et d'événements majeurs impactant les réseaux urbains.

Les recherches présentées dans cette dissertation sont motivées par le besoin de définir de façon fiable la résilience des réseaux de transports pour comprendre leurs vulnérabilités. Pour ce faire, la méthodologie avancée a pour but de cherche à caractériser conjointement la topologie du réseau de transport et les dynamiques de trafic dans la caractérisation de la résilience. La multimodalité des réseaux de transports urbains se doit d'être considérée puisqu'elle accroît la redondance du réseau de transport via les différents modes de transports. Néanmoins, les larges ensembles de données qu'elle conduit à appréhender nous obligent à simplifier ces réseaux pour une caractérisation rapide, en quasi-temps réel, de la résilience. La connaissance ainsi acquise vise à améliorer leur fonctionnement lors de perturbations et à anticiper leurs pertes de performances par la conception de réseaux plus résilients, plus en mesure de maintenir un niveau de performances acceptable en toutes circonstances.

Dans l'état de l'art, deux approches majoritaires permettent de quantifier la résilience des réseaux. D'une part, l'approche topologique basée sur la théorie des graphes, qui caractérise la résilience statique des

éléments du réseau en s'intéressant à la redondance dans le réseau ou encore à sa connectivité. D'autre part, l'approche dynamique qui, considérant les dynamiques de trafic, en exploite la théorie pour quantifier la résilience induite par les usagers et les performances du réseau de transport. Dans ce cadre, Les mesures de centralités qui ont pour objectif de classer les composants d'un graphe en fonction de leur importance, sont beaucoup utilisées dans l'analyse de la caractérisation de la résilience des réseaux de transport.

Le premier objectif consiste à combiner les deux approches topologique et dynamique majoritairement utilisées pour caractériser la résilience, souvent menées séparément malgré leur complémentarité. En calculant les mesures de centralité sur un graphe pondéré dynamiquement qui permet de capturer les conditions de trafic et en adaptant leurs formules pour tenir compte de la demande des utilisateurs, nous sommes capables de considérer la topologie du réseau et les dynamiques de trafic dans la caractérisation de la résilience. Les résultats obtenus prouvent la capacité des mesures de centralités à capturer les dynamiques de trafic en plus de la topologie du réseau en étant calculées sur un graphe dynamique. En effet, nous observons une évolution de ces mesures de centralités en lien avec l'évolution des conditions de trafic simulées ou réelles. Ainsi, la criticité de certains composants du réseau (routes ou intersections) est modifiée au cours du temps. Une étude de corrélation entre l'évolution d'une mesure de centralité et d'un flux de véhicule a été menée et a permis de confirmer la capacité des mesures de centralité à capturer les dynamiques de trafic lorsque ces dernières sont calculées sur un graphe dynamique. Les routes congestionnées ont tendance à présenter une anti-corrélation entre la mesure de centralité et le flux, les routes avec un comportement non-corrélées étant inutilisées ou vulnérables topologiquement, alors que les routes présentant un comportement corrélé présentent majoritairement des conditions de trafic fluides.

Pour émuler l'impact de perturbations, nous considérons des données tant simulées que réelles. Une méthodologie de test de résistance, majoritairement étudiée dans les domaines du nucléaire et comme de la finance et qui permet de simuler les pires scénarios de catastrophes en vue d'analyser l'impact et la réaction du réseau, est développée pour observer le comportement du réseau de transport. Ici encore, l'utilisation de mesures de centralités calculées sur un graphe pondéré par des données de trafic (en l'occurrence les temps de parcours), permet une caractérisation des performances du réseau de transport en fonction de l'évolution des conditions de ce trafic. Ainsi, l'impact de la perturbation sur le réseau peut être quantifiée et renseigne donc sur la résilience du réseau.

Une fois la résilience du réseau de transports caractérisée, des stratégies pour son amélioration peuvent/doivent être mises en place pour limiter l'impact négatif d'une potentielle perturbation. Celles-ci sont proposées en amont d'un tel événement pour améliorer la résilience du réseau de transport en réponse. Elles consistent majoritairement en une amélioration de la robustesse du réseau via l'addition d'itinéraires ou le développement d'un nouveau mode de transport visant à compléter l'offre de transport existante. Ces stratégies s'intéressent également au déploiement optimal de services publics visant à réagir efficacement à une perturbation en vue de retrouver au plus vite des conditions de trafic optimales. Concernant les stratégies qui interviennent après la perturbation, une distinction peut être faite entre le court et le long terme. Alors que dans un premier temps il faut retrouver des conditions de trafic acceptables le plus rapidement possible via le déblayage des routes ou la mise en place de service de transports alternatifs, par la suite , les stratégies visent essentiellement à concevoir un futur réseau plus robuste.

Nous avons donc proposé deux types de stratégies visant à définir un réseau de transport plus résilient via l'addition d'un nouveau mode de transport. Dans un premier temps, nous développons une méthodologie, peu coûteuse en temps de calcul, pour optimiser la création d'un tel moyen de manière à maximiser le gain de performance et en améliorer sa la résilience globale du réseau. L'intérêt d'une telle méthodologie est double. A court terme, en condition dégradée, cette méthode agit comme un outil d'aide à la décision pour la mise en place rapide d'une ligne de bus par exemple, visant à préserver autant que possible les performances habituelles. A long terme, elle permet de déterminer les lignes de transports en communs à privilégier lors de la construction d'un nouveau mode de transport en planifiant son architecture avec le but de maximiser les gains de performance le plus rapidement possible. Pour ce faire, nous caractérisons la résilience du réseau de transport existants en considérant les aménagements à prévoir, au moyen de mesures

de centralité. Une méthodologie de simplification de graphe a d'ailleurs été imaginée pour maintenir un temps de calcul acceptable pour des réseaux de transports multimodaux de large échelle.

Dans un second temps, nous proposons deux formulations visant à optimiser la mise en place d'un système de park-and-ride combiné à un service de transport en commun. Ces formulations sont stochastiques pour considérer un ensemble de situations normales et dégradées pour lequel le système sera optimisé. Le système de park-and-ride est ainsi sensible aux perturbations régulières qui affectent le réseau de transports. La première consiste à maximiser l'utilisation du système de transport proposé qui vient compléter l'offre de service actuelle. En simulant le choix du mode de transport via la formulation logit et en considérant une formulation stochastique pour tenir compte de différentes conditions de trafic, nous sommes en mesure de déterminer les localisations optimales pour les points de départs (pick ups) et les points d'arrivée (drop offs) ainsi que la répartition des usagers sur le système de park-and-ride. Afin de résoudre ce problème sur un large réseau de transport, nous avons développé un algorithme de relaxation lagrangienne associé à une heuristique pour réduire les temps de calculs. L'étude de cas portant sur la ville de Lyon nous a permis de conforter l'intérêt de notre algorithme pour résoudre un tel problème. La seconde formulation vise à minimiser les coûts de construction du système de park-and-ride, les coûts d'exploitation avec une optimisation de la flotte de véhicules utilisée, et les coûts de trajet pour les usagers du système. Dans ce cas, le problème nous fournit les emplacements optimaux pour le positionnement des pick ups et des drop offs, la répartition de la demande sur les différents itinéraires proposés par le système de park-and-ride mais aussi le dimensionnement, le type, ainsi que la répartition de véhicules nécessaire pour satisfaire la demande sur chacun des itinéraires. Cette seconde formulation, sensible aux conditions de trafic dégradées, a été testée sur un petit réseau et le développement d'un algorithme de génération de colonnes pour traiter un large réseau de transports urbains est en cours de développement afin d'appliquer cette formulation sur de larges aires urbaines. Une combinaison des deux formulations semblerait prometteuse pour le déploiement d'un tel système adapté aux perturbations récurrentes en vue de proposer un mode de transport résilient.

Au cours de cette dissertation nous avons proposé une vue globale de la résilience des réseaux de transports urbains. Après avoir présenté l'état de l'art existant, nous avons détaillé notre méthodologie pour déterminer une telle caractéristique en considérant la topologie du réseau ainsi que les dynamiques de trafic. Sa caractérisation pour des réseaux de transports urbains et péri-urbains via l'utilisation de données simulées ou réelles est ensuite détaillée tout comme la capacité de nos mesures à capturer l'impact de perturbations, afin de valider notre méthodologie. Enfin, à des fins d'illustration de notre étude, nous avons élaboré et testé deux stratégies visant à améliorer la résilience de réseaux de transports urbains via l'ajout d'un mode de transport alternatif au réseau existant.

Mots Clés : Résilience des réseaux de transport, Réseaux complexes, Perturbations, Test de résistance, Conception du réseau

Acknowledgment

This project would not have been possible without the support of many people.

First, I would like to thank my supervisors, Dr. Angelo Furno and Prof. Nour-Eddin El Faouzi. Both expertises were invaluable in formulating the research questions and methodology. Their insightful feedback pushed me to sharpen my thinking and brought my work to a higher level. They oriented my research work, allowed me to attend to conferences worldwide or online, and above all never stopped supporting me.

While exploring the last chapter of this thesis, I have received a significant support from Dr. David Rey. He taughs me a lot about the optimization problems formulation and their resolutions. I would like to thank him very deeply and it was a great pleasure to work with him and explore this field during my thesis.

I would express my gratitude to the other members of my PhD committee Dr. Bidisha Ghosh, Prof. Aghezzaf El Houssaine, Prof. Laure Tougne for all their comments and reviews. I felt honored to have my work examined by them and I would like to thank them again for the day of my PhD defense, which I will remember.

My first research experience is the reason of where I am today. I had the deep honor to join the Department of Civil, Structural and Environmental Engineering laboratory at the Trinity College of Dublin, on April 2017, for a five months internship under the supervision of Dr. Bidisha Ghosh. Since this wonderful research experience, I have always felt like any good thing happening in my young academic career would be related to this internship.

I would like to thank the Neovya's team and especially Dr. Aurélien Duret, Dr. Etienne Hans and Dr. Guillem Mariotte for the help in using their traffic simulator Hubsim and the model calibration.

Thank you to Prof. Eugenio Zimeo, and M. Mathieu Petit with whom I had the honor to work with along my thesis, as well as M. Loic Bonnetain, with who I also shared the thesis experience and the office.

I would like to acknowledge my colleagues from the LICIT laboratory for their wonderful collaboration. Cécile D., Loïc and Louis with whom I had the honor to share the office (formerly named "trainee office") and good moments, Manon and Cyril who made the conferences and seminars much more interesting and pleasant, Aurélien C. who has been an example from his experience and all the others, Andres who has always been good advice and whose discussions were always interesting, Kindjal who is always up for sharing good times and discovering Lyon and the French culture, Pierre-Antoine whose kindness and wisdom were invaluable and who was always listening and happy to advise, Matthieu with whom I had the good fortune to work and share discussions, Pierre whose running and hiking stories motivate me to try it, Umberto who has always be very friendly and gave me the desire to visit Mexico, Sarah whose kindness and happiness was always appreciable, Sonia who patiently guided me through administrative tasks, Bernard whose historic and philosophic discussions were always instructive, Christine, Cécile B., Aurélien D., Nicolas, Delphine, Jean, Arthur, Colette, Jean-Luc and Ludovic (and again Nour-Eddin and Angelo) who after having been fabulous teachers at the ENTPE have become very nice colleagues. I am deeply grateful to Ms. Anne-Christine Demanny who brings a good atmosphere to the laboratory and has always helped me a lot. Thank you again

for proofreading my manuscript and your precious help with English.

I thank the Ministère de Transition Ecologique (MTE) and all the committee members for funding and opportunity to complete my formation with a pursuit at the doctoral level. I also want to thank the Mobilité Transition Numérique project, as well as the French ANR research project PROMENADE, which contribute to funding for some of the thesis missions.

My last, sincere and deep affectionate thoughts are for my friends and my beloved family: my grandparents, my parents, my brother and my boyfriend. They have guided me through adversity, and they have all my admiration and love.

Contents

List of Figures

List of Tables

Acronyms

γ Gamma Index. 24, 27

$\langle DSNDC \rangle$ Demand-Sensitive Network Density. xviii, 30, 92, 97, 98

$\langle NDC \rangle$ Network Density. xvi, xvii, xviii, 27, 28, 46, 48, 49, 58, 61, 68, 71, 72, 73, 74, 81, 92, 95, 96, 100, 129, 130

A Accessibility. xix, 33, 131, 135, 136, 137

AE Average Efficiency. xvi, xvii, xviii, xxi, xxii, xxiii, 27, 28, 29, 30, 31, 44, 45, 48, 49, 51, 58, 75, 76, 82, 92, 95, 96, 100, 130, 140, 141, 142, 143, 144

BC Betweenness Centrality. 25, 26, 30

CDL Capacity Disruption Level. 24

City Catchement Analysis Tool CityCAT. 13

CM Centrality Measures. xxi, xxii, xxiii, 24, 25, 26, 29, 30, 31, 32, 33, 35, 40, 52, 53, 58, 59, 61, 63, 66, 81, 92, 129, 130, 131, 139, 140, 141, 142, 143, 144

CPV Cost Per Vehicle. 23

CR Capacity Reduction. xxi, xxii, xxiii, 140, 141, 142, 143, 144

DCI Demand- / Capacity-based Indicators. xxi, xxii, xxiii, 139, 140, 141, 142, 143, 144

DS Demand-Sensitive. xvi, xvii, xxi, xxii, xxiii, 35, 53, 54, 55, 56, 57, 58, 79, 82, 140, 141, 142, 143, 144

DSAE Demand-Sensitive Average Efficiency. xviii, 90, 92, 97, 98

DSEBC Demand-Sensitive Edge Betweenness Centrality. xvi, xviii, 31, 52, 53, 59, 90, 92, 99, 100, 130

DSNBC Demand-Sensitive Node Betweenness Centrality. 31

DSNCC Demand-Sensitive Node Closeness Centrality. xviii, 31, 90, 92, 98, 99

DSNDC Demand-Sensitive Node Degree Centrality. 30, 92

E Exposure. xxi, xxii, xxiii, 23, 24, 140, 141, 142, 143, 144

EBC Edge Betweenness Centrality. xv, xvi, xvii, xviii, xxi, xxii, xxiii, 25, 26, 29, 30, 35, 40, 41, 42, 43, 44, 45, 47, 48, 50, 51, 52, 53, 54, 55, 56, 57, 58, 59, 61, 63, 64, 65, 77, 78, 79, 80, 81, 82, 87, 90, 92, 95, 97, 100, 130, 140, 141, 142, 143, 144

ECMT European Conference of Ministers of Transport. 22

EE entries-exits. xvi, 53, 54, 55, 56, 57, 58, 82

FCD Floating Car Data. xvii, 14, 61, 63, 64, 75, 77, 82, 111, 112, 136

FD Fundamental Diagram. 11

FEMA Federal Emergency Management Agency. 13, 89

FF Free-Flow. xviii, 53, 54, 55, 56, 57, 79, 80, 81, 82

GCC Giant Connected Component. xxi, xxii, xxiii, 27, 140, 141, 142, 143, 144

GE Global Efficiency. 30

GEBC Global Edge Betweenness Centrality. xv, xvi, 26, 41, 42, 43, 48, 58, 77, 78, 82

GPS Global Positioning System. 63, 65, 79

H Heterogenity. xvii, 28, 61, 67, 71, 72, 73, 74, 80, 81

HAZUS HAZards US. 89

HD Historical Data. xxi, xxii, xxiii, 140, 141, 142, 143, 144

I Importance. xxi, xxii, xxiii, 23, 140, 141, 142, 143, 144

INFRARISK Novel Indicators for Identifying Critical INFRAstructure at RISK from Natural Hazards. 89

LA Lagrangian Relaxation Algorithm. xix, 83, 104, 105, 106, 108, 109, 112, 113, 114, 115, 116, 117, 127, 131

LB Lower Bound. 105, 113, 114

LM Lagrange Multipliers. 104, 105, 106, 109, 110

LR Lagrangian Relaxation. 104, 105, 106, 108, 117, 131

MC Model Coupling. xxi, xxii, xxiii, 140, 141, 142, 143, 144

MFD Macroscopic Fundamental Diagram. 11, 22, 23, 142

MILP Mixed-Integer Linear Programming. 103, 112, 113, 114, 115, 116, 117, 119, 124, 127, 131

MMN Multi-Modal Network. xxi, xxii, xxiii, 140, 141, 142, 143, 144

NBC Node Betweenness Centrality. 25, 26, 27, 30, 31

NCC Node Closeness Centrality. xvi, xvii, xxi, xxii, xxiii, 26, 27, 30, 31, 35, 40, 44, 45, 46, 48, 49, 50, 51, 52, 59, 61, 63, 64, 75, 76, 77, 82, 87, 92, 95, 96, 97, 100, 130, 140, 141, 142, 143, 144

NDC Node Degree Centrality. xvi, xvii, xxi, xxii, xxiii, 25, 27, 28, 29, 30, 32, 35, 40, 46, 47, 48, 49, 50, 51, 52, 58, 59, 61, 63, 66, 67, 68, 69, 70, 71, 72, 73, 74, 75, 81, 82, 92, 100, 129, 130, 131, 140, 141, 142, 143, 144

NPV Net Present Value. 23

NRI Network Resilience Index. 24

NRT Network Trip Robustness. 24

OD origin-destination. 20, 24, 31, 37, 39, 41, 42, 43, 45, 52, 53, 58, 101, 102, 103, 110, 118, 119

OECD Organisation for Economic Co-operation and Development. 22

P&R Park-and-Ride. xxi, 4, 83, 87, 101, 102, 103, 104, 105, 106, 107, 110, 111, 112, 113, 114, 116, 117, 118, 119, 121, 123, 126, 127, 129, 130, 131, 132, 145, 146

PE Passenger-Exposure. 24

PHD Person Hours Delay. 23

POIs Points Of Interest. 31, 135, 136

PT Public Transport. 23

PTN Public Transport Network. xxi, xxii, xxiii, 140, 141, 142, 143, 144

QCB Quai Claude Bernard. 80, 81

QDG Quai Dr. Gailleton. 80, 81

R Removal. xxi, xxii, xxiii, 140, 141, 142, 143, 144

RAIN Risk Analysis of Infrastructure Networks in Response to Extreme Weather. 89

REINFORCE Rapid augmentation of large-scale multi-modal transport networks for resilience enhancement. xviii, 4, 83, 90, 91, 92, 95, 98, 100, 129, 130, 132

RESOLUTE RESilience management guidelines and Operationalization appLied to Urban Transport Environment. 89

RN Road Network. xxi, xxii, xxiii, 140, 141, 142, 143, 144

S Symmetry. xvii, 28, 61, 71, 72, 73, 74, 81

SNAMUTS Spatial Network Analysis for Multimodal Urban Transport Systems. 32

STC Stress Test Criticality. 24

SUMO Simulation of Urban MObility. 13

TT Travel Times. xvi, xvii, xviii, 53, 54, 55, 56, 57, 58, 79, 80, 81, 82

TTI Travel time-based Indicators. xxi, xxii, xxiii, 139, 140, 141, 142, 143, 144

U Unweighted. xvii, xviii, xxi, xxii, xxiii, 53, 54, 55, 56, 57, 79, 80, 140, 141, 142, 143, 144

UB Upper Bound. xix, 105, 115

US United States. 88

V/C Volume / Capacity. xxi, xxii, xxiii, 22, 24, 29, 140, 141, 142, 143, 144

W Weighted. xxi, xxii, xxiii, 140, 141, 142, 143, 144

Introduction

Urban population is projected to reach 2.5 billion in 2050, more than two-thirds of the population (United Nations, 2018). One of the biggest challenges facing growing urban areas is thus the increasing mobility demand for all modes of transport, causing congestion, crowding, noise and emissions to rise (Cats and Jenelius, 2018). Because the infrastructure systems are often designed with the objective of minimizing the construction, maintenance and operational costs, they work close to their capacity with small margins of reserve capacity and little redundancy (Mattsson and Jenelius, 2015). Indeed, some transport networks already operate at their capacity limits (ITF, 2016; Dolinayova et al., 2020). Knowing that an increase of capacity often reduces the redundancy, the system becomes more vulnerable (Goldberg, 1975). This is typically the case in many metropolitan areas with rapid and important urbanization, especially in developing countries where the transport networks are insufficient, causing severe traffic jams (Rana, 2011). According to the INRIX Global Traffic Scorecard (INRIX, 2020), over half of the 200 studied cities, across 38 countries, registered more than 100 hours lost in congestion per driver and year. By causing delays, inconvenience, and economic losses, as well as air pollution, traffic congestion is a perpetual problem for the sustainability of transportation development (Afrin and Yodo, 2020). Urban congestion costs are estimated to account between €75 billion according to INRIX company (INRIX, 2020) and €105 billion according to Litman (2021). Furthermore, the multimodal urban transport networks, essential to our societies are impacted by incidents and adverse conditions which vary in nature, intensity, and origin, and reduce their performances (Kramarz and Przybylska, 2019). Disruptions could be originated from natural, human or technical factors (Cats et al., 2017; Husdal, 2004), and a distinction can be made between internal (technical failures, accidents) and external (attacks, adverse weather) causes of disruptions (Mattsson and Jenelius, 2015). Their impact differs in both spatial and temporal dimensions.

Extreme events and climate change

Public transport strikes impact the mode choice and disturb the total network by increasing the use of personal vehicles for a few hours or a few days; bridge collapses strongly impact the transport network by totally removing an important edge until its reconstruction; special events such as Olympic Games disrupt normal traffic conditions by introducing a highly concentrated travel demand for months, natural hazards and extreme-weather events such as earthquakes or hurricanes induce important infrastructure damages, and negatively impact the network (Zhu and Levinson, 2011). It is important to note that, as a consequence of climate change, the frequency and intensity of these events are expected to increase significantly (Pregnolato et al., 2017). Some recent events confirm the forecasts: Alex's storm on 2^{nd} October 2020 which cut off access to Roya Valley Taylor (2020),the heatwave in Canada and Western America which caused several roads closure during June and July 2021 because of the asphalt bucking due to burning temperatures (Therrien, 2021), the high-intensity rainfall on 14^{th} July 2021 in western Germany where roads were cut off (BBC, 2021b), the wildfire on 17^{th} August 2021 in the south of France which provoked road closures and detours (BBC, 2021a).The technical factors encompass the recurring technical problems impacting the public transport (Whyte, 2021), the bridge failures which strongly impact the transport networks (NBC, 2018).Finally, the human factors are due to the people errors such as the blockage of the Suez Canal at the end of March 2021 which causes important maritime traffic jams (The Associated Press, 2021a), or

the recurrent car crashes which impacts the traffic conditions, the power outage that disrupted half of New York City's subway system for several hours caused by someone accidentally pressing an "Emergency Power Off" button (The Associated Press, 2021b).

Resilience definition

According to Lyons (2004) society and transport are dependent: "transport does not merely serve society: it shapes society, as in turn society shapes transport". Transport networks, which aim at moving goods, people or information, from one node to all others (Liu, 2011; Aldagheiri, 2009), are essential for our societies because of their influence on the spatial variation of many activities (White and Senior, 1983), by impacting disease spread, congestion, urban sprawl or city structure (Barthélemy, 2011). The identification of events are crucial for decision-makers to initiate mitigation strategies to improve transportation system resilience and thus reduce network vulnerabilities (Afrin and Yodo, 2020). Although transport network resilience has gained attention in the past decades, since its apparition in the ecological field (Holling, 1973), resilience has no single agreed definition. For Janić (2015) resilience is the ability of a system to operate under variable and unexpected conditions without substantially compromising its planned performances. Haimes (2009) proposes a similar definition with the addition of the recovery aspect: the system has to recover within an acceptable time and composite costs and risks. Dekker et al. (2008) assume that a resilient system is able to adapt its functioning prior to, during, or following changes and disturbances. Another popular definition of resilience is the one of Bruneau et al. (2003) who separate resilience in three parts phases, with respect to the occurrence of a disruption: *pre-perturbation resilience* aims at mitigating the impact of hazards before their occurrence thanks to the network robustness ; *perturbation resilience* aims at limiting damages during the perturbation and is known as the network reactivity ; *post-perturbation resilience* aims at rapidly regaining the initial level of performance after the disruption and corresponds to network recovery. To sum up, a resilient system may fluctuate between states as long as it can absorb shocks, in the sense that its qualitative behavior does not change thanks to its robustness and its redundancy, quickly recovers in presence of performance losses, and adapts itself to future disruptions (Woods, 2015; Hollnagel, 2008; Berkeley and Wallace, 2010).

Resilience quantification

By relying on the calculation of network performance metrics, resilience is quantified by comparing the operations of transport networks in normal and disturbed conditions. The knowledge of transport network resilience is helpful to improve the management of transport networks but also to develop planning and decision support tools, which are crucial in the event of a disruption. These goals should improve, in all circumstances, the control of the situation and reduce the negative impacts on transport systems. To be prepared to extreme events, the accurate understanding of the network behavior is crucial. Disruption modelling is needed to simulate the impact of extreme events on transport network. Whereas some works focus on the use of historical data (Zhu et al., 2017, 2016; Miller et al., 2013; Mudigonda et al., 2019; Lu et al., 2016; Bíl et al., 2015), some researches deal with the merging of catastrophe models with traffic simulators (Yin et al., 2017; Pregnolato et al., 2017; Postance et al., 2017; Grossi and Kunreuther, 2005; Yossyafra et al., 2018), and some analyses focus on the network topology by examining the impact of random or targeted graph components removal (Chen and Hero, 2013; Shalaby et al., 2016; Holme et al., 2002; Aydin et al., 2018; Boldi et al., 2013). Gauthier et al. (2018) suggest to apply a stress test methodology, widely used for banking systems, nuclear risk, and biology analysis (Haldane, 2009; Goldschlager et al., 1976; Kini et al., 2018; Battiston et al., 2017), for quantifying the adverse impacts. Regarding the characterization of resilience, nowadays it is assessed either statically, based on the network topology using graph theory (Shalaby et al., 2016; Zhang et al., 2015; Cheng et al., 2015), or dynamically, by analyzing the evolution

of traffic variables (Shalaby et al., 2016; Murray-Tuite, 2006; Jenelius et al., 2006). Because topological approaches are unable to capture the time-dependent aspects of resilience, it is essential to combine both approaches because of their complementarity (Shalaby et al., 2016; Gauthier et al., 2018; Henry et al., 2019b). Both structural and dynamical resilience analyses, often lead separately, are essential to a better understanding of network vulnerabilities. The combination of the two approaches (*i.e.*, the topological and the dynamic ones) is rare (Gauthier et al., 2018) as the problem of characterizing resilience in multimodal urban transport (Aleta et al., 2017), while the multimodality consideration will permit a more realistic assessment of transport resilience (Aleta et al., 2017).

Research purpose

In this context, we aim at accurately characterizing transport network resilience by both considering network topology and traffic dynamics resulting in combining static and dynamic existing approaches. Indeed, the characterisation of the transport network behavior in presence of disruptions is needed to understand the impact the latter have on traffic conditions and network functioning. This is also needed to plan some strategies of improvement, either to maintain a level of performance during the event, or increase network robustness as a form of preparedness for disruption.

This thesis addresses the following research questions:

(i) How to accurately model the transport network to consider both traffic dynamics and network topology?

The accurate modelling or detection of disruptions is also essential to fully understand the transport network behavior and adapt it to improve its operations whatever the traffic conditions or the topological modifications (tunnel closure, infrastructure work, bridge collapse, etc).

(ii) How to properly model disruptions to emulate their impacts on the transport network for resilience study?

Once a satisfying transport network model is built and disruptions are modeled, resilience has to be characterized. Existing approaches have to be adapted and extended to simultaneously consider traffic dynamics and network topology, typically studied separately. The indicators must capture the impacts of disruptions on both aspects.

(iii) How to both consider network topology and traffic conditions in resilience characterization? How to design resilience metrics that capture both aspects?

The consideration of the transport multimodality is interesting by providing resilience adapted strategies in increasing the redundancy of the transport network, by proposing alternative paths. Indeed, De Domenico et al. (2014) prove how the whole public transport network in London is more resilient to random failures than its individual layers separately. Because the study focuses on a large scale urban areas with large data sets to model traffic conditions, transport network simplifications and code optimization need to be implemented.

(iv) How to accurately reproduce the large scale urban multimodal networks in order to quantify their resilience? How to deal with large data sets in order to obtain results in a reasonable computational time, possibly close to real time?

As a final goal, we aim at proposing strategies to improve transport network resilience.

(v) How to develop strategies to improve resilience of transport network in order to maintain an acceptable level of performances? How to design the transport network to make it more resilient?

This dissertation aims at considering and addressing these questions by proposing a framework that allows us: *i)* to represent the (multimodal) transport network for vulnerability characterization by jointly taking into account traffic dynamics and network topology; *ii)* identifying a set of relevant metrics to quantify the vulnerability of the modelled transport network; *iii)* injecting disruptions in the network by means of stress testing to define perturbation scenarios and to capture, via the aforementioned metrics, those scenarios that stress the network the most; *iv)* improving resilience of the transport network via multiple augmentation/monitoring solutions.

To this purpose, analytical frameworks were needed to properly model both transport topology and dynamic traffic conditions. Resilience analyses based on simulated data have been performed using both microscopic and macroscopic simulators to characterize resilience and conduct a stress test methodology aiming at evaluating the impact of extreme events that negatively impact the transport network. To support the simulated based conclusions and further extend our research, we also used real data. The latter have been leveraged to identify real disruptions by observing significant variations in terms of the average travel times with respect to typical behaviors. Finally, a modelling framework for the design of resilient networks is introduced by proposing a quick-to-compute methodology to build a new transport mode and develop an optimal Park-and-Ride (P&R) system. Such a system is a sustainable transport mode that will reduce the circulation of privately-owned vehicles and is thus expected to lead to a more resilient mobility framework by improving road traffic conditions.

Structure of the manuscript

The organization of the manuscript is as follows: Chapter 1 deals with the modelling of a transport network, considering both network topology and traffic dynamics, for network resilience assessment context. Graph theory, mainly used in the representation of a transport network and useful to reproduce topological disruptions, with the removal of network components, is introduced. The state of the art in traffic modelling, used to simulate traffic conditions, is also included in this chapter as well as the approach for modelling of disruptions with the presentation of the stress test methodology, the coupling of catastrophe models and traffic ones as well as the use of historical data. A hybrid representation encompassing network topology and traffic dynamics with a dynamic graph is presented in the chapter. Finally, the representation of transport network multimodality using multi-layer graphs is discussed. Chapter 2 covers the definition of resilience and the associated notions: robustness, vulnerability and reliability. The main network performance indicators analyzed along the thesis are summarized with distinctions between the dynamic and static approaches mainly used in resilience characterization and the global and the local network characterizations. The network performances indicators extended to the proposed hybrid representation of the transport network and to its multimodal nature are detailed. Chapter 3 focuses on the simulated data presentation and the analysis lead with the aim of quantifying transport network resilience using dynamically weighted graphs and some related indicators issued from graph theory. The validation on the real data is analyzed in Chapter 4 where similar analysis are lead to support our findings. Finally, Chapter 5 presents the developed strategies aiming at designing a resilience-oriented transport network. An overview of resilience improvement strategies before or after the disruption occurrence is summarized.Two strategies are developed to improve the development of a resilience-oriented network design. The first one, REINFORCE's method, aims at prioritizing the deployment of the multiple lines or modes that a transport operator might want to propose to increase its offer. As a short-term strategy, the methodology is helpful to quickly deploy bus lines aiming at maximizing the transport network performances gain, whereas, as a long-term strategy. The methodology aims at planning the construction of a transport mode by ordering the lines based on the gain of performances they might offer. The second strategy aims at optimizing the deployment of a P&R system adapted to recurrent disruptions with stochastic problem formulations. On the one hand, the P&R deployment maximizes its ridership whatever the traffic conditions. On the other hand, the P&R deployment minimizes the construction, social and operational costs considering a set of disturbances.

Conclusions and Future Work reflect on the contributions of the dissertation and the future work opened by the funding of this thesis.

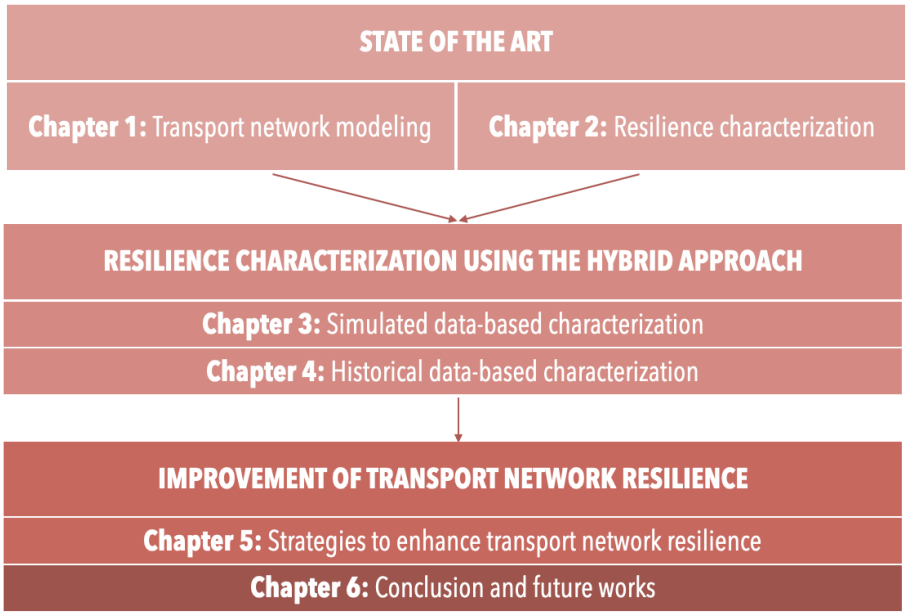

Figure 1: Thesis organisation

Publications

Along with this work, the following research has been published in peer-reviewed journals and international conference, all listed below. Most of the chapters in this manuscript are updated and enhanced versions of these papers. They all consist of original works first-authored by the PhD candidate.

(a) Peer-Reviewed Journal Publications

- E. Henry, A. Furno, N.-E. El Faouzi, Approach to Quantify the Impact of Disruptions on Traffic Conditions Using Dynamic Weighted Resilience Metrics of Transport Networks, *Transport Research Record*, journal of the Transportation Research Board, 2020, issue 4, volume 2675, pp: 61-78.
- E. Henry, A. Furno, N.-E. El Faouzi, REINFORCE: Rapid augmentation of large-scale multimodal transport networks for resilience enhancement, *Applied Network Science*, 2021, issue 74, volume 6.
- E. Henry, A. Furno, N.-E. El Faouzi, D. Rey, Locating Park-and-Ride Facilities for Resilient On-Demand Urban Mobility. *Transportation Research Part E: Logistics and Transportation*, 2022, volume 158.

(b) Peer-Reviewed Conference Publications

- E. Henry, M. Petit, A. Furno, N.-E. El Faouzi, Quick Sub-optimal Augmentation of Large Scale Multimodal Transport Networks, 2020, 9^{th} *International Conference on Complex Networks*, December 2020, Madrid, Spain.
- E. Henry, A. Furno, N.-E. El Faouzi, D. Rey, Optimal Park-and-ride Facility Location and Fleet Sizing to Enhance resilience of Transport Networks, 2020, 8^{th} *International Symposium on Transport Network Reliability*, June 2021, Stockholm, Sweden.
- E. Henry, A. Furno, N.-E. El Faouzi, Dynamic Weighted Resilience Metrics of Transport Networks: an Approach to Quantify the Impact of Disruptions on Traffic Conditions, 99^{th} *Annual Meeting of Transportation Research Board*, January 2020, Washington D.C., USA.
- E. Henry, A. Furno, N.-E. El Faouzi, An Accessibility-based Approach to Characterize the Dynamic Vulnerabilities of Multimodal Urban Transport Networks, 9^{th} *Symposium of the European Association for Research in Transportation, hEART 2020*, February 2021, Lyon, France.
- E. Henry, L. Bonnetain, A. Furno, N.-E. El Faouzi, E. Zimeo, Spatio-temporal Correlations of Betweenness Centrality and Traffic Metrics, MT-ITS 2019, 6^{th} *International Conference on Models and Technologies for Intelligent Transportation Systems*, June 2019, Cracovie, Poland.
- E. Henry, A. Furno, N.-E. El Faouzi, A Graph-based Approach with Simulated Traffic Dynamics for the Analysis of Transportation Resilience in Smart Cities, 98^{th} *Annual Meeting of Transportation Research Board*, January 2019, Washington D.C., USA.
- E. Henry, A. Furno, N.-E. El Faouzi, Resilience Analysis of Transport Networks using a Dynamic Graph, 1^{st} *International School on Informatics and Dynamics in Complex Networks*, Oct 2018, Catania, Italy.

Chapter 1

Overview of the Transport Network Modelling under Disruptions

This chapter deals with the modelling of a transport network for resilience quantification. As pointed in the Introduction, in resilience context two major approaches exist: a static one based on network topology and a dynamic one based on traffic conditions. Hence the interest of proposing an accurate modelling of the transport network, encompassing both the design of the network and the traffic conditions. This chapter also addresses the disruption modelling related to the network topology or to the traffic conditions, closely linked to the modelling of the network. After reviewing the network topology modelling and the traffic conditions one separately, we present a hybrid modelling approach which leads to the accurate consideration of both aspects in the representation of a transport network. The monomodal network representation is then extended to a multimodal one.

Section 1.1 focuses on the topology representation of a road network. By modelling the roads with the edges and the intersections by the nodes, it is possible to analyze the network topology by means of graph theory (Section 1.1.1). Indeed, the redundancy of the paths and the connectivity between the components, important in resilience characterization, depend on the network topology. The topological-based modelling of disruptions and its limits are also introduced (Section 1.1.3). Section 1.2 reviews the state of the art related to the modelling of the transport network by emulating the traffic dynamics using historical or simulated data (Section 1.2.1). The use of traffic simulation is essential in the modelling of disruptions, and especially in the stress testing methodology (Section 1.2.2.1) which proves its efficiency in some fields and appears to be promising in transport network resilience analysis. It refers to a range of techniques used to assess the vulnerability of a complex system by analysing a unique risk or a combination of risks. The hybridisation of both traffic dynamics and network topology, allowing a full representation of the transport network is presented in Section 1.3. Such hybrid modelling of the transport network is useful for the combination of both static and dynamic approaches. The literature related to the modelling of multimodal transport network is introduced in Section 1.4. Finally, Section 1.5 discusses the approach used to model the transport networks in the manuscript, for both monomodal and multimodal transport networks, respecting the constraints of computational time and data merging (network topology and traffic dynamics).

1.1 Network Topology and Associated Disruptions

The simplest representation of a transport network consists in modelling it as a graph with transport stops or roads intersections, represented as nodes, and their potential connections, represented as edges (Thomson and Richardson, 1995; Barthélemy, 2011; Jafino et al., 2020). Such modelling approach focuses on the representation of the network topology which defines the manner in which the edges and nodes of a network are arranged and how the flow could travel in the network. As a first step we only focus on the monomodal network representation rather than a multimodal network which is the subject of Section 1.4.

1.1.1 Graph Theory

Graph theory appeared in 1735, when solving the problem of the seven Königsberg bridges (Lhomme, 2012). The problem consists in crossing the seven bridges in the Pregel River, crossing each bridge only once, and returning to the point of origin. The Swiss mathematician Leonhard Euler solved this problem, demonstrating through a representation, called graph, the impossibility of a journey with these characteristics (Barwaldt et al., 2014). Graph theory already proves its efficacy in numerous fields and especially in the transport one. This theory is highly employed in resilience analysis of the transport network. Indeed, graph theory is "suitable for identifying structural criticalities" (Eusgeld et al., 2009). Barwaldt et al. (2014) use graph theory to implement a bike lane in Santo Angelo, Brasil, by choosing a path with minimal costs and time. Freiria et al. (2015) identify the most important roads in a Portuguese network. Shalaby et al. (2016) study performances of public transport network in Toronto and USA. Tu et al. (2010) analyze the topological vulnerability of Sioux Falls network.

Graph modelling is a mathematical approach used to describe *things* with *relationships* (Bettilyon, 2019). Graph theory aims at solving complex problems by simplifying their representation using a graph $G = (V, E)$ composed of a set of vertices V which are the fundamental units of a graph, connected in pairs by edges $E \subseteq V \times V$. One main advantage of graph theory is its capability of modelling numerous complex interactions within systems. According to Trudeau (1993), a graph is an object composed by two sets, called *vertex* set and *edge* set. The vertex set is a finite non-empty set. The edge set may be empty, but otherwise its elements are two-element subsets of the vertex set. The connections between the vertices V by the edges E are summarized in the adjacency matrix $A(G)$ which is a square matrix whose size equals the number of vertices. If an edge connects the vertices i and j, $A(G)_{ij} = 1$ else, $A(G)_{ij} = 0$. In a graph, a *walk* is a finite nonempty sequence of vertices and edges which could be repeated (Diestel, 2000; Bondy and Murty, 1976; Gibbons, 1985). A *cycle* appears if the walk is closed, meaning that the origin and the destination are the same and a *path* corresponds to a walk without vertices or edges repetition. If some vertices are not connected to some other vertices by a path, the graph is composed by several *components*. A *component* is a subgraph in which any two vertices are connected to each other by paths. A *shortest path* represents a path with a minimum distance. Originally, this distance is computed by counting the number of crossed edges. The *neighbourhood* of a generic vertex v is the graph composed of the vertices adjacent to the vertex v and all edges connecting these adjacent vertices.

Two edges properties, the direction and the weight, change the type of the graph. The direction of the edges is considered in a directed graph where the edges represent a one-way relationship from a node to another node, contrary to an undirected graph in which the edges represent a bidirectional relationship. Such a bidirectional relationship involves two edges in a directed graph: an edge from i to j and another edge from j to i. In an undirected graph, its adjacency matrix is symmetrical unlike the one of a directed graph. Graph could be weighted, meaning that a weight, which is a numerical value, is attached to each individual edge. The distance between two vertices is thus equal to the sum of the crossed edges' weights and the coefficients of the adjacency matrix are then equal to the weight w_{ij} of the specific edge $A(G)_{ij} = w_{ij}$. If the edges do not have weights, the graph is said to be unweighted and the distance is equal to the original

value: the number of crossed edges to join the two vertices. Edge weight allows to consider some traffic indicators, such as the length (Ducruet and Lugo, 2013; Dall'Asta et al., 2006), the travel time (Gauthier et al., 2018; Yin et al., 2017) or the flow (Yoo and Yeo, 2016; Akbarzadeh et al., 2019). Nonetheless, to consider traffic dynamics, it is crucial to consider the temporal aspect.

The main difference between time-independent and time-dependent route planning is the type of edge weights (Pajor, 2009). Whereas for time-independent route planning it is sufficient to have constant weights, for time-dependent route planning, functions are necessary to accommodate the weights of the edges at different times of day and thus obtain a temporal graph (Tang, 2011). Such temporal graph, with time-dependent weights, representing the traffic conditions, is relevant for our objective of merging the network topology modelling with the traffic conditions.

1.1.2 Transport Network Topology Modelling

In the literature, there are different manners of modelling the topology of a transport network. Kurant and Thiran (2006) analyze the three existing approaches in the literature review that define three different *spaces* to spatially model the transport network (Figure 1.1a). The first approach is the *space-of-changes* (Figure 1.1b), also called *P*-space (Von Ferber et al., 2008; Hu and Zhu, 2009; Berche et al., 2009; Yang et al., 2012; Rocha, 2017; Alessandretti et al., 2016), which connects two public transport stations (respectively or road intersections) by an edge when there is at least one vehicle that stops at both stations (respectively crosses both road intersections) without considering the physical distance. The second approach is the *space-of-stations* (Figure 1.1c) which connects two stations (respectively road intersections) if they are physically directly connected. The last approach is the *space-of-stops* (Figure 1.1d), also called *L*-space (Hu and Zhu, 2009; Berche et al., 2009; Von Ferber et al., 2008), which connects two stations (respectively or road intersections) if they are two consecutive stops (respectively intersections) on a route with at least one vehicle. In such an approach, the distance of a path is equal to the minimal number of crossed stations (respectively intersections). The last approach, reflects the real physical network, essential for the network topology analysis, and is seen as the primal approach (Porta et al., 2006). This representation appears as the most intuitive with a strong connection to the geographic dimensions: "the primal road-centerline-between-nodes representation of street patterns, where intersections are nodes and streets are (weighted) edges, evidently appears the most valuable option" (Porta et al., 2006). The weighting of the graph by the edge length or travel time allows to measure in spatial or temporal terms the distance rather than in

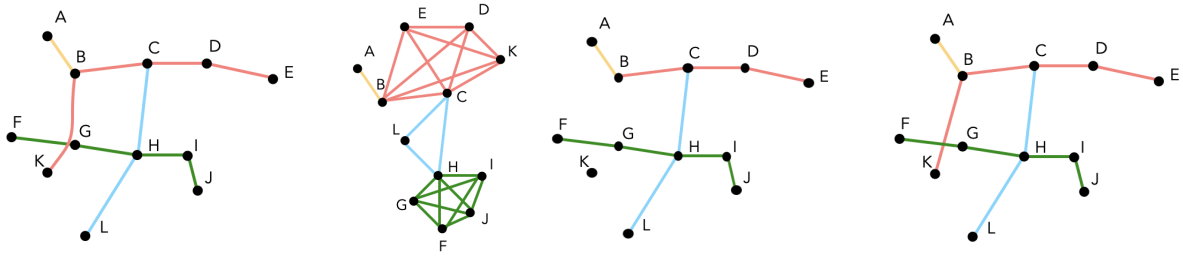

(a) Transport network **(b)** Space-of-changes **(c)** Space-of-stations **(d)** Space-of-stops

Figure 1.1: An illustration of the transportation network topology in three spaces. (a) The routes of four transport lines. The route of Red line passes through node G on the way from B to K, but the transport mode does not stop there. (b) The topology in space–of–changes. Each route results in a clique. (c) The topology in space–of–stations. (d) The topology in space–of–stops. The "shortcut" B-K is a legitimate edge in this space. This graph reflects the topology of the real-life infrastructure (Kurant and Thiran, 2006).

topological terms when the distance is computed by the number of crossed edges. In the following, we thus assume that a route is simply a single physical edge between two locations and an intersection is a merge or diverge junction of several road sections to conserve the transport network topology (Sossoe, 2017).

1.1.3 Topology-based Disruptions

Topological approaches aim at quantifying network resilience by looking at the connectivity properties of the network (Figure 1.2a), by using graph theory. In such an approach, network resilience is quantified by the impact of the removal of a component, corresponding to an edge (Figure 1.2c) or a node (Figure 1.2b), with static metrics (Shalaby et al., 2016). The removal can be random or targeted, by quantifying the impact induced by the removal of the most attractive component (edge or node) in the network. By ranking the components according to their importance in the network functioning, Shalaby et al. (2016) prove that the negative impact is worst with targeted failures than with random ones. Holme et al. (2002) similarly conclude its attack analysis: "the impact is stronger by iteratively removing the most important component than removing the initial most important components due to the network structure changes". Aydin et al. (2018) analyze the impact of seismic hazards over the road network by removing edges randomly, based on their kernel density or based on the community structures. Nonetheless, such modelling is able to represent infrastructure failures only and does not consider traffic conditions. Rather than fully removing a node or an edge, its weight could be modified to emulate a capacity reduction (Figure 1.2d) or a travel time increase to modify the network properties by being more faithful to some recurrent disruptions impacting the transport network (Cats et al., 2017; Cats and Jenelius, 2018; Gauthier et al., 2018). Such an approach allows to better quantify minor daily disruptive events. Finally, whatever the disturbance intensity, various disruptive events, like floods, snow-storms, fires, etc., may easily affect entire areas and cannot be modeled by the previous approach consisting in removing or modifying the property of a unique component. Jenelius and Mattsson (2012) ensure that "area-covering disruptions will have severe consequences that are quite different from those of single link failures". Although topological vulnerability studies can provide important general insights and indicate various structural weaknesses in transport networks, they are in some respects too simplistic to be useful for assessing actual policy actions in a specific transport system.

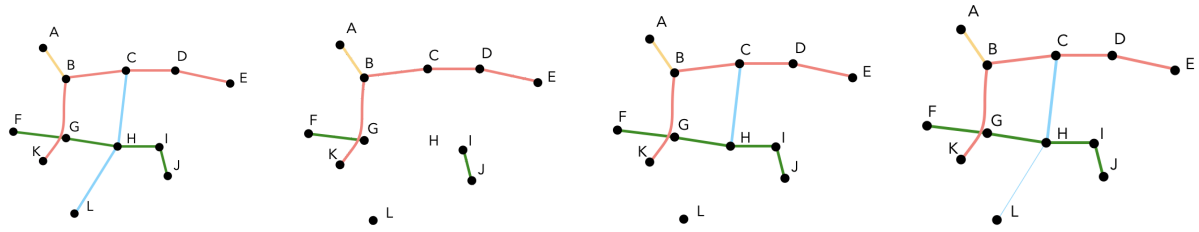

(a) Transport network **(b)** Node removal **(c)** Edge removal **(d)** Capacity reduction

Figure 1.2: Topology-based disruptions on the transport network (a). The node removal consists in deleting a node, here H, and the connected edges, G-H, H-I, C-H and H-L (b). The edge removal prohibits the original connection between the nodes H and L (c). We assume that the width of the edges is proportional to their weight. Less vehicles can cross the edge H-L (d).

1.2 Traffic Dynamics and Disruption Modelling

As noticed by Kurant and Thiran (2006), the knowledge of real-life traffic pattern is crucial to well understand and analyze transportation systems. Traffic modelling is essential to understand and investigate the evolution of traffic conditions under normal condition and in presence of a disruption. The first theory of traffic flow was introduced by Lighthill and Whitham (1955) and Richards (1956). Traffic flow theory aims at determining all relevant traffic flow quantities at different granularities. Indeed, the field of traffic modelling is usually divided into three categories following the different types of granularities possibly adopted in the models: macroscopic, mesoscopic and microscopic. By relating the interactions between travellers and infrastructure, traffic flow theory provides information about the transport network movement and the traffic congestion problems. The fundamental variables of traffic flow are the speed v, the volume of traffic q and the density k. They are related through the fundamental relation $q = k \times v$. From this relation derives the Fundamental Diagram (FD). Such diagram enlightens about the maximal capacity intensity, the critical density, the jam density, and the average speed (Hoogendoorn and Knoop, 2015).

1.2.1 Traffic Simulation Levels

As noticed, three levels of granularities exist for the traffic flow models: macroscopic, mesoscopic and microscopic. Macroscopic level models are based on a regional description of the network and the use of aggregate traffic variables. Such models consider the average state of traffic (Hoogendoorn and Knoop, 2012). The advantages of this type of models are the low computation cost and the possibility to use well-defined empirical relations, at global scale, between the main traffic variables: flow, density and speed. Mesoscopic scale simulates traffic for smaller network elements, like roads or for groups of cars. These models represent the behavior of drivers without explicitly distinguishing their time–space behavior. Both macroscopic and mesoscopic models are interested in the viewpoint of the collective vehicular flow (Hoogendoorn and Bovy, 2001). Finally, microscopic models are agent-based ones with the decision variables chosen at the driver level under the influence of vehicles in their proximity, implying a high computational cost and also greater stochasticity in the results (Hoogendoorn and Knoop, 2012). Contrary to macroscopic and mesoscopic models, such modelling requires an explicit and detailed modelling of the road sections, intersections, roundabouts and so on (Barcelo et al., 2007).

1.2.1.1 Macroscopic Simulation

Macroscopic models give a general description of vehicles and traffic as a continuum (Adebisi, 2017). Macroscopic simulation models were originally developed to model traffic in distinct transportation subnetworks, such as freeways, corridors, surface-street grid networks, and rural highways. Such models assume that the aggregate behavior of drivers depends on the traffic conditions in the drivers' direct environments (Hoogendoorn and Bovy, 2001). These models are suitable for large-scale simulations of traffic flow in networks. Nevertheless, macroscopic models are not very suited for analysing inherently microscopic characteristics of the flow. Macroscopic urban dynamics are based on the deterministic relationships of the flow, speed, and density of the traffic stream and should be modeled using a Macroscopic Fundamental Diagram (MFD), based on the variation of the accumulation of circulating vehicles in a given area Mariotte et al. (2017). Introduced in the late 2000s (Daganzo and Geroliminis, 2008), the area-based FD, which characterizes road by relating three traffic variables, called MFD, relates the output flow and the number of vehicles in a large network, and gives insights about the state of a zone over a road network. Already used in traffic control (Qian, 2009), the MFD could offer good opportunities in resilience analysis. Kim and Yeo (2016) assess resilience of a part of the transport network in the city of Seoul, South Korea, by using information issued from this traffic tool and by assessing some area properties such as the outflow or the traffic density.

1.2.1.2 Mesoscopic Simulation

The mesoscopic analysis of the traffic conditions combines both macroscopic and microscopic models. Such models describe traffic flow at a medium detailed level. This analysis level describes the aggregated vehicle behavior whereas the behavior rules are defined for individual vehicles. Such models represent a good compromise according to the aim of the study, by being more faithful to the vehicles behaviors than macroscopic model and quicker in terms of computational times than microscopic model. This level of analysis is based on the gas kinetic models, originally used in contemporary physics to describe the motion of large numbers of small moving particles in a gas. Applied to the motion of vehicles in a traffic stream, similar models can be used to describe the variation of the speed distribution of vehicles (Kessels et al., 2015). Mesoscopic models have the advantage that they enable description behaviors of individual vehicles, without the need to describe their individual time–space behavior (Hoogendoorn and Bovy, 2001). The Lighthill-Whitham-Richards model (Lighthill and Whitham, 1955; Richards, 1956) is suitable to model traffic dynamics at a mesoscopic scale (Duret et al., 2016; Laval and Leclercq, 2013). Such a model is the analogy of vehicles in traffic flow and particles in a fluid.

1.2.1.3 Microscopic Simulation

Microscopic models simulate the movement of individual vehicles based on car-following theory and lane-changing one. Microscopic traffic models define the operation of a traffic system based on individual vehicle characteristics, and are thus efficient to evaluate traffic congestion as well as drivers response to a disruption on the transport network. Nonetheless, these models are time consuming, costly, and can be difficult to calibrate (Adebisi, 2017).

These models are detailed at a fine scale and typically include all streets and components of the transportation system that impact travel. Such elements can include intersection control, pedestrian crossings, transit stops, and even the inclusion of traffic measures. Microscopic models are calibrated using disaggregate data. They are regarded as non-continuum models, which require the input of parameters such as lane changing, free flowing, car following (Newell, 2002) and route choices in their calibration. Each vehicle moves in response to the behaviors of the other vehicles by maintaining the legal safe distance of the preceding vehicle and respecting the legal speed. This response is expressed in terms of acceleration. The microscopic models compute the dynamics of individual vehicles over a multimodal transport network, by generating the spatio-temporal traces of vehicles, and compute transit times every time unit (*e.g.*, second), allowing to extract many traffic indicators. In such simulator, the vehicles route choice is defined according to the traffic conditions upon their generation.

1.2.2 Disruption Modelling

Traffic is frequently impacted by extreme weather (Pregnolato et al., 2017; Kyte et al., 2001; Hooper et al., 2014; Jaroszweski et al., 2014; Bíl et al., 2015) and daily disruptions (Marra et al., 2019; Afrin and Yodo, 2020; Suryani, 2019; Zhu and Levinson, 2011). Their modelling, issued from simulated or historical data, is crucial in transportation network resilience analysis. Two strategies are based on simulated data analysis. First, the stress test methodology (Section 1.2.2.1), widely used in bank and nuclear sectors, aims at simulating extreme but plausible situations in order to evaluate their consequences and the resistance of the network. Second, the coupling of both catastrophe and traffic models (Section 1.2.2.2), mainly used to quantify the impact of floods, aims at simulating the drivers behavior in presence of a disruption. The analysis of historical data (Section 1.2.2.3) provides information about the consequences of happened events over the traffic. Whatever the used methodology, the studied disruptions depend on the availability of data and models (Mattsson and Jenelius, 2015).

1.2.2.1 Stress Testing

The stress test methodology aims at simulating some situations to be prepared in case of disruptive events in order to identify critical points to strengthen them or to know how to react if it occurs (IAA, 2013). According to Lam et al. (2018), "a stress test is a quantitative assessment designed to evaluate the ability of a network to perform adequately during and after the occurrence of hazard events". It may also be defined as "the process of determining the ability of a network to maintain a certain level of effectiveness under unfavorable conditions" (Clarke and Obrien, 2016). By comparing the outputs, determined by different scenarios, including the reference one, the impact induced by a disruption is known (Mercier et al., 2013) The risk factors are simulated thanks to the elaboration of scenarios, reproducing the events. Scenarios have to be as plausible, coherent and reliable, as possible. It is a difficult task and can "involve a great deal of expertise and judgment" (Blaschke et al., 2001). Such a methodology is well developed and considered as an important tool to assess the safety, security and resilience of the relevant system in the banking and nuclear sectors (Galbusera et al., 2014). In this way, stress test can be useful for critical infrastructures resilience in testing transport network under abnormal conditions (Cooperation Work Programme, 2014). This methodology is rarely used in the transport field but appears like a promising solution concerning the simulation of perturbations (Gauthier et al., 2018). According to Galbusera et al. (2014) the application of this methodology will improve critical infrastructure resilience by knowing their weakness. To apply the stress test methodology, many simulations have to be ran in order to quantify the impact of some extreme, but plausible, events. For this reason, the use of microscopic simulators is not the more appropriate one in urban areas due to the large computational time. The mesoscopic and macroscopic simulators have to be preferred.

1.2.2.2 Model Coupling

Another disruptions impact modelling consists in the coupling of both catastrophe model to simulate the consequences of the events, and traffic simulators to reproduce the drivers behaviors in reaction to the disturbed situation. By coupling a traffic simulator with catastrophe models, some disruption impacts, mostly flood ones, are evaluated. A catastrophe model is composed of four basic components (Grossi et al., 2019). First the risk of the natural hazard is characterized. Next, the inventory of the risk is detailed such as the location and all the parameters impacting the vulnerability at the specific location. Both hazard and inventory aim at calculating the vulnerability which is the susceptibility to damages of the infrastructure. Finally, the loss of performance is evaluated. Pregnolato et al. (2017) analyze the rainfall and flooding impact on the transport network of Newcastle, United Kingdom, by coupling traffic modelling to the CityCAT (City Catchement Analysis Tool) flooding model. Yin et al. (2017) couple two dimensional hydraulic scenarios developed by the Federal Emergency Management Agency (FEMA), to the road network of New York with the aim of studying exit strategies. Postance et al. (2017) model the impact of a landslide, based on the GeoSure GeoSure classification, over the Scottish road network where the traffic is simulated using SUMO (Simulation of Urban MObility). Luin and Petelin (2020) couple tunnel ventilation, evacuation, and traffic models to analyze the impact of accident in such transport infrastructure. Finally, Raimbault (2015) observe the urban growth impact over transport networks using an algorithm method to provide the co-evolution of transportation networks and urban land-use. Such a methodology should be extended to other natural hazards models or to terrorist attacks. Indeed, Grossi and Kunreuther (2005) detail the four basic components of a catastrophe model for the terrorist attack. Because the catastrophe model accurately reproduces the impact of disruptions, mostly issued from natural hazards, the coupling with traffic simulator is promising to analyze transport network resilience. Nonetheless, such disruption modelling depends on a huge amount of data, increasing the model complexity and the computational time, as well as the availability and the accuracy of such catastrophe models.

1.2.2.3 Historical Data-based Modelling

The historical data recorded during disrupted events provides information about their impacts on transport network. Schäfer et al. (2002) use Floating Car Data (FCD) issued from taxis in European capital cities to observe the speed evolution, and prove that the most significant speed variations are induced by special events, bad weather conditions or roadwork. Calabrese et al. (2010) study the mobility during special events, located in 6 different places in the Boston Metropolitan area, using 1 million cell-phone traces. By analyzing the origins of people attending an event, the authors prove the strong correlation with the type of event. Pan et al. (2012) use real traffic data to accurately predict the traffic conditions and the event impact. Melnikov et al. (2015) analyze the impact on the road traffic of the modal change from the electric public transport system to the private vehicle, induced by a major power failure in North Holland. By comparing the propagation of traffic jams during the blackout and under normal conditions, using the traffic flow and speed data, the authors highlight the most impacted areas. Zhou et al. (2015) lead an analysis to identify the critical locations of the Wuhan Chinese road network using taxi trip trajectory dataset, related to approximately 12 000 taxis, collected during the month of September in 2009. Bíl et al. (2015) analyze the impact caused by some events on the Dutch road network between 1997 and 2010. Zhu et al. (2016) quantify the New York transportation network resilience during the hurricane Irene and Sandy, using taxi trip and subway data. Zhu et al. (2017) also analyze the impact of both hurricanes in New York by computing the loss of resilience, based on the recovery rate, defined as the ratio of the number of trips during a certain hurricane period divided by the number of trips during a corresponding normal period. Lu et al. (2016) study mobile data in Bangladesh impacted by the cyclone Mahasen in 2013 over four months of data. The call frequency, the use of mobile phone credit and the moves before, during and after the cyclone allow to model the human behavior and the transport mode use in presence of such disruption. Donovan and Work (2017) prove the ability of detecting abnormal situation using taxi trip data. Tympakianaki et al. (2018) use historical information issued from traffic sensors and FCD to analyze the multimodal impacts of transport network disruptions. By studying the spatio-temporal network changes and the multimodal effects between normal conditions and during a tunnel closure, the authors show that the disturbed situation highly impact the network traffic conditions due to the redistribution of vehicles on alternative path, as well as the public transport which attract some of people. Nonetheless, Calvert and Snelder (2018) argue that some events are too rare to accurately derive from empirical data. Indeed, with the use of historical data, the set of analyzed disrupted events is limited to what already happened and what has been recorded, restricting the modelling of disruptions. Although historical data aims at analyzing the real consequences of a disruption over a transport network, the limited availability of data is not sufficient to prepare the network and adapt the response of the traffic operators in order to minimize the impact of a disruption.

1.3 Traffic Dynamics and Network Topology Hybridisation

Because the structure of a network often affects its function (Strogatz, 2001; Akbarzadeh et al., 2017), deciphering the topology and dynamics of the underlying networks is a prerequisite to a full understanding of connected, interacting systems. Nonetheless, the simplistic way in which the transport system is often represented as an abstract network does not allow for a very realistic description of the behavioural responses to a disruption (Mattsson and Jenelius, 2015). According to Van Nes (2002), "the main characteristics of any transportation network from the traveller's point of view are travel costs and travel time, with the latter determined by network characteristics such as network speed, space and time accessibility". Because, human mobility is dynamic and highly time-dependent (Kazerani and Winter), we could weight the graph with an edge time-dependent weight (Section 1.1.1). A *temporal graph*, also known as *time-varying graph*, *dynamic graph* or *evolving graph* is a specific graph where vertices connections evolve in time by being removed or modified with new weights (Tang, 2011; Nicosia et al., 2013; Kostakos, 2009). Such network differs from a static network in the sense that a different adjacency matrix is given at each time stamp (Rocha,

2017). In the literature, there are four basic kinds of dynamic graphs (Harary and Gupta, 1997): the node (respectively edge) -dynamic graph in which some nodes (respectively edges) could be added or removed from the graph and the node (respectively edge) weighted dynamic graph in which the labels, associated to the nodes (respectively edges), are time-dependent and vary in time. All these models are interesting in the transport network analysis. Whereas the weighted dynamic graph allows to reproduce the time-varying traffic conditions, the dynamic graph aims at modelling the network modification induced by a disruption. A temporal graph could be seen as a succession of static graphs. The graph is thus composed by a new set of edges and nodes at each time stamp. In their article, Yang et al. (2018) establish a real-time path planning application, based on real-time traffic conditions, for providing shortest paths with minimum travel time on a dynamic weighted graph. Huang et al. (2007) propose a shortest path algorithm adapted to such graph aiming at modelling transport network with their dynamic traffic conditions. Cats and Jenelius (2014) build a dynamically riding time-weighted graph to assess the dynamic vulnerability of the Stockholm public transport network. Peng et al. (2020) predict the urban passenger traffic flows at transit stop using a dynamic graph, weighted by historically passenger traffic flows to model traffic station relationships. The authors conclude that using dynamic spatial-temporal incidence graphs is more suitable to model external changes and influences. Such dynamic graphs are crucial to model transport networks with their traffic dynamics. Indeed, by modifying the edge weights, or by removing some of them, the traffic conditions should be modeled as well as the disruptions impact.

1.4 Multimodal Transport Network Modelling

As discussed Kivelä et al. (2014) "to represent systems that consist of networks at multiple levels or with multiple types of edges, we consider structures that have *layers* in addition to vertices and edges". Networks with multiple layers can encapsulate a much more detailed description of a system than simple networks. A multilayer graph is composed of vertices V and edges E, like a simple graph (Section 1.1.1), but the multilayer graph is also composed of layers L which may belong to different sets such as relationships or time stamps. In a multilayer network, there are two kinds of edges: the ones that remain inside of a layer, called *intra-layer edges*, and the ones that cross layers, called *inter-layer edges*. Kivelä et al. (2014) model the multimodal transport network as a weighted directed multilayer graph, $G = (V, E, L)$, with $L = \{L_m\}_{m=1}^{M}$ the set of elementary layers, each representing a specific transport mode m, V the set of nodes and E the set of edges. Each layer contains a node subset $V_l \subset V$, which corresponds, respectively, to the set of intersections and the intra-layer segments composing the transport mode m represented on layer $l \in L$, and an edge subset $E_l \subset E$. The edge set E is also composed by inter-layer edges $E_{l'}$ that allow to cross the layers, *i.e.*, to switch between two different transport modes composing the graph. There are two main types of multilayer networks, multiplex networks and interconnected networks (Kivelä et al., 2014; Kinsley et al., 2020). In multiplex networks, inter-layer edges can only connect nodes that represent the same actor in different layers. Therefore, multiplex networks typically represent sets of interactions between the same entities. In interconnected networks, inter-layer edges can connect between different actors, and therefore different layers typically represent different entities.

To model the multimodal transport networks, different strategies exist in the literature. Cardillo et al. (2013) study the dynamics of the European air transport network using a multiplex network to compare the approach with the single-plex one in characterizing resilience of the system against random flight failure. The 15 layers of the multiplex graph correspond to the biggest airline company and the vertices represent the airports. On each layer, the edges are the flights between the airports, operated by the airline. In their article, De Domenico et al. (2014) analyze the navigability in the travel cost weighted interconnected multilayer network of public transport of London under random failures. By comparing the efficiency they prove the high influence of layers' topology, interconnection strengths, and walk strategy in exploring the multiplex. To consider both the multimodality of an urban transport network and the dynamic induced by the traffic, Gallotti and Barthelemy (2015) build a multilayer temporal graph to reproduce the network of public

transport in Great Britain. Aleta et al. (2017) study the interconnected structure of 9 different cities in Europe by representing the corresponding urban transport network using a multiplex network. In the multiplex representation, the modes are connected through the closest nodes of each mode, by an edge weighted by the distance, if the distance does not exceed 100 meters. Two representations are analyzed: on the one hand, in the per-line representation, each line corresponds to a layer, on the other hand, in the per-transport-mode representation, each layer represents the group of lines belonging to the same transport mode. By analyzing the sum of the degree for a node in each layer, the authors conclude that both representations are useful and complementary to understand the functioning, as well as the vulnerabilities, of transportation systems. Sossoe (2017) defines a multimodal transport network as a collection of networks, each network corresponding to one transport mode. Some connections between the transport modes, represented as transfer nodes or edges (Van Nes, 2002), permit to change from mode to mode. This is as simple as a physical network in which people could travel from one location to another location through at least two means of mobility (Fawzy Mahrous, 2012; Mandloi and Thill, 2010; Chen et al., 2011).

1.5 Concluding Remarks and Discussions

In a nutshell, we aim at modelling urban transport networks considering both the topology and the traffic conditions. By using a dynamically weighted graph, introduced as the *hybridisation approach* and detailed in Section 1.3, both transport network aspects are considered by leveraging traffic conditions as time-varying weights associated to the edges. The time-varying weights are equal or based on the edge travel time evolution issued from simulated data (Chapter 3) or real ones (Chapter 4). To go further and improve the significance of the edge weights, we adopt a discretization process, we reasonably assume that paths are equally chosen by a user if they are perceived equivalent with a similar total length, *e.g.*, total travel time. This idea relates to the bounded rationality principle (Gigerenzer and Selten, 2001) and corresponds to a choice done with flexible criteria with limited information processing resources and limited consideration of alternatives paths (Sivak, 2002).

Regarding the multimodality consideration, each transport mode is modeled in a specific layer. To maintain an acceptable computational time in the characterization of resilience for large scale multimodal transport network we propose an approach of a graph simplification, detailed in Section 5.2. Each layer models a spatially aggregated transport mode weighted by the average travel time. To aggregate the different transport mode graphs, we use small areas, defined by a walkable distance. The inter-layer edges weighted by an average walking time, modelling the modal shift, connects the layers inside an area if at least two transport modes are present.

To model disruptions, different methodologies are applied. On the one hand the stress test methodology is employed by modelling some extreme conditions, close to real situations, with edge removals, capacity or speed reductions (Chapter 3). The use of simulated data aims at modelling extreme traffic conditions that could occur in order to understand the more vulnerable network components. Moreover, this allows to test some strategies to improve the network resilience and observe the transport users' behaviors. On the other hand, some abnormal conditions are analyzed via historical real data (Chapter 4). By analyzing real events, we try to capture the real users' behaviors rather than simulated ones and characterize the impact of real events rather than simulated ones.

Chapter 2

Transport Network Resilience Quantification Approaches

This chapter presents the literature review related to resilience quantification. As presented in the Introduction, transport networks are impacted by some disruptions which negatively impact their performances. Improving resilience of the transport networks will allow them to maintain an acceptable level of performance in all circumstances. Currently, the assessment of transport network resilience is led via two different major approaches based on the two major components of the transport network: topology and traffic dynamics (Chapter 1). Topological approaches aim to quantify network resilience, especially according to the perspective of robustness, by looking at the connectivity properties of the network, whereas dynamic ones characterize resilience by considering actual or simulated traffic dynamics, using demand-sensitive indicators. The hybridization of both approaches is rare but promising, based on the idea of joining graph theory with simulated or data-inferred traffic conditions. Indeed, topological approaches are traditionally unable to capture the time-dependent aspects of resilience and dynamic ones tend to use heavy simulations which demand large execution time.

Section 2.1 defines resilience and summarizes the different notions of reliability (Section 2.1.1), vulnerability (Section 2.1.2), and robustness (Section 2.1.3), comprised in this complex term, mainly used in the literature. Section 2.2 deals with the presentation of major network performances indicators. A distinction is made between traffic conditions-based measures (Section 2.2.1), related to the traffic flow as well as the travel time evolution, and the topological-based indicators (Section 2.2.2) characterizing the network performances either at global scale or at local one, related to the transport network topology. The hybridization of both transport network properties which are traffic dynamics, and network topology is essential to fully characterize the transport network resilience. Such kinds of approach is presented in Section 2.2.3 with the corresponding indicators. Section 2.3 summarizes the analysis of resilience led on multimodal transport networks. Finally, Section 2.4 presents the indicators analyze in the rest of the manuscript and their extension or modification to consider all the aspects of the transport networks as the multimodality.

Contents

2.1 Resilience Definitions and Associated Components

The vocable of *resilience* has its origins in the Latin word *resiliere*, which means to *bounce back* (Henry and Emmanuel Ramirez-Marquez, 2012). This concept is rather new and appeared in the ecological field as the ability of a system to absorb external stresses (Holling, 1973). Since its appearance, resilience has been studied in different domains like in communication networks where Sterbenz et al. (2010) define resilience as "the ability of the network to provide and maintain an acceptable level of service in the face of various faults and challenges to normal operation". For Hashimoto et al. (1982), resilience measures how fast a system is likely to return to a satisfactory state once the system has entered an unsatisfactory one. Concerning transport resilience, it arrived later but acquired acknowledgments across other subject areas which can be harnessed in transport networks. Many definitions are present in the literature (Doll and Lyon, 1998). According to Dekker et al. (2008), "a resilient system is able effectively to adjust its functioning prior to, during, or following changes and disturbances, so that it can continue to perform as required after a disruption or a major mishap, and in the presence of continuous stresses". For Heaslip et al. (2009), resilience is "the ability for the system to maintain its demonstrated level of service or to restore itself to that level of service in a specified time frame". Murray-Tuite (2006) characterizes resilience as an indicator of the "system performance under unusual conditions, recovery speed, and the amount of outside assistance required for restoration to its original functional state". Under normal conditions the network performances are acceptable and the network robustness aims at maintaining this level of performances against small disruptions, when a major disturbance occurs the level of performances drops until the recovery phase which aims at regain the initial level of performances after the perturbation.

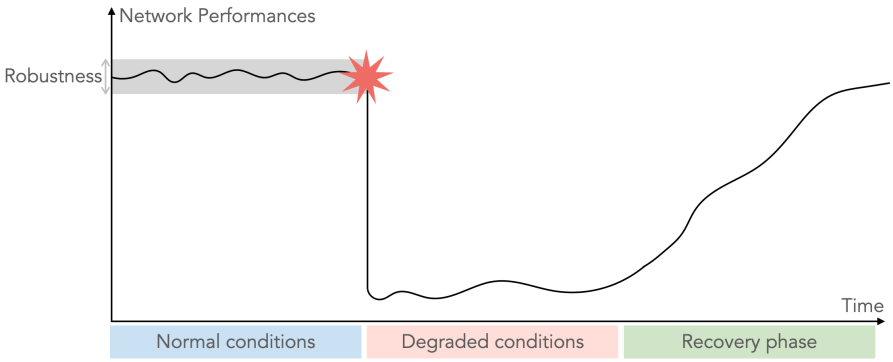

Figure 2.1: Definition of resilience.

One of the most quoted definition is the one of Bruneau et al. (2003) (Figure 2.1) who break down the notion of resilience in three temporal phases: *i) before perturbation*, corresponding to the notion of robustness, *ii) during perturbation*, corresponding to the notion of reactivity, and *iii) after perturbation*, corresponding to the notion of recovery. Berkeley and Wallace (2010) extend the definition above by including a *feedback phase* corresponding to the notion of adaptability. Woods (2015) defines four concepts for resilience. Resilience as a *rebound*, as *robustness*, as the *opposite of brittleness* and as the *ability to adapt to future surprises*. First one (*rebound*) must know how respond to disruptions by adjusting the transport network functioning. Second one (*robustness*) must know how to contain the current disturbed situation. Third one (*opposite of brittleness*) must know how do systems stretch to handle surprises. Finally, one (*ability to adapt to future surprises*) have to learn from experience to be prepared in the future. These four dimensions for resilience are also depicted by Bruneau et al. (2003): *robustness*, *redundancy*, *resourcefulness* and *rapidity*. Both *resourcefulness* and *rapidity* become relevant when the network is affected and respectively relates to deploying emergency measures and to the importance of a rapid return to an acceptable level of

service. In the field of transportation, Mattsson and Jenelius (2015) recently advocate the lack of adequate research on the topic, particularly with respect to the post-disaster phase. Since then, resilience emerges as a vast domain of investigation, with a growing and active community. In this context, definitions, metrics and approaches stemming from other research fields and domains, such as telecommunications or computer systems and networks, are proving to be crucial in the transport domain as well (Sterbenz et al., 2010; Cohen et al., 2000). Transport resilience has mainly dealt with extreme events such as floods (Litman, 2006), earthquakes (Nakanishi et al., 2013), and disasters in general (Mattsson and Jenelius, 2015; Zhang et al., 2015; Adjetey-Bahun et al., 2016). According to Hashimoto et al. (1982), system performances can be described from three different viewpoints: "*i) how often the system fails* (reliability), *ii) how quickly the system returns to a satisfactory state once a failure has occurred* (resiliency), and *iii) how significant the likely consequences of failure may be* (vulnerability)". Murray and Grubesic (2007) ensure that both vulnerability and reliability "are especially important when examining the ability of critical infrastructure to provide continuity in operation". Finally, Calvert and Snelder (2018) indicate that the "resilience is related much closer to robustness and vulnerability than to reliability".

2.1.1 Reliability

Reliability is typically defined as the probability of being functional or operational in post-disaster time (Balakrishnan et al., 2009). According to Wakabayashi and Iida (1992) reliability is "the probability that a system will perform its purpose adequately for the period of time intended under the operating conditions encountered". For Murray and Grubesic (2007), the network reliability is "the ability of a network to carry out a desired network operation despite the failure of network components". A vulnerable network is not necessarily unreliable if it maintains an acceptable level of performances when subjected to a disruption (Murray and Grubesic, 2007; Mattsson and Jenelius, 2015). However, both reliability and vulnerability are important to the continuity of critical infrastructure operations (Murray and Grubesic, 2007). In the transport literature, reliability is used more generally to describe the stability, certainty and predictability of travel conditions (Mattsson and Jenelius, 2015). For Immers et al. (2004) this is the "degree of certainty with which a traveller is able to estimate his own travel time", which depends on available information, on alternative travel options and on the probability distribution as well as the stability of travel times. Nicholson (2003) notices the lack of users' perception consideration in this definition of system vulnerability which is often only focused on transport planners point of view. According to Nicholson (2003), the unreliability of network comes from either a flow variation or a capacity one. In the literature, reliability is defined with respect to different aspects. First, the *connectivity reliability*, also called *terminal reliability* (Wakabayashi and Iida, 1992; Hongwei and Xizhao, 2015; Chen et al., 2007b) and introduced by Mine and Kawai (1982), which considers the probability that a pair of nodes in a network remains connected. Second, the *experienced terminal reliability* which is based on the probability of experiencing a disruption during the path (Bell and Schmöcker, 2002) or the probability that a network can accommodate a demand level (Chen and Tzeng, 1999). Third, the *travel time reliability* (Bhouri et al., 2012; Chen et al., 2003; Carrion and Levinson, 2012) which considers the probability that a trip between a given OD pair can be completed successfully within a specified time interval (defined as the travel time in normal condition) plus a safety margin (Cassir, 2001) and could be extended to the *travel cost reliability* (Schmöcker and Bell, 2002). The *capacity reliability* which is the probability that the capacity of the network is greater than or equal to the required demand (Chen et al., 2002, 1999; Kuang et al., 2013; Church and Scaparra, 2007) and finally the *flow-decrement reliability*, introduced by Du and Nicholson (1991), which is the probability that the flow reduction is lower than a specific threshold under a degradable network (Chen et al., 2013). Other aspects of reliability, including the *behavioral-related reliability* based on the behavioral responses (Chen et al., 2002; Shariat-Mohaymany and Babaei, 2010; Bell, 2000), are related to the reliability definition which aims at computing the level of service whatever the traffic conditions (Calvert and Snelder, 2018).

2.1.2 Vulnerability

While reliability refers to the possibility of maintaining the level of performance, the system vulnerability focuses on the potential for disrupting the element of critical infrastructure generating a loss of performance (Murray and Grubesic, 2007). Berdica (2002) defines vulnerability as the susceptibility that disruptions could cause considerable reductions in network service or the ability to use a particular route at a given time. As for resilience, a distinction between the topological vulnerability, where the transport network is modeled as a simple graph, and the system-based vulnerability, based on real transport system in the demand and supply models, is also made (Mattsson and Jenelius, 2015). There are differing opinions on the network vulnerability concept. Indeed, Taylor and D'Este (2007) propose a slightly different definition of the concept by ensuring that vulnerability is strongly related to the consequences of link failure, irrespective of the probability of failure. For Guze (2019), the vulnerability describes consequences in terms of increased travel time or limited availability of services, when travelling in a transport networks in presence of a disruption. Husdal (2004) defines a network as vulnerable by considering its non-serviceability, non-accessibility, and variability under certain circumstances, due to the lack of redundancy, robustness, and resilience in the network and consider equivalent (under certain circumstances) the notion of vulnerability and unreliability. According to Calvert and Snelder (2018), vulnerability considers the improper working of a system. The authors affirm that "vulnerability may be considered as a two-component concept in which probability and consequence are the two main attributes". For Hashimoto et al. (1982), vulnerability refers to the magnitude of a failure considering its probability of occurrence. This definition is closer to the notion of risk, introduced by Berdica (2002) as a combination of the probability of an event with a negative impact to take place and the extent of the resulting consequences once that event has taken place. For Jenelius and Mattsson (2015), vulnerability is the societal risk of road infrastructure disruptions. Risk evaluation and management aims at identifying hazards with their probabilities and consequences, assessing the acceptability of the risk and taking action to avoid unacceptable risks.

2.1.3 Robustness

Robustness refers to the connectivity loss in presence of disruption (Pagani et al., 2019). This concept differs from reliability by considering how a network can maintain its function while suffering a disturbance (Calvert and Snelder, 2018). According to (Bankes, 2010), robustness refers to the "ability to withstand or survive external shocks, to be stable in spite of uncertainty". Jen (2003) provides a similar definition by considering robustness as the "ability of a system to withstand perturbations in structure without change in function". Cats (2016) assumes that the system robustness is the capacity to absorb disturbances with a minimal impact on system performances. Although close to resilience, robustness emerges as a concept that can be used to directly assess network performances whereas resilience is a concept that focuses on understanding the ability of systems to persist over time against external shocks (Capano and Woo, 2017). In the literature, some works focusing on the characterization of resilience only consider robustness (Steen and Aven, 2011). According to Mahdavi et al. (2020), robustness can be expressed by the change in topological properties of the network. A popular measure of network robustness is the number of nodes that must be removed to break it down (Boldi et al., 2013). Sullivan et al. (2010) affirm that a robust network has the capability to compensate for disruptions on network links with relative ease and with only a small deterioration of performances. To improve robustness, Immers et al. (2004) propose to introduce a certain amount of redundancy or spare capacity into the system and to minimize the inter-dependencies to limit cascade failure, which is an iterative processes in which a single failure leads to subsequent ones. The authors ensure that a transport network could considerably suffer from a lack of redundancy or an insufficient spare capacity. Jenelius (2010) considers the importance of edges as rerouting alternatives when other edges in the road network are disrupted. Robustness is a necessary condition to make a system resilient (Cuadra et al., 2015).

2.2 Network Performances Quantification

Recently, most academics have focused on the connectivity and reliability of networks and tested their robustness and vulnerability. According to Bruneau et al. (2003), the failure probability defined by reliability (Section 2.1.1) and vulnerability (Section 2.1.2), the consequences of failure related to robustness (Section 2.1.3) and the recovery time should be used to quantify resilience. Quantifying the performances of a transport network, both considering network topology and traffic dynamics, is crucial to observe the impact of a disruption. Tamvakis and Xenidis (2013) ensure that resilience quantification is currently "performed by measuring either the system's variation of performance in time or some selected system's properties that are considered as indicators of system's resilience". Jafino et al. (2020) notice that the aim of the criticality analysis is to rank the components of a system based on their criticality scores rather than calculate the criticality scores for each transport network component. As presented in the introduction of this chapter both approaches based on traffic dynamic (Section 1.2) and network topology (Section 1.1), are used in the transport network resilience analysis with their own specific metrics (Jafino et al., 2020; Ducruet and Lugo, 2013; Mattsson and Jenelius, 2015).

2.2.1 Traffic Conditions-based Measures

Traffic indicators such as the queue length, the speed evolution, the travel time or the flow of vehicles provides information about the traffic conditions and thus about network resilience when computed in presence of disruption (Murray-Tuite, 2006; Balal et al., 2019). Knoop et al. (2012) compare ten potential metrics based on traffic indicators such as flow, free flow speed, capacity, jam density, road length, number of lanes and found very low correlations between the ranking produced by these metrics. This implies that looking for a single best metric is not feasible, as different metrics produce distinctive rankings (Jafino et al., 2020). According to the OECD (Organisation for Economic Co-operation and Development) and ECMT (European Conference of Ministers of Transport) the congestion is a physical phenomenon relating to the manner in which vehicles impede each others' progression. However, congestion is a relative phenomenon relating to users' expectations towards the road system performance. Because of this twofold source, congestion cannot be captured through a unique metric. Most of the metrics are based on comparisons of traffic conditions under normal and disturbed scenarios and focus on the fundamental traffic variables (Section 1.2). In general, the evolution of traffic flow and travel time are the two main studied characteristics.

2.2.1.1 Flow-based Measures

Chan et al. (2015) characterize resilience through the loss of services per day computed by the vehicle-miles revenue to assess system performance in the face of a major weather disruption. Cox et al. (2011) and Jin et al. (2014) focus on the analysis of the amount of satisfied subway travel demand after a disruption. Qiang and Nagurney (2011) quantify resilience by analyzing the satisfied and the unsatisfied demand in presence of disruptions. Such a measure is close to the Volume / Capacity (V/C) ratio one, widely used in resilience analysis, which aims at computing the level of congestion by dividing the volume of traffic by the capacity (Oliveira et al., 2014; Murray-Tuite, 2006; Mahdavi et al., 2020). In this way, Geroliminis and Daganzo (2007) introduce the Macroscopic Fundamental Diagram (MFD) (Section 1.2.1.1), which "is elegant and attractive because it provides a global view of traffic behavior and performance at a network level", according to Leclercq and Geroliminis (2013). The evolution of network performances under a disturbance could be represented by this tool. Kim and Yeo (2016) propose to study resilience of urban transport network using the MFD, to quantify the performance loss. Hoogendoorn et al. (2015) show the ability of the MFD to fit traffic dynamics using Dutch freeway ring road data. Amini et al. (2018) aim at developing a performance indicator to evaluate the impact of real-time traffic control strategies on resilience of the road network using the MFD. Dong et al. (2017) propose to detect the critical edges of an urban network by using the MFD.

From their study, the authors conclude that the MFD is suitable for traffic management and intelligent control, as well as for evaluating the design effect of the urban network. Nonetheless such measures do not consider network topology in the analysis of resilience. Zhou et al. (2015) identify the intersections of an urban transportation network which are characterized by good connectivity, serving a high density of trip trajectories, and exhibiting multiple traversing patterns of trip trajectories as potential functionally critical network locations. Jenelius (2010) proposes a flow-based redundancy importance measure. The measure considers the net amount of flow that is rerouted to the link of interest when other links are closed, by comparing the flow of a road in presence of disruption and under normal conditions. Moreover, several models have been developed to detect facilities whose loss put the most system flow at risk to evaluate the network vulnerability (Murray et al., 2007; Matisziw and Murray, 2009; Myung and Kim, 2004). Hong et al. (2019) notice that most studies focus on monomodal transport network resilience characterisation.

2.2.1.2 Travel Time-based Measures

As a first measure, the travel time variation provides information about traffic dynamics and the impact of a disruption over the transport network. Such an indicator is essential in the travel time reliability characterization which is the probability that a trip can be completed within a specified time interval (Mattsson and Jenelius, 2015). To characterize the congestion, Zhang and Lomax (2008) propose an index equal to the ratio of the trip time under real traffic congestion over the trip time under free flow congestion. Martinez-Pastor et al. (2016) called such metric as the *perturbation measure*. Van Lint et al. (2008) classify quantitative indices for travel time reliability into four categories: statistical indices based on the distribution of travel time empirical data (Sun et al., 2016), buffer indices based on the extra length of travel time required for punctuality (Lomax et al., 2003; Van Lint et al., 2008), tardy trip indices based on the measure of the threshold of acceptable lateness (Lomax et al., 2003; Van Lint et al., 2008), and probabilistic indices based on the proportion of trips whose travel times exceed a pre-determined travel time threshold (Van Lint et al., 2008). Jones and Anciaes (2016) list some measures of congestion and road network performance based on the travel time (excess travel time, excess travel rate, journey time variability, excess PT waiting time, excess PT travel time). Derived from this traffic variable evolution, Pregnolato et al. (2017) analyze the Person Hours Delay (PHD) which is the difference in the aggregate journey time recorded in a specific scenario and the baseline one. To monetize this delay, the authors introduce the Cost Per Vehicle (CPV) and the Net Present Value (NPV). Mudigonda et al. (2019) compute the recovery rate to analyze network resilience through the travel time and the passenger trips recorded during the hurricane Sandy. In the dynamic resiliency quantification of the public transport network of New Dehli, Mahdavi et al. (2020) compute the travel time reliability (Section 2.1.1) to describe the degradation of performance of the operation with respect to delays in the service. The delays are quantified with the difference between scheduled and real services that is called on-time performance, and correspond to the additional waiting time imposed to passengers who experienced a disruption. Chang et al. (2020) observe the performance in frequency to analyze the loss of performances between the scheduled and the realized frequencies of a Seoul metro line. The metrics based on the costs of delays are possible indicators and give information about the network vulnerability (Cantillo et al., 2018). By comparing the travel cost evolution in presence of disruption, (Jenelius et al., 2006) characterize the Importance (I) (2.1a) of an edge with respect to the network by disrupting it, and its Exposure (E) (2.1b), which is the expected increase in travel cost for a random link failure.

$$I(e) = \frac{\sum_{ij \in N \times N} w_{ij}(c^*_{ij} - c_{ij})}{\sum_{ij \in N \times N} w_{ij}} \tag{2.1a}$$

$$E(e) = \frac{\sum_{ij \in N \times N} w_{ij}(c^*_{ij} - c_{ij})}{L^{nc} \sum_{ij \in N \times N} w_{ij}} \tag{2.1b}$$

where N represents the set of nodes of the transport network, w_{ij} is the weight of the OD. If all the weights w_{ij} are all equal, all OD are equally important. The c_{ij} is the travel cost between the OD pair in the normal scenario and c^*_{ij} in the disturbed scenario. L^{nc} is the number of non-cut links. A non-cut link is a link that causes finite increases in travel cost when closed in presence of a link closure.

Gauthier et al. (2018) extend the importance with the Stress Test Criticality (STC) metric (2.2), based on the aggregation of the performance loss values, computed by comparing the travel cost in presence of disruption and under normal condition, for different capacity-disruption levels.

$$STC(e) = \int_{CDL} \sum_{v \in V} \frac{c_v^d(e, CDL) - c_v^0(e)}{n} \tag{2.2}$$

where CDL is the capacity disruption level, V is the set of vehicles and c_v is the travel cost for the edge e and the vehicle v under normal ^{0} or disrupted ^{d} conditions.

2.2.1.3 Travel Time and Flow-based Measures

To consider the impact on the flow, Cats et al. (2016) extend the E and define a Passenger-Exposure (PE) metric which corresponds to the total number of hours that an edge is subject to disruptions multiplied by the passenger flow on this edge, during a given time period. Scott et al. (2006) propose the Network Resilience Index (NRI) based on both the variation of the travel time and the flow in presence of an edge removing. By comparing the results with the V/C ratio, the authors conclude that the NRI provides a better indication of the value associated with individual edges of a highway network because of the consideration of the spatial relationships and rerouting possibilities associated with the networks topology, the OD demand and the capacity of individual highway segments in this second index. The NRI also presents an advantage compared to the Gamma Index (γ) which only accounts for network topology by ranging the network connectivity between 0 and 1 without considering the traffic flow. This index measures the relationship between the number of links and the maximum number of possible links in a network, linking every pair of distinct vertices by a unique edge. A value of 1 is synonymous with completely connected network. Sullivan et al. (2010) enlarge this measure to provide a global characterization of the network rather than a local one. By summing the NRI for all the individual and dividing by the total trip demand in the network, the authors create the Network Trip Robustness (NRT). The authors consider the capacity reduction of the edge rather than a total removing to evaluate the impact of frequent network disruptions and to identify and rank the most critical links in the network using three test networks with different levels of connectivity. Oliveira et al. (2014) also characterize the performances of a road network using the NRI, the V/C ratio but also the congestion index, introduced by Zhang and Lomax (2008), which aims at measuring the level of congestion of a road as the ratio between the travel time under congested and free-flow traffic conditions.

2.2.2 Topological-based Measures

Regarding network topology based approach, the Centrality Measures (CM), issued from graph theory (Section 1.1.1), compute the importance of any given component (node or edge) in a network (Disney, 2020) and are a vital tool for understanding networks. The CM, often used in graph analysis including the transport field, aims at quantifying both the global network (Section 2.2.2.2) performances and the local ones (Section 2.2.2.1) by providing the importance of a network component (node or edge) (Ducruet and Lugo, 2013). The granularity of the study influence the result more than the properties of the network. The choice of scale is essential because of the implied structural changes (Duan and Lu, 2014). Porta et al. (2006)

perform an analysis of such metrics on different transport networks and classify them depending on the position and the role of a component regarding the network. Scheurer et al. (2007) apply CM on Melbourne's public transports. Zhang et al. (2011) (5 different kinds of network topologies) prove the importance of topological analysis, defining the connectivity and the accessibility, to assess transport network resilience. The more the network has redundant paths, the better resilience is.

2.2.2.1 Local Characterization

To locally characterize the network connectivity, the Node Degree Centrality (NDC) (2.3), defined as the total number of connected edges linked to a vertex, is useful (Barabási and Albert, 1999).

$$NDC_u = |\{E_{uv}, \quad \forall v \in N_u\}| + |\{E_{vu}, \quad \forall v \in N_u\}| \tag{2.3}$$

where $|\{E_{uv}, \quad \forall v \in N_u\}|$ is the cardinally of the set of edges going from u to the the neighbors nodes $v \in N_u$, and $|\{E_{vu}, \quad \forall v \in N_u\}|$ is the cardinally of the set of edges going from the neighbors nodes v to the node u. In an undirected graph, the NDC is only equal to $|\{E_{uv}, \quad \forall v \in N_u\}|$ corresponding to the cardinality of the set of edges between u and all the neighbors nodes.

It can be interpreted as the capacity of a node to directly join another node through the network. The larger the NDC, the more central the node due to the number of connections. In a directed graph (2.3), a distinction between in-NDC and out-NDC is done to differentiate the entering edges to a node ($\{E_{vu}, \quad \forall v \in N_u\}$) from the outgoing ones ($\{E_{uv}, \quad \forall v \in N_u\}$). To capture the redundancy of a network, Dueñas-Osorio (2005) propose a redundancy index (Hong et al., 2019; Yang et al., 2018; Chopra et al., 2016; Zhang et al., 2019; Liu and Tan, 2013; Lhomme et al., 2013), similar to the NDC, which counts the number of independent paths from a vertex u, to each of the vertices with a distance of two vertices $w \in N_v \forall v \in N_u$. The most redundant simple graph is a complete graph less redundant one is a completely fragmented graph, with no edge. Finally, the connectivity of a network should be characterized by the Clustering Coefficient which measures the number of triangles in a graph, and characterizes the cohesiveness of the neighborhood of a node (Soh et al., 2010; Wang et al., 2020; Shang et al., 2020b).

To describe network efficiency at local scale, the Betweenness Centrality (BC) (2.4a) and (2.4b) (Freeman, 1979) is among the preferred ones in the transport field and is largely used to identify bottlenecks of the transport networks (Zhang et al., 2011; Derrible, 2012; Gauthier et al., 2018; Furno et al., 2018; Akbarzadeh et al., 2017).

$$EBC_e = \frac{1}{(|V|(|V|-1))} \sum_{\substack{u,v \in V \times V \\ u \neq v}} \frac{\sigma_{uv}(e)}{\sigma_{uv}} \tag{2.4a}$$

$$NBC_n = \frac{1}{(|V|(|V|-1))} \sum_{\substack{u,v \in V \times V \\ u \neq v}} \frac{\sigma_{uv}(n)}{\sigma_{uv}} \tag{2.4b}$$

where σ_{uv} the number of shortest path joining nodes u and v in the graph and $\sigma_{uv}(e)$ (respectively $\sigma_{uv}(n)$) the number of shortest path joining u to v crossing the edge e (respectively the node n). Factor $1/(|V|(|V|-1))$ is induced by the metric normalization.

This metric is computable over edges (Edge Betweenness Centrality (EBC)) (respectively nodes (Node Betweenness Centrality (NBC))) and characterizes the importance of an edge (respectively a node) regarding

the number of times the edge (respectively the node) is crossed by a shortest path. Although an edge (respectively a node) with a high EBC (respectively NBC) is vulnerable in terms of resilience, it also means that the edge (respectively the node) is very attractive and important to sustain flow in the graph, being crossed by a high number of shortest paths. To observe the evolution of such EBC measures, we compute the Global Edge Betweenness Centrality (GEBC), equal to the sum of all the EBC values (2.5).

$$GEBC = \sum_{e \in E} EBC_e \tag{2.5}$$

In their analysis, Porta Sergio et al. (2009) and Porta et al. (2012) observe the existing link between some CM (EBC, Node Closeness Centrality (NCC), Straightness Centrality) and the economic activities in different cities. Limits of these measurements come from the lack of traffic data using. According to Furno et al. (2021), most of the existing works consider networks and their attributes (*e.g.*, weights) as static entities which is an unrealistic modelling approach as traffic, and consequently edge weights, rapidly evolve as a consequence of change in travel demand, accidents, congestion, etc. In order to counter that, some researches include a graph weighting procedure based on the demand or the travel time for instance (Gauthier et al., 2018). Indeed, the addition of network properties to edges, provides accurate results for metrics which become more realistic (Altshuler et al., 2011). In this sense, improving BC definition and computation represents a real opportunity in the network resilience analysis. Cats and Jenelius (2014) extend the traditional BC measure to focus on vehicles and passengers to quantify resilience of a public transport network. The centrality for vehicle compares the number of vehicles belonging to a specific line entering an edge in a given time stamp and the expected number of departures during the time interval. The centrality for passengers compares the number of passengers from an origin to a destination entering an edge during the time interval and the total number of passengers travelling between the same origin and the destination.

Another widely used metric to assess the network performance at local scale is the Node Closeness Centrality (NCC) (Freeman, 1979) (2.6), which quantifies how a given node is far from all the other ones by summing the reciprocal of the length of the shortest paths.

$$NCC_u = (|V| - 1) \sum_{\substack{v \in V_u \\ u \neq v}} \frac{1}{l_{vu}^{sp}} \tag{2.6}$$

where V_u is the set of nodes reaching from u, $|V_u|$ its cardinality and l_{vu}^{sp} is the length of the shortest path going from the nodes v to u in the graph. Factor $(|V| - 1)$ is induced by the metric normalization.

The higher the NCC, the shorter the shortest paths. Ilbeigi (2019) ensures that " the greater the NCC is, the higher the connectivity in the network". A node with a high NCC is in a short range from the rest of the network. According to Crescenzi et al. (2016) "having high NCC can have positive impact on the vertex itself".

The presented local metrics are used both on road network analysis and public transport ones (Crucitti et al., 2006; Berche et al., 2009; Chan et al., 2015; Zhang et al., 2011). Brandes et al. (2016) assume that both NBC and NCC are related. Extensions of these CM to weighted graph are proposed in the literature (Opsahl et al., 2008; Wei et al., 2012; Gauthier et al., 2018).

Other CM are used in the literature to characterize the transport network topology, such as the Straightness Centrality (Yin et al., 2018; Crucitti et al., 2006; Sevtsuk and Mekonnen, 2012) which illustrates the length of the shortest path connections from each node to the surrounding points as compared with the shortest distance between two nodes, computed with the Euclidean distance and corresponding to a straight path. The Spectral Centrality is another measure counting the number of walks going from an origin to

a destination with a decreasing importance in relation with its length (Nicosia et al., 2013; Perra and Fortunato, 2008; Boulmakoul et al., 2017). The Eigen-Vector Centrality and the Page-Rank Centrality, both based on the principle that the importance of a node depends on the importance of its neighbors, are also used in the transportation field (Perra and Fortunato, 2008; Mouronte-López, 2021).

2.2.2.2 Global Characterization

To characterize the global topological evolution of a network, two major elements are studied: the change in connectivity and the change in the shortest path length. Number of studies focus on the computation of the performance loss by quantifying the Average Efficiency (AE) (2.7) (Latora and Marchiori, 2001) before and after a disruption (Zhang et al., 2018a; Saadat et al., 2020; Nagurney and Qiang, 2008).

$$AE = \frac{1}{|V|(|V|-1)} \sum_{\substack{u,v \in V \times V \\ u \neq v}} \frac{1}{l_{uv}^{sp}} \tag{2.7}$$

where l_{uv}^{sp} is the length of the shortest path going from u to v,V is the set of vertices, $|V|$ its cardinality.

According to Mattsson and Jenelius (2015), such a measure is helpful to compare different networks and is frequently employed in the related literature (Bíl et al., 2015; Aydin et al., 2018; Duan and Lu, 2014; Crucitti et al., 2006). It quantifies how efficiently information (or any other kind of flow) is exchanged over the network. Higher values of AE denote that the network is efficient by reducing the length of the shortest paths. Zhang et al. (2015) compute the average reciprocal distance computed over an unweighted network to observe the impact of a disruption before and after it happened. Filippidou and Kotidis (2016) consider the percentage change in the average shortest path length between the initial graph and the one augmented by some edges. The defined metric is the Gain, highly related to the AE. Hong et al. (2019) analyze the average path length and the network diameter, which measures the longest graph distance that exists between any two nodes in a network, to characterize the bus network and the subway network in Seoul metropolitan area (Li and Han, 2017). Derived from the AE, the Information Centrality compares the relative drop of AE after a node removal to characterize its importance in the network. Crucitti et al. (2006) examine the topology of eighteen cities using this global measure combined, among others, with the NBC and the NCC. The authors conclude that each centrality captures a different aspect of one place regarding the rest of the network.

The network efficiency and the network connectivity globally characterize the network structure. Hong et al. (2019) also analyze both the average path length, called the characteristic path length of the network (Li and Han, 2017), and the connectivity using the γ, very useful to transport planners and practitioners as it estimates how easy it is to travel from one station to another. The connectivity loss expresses the average reduction in the ability of vertices to receive flow from sources. A weighted formulation is proposed by Pitilakis et al. (2016). This index upgrades the simple connectivity loss by weighting the number of sources connected to a vertex, in seismic and non-seismic conditions. The Giant Connected Component (GCC) is the largest set of connected nodes in a graph. Even in presence of a disruption, it is essential that the GCC is preserved and that all nodes are connected to each other. This component is used to evaluate robustness of networks by removing nodes or links and measuring changes and Berche et al. (2009) define it as a "useful quantity". Wang et al. (2011) define the network structure of China's air transport network using the NDC distribution (Barabási and Albert, 1999), the average path length (Watts and Strogatz, 1998) and the clustering coefficient, close to the Network Density ($\langle NDC \rangle$) (2.8) which is the average network NDC.

$$\langle NDC \rangle = \sum_{u \in V} \frac{NDC_u}{|V|} \tag{2.8}$$

where NDC_u is the NDC of the node u and $|V|$ the cardinality of the set of vertices.

The Node Degree Centrality (NDC) (2.3) distribution is an important indicator for network characterization (Da F Costa et al., 2007; Gao and Albert-László Barabási, 2016; Aliakbary et al., 2018). Li and Han (2017) ensure that the Node Degree Centrality (NDC) distribution is one of the most important parameters to describe the complex characteristics of the network. Mahdavi et al. (2020) characterize robustness of the network by quantifying the change in terms of NDC distribution and assortativity (Newman, 2002) which measures the similarity of connections in the graph with respect to the NDC and the AE. Finally, the $\langle NDC \rangle$ characterizes the nodes connectivity in the whole network, which is an important aspect from the perspective of redundancy and capability to absorb perturbations. The denser the graph, the more connections exist between nodes.

Jacob et al. (2017) use the NDC distribution to compute the Heterogenity (H) which varies directly with the NDC-spectrum. The H of a network, also known as *graph irregularity*, provides global information on the diversity of network nodes connectivity (Jacob et al., 2017; Estrada, 2010). The H of a complex network is essential to understand the behaviors and the functions because such a characteristic is the source of many network properties (Wu et al., 2010). The definition of this metric can also be extended to the case of a weighted network (*i.e.*, weighted NDC), as described in (Barrat et al., 2004; Newman, 2004; Opsahl et al., 2008, 2010; Dall'Asta et al., 2006). As with the traditional NDC, the weighted NDC of the generic node i can be distinguished into in-NDC and out-NDC centrality, being equal to the sum of the edge weights that join the node i to its predecessors (respectively successors) j. Computed over a weighted graph, H could take traffic dynamics into account and therefore be sensitive to perturbations and providing information on network resilience. The definition of H is typically based on NDC (2.3).

Gao and Albert-László Barabási (2016) also propose a H metric, computed over a directed weighted graph, based on the in-NDC (number of edges pointing in to the node) and out-NDC (number of edges pointing out of the node) density functions (2.9).

$$H = \frac{\sigma_{in}\sigma_{out}}{\langle NDC \rangle} \tag{2.9}$$

where σ^2_{in} (respectively σ^2_{out}) is the variance of density function of the weighted in-NDC $P(NDC_{in})$ (respectively out-NDC $P(NDC_{out})$) and $\langle NDC \rangle$ is the average NDC or network density.

In their work, Gao and Albert-László Barabási (2016) propose a methodology to quantify resilience of different types of multi-dimensional systems (*i.e.*, gene regulatory, ecological and power supply networks). The authors prove that resilience properties can be effectively grasped via a combination of network metrics that includes: Heterogenity (H), Network Density ($\langle NDC \rangle$) (*i.e.*, average NDC (2.8)) and network Symmetry (S) (2.10a). S is defined as the correlation coefficient of in-NDC and out-NDC.

$$S = \frac{\langle NDC_{in} NDC_{out} \rangle - \langle NDC_{in} \rangle \langle NDC_{out} \rangle}{\sigma_{in}\sigma_{out}} \tag{2.10a}$$

where $\langle NDC_{in} \rangle$ (respectively $\langle NDC_{out} \rangle$) is the average in-NDC (respectively out-NDC), $\langle NDC_{in} NDC_{out} \rangle$ the scalar product of both vectors (in-NDC and out-NDC) and σ^2_{in} (respectively σ^2_{out}) is the variance of density function of the weighted in-NDC $P(NDC_{in})$ (respectively out-NDC $P(NDC_{out})$)

A macroscopic resilience parameter β_{eff} (2.11) is then defined as a function of the aforementioned metrics for bacterial and gene regulatory networks.

$$\beta_{eff} = \langle NDC \rangle + S \times h \tag{2.11}$$

The β_{eff} coefficient is defined based on the Michaelis-Menten equation (Michaelis and Menten, 2009) that defines the dynamics of regulatory networks. In other words, by defining a function that characterizes the network dynamics, the authors determine the critical transition plane β^c_{eff}, separating the desired resilient state, from the undesired one, *i.e.*, non-resilient. In the transport field, the fundamental diagram defines network dynamics by relating the speed and the vehicle concentration. To obtain the same trend as the Michaelis-Menten one, we can relate free flow speed minus the observed one to the concentration.

2.2.3 Hybrid Approaches

In order to fully characterize the transport network performances, both network topology and the traffic conditions have to be considered with the dynamically weighted CM based on network topology and the traffic conditions.

Topological approaches are simplistic in the sense that they do not incorporate dynamic information about traffic and time-varying characteristics of the network. Shalaby et al. (2016) and Gauthier et al. (2018) compare public transport and road networks resilience quantified with both approaches. Gauthier et al. (2018) demonstrate the importance of this combination as topological approaches are traditionally unable to grasp the time-dependent aspects of resilience. As discussed in Kazerani and Winter, human mobility is dynamic and highly time-dependent. Therefore, it appears crucial to consider time and demand information in the computation of CM. Along their analysis, Dall'Asta et al. (2006) show that complex networks are more fragile than expected from the analysis of topological quantities when the traffic characteristics are taken into account. Most of the CM have been generalised to weighted networks (Opsahl et al., 2010; Newman, 2004; Barrat et al., 2004; Opsahl et al., 2008; Newman, 2001). The shortest paths dependent one have been extended using the Dijkstra's algorithm (Dijkstra, 1971) for the shortest paths computation. By visiting all nodes in the graph, the algorithm returns the shortest paths as the paths with the minimum sum of the weights of the crossed edges. Indeed, in a weighted graph, the shortest path corresponds to the path between two vertices which minimizes the sum of the weights of the edges belonging to the path. The length of such a shortest path is equal to the sum of the weights of the edges belonging to the shortest path.

To characterize the dynamic resiliency of the public transport of New Delhi, Mahdavi et al. (2020) focus on network topology and traffic dynamics as suggested in the literature (Gauthier et al., 2018; Cats and Jenelius, 2018). The authors develop an index that covers the magnitude of changes in the network performances in terms of robustness with CM (NDC, AE), travel time reliability and residual capacity with traffic indicators (V/C ratio, number of affected passengers and waiting time). Li et al. (2019) define a hybrid local metric based on the sum of nodes performances defined as the weighted NDC and the number of alternative paths to all the other nodes in the network, as well as their lengths. Using a weighted sum of these local characterizations, the authors quantify resilience of the global network by observing the loss of performances in presence of a disruption, with respect to the normal conditions (Zhang et al., 2018a; Saadat et al., 2020; Chang et al., 2020). Cheng et al. (2015) compared results obtained by EBC weighted or not. Gauthier et al. (2018) and Cats et al. (2017) focus on the ranking of the network components using the EBC computed over a weighted graph. Because in such a graph the shortest paths correspond to the sequence of edges with minimal weights connecting two nodes, the edge weights permit to consider road characteristics information like the travel time, and ensure that traffic dynamics are considered in CM based on the shortest path computation. Wang et al. (2008) examine the mathematical relationships existing between EBC and edge weights in a weighted graph. As an important result, the authors identify the relationships that hold for edges to have higher EBC. Specifically, Wang et al. (2008) prove that if the network is in a weakly disordered regime, edges with smaller weight tends to carry more traffic in the network, thus introducing negative correlation between edge EBC and edge weights. Such a property is important in transportation networks and to have an interesting application to understand how traffic redistributes in this kind of networks. By observing the change in travel time, computed over a graph, some articles tend

to characterize transport networks resilience. Akbarzadeh et al. (2019) observe the impact of the weight in the critical links detection and suggest, by computing the loss of GE, that "reinforcing an urban network in terms of its robustness could be best achieved by reinforcing the links located on the borders of its clusters rather than links with highest flow, congestion, or EBC". Akbarzadeh et al. (2017) observe the impact of the weight on the Node Betweenness Centrality (NBC), by comparing the metric results computed over an unweighted graph and a weighted one. The authors analyze different weights (traffic flow, edge length, reciprocal capacity, congestion, time) and conclude that the travel time and the reciprocal of capacity yielded similar NBC results when used to weight links and that these two measures were relatively highly correlated with node flow. In the literature review, different methods are presented to weight the NDC in order to capture traffic dynamics. One possibility is to sum all the weights of the edges connected to the studied vertex (Barrat et al., 2004; Newman, 2004; Opsahl et al., 2008, 2010; Jacob et al., 2017; Dall'Asta et al., 2006). When computed over a travel time weighted graph, the AE aims at comparing the difference in travel time induced by specific traffic conditions.

Various CM have been studied on both nodes and edges in relation to global traffic network properties such as vulnerability, attractiveness or criticality, also suggesting to consider network centrality indicators as predictors of traffic flow conditions (*e.g.*, Betweenness Centrality (BC) in (Ye et al., 2016), Node Closeness Centrality (NCC) in (Leung et al., 2011; Jayasinghe and TalatMunshi, 2014; Ye et al., 2016) and Node Degree Centrality (NDC) in (Leung et al., 2011; Zhao et al., 2017)). In this context, Jayasinghe and TalatMunshi (2014) and Jayasinghe et al. (2017) evaluate the correlation existing between different CM and the transit demand observed in the proximity of public transport stops of Ahmedabad city, India (Jayasinghe and TalatMunshi, 2014), and the Colombo Metropolitan Area, Sri Lanka (Jayasinghe et al., 2017). Akbarzadeh and Estrada (2018) prove that the communicability shortest paths attract more flows than the traditional shortest paths. In accordance with these works, the travel demand is considered in the computation of NDC, by defining its demand-sensitive adaptation DSNDC (2.12a). Similarly, DSNDC represents the Demand-Sensitive Network Density ($\langle DSNDC \rangle$).

$$DSNDC_u = \delta_u.(|E_{uv}| + |E_{vu}|) \tag{2.12a}$$

$$\delta_u = \sum_{v \in V_u} \alpha_{uv} + \alpha_{vu} \tag{2.12b}$$

where δ_u is the travel demand departing from and arriving to node u, $|\{E_{uv}, \quad \forall v \in N_u\}|$ is the cardinally of the set of edges going from u to the the neighbors nodes $v \in N_u$, and $|\{E_{vu}, \quad \forall v \in N_u\}|$ is the cardinally of the set of edges going from the neighbors nodes v to the node u.

Rather than only considering the number of connected edges, the DSNDC (2.12a) accounts for the number of travelers departing from and arriving to the generic node u. In that sense, the α_{uv} coefficients (α_{vu}, respectively) represent the part of the total travel demand going from the node u to the node v (from v to u, respectively).

Concerning the AE metric, the travel demand is considered by weighting the efficiency of each path by using the same α_{uv} factor describing the part of the total travel demand it serves.

$$DSAE = \frac{1}{|V|(|V|-1)} \sum_{\substack{u,v \in V \times V \\ u \neq v}} \alpha_{uv}.\frac{1}{l_{uv}^{sp}} \tag{2.13}$$

The larger the demand associated to a specific pairs of nodes (u, v), the more such path will contribute to the AE. With such formula modifications, both travel time and travel demand data will have an impact

on the computation of the AE, as from (2.13), *i.e.*, shortest paths serving larger parts of the travel demand will therefore have a stronger impact on network efficiency.

By modifying the definition of the NBC, Altshuler et al. (2011) consider the demand in the node importance characterization and prove the better correlation of such modified DSNBC to capture traffic dynamics. Similar conclusions are stated in our article Henry et al. (2019a) (Section 3.4). Indeed, using simulated data, we proved the existence of a spatio-temporal correlation between the Demand-Sensitive Edge Betweenness Centrality (DSEBC) (2.14) and the traffic flow. In such DSEBC formulation, the importance of an edge with respect to the network depends both on the number of shortest paths crossing the edge and on the part of demand that travels through the edge for a specific pair of OD nodes.

$$DSEBC_{uv} = \sum_{\substack{u,v \in V \times V \\ u \neq v}} \alpha_{uv} . \frac{\sigma_{uv}(e)}{\sigma_{uv}} \tag{2.14}$$

$$DSNCC_u = \sum_{\substack{v \in V_u \\ u \neq v}} \alpha_{vu} . \frac{1}{l_{vu}^{sp}} \tag{2.15}$$

The demand-related coefficient α_{uv} could be defined and estimated in different ways. Gao et al. (2013) use mobile phone data to estimate them. Leung et al. (2011) consider instead the amount of Points Of Interest (POIs) (*e.g.*, restaurants) located in the proximity of each network node. The authors (Gao et al., 2013) derive these coefficients from the function (*i.e.*, class) of the adjacent road segments, whereas Ren et al. (2014) use a cost-based function derived from the radiation mobility model, based on the assumption that the individual will be choosing the place that has the lowest travel cost on the network with a benefit factor at least as large as the possible. Ye et al. (2016) propose to estimate demand via taxi trips. The Demand-Sensitive Node Closeness Centrality (DSNCC) (2.15) aims at considering the demand a node attracts in its importance characterization. Such a metric, extended from the NCC definition, quantifies the node importance depending on both the needed time (when computed over a travel time weighted graph) to reach the node from all others, and the number of people wanting to join the node. Finally, the quicker the node is reachable, and the larger the demand is to join the node as a destination, the higher the DSNCC.

The consideration of traffic dynamics, such as the travel demand and the temporal evolution of the traffic conditions, is essential for the quantification of performances and vulnerabilities of mobility networks when computing complex network metrics on transportation graphs. Indeed, Kazerani and Winter suggest to use data on travel demand to weight shortest paths in the computation of centrality metrics. As introduced in Section 2.2.3, by modifying the definition of the NBC, Altshuler et al. (2011) consider the demand in the node importance characterization. Moreover, by weighting the graph with traffic indicators, free-flow travel time for peak and non-peak hours, the authors capture traffic conditions in the NBC computation. Indeed, the shortest paths are no longer the path containing the lowest number of crossed edges but the ones with the lowest travel time. By computing the modified NBC (equivalent to the DSNBC) over the weighted graph, the authors notice a different distribution with respect to the unweighted classical DSNBC definition, with a better correlation to typical flow information in the first situation. Such a result supports the importance to include the dynamic and temporal nature of human travel demand for realizing traffic flow prediction or characterizing the network performances. Similar conclusions are found in (Puzis et al., 2013; Leung et al., 2011). Cheng et al. (2013), Cheng et al. (2015) and Yoo and Yeo (2016) extended definitions of the CM, to provide the importance of the components by including commuter flows and temporal delays in the computation of the network performance. Following similar approaches, Zhao et al. (2017) ensure that the use of modified CM, considering both geometric properties and traffic information of the road network, lead to an improved traffic flow analysis and accurate predictions of flows at different network levels.

2.3 Multimodal Transport Network Resilience Approaches

On the one hand, "public transport used road space more efficiently than cars by carrying more people in almost the same space" (Wu et al., 2018). In this way, the reduction of congestion and consequently the improvement of resilience is expected thanks to the increasing use of public transport. Indeed, an improved and more attractive public transport system also improves traffic conditions by relieving the pressure on the roads. To analyze that it is necessary to take in account the multimodality of the network across the study. On the other hand, this aspect will permit to take in account existing possibilities of modal shift when a damage occurs. For instance, in Lyon, France, during an incident blocking the metro, the public transport operator makes available buses to pursue the service as well as possible. The most common but unsatisfied method to analyze a multilayer network is the same as for a normal network. According to Kivelä et al. (2014) "the best way is to begin from initial and fundamental concepts stated for graph theory and adapt them to create new methods and metrics in order to analyze multilayer networks".

In the transportation context, multilayer representations provide a deep understanding of the multimodal transport network. Nevertheless, only few study already deals with this method and "still represent isolated cases" (Aleta et al., 2017). Moreover, done studies consider a single network which does not interact with other ones, or focus on representing a mode per layer which is still aggregated. Buldyrev et al. (2010) analyze the cascade effect in interdependent networks. De Domenico et al. (2014) measure the necessary time to cover network thanks to random walks. Du et al. (2016) deal with resilience of Chinese Airline Network with removal of nodes. The network is divided in three layers by the k-core decomposition. Conversely, "modern systems are becoming more and more coupled together" (Buldyrev et al., 2010) and it is interesting "to study the interdependency and resilience of the system while to have a realistic model of human mobility the single line per layer perspective should be adopted" (Aleta et al., 2017). In conclusion, both representations will be needed in the work. The first will serve to construct cascade effects of stress tests due to the interdependency of transport networks (Buldyrev et al., 2010). The second will allow to simulate accurately how the network works under disruption.

Regarding the multimodal transport networks, dynamically weighted CM (Section 2.2.3) has also been created for multilayer networks. For instance, De Domenico et al. (2015) present CM based on dynamical properties for this type of network. Bródka et al. (2011) and Bródka et al. (2012) analyze aggregated multilayer network in the social field. They deal with metrics to establish a neighborhood analysis and especially centralities ones as the cross-layer degree centrality and the cross-layer clustering coefficient. Kivelä et al. (2014) specify that the node neighborhood definition consists in "counting the number of different types of edges and considering the directions of the edges". Du et al. (2014) propose a methodology applicable in logistics transportation network vulnerability assessment. They develop a vulnerability index of facilities in the multimodal logistics transport networks including road and rail networks, using the ratio between the network's normal performance as the reference status and the degraded ones. The performances are recorded through a generalized cost composed of the per-edge economic cost of logistics transport and the per-edge logistics travel time. De Domenico et al. (2013) develop a framework to study general multilayer networks with the generalization of several graph-based indicators such as the NDC, the clustering coefficients, the eigen-vector centrality, and the modularity. Battiston et al. (2014) analyze the multilayer network of Indonesian terrorists using the entropy and the participation coefficient, based on the NDC, the overlapping degree. They also analyzed the clustering coefficient, the interdependence of vertices and the eigen-vector centrality. Another centrality measure had been adapted to multilayer networks like present De Domenico et al. (2015). The interactive decision tool Spatial Network Analysis for Multimodal Urban Transport Systems (SNAMUTS) aims at defining the cities transport network resilience using CM. The shortest paths used in the centrality metrics are computable over multilayer graph (Solé-Ribalta et al., 2019; Brodka et al., 2011). A penalization for the layer crossing in such computation is possible. Delling et al. (2009) present a multimodal variant of Dijkstra's algorithm (Dijkstra, 1971), used to compute the shortest paths over a multilayer directed weighted graph. It is interesting to note that multilayer networks analysis could consist in comparing the intra-layer edges of the different layers of the network: Bianconi (2013)

computes overlaps between layers, Barigozzi et al. (2010) analyze the correlations between the distributions of the layers, etc.

2.4 Concluding Remarks and Discussions

Because we aim at modelling the transport network using a dynamically weighted graph (Section 1.3) to consider both network topology and traffic dynamics in the quantification of resilience, we must use adapted indicators (Section 2.2.3). The use of weighted CM is optimal because of their easy implementation and the huge related literature proving their interests (Ghanem et al., 2018; Brandes and Fleischer, 2005; Furno et al., 2021, 2018; Shalaby et al., 2016). Computed over a weighted graph, the indicators capture the traffic condition in their computation (Gauthier et al., 2018). The modification of the CM which considers the travel demand in the component importance characterization and thus supplement traffic dynamics consideration in the characterization of resilience. Regarding the implementation and the extension of these indicators to dynamically weighted graph and multilayers ones (Section 2.3), by modifying the shortest path computation algorithm, on which CM are currently based, these indicators are easily customizable (Tang, 2011; Kivelä et al., 2014).

A presentation of another used metric, called Accessibility (A), is presented in Appendix A with a short work. Moreover, a non-exhaustive list of about 100 transportation resilience analysis is available at the end of the manuscript from Table 9 to Table 13 (Appendix B).

Chapter 3

Simulated Data-based Analysis and Stress Tests Evaluations

This chapter focuses on the presentation of the simulations and the analysis performed with the aim of quantifying transport network resilience using dynamically weighted graphs, presented in Chapter 1, and some related indicators issued from graph theory, introduced in Chapter 2.

To build the dynamically weighted graph, we use simulated data issued from the macroscopic/mesoscopic simulator HubSim (Section 3.1.2), developed by Neovya company, and the microscopic traffic simulator SymuVia (Section 3.1.1), developed by our research group. These two simulators allow us to respectively study a peri-urban transport network and an urban transport network.

We characterize the resilience using the following CM: the Edge Betweenness Centrality (EBC), the Node Closeness Centrality (NCC), the Node Degree Centrality (NDC), and their Demand-Sensitive (DS) extensions. The ability of the weighted CM to capture the traffic conditions is presented in Section 3.2. Finally, Section 3.4 presents a comparison of these resilience indicators, dependent on the topology and the traffic conditions, with purely traffic ones through a correlation analysis.

This chapter contributes to the state of the art by demonstrating the ability the presented hybrid approach to consider both transport network topology and traffic conditions in the characterization of resilience. Computed over a graph with dynamic weights, modelling the traffic dynamics, the CM become sensitive to traffic conditions and able to capture the impact of disruptions. The importance of accurately reproduce the drivers' behaviors is demonstrated, as well as the relation between the CM and the traffic indicators. In this chapter we use simulated data.

Section 3.4 is an updated and enhanced version of the conference paper Henry et al. (2019a).

Contents

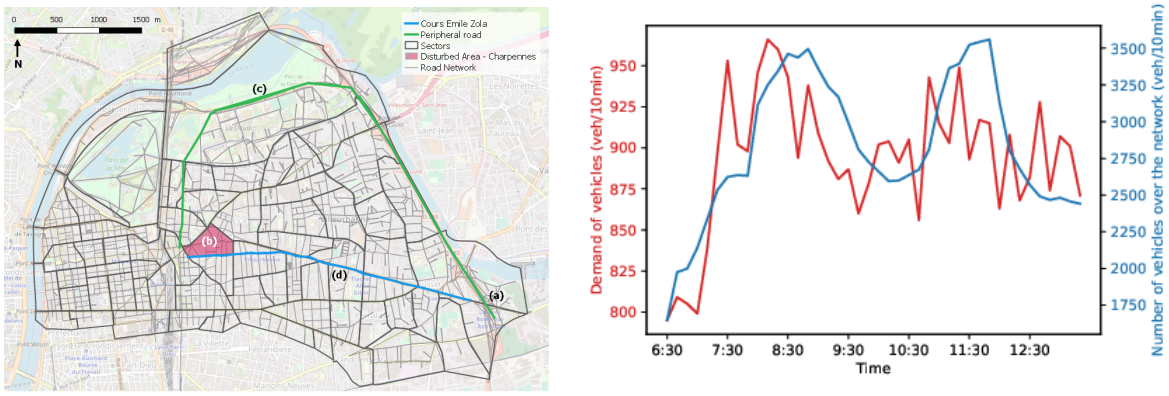

(a) Network topology

(b) Demand and number of vehicles

Figure 3.1: The simulated network (a) and the demand profile (red) vs. the number of vehicles in the network (blue) (b)

3.1 Simulated Data Description

In this chapter we aim at analyzing transport network resilience using simulated data, computed both with the open-source traffic simulator SymuVia, developed by our research group, and the HubSim platform, developed by Neovya. With the first simulator, we work on an urban transport network which is a part of Lyon, France, whereas with the second simulator, we focus our analysis on a peri-urban transport network, around Lyon, France, to reduce the graph size and run a large number of simulations with the aim of applying a stress test methodology.

3.1.1 SymuVia Simulation Tool: urban transport network

The simulator represents individual vehicles (Section 1.2.1.3) and computes transit times every second, based on the LWR model (Lighthill and Whitham, 1955; Richards, 1956). The vehicles are distributed over the network according to the traffic conditions at the moment the vehicle is generated. Before running a simulation, duration, OD demand and speed limit per edge have to be defined. Based on the generated spatio-temporal traces of the vehicles, the simulator allows to compute aggregate traffic indicators such as the flow and the travel time observed over each edge of the network within a user-specified period of observation. We perform simulations over a portion of the road network of Lyon, France, including its 3^{rd} and 6^{th} city district, and a part of the neighbor city of Villeurbanne, France (Figure 3.1a). Such an area allows to run a microscopic simulation (Section 1.2.1.3) with an acceptable computation time and area size to observe vehicles traces. Among the simulation inputs, we highlight the OD matrix, available over this part of Lyon, which includes three realistic areas with different social and economical characteristics: *i)* the 3^{rd} borough is the central business district of Lyon, as well as the most populated area of the city; *ii)* the 6^{th} district has instead a dominant commercial function and a large population; *iii)* Villeurbanne is a more popular city hosting one of the largest university district of the region. The final network is composed of 3 324 edges and 1 774 nodes, represented as a directed graph coded in Python 3.6 by using the NetworkX library (Hagberg et al., 2008). The simulation is run over a period of 7 hours, from 6 : 30 am to 1 : 30 pm, with the global demand profile reported in Figure 3.1b. The expected demand and the number of vehicles in the network along the simulation are shown in red and blue, respectively. The demand has a typical 2-peaks profile, one around 8 : 30 am and a second one around 12 : 00 pm, condensed in a 7-hours interval for computational efficiency. The route-choice assignment coefficients, which control vehicle distribution over different alternative paths associated to the OD pairs, have been configured to change along the simulation.

(a) Network topology

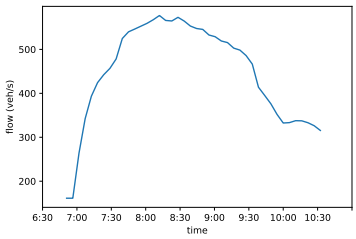

(b) Flow of vehicles

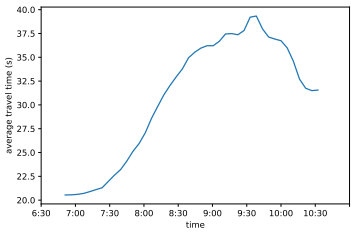

(c) Average travel time

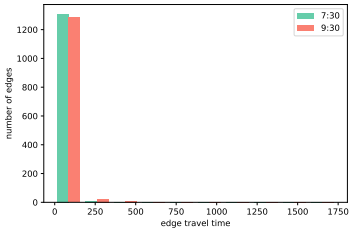

(d) Travel time distributions at 7 : 30 am and 9 : 30 am

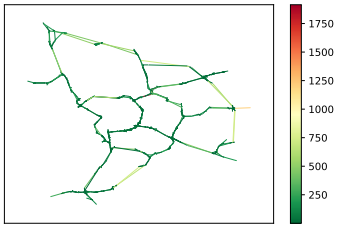

(e) Travel time distribution (s) (7 : 30)

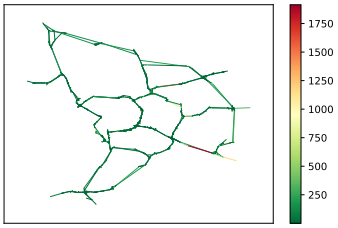

(f) Travel time distribution (s) (9 : 30)

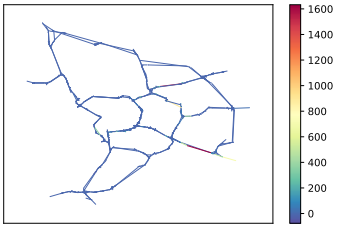

(g) Travel time increases (s) (9 : 30 - 7 : 30)

Figure 3.2: The simulated network (a), the number of vehicles in the network (b), the average travel time along the simulation (c), the travel time distributions at 7 : 30 am and 9 : 30 am (d), the spatial allocation at 7 : 30 am (e), at 9 : 30 am (f) and the travel time increase between 9 : 30 am and 7 : 30 am (g).

3.1.2 HubSim Simulation Tool: peri-urban transport network

This macroscopic simulator intelligently combines scientific algorithms, machine learning and data science to offer speed of calculation. HubSim simulations have been performed on the peri-urban road network of Lyon, France (Figure 3.2a). The Westernmost roads are the *A*6 highway and the *A*7 that link Paris to the French Riviera by crossing the city of Lyon. The central ring road is the Lyon peripheral road that offers a road axis to quickly bypass the city. The *A*46 is the second East bypass of Lyon with the *A*432. The *A*42 highway joins Switzerland whereas the *A*43 highway joins Italy through the Frejus' tunnel. The final network is composed of 1 323 edges and 1 238 nodes, also represented as a directed graph coded in Python 3.6 by using the NetworkX library (Hagberg et al., 2008). Ran on such graph size, the simulator can

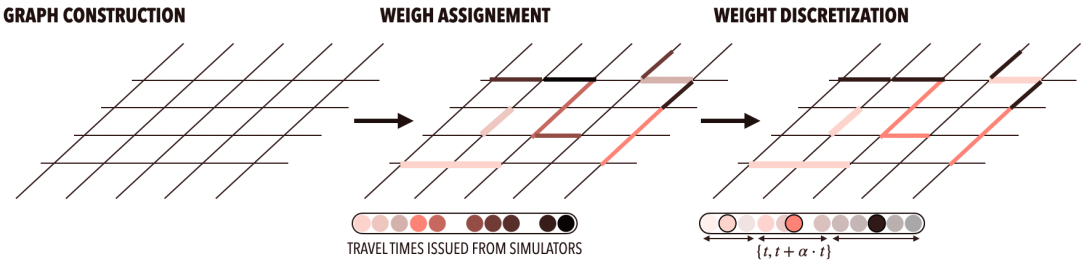

Figure 3.3: Used methodology to build a dynamic graph weighted by the simulated travel time with a weight discretization.

provide results in a reduced computational time (around 1 minute per simulation). Specifically, we applied a stress test methodology by simulating different disruptions and test some improving strategies with the aim of diminishing the negative impact of the disturbance. For instance, we model the impact of the summer holidays by reducing the speed over the *A7* highway, car crashes effect on a major peripheral road, extreme weather by means of a global reduction of speed, etc.

3.1.3 Dynamic Graph Construction

We propose to adopt dynamic graph modelling to leverage traffic conditions as time-varying weights associated to the edges (Chapter 1). The complete used methodology is detailed in Figure 3.3. To weight our graph and model traffic dynamics, we leverage either the SymuVia microscopic traffic simulator (Section 1.2.1.3) or the macroscopic/mesoscopic traffic simulator HubSim (Section 1.2.1.1 and Section 1.2.1.2). The simulator allows for extracting speeds averaged by 10-minutes time stamps. Thus, by dividing the edge length by the average travel speed, periodically measured via simulation, we can weight the edges by their travel time.

In order to improve the significance of the edge weights, we adopt a discretization process to model the bounded rationality principle (Jones, 1999) and identify groups of equivalent shortest paths between pairs of OD, which represents the set of paths that a traveller could select (Figure 3.4). To discretize weights, we group them according to their travel time. For the first interval, we consider the shortest edge travel time t and consider equal all edges whose length is in the range $[t, t + \alpha \cdot t]$. All these edges received the mean value as weight. The minimal value of the second interval is equal to $t + \alpha \cdot t$ while the maximal one is equal to $(t + \alpha \cdot t) \cdot (1 + \alpha)$, the mean value of this second range becomes the weight for the edges belonging to this interval. The process is iterated while the longest edge travel time is not included in an interval.

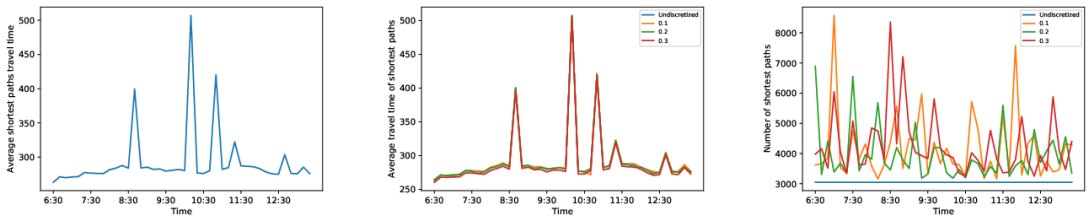

(a) Average shortest paths travel time **(b)** Average shortest paths travel time **(c)** Number of shortest paths for varying values of α

Figure 3.4: Evolution of the average shortest path duration between 6:30am and 1:30pm and the number of shortest paths with and without the weight discretization, representing the bounded rationality.

As we noticed in Figure 3.4a and Figure 3.4b, such discretization process does not modify the average

shortest path length, but impact the number of shortest paths which increases with the rise of α in the range $[0.1, 0.3]$ (Figure 3.4c).

3.2 Traffic condition-Sensitive Centrality Measures

As a first step, we compute traffic condition-sensitive CM over the graph weighted by simulated data, issued from SymuVia (Section 3.1.1) and HubSim (Section 3.1.2). By these analyses, we observe the impact of traffic condition consideration on CM. As introduced in Chapter 2, CM are influenced by the graph weighting and thus sensitive to the traffic conditions. Computed over a weighted graph, the shortest path is no longer the path with the smallest number of crossed edges but the one with the smallest weight. The NDC is no longer the number of connected edges but the sum of their weight. This traffic condition dependence is demonstrated with the EBC computation over a statically weighted graph in Section 3.2.1 where we compare the results for an unweighted graph, a graph where edges are weighted by the length, and a graph where edges are weighted by the free flow travel time. Next Section 3.2.2 focuses on the computation of the EBC, the NCC and the NDC over a dynamically travel time weighted graph with a specific attention on the impact of weight discretization at both global and local scales in urban areas.

3.2.1 Weighted Edge Betweenness Centrality: Static Case

Weighting EBC by static traffic information such as road segment length or the free flow travel time is a first step towards merging topological and dynamic resilience approaches. In Figure 3.5a and Figure 3.5d, we present the values of unweighted EBC. In the peri-urban network (Figure 3.5a), the longest edges (highways *A*7 and *A*46) exhibit the highest EBC values. Similar observations can be done for the urban network of Lyon (Figure 3.5d), the ring road, represented in green with label (c) in Figure 3.1a, possesses the highest EBC due to the long length of the corresponding road segments. For instance, this is the shortest path because of the low number of crossed hops, to go from the interchange, labeled (a) in Figure 3.1a to the red sector, labeled (b) in Figure 3.1a. In Figure 3.5b and Figure 3.5e, we consider the edge length in the EBC

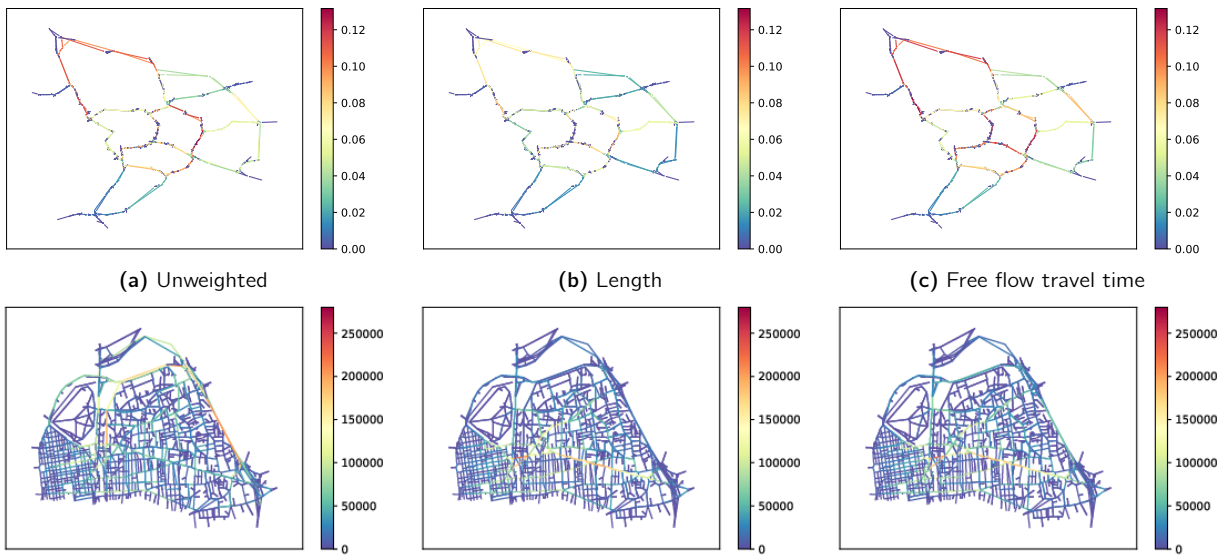

(a) Unweighted **(b)** Length **(c)** Free flow travel time

(d) Unweighted **(e)** Length **(f)** Free flow travel time

Figure 3.5: Comparison of unweighted, edge length weighted and edge free flow travel time weighted EBC over the peri-urban network of Lyon ((a)-(c)) and a part of the Lyon's urban network ((d)-(f)).

computation. For the peri-urban network (Figure 3.5b), we notice a reduction in the longest edges EBC due to the weighting. Due to the length of these edges, shortest paths are modified and no longer cross these edges. For the urban network (Figure 3.5e), the shortest path for the same OD pair (to go from the interchange (Figure 3.1a (a)) to the red sector (Figure 3.1a (b)) becomes "Cours Emile Zola" (Figure 3.1a (d)), with a distance of about 3km while the ring road one is approximately 6km. By considering road segment lengths as the weight of the ring road EBC value approaches zero, which is not consistent with real world situation. Indeed, the ring road, even if longer in terms of length, possesses a high limit speed, which has to be taken into account in the shortest path computation. In Figure 3.5c and Figure 3.5f, edges are weighted by their free flow travel time. Regarding the peri-urban network (Figure 3.5c), the west peripheral road, as the northern highways, are highlighted due to their time efficiency. By weighting edges by their free flow travel time, the ring road travel time benefit is considered in the urban network. Figure 3.5f shows an increase of ring road EBC, due to its presence across some shortest paths. However, in realistic scenarios, the actual travel time of each road segment significantly impacts the path choice.

3.2.2 Weighted Edge Betweenness Centrality: Dynamic Case

In the following, we analyze the impact of the dynamic traffic conditions on the Edge Betweenness Centrality (EBC) (2.4a) and the Global Edge Betweenness Centrality (GEBC) (2.5) which corresponds to the sum of all the EBC values to globally characterize this metric. By leveraging the previously described dynamically weighted graph (Section 3.1.3) to model the road network, the EBC of each edge, whose computations are based on the identification of the weighted shortest paths between each possible pair of OD via Dijkstra's algorithm (Dijkstra, 1971), becomes a function of the time. It is worth to remind that the EBC characterizes the importance of an edge depending on the number of shortest paths crossing it and the total number of shortest paths. The time-dependency of the EBC permits to better capture the functioning of the transport network by considering dynamic features of the roads such as the travel times, neglected in the basic unweighted definitions of the EBC. By evolving both because of regular traffic dynamics (*i.e.*, travel time variations) and, possibly, as a consequence of unpredictable events (*i.e.*, disruptions) the edge weights influence and modify the shortest paths implying an evolution of the EBC over time as a consequence of the changes taking place in the weighted graph. We apply the EBC and the GEBC over a travel time weighted graph. The impact of the weight discretization is observed on both local and global scale on the urban transport network of Lyon (Figure 3.1a) (Section 3.2.2.1). For the urban network, the metrics are computed under normal and highly congested situations to observe the sensitivity of the EBC and the GEBC to the traffic conditions.

3.2.2.1 Implementation on Urban Transport Network

The blue curve in Figure 3.6a corresponds to the GEBC evolution with a non-discretized travel time. It highlights the change in performance over time, related to the evolution of vehicle number in response to the input demand, both reported in Figure 3.1b. With the increase of vehicles present over the network the sum of the EBC computed over all edges, named GEBC rises. In such case, the EBC is not normalized. According to the users bounded rationality principle, the path choice has to be less demanding to obtain a resilience analysis relating to network usage. By weighting the edges with a continuous travel time measure, there is typically only one shortest path between each pair of OD, which makes the model unrealistic from a user's perspective, and therefore, resilience metrics inefficient, such as EBC, as they rely on the identification of the number of shortest paths that traverse each node or edge. With the increase of the number of shortest paths (Figure 3.4c) due to the weight discretization, observed for α equal to 0.1 to 0.3, more possibilities exist to join two nodes. In traffic perspective, this implies that EBC will capture the criticality of the possible taken paths by drivers rather than the topologically shortest one. Only slight changes are visible, in case of discretized weights. Indeed, Figure 3.6a presents almost superimposed curves like the average paths travel

time for all OD pairs (Figure 3.4b). To observe the impact of discretization in presence of congestion, we run a simulation from 6 : 30 am to 1 : 30 pm in presence of a blockage. At global level, we notice a continuous increase in the number of vehicles over the network (Figure 3.6c). This implies a global decrease of performances (Figure 3.6b) with the increased peaks of GEBC due to either the larger set of edges with a positive EBC value implied by the road deviations and the shortest paths modification, or the increase of some edge EBC which becomes more critical by being crossed by a larger set of shortest paths. Indeed, the concentration of some OD shortest paths over specific edges is represented as an increase in the GEBC, making the network more vulnerable. Global results still do not change significantly with the discretization.

At local scale, the change in EBC distribution at 8 : 30 am is not so impacted (Figure 3.7a and Figure 3.7b) under normal traffic conditions whereas, in presence of congestion, the distribution of EBC is

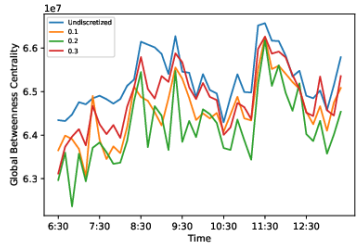

(a) Evolution of discretized travel time weighted GEBC under normal conditions

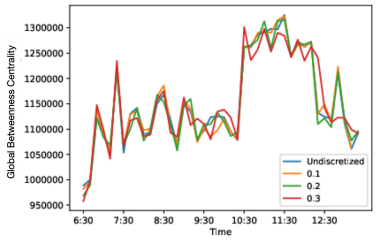

(b) Evolution of travel time weighted GEBC with a congestion

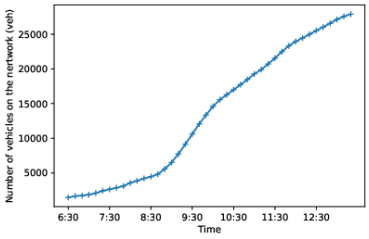

(c) Number of vehicles in the network in presence of congestion

Figure 3.6: GEBC evolution without the weight discretization, under normal conditions (a) and in presence of a congestion (b) whose evolution of the number of vehicles is detailed in (c) for the urban transport network.

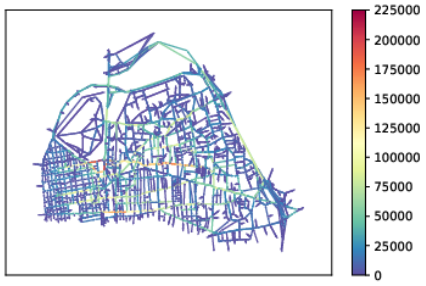

(a) EBC with "real" weights - normal conditions

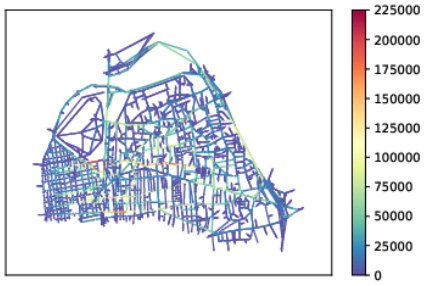

(b) EBC with discretized weights - normal conditions

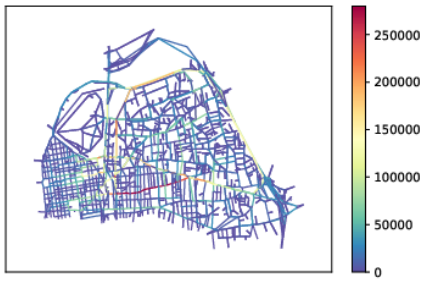

(c) EBC with "real" weights - congestion

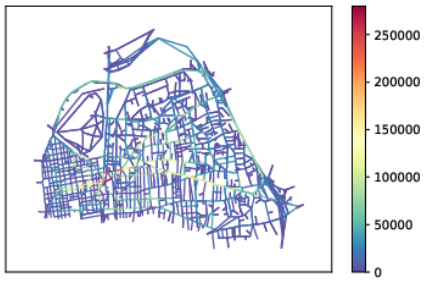

(d) EBC with discretized weights - congestion

Figure 3.7: EBC spatial distribution at 8 : 30 am for non-discretized ((a) and (c)) and discretized weights ((b) and (d)) ($[t, 0.2 \cdot t]$) under normal conditions ((a) and (b)) and in presence of congestion ((b) and (d)) for the urban transport network.

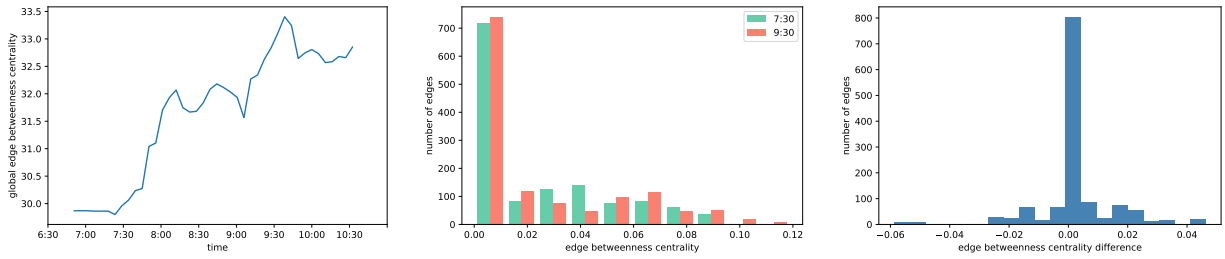

(a) GEBC evolution **(b)** EBC distribution **(c)** EBC difference (9 : 30 - 7 : 30)

Figure 3.8: Global EBC evolution along the simulation duration (a), EBC distribution at 7 : 30 am and 9 : 30 am (b) and the difference in the EBC distributions (c) for the peri-urban transport network.

completely different at 8 : 30 am. As the EBC is dependent on the shortest paths number and composition, by increasing them via our discretization method, redundant shortest paths exist for a same itinerary and therefore more edges are crossed by them. The criticality is thus spread over travel-time-equivalent redundant paths, modifying results. The major impact of this step is underlined by results issued from congested simulation where EBC spatial distributions are completely modified (Figure 3.7c and Figure 3.7d). In the non-discretized weights case (Figure 3.7c) some roads are distinguished by their EBC value as the ring road. When weights are discretized (Figure 3.7d) EBC is slightly better distributed over the network, although we see a group of critical edges close to the center of the network. When using the EBC with travel time weights, that are discretized, we have a more realistic representation of the vulnerable edges of the network.

3.2.2.2 Implementation on Peri-urban Transport Network

In the peri-urban network of Lyon (Figure 3.2a), the weight discretization (Section 3.1.3) has no impact on the number of shortest paths between pairs of OD, which are always unique, due to the weak redundancy of the modelled network and the significant travel time difference between the alternative paths. For this reason, all the results are computed for non-discretized travel times.

Figure 3.8a highlights the traffic condition dependency of the normalized EBC. Indeed, the GEBC evolution follows the average travel time one (Figure 3.2c). The change in performance means that the network is unbalanced, *i.e.*, there are certain edges traversed by more shortest paths (and therefore typically attracting more traffic) than other ones. The appearance of traffic slowdowns increases the travel time of the traversed edges. Thus, the value of travel time associated to the shortest paths at the successive time slots rises. The two following situations can occur: either vehicles continue traversing the same path, which will show, in the following time slots, a larger travel time because of congestion, or vehicles switch to a new path, which has a certain travel time, very likely larger than the one traversed during the previous time slot. The EBC distributions at both 7 : 30 am and 9 : 30 am (Figure 3.8b) support these findings. At 9 : 30 am, the number of quasi 0-EBC edges is increased, meaning that the set of edges not traversed by shortest paths is larger whereas some edges present a huge rise of importance in terms of shortest paths.

Figure 3.9 shows the spatial distribution of the EBC values observed in Figure 3.8b at 7 : 30 am and 9 : 30 am. A lot of changes are observed between both spatial EBC distribution. By observing the travel time evolution between both time period (Figure 3.2e, Figure 3.2f and Figure 3.2g), we observe a travel time increase over the highways *A*7, *A*43 and *A*46, and the departmental road *D*302. As noticed in Figure 3.9c which presents the difference in the spatial distribution of the EBC between 9 : 30 am (Figure 3.9b) and 7 : 30 am (Figure 3.9a), the EBC of many edges ($\approx$ 800 edges) is unchanged (yellow). Some edges present a reduction of their EBC (green and blue) (Figure 3.9c). The edges that presented a major reduction in the EBC values (≈ -0.04) are located over edges belonging to the *A*43 and the junction between the *A*46 and the *D*302. Due to the travel time increase over these edges (Figure 3.2g), shortest paths are deviated over

other paths crossing edges with a lower travel time. The EBC of the edges belonging to the *A*46 and the *D*302 is thus reduced. Other edges highlight an increase of their EBC (orande and red) (Figure 3.9c). A huge increase in the EBC values ($\approx +0.04$) is observed for the edges belonging to the *A*432, which becomes a new alternative in terms of shortest paths. Due to the huge travel time increase of the edge located at the junction between the *A*43 and the *N*346 (Figure 3.2f and Figure 3.2g), it becomes more attractive to get around it using the *A*432, the *A*46, the *D*302, the *N*346 and even retrace one's path using the opposite portion of the *A*43 rather than use the edge. The other alternative, crossing the *A*6, the *A*7 and the *D*301 is also impacted by the travel time increase of the edge located at the junction between the *A*43 and the *N*346 (Figure 3.2f and Figure 3.2g) as demonstrated by the rise of their edges EBC values ($\approx +0.02$) (Figure 3.9c).

3.2.3 Dynamically Weighted Node Closeness Centrality

After analyzing the impact of the dynamic traffic conditions on the EBC, we observe the ability of the Node Closeness Centrality (NCC) to capture the traffic dynamics. The NCC (2.6) is also based on the shortest path computation which becomes weight dependent when using the Dijkstra's algorithm (Dijkstra, 1971). Nonetheless, for such a measure the weight discretization is not so important due to its formula (2.6). Indeed, the NCC depends on the length of the shortest path and not on the number of shortest paths. For this reason, we present the global results on both urban (Figure 3.1a) (Section 3.2.3.1) and peri-urban (Figure 3.2a) (Section 3.2.3.2) networks with non-discretized travel times. We only focus the spatial analysis on the peri-urban transport network whose simulation is quicker and sufficient to observe the dependence of the NCC to the traffic conditions. Computed over a dynamically weighted graph (Section 3.1.3), the NCC becomes time-dependent. To globally analyze the metric evolution, we compute the Average Efficiency (AE) at each time stamps on the peri-urban transport network of Lyon (Figure 3.2a) (Section 3.1.2).

3.2.3.1 Urban Network Use Case

Regarding the urban network of Lyon (Figure 3.1a) under normal conditions, the global increase of travel time, as well as the shortest path travel time, especially at 8 : 40 am, 10 : 10 am and 11 : 20 am (Figure 3.4a), induced by the increase of vehicles present over the network (Figure 3.1b), leads therefore to a decrease of AE (Figure 3.10a), inversely proportional to the length (*i.e.*, total travel time) of the shortest paths (Figure 3.4a). As noticed in Figure 3.4b, the length of the shortest paths, on which the calculation of the AE is based, is not so impacted by the weight discretization. Such an observation supports our idea that the discretization has a negligible impact on the NCC and the AE computations. When computing over the urban network of Lyon in presence of congestion (Figure 3.6c), the AE (Figure 3.10b) continuously decreases because of the huge degradation of traffic conditions. The weight discretization does not impact

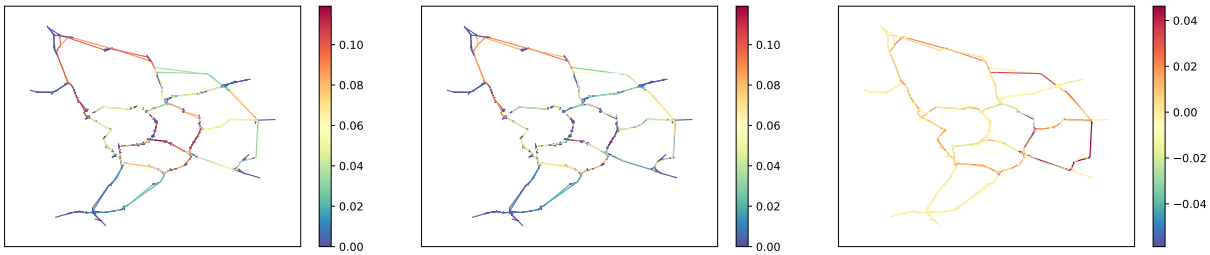

(a) EBC (7 : 30) **(b)** EBC (9 : 30) **(c)** EBC difference (9 : 30 - 7 : 30)

Figure 3.9: EBC spatial distribution at 7 : 30 am (a), at 9 : 30 am (b) and the difference between 9 : 30 am and 7 : 30 am (c) for the peri-urban transport network.

the metric (Figure 3.10c), as we anticipated. The minor change only depends on the shortest paths length and is not essential in our analysis.

3.2.3.2 Peri-Urban Network Use Case

In Figure 3.11a, we present the AE evolution. We notice a decrease in the values of this metric, beginning at 7 : 30am, related to the travel time evolution (Figure 3.2c). The longer the travel time of the shortest paths, the lower the NCC. After 9 : 45 am, the measure rises again until the end of the simulation period, in accordance with the travel time evolution (Figure 3.2c). The NCC distribution computed at 7 : 30am and 9 : 30am (Figure 3.11b), supports the conclusions based on the AE. At 9 : 30am, the distribution is shifted to the left, due to the reduction of some nodes NCC because of the increase of travel time. By being further from each others, the nodes present a lower NCC.

The spatial distribution of the NCC is presented in Figure 3.12 at both 7 : 30 am (Figure 3.12a) and 9 : 30 am (Figure 3.12b) with a focus on the NCC evolution between 7 : 30 am and 9 : 30 am (Figure 3.12c). In accordance with the NCC distribution (Figure 3.11b), at 7 : 30 am (green to orange nodes) (Figure 3.12a), the number of nodes with a high NCC value is larger than at 9 : 30 am (green to yellow nodes) (Figure 3.12b). The difference in the NCC results (Figure 3.12c) supports these observations. Almost all the nodes present a negative difference between the two time steps, meaning that it is, on average, longer to reach most of the nodes at 9 : 30 am than at 7 : 30 am from all other the network locations. The nodes presenting the major change in the NCC value ($\approx -3e^{-4}$) (Figure 3.12c), are located both on the *N*346 and the *A*43 where the longer travel time increases are observed (Figure 3.2e, Figure 3.2f and Figure 3.2g). The others NCC are weaker ($\approx -1.5e^{-4}$) (Figure 3.12c) and induced by the generalized travel time increase (Figure 3.2c), as well as the change of shortest routes between OD pairs as noticed in the EBC analysis (Section 3.2.2.2).

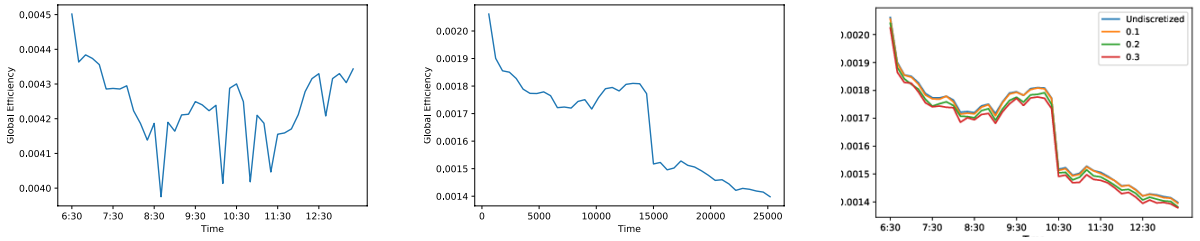

(a) Travel time weighted AE of the urban network under normal conditions

(b) Travel time weighted AE of the urban network in presence of congestion

(c) Discretized Travel time weighted AE of the urban network in presence of congestion

Figure 3.10: Evolution of the AE over the urban networks of Lyon under normal conditions (a) and in presence of congestion (b). The discretization of this weight impact is shown in presence of congestion (c).

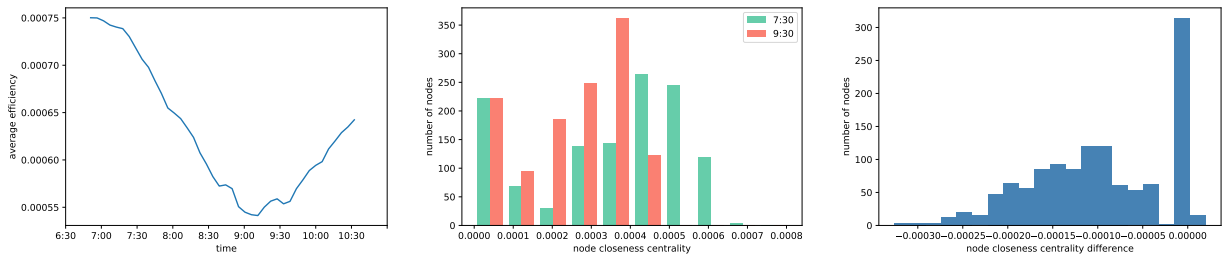

(a) AE time serie evolution

(b) NCC distribution

(c) NCC difference (9 : 30 - 7 : 30)

Figure 3.11: AE evolution along the simulation duration (a), NCC distribution at 7 : 30 and 9 : 30 (b) and the difference in the NCC distributions (c).

3.2.4 Dynamically Weighted Node Degree Centrality

To account for traffic dynamics in the weighted Node Degree Centrality (NDC) computation, with the aim of merging topological and dynamic approaches, the first step consists of obtaining a graph whose weights describe how effectively the edge connects nodes by considering the actual traffic conditions. We assume that in free flow conditions, all nodes are connected at the best possible level, *i.e.*, all edges have a weight equal to one. When travel time increases, we assume edge weights progressively decrease to zero, with zero corresponding to the case of a completely saturated edge, *i.e.*, a road segment where vehicles are completely stuck. Such weight corresponds to the congestion index (Zhang and Lomax, 2008), also called perturbation measure (Martinez-Pastor et al., 2016), used to characterize transport network resilience. We lead the analysis over the peri-urban network of Lyon (Figure 3.2a).

Figure 3.13a presents the evolution of the average NDC, noted as the $\langle NDC \rangle$ (2.8), during the simulation time period. The lower the $\langle NDC \rangle$, the lower the node connectivity. Because of a travel time increase, the level of connectivity of an edge is considered to be degraded due to the reduction in the level of service. For this reason, the higher the average travel time (Figure 3.2c), the lower the $\langle NDC \rangle$. After a decrease from 7 : 00 am to 9 : 30 am (Figure 3.13a), the metric rises at the end of the simulation when the travel time decreases again (Figure 3.2c). The reduction in the $\langle NDC \rangle$ can be also highlighting by the shift to the left of the NDC distribution shifting presented in Figure 3.13b between 7 : 30 am and 9 : 30 am. Indeed, the worse the traffic conditions (Figure 3.2c and Figure 3.2d), the more the network connectivity is degraded and the NDC, appears shifted towards zero.

The spatial distribution of the NDC is presented in Figure 3.13 at 7 : 30 am (Figure 3.14a) and at 9 : 30 am (Figure 3.14b). Figure 3.14c shows the difference in the NDC value at 9 : 30 am compared to 7 : 30 am, in relation to the traffic conditions evolution (Figure 3.2d). In accordance with the NDC distribution shifting to zero (Figure 3.13b), the nodes differences between both spatial NDC distribution (Figure 3.14c) are mostly negative (≈ -1.5). Also in this case, the nodes adjacent to the edges presenting the major travel

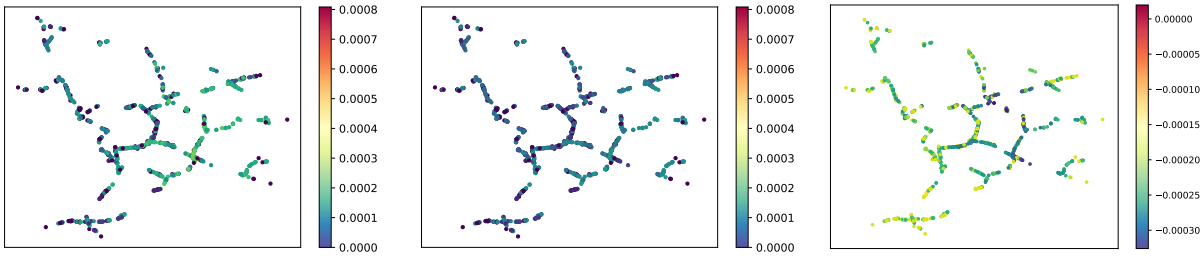

(a) NCC (7 : 30) **(b)** NCC (9 : 30) **(c)** NCC difference (9 : 30 - 7 : 30)

Figure 3.12: NCC distribution at 7 : 30 am (a), at 9 : 30 am (b) and the difference between 9 : 30 am and 7 : 30 am (c).

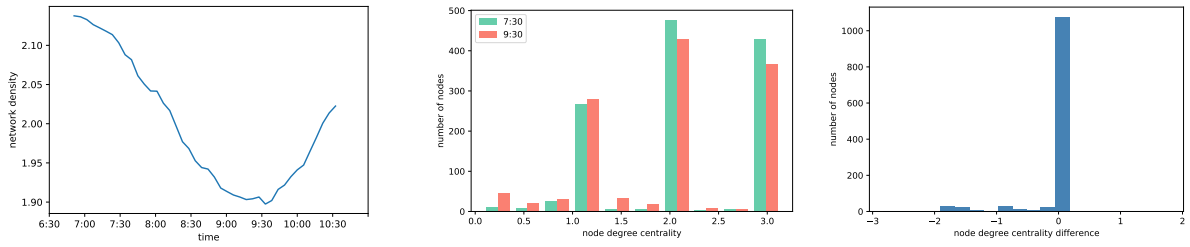

(a) $\langle NDC \rangle$ evolution **(b)** NDC distribution **(c)** NDC difference (9 : 30 - 7 : 30)

Figure 3.13: $\langle NDC \rangle$ evolution along the simulation duration, NDC distribution at 7 : 30 and 9 : 30 and the difference in the NDC distributions (c).

time increase (Figure 3.2g), (*i.e.*, on the *N*346 and the *A*43), are the ones with the higher decrease in the NDC.

To summarize, using a dynamic weighted graph, we relate static and dynamic approaches issued from the literature interesting in transport network resilience. The proposed metrics present a relevant dependence on traffic conditions besides purely topological properties. The choice of travel time weighting is motivated by the analysis led in Section 3.2.1. By reproducing the use of road network through the adaptation of edge weights, we can quantify network resilience in relation to both its topology and its traffic conditions. It is essential to reliably reproduce network usages for an accurate resilience analysis regarding the significant change in EBC distribution.

3.3 Stress Testing on the Peri-Urban Network

The impact of disruptions is analyzed using a stress test methodology. Three disrupted scenarios (Figure 3.15) are compared to a baseline scenario, using the HubSim simulator (Section 3.1.2). First, we analyze the impact of a car crash blocking one lane from 7 : 00 am to 9 : 00 am, located at an entry of the peripheral road (Figure 3.2a) where most of the car crashes occur over this road. The flow (Figure 3.15c) is reduced in a first time from 8 : 30 am to 9 : 30 am. Then, it regains and even exceeds the reference value (blue curve), obtained when the simulation is ran without any disruption, allowing to evacuating the vehicles which have been blocked during the car crash (orange curve). Second, we consider a global speed reduction of 15% compared to the free flow one, over the whole road network, obviously impacts the average speed (Figure 3.15b). Nonetheless, such a disruption (green curve) has no impact on the flow (Figure 3.15c).

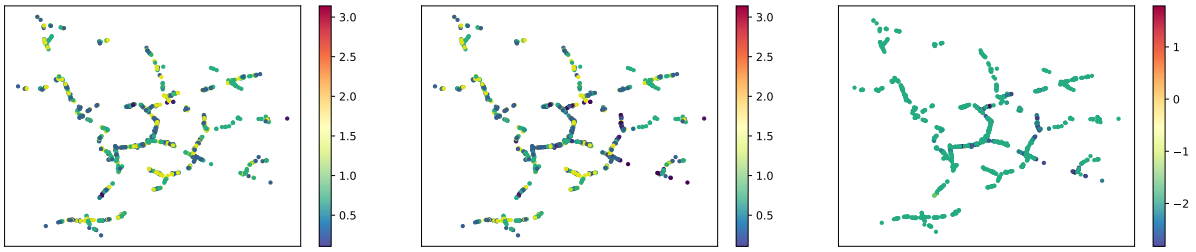

(a) NDC (7 : 30) **(b)** NDC (9 : 30) **(c)** NDC difference (9 : 30 - 7 : 30)

Figure 3.14: NDC distribution at 7 : 30 am (a), at 9 : 30 am (b) and the difference between 9 : 30 am and 7 : 30 am (c).

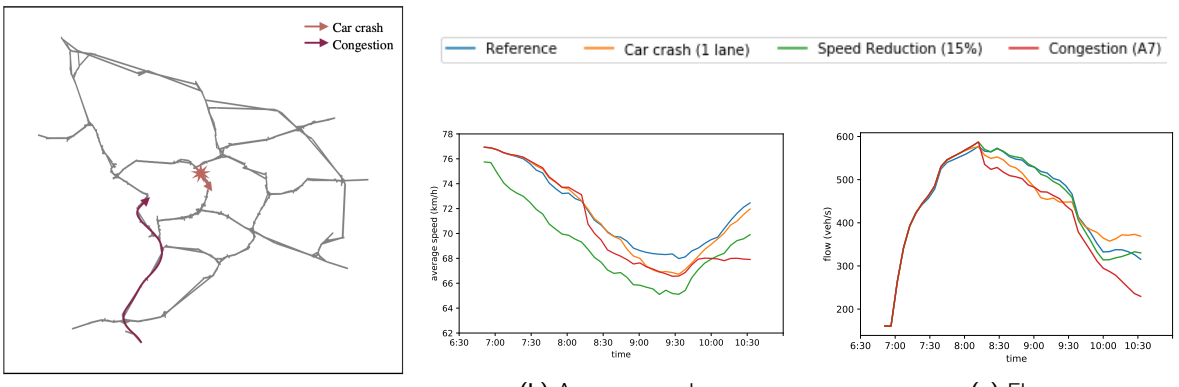

(a) Disruptions **(b)** Average speed **(c)** Flow

Figure 3.15: Localisation of the car crash and the congestion (a). Average speed (b) and flow (c) under normal conditions and in presence of the three disruptions.

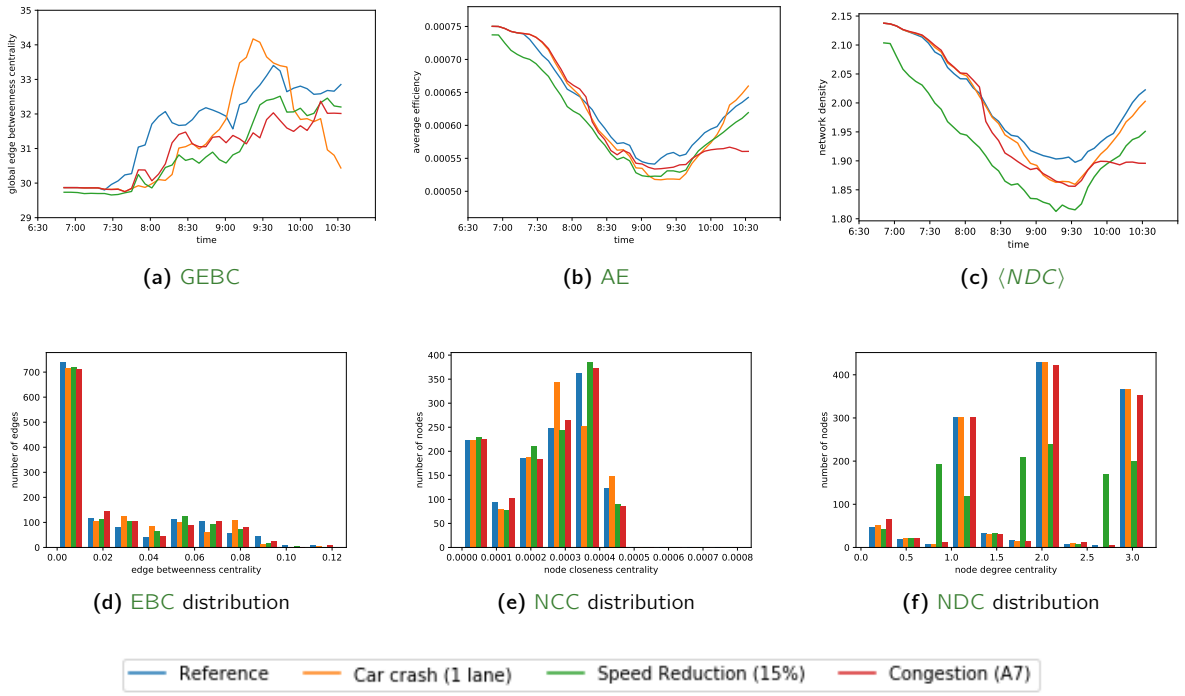

(a) GEBC **(b)** AE **(c)** $\langle NDC \rangle$

(d) EBC distribution **(e)** NCC distribution **(f)** NDC distribution

Figure 3.16: Global evolution of the network performances computed with the GEBC (a), the AE (b) and the $\langle NDC \rangle$ (c) under normal conditions and in presence of three simulated disruptions. The distribution of the EBC (d), the NCC (e) and the NDC (f) at 9 : 30 am.

Such a reduction is comparable to the impact of a snowfall (Figure 4.3). Finally, we observe the impact of a strong congestion over the highway *A*7 on South-North direction (Figure 3.2a), assuming that the flow is reduced of 78% from 8 : 00 am until the end of the simulation. During the summer, this highway, joining South of France to Paris, is congested every week-ends because of the return of vacations. The impact over the flow begins at 8 : 30 am. The flow is reduced until the end of the simulation without regaining the reference value (Figure 3.15c) (red curve). Whereas the car crash and the congestion are localized events (Figure 3.15a), the speed reduction uniformly impacts the whole transport network.

Figure 3.16a-Figure 3.16c presents the global characterization of the network performance using the AE, the GEBC and the $\langle NDC \rangle$, while Figure 3.16d-Figure 3.16f focus on the distributions of the NCC, the EBC, and the NDC at 9 : 30 am, when the conditions are the most degraded (Figure 3.15). The car crash, whose main impact is localized on the peripheral road from 7 : 00 am to 9 : 00 am, negatively impact the global network performance from 8 : 30 am to 10 : 00 am, by reducing the speed during this time period (Figure 3.15b), as well as the AE (Figure 3.16b) and the $\langle NDC \rangle$ (Figure 3.16c). Before 8 : 30 am and after 10 : 00 am, the network performance are close, almost equal, to the one recorded during the normal traffic conditions. We notice that the GEBC is hugely increased from 8 : 00 am to 9 : 30 am, compared to its initial and its final values (Figure 3.16a). Because the car crash occurs on the peripheral road at 7 : 00 am with a reopening of the impacted lane at 9 : 00 am, the shortest paths are deviated to the *N*346 or to the *A*432, which both extends the number of crossed edges with a positive EBC values and concentrate the shortest paths over the same edges with a reduction of alternative routes (Figure 3.16d). We notice that under normal conditions, the GEBC is higher than for the other disturbed conditions due to the presence of a higher number of edges with high value of EBC (higher than 0.09) which probably corresponds to numerous edges belonging to the peripheral road. Regarding the speed reduction, the trend of the GEBC is similar to the one obtained under normal conditions, although the GEBC is a bit lower with the speed reduction. Both the AE and the $\langle NDC \rangle$ are reduced with such disruptions because of the reduction in the

network efficiency. By reducing the speed, the node are farther from each others, diminishing the measures. The NCC and the NDC distributions support these observations by being shifted to the zero. Finally, the congestion, occurring on the highway $A7$ from $7:00$ am, negatively impacts the network performance from $8:30$ am, until the end of the simulation. The average speed is highly reduced at $8:30$ am, from 74 km/h to 68 km/h (Figure 3.15b). Contrary to the other disruptions, the congestion lasts from $7:00$ am to the end of the simulation, and consequently, does not highlight a "recovery" in the network performance at the end of simulation. Both the NCC (Figure 3.16b) and the $\langle NDC \rangle$ (Figure 3.16c) present such a trend with a reduction of AE and $\langle NDC \rangle$ from $8:30$ am until the end of the simulation without presenting an improvement in the measure at the end of the simulation. At $9:30$ am, the NCC distribution (Figure 3.16e) is slightly shifted to zero, as well as the NDC distribution (Figure 3.16f).

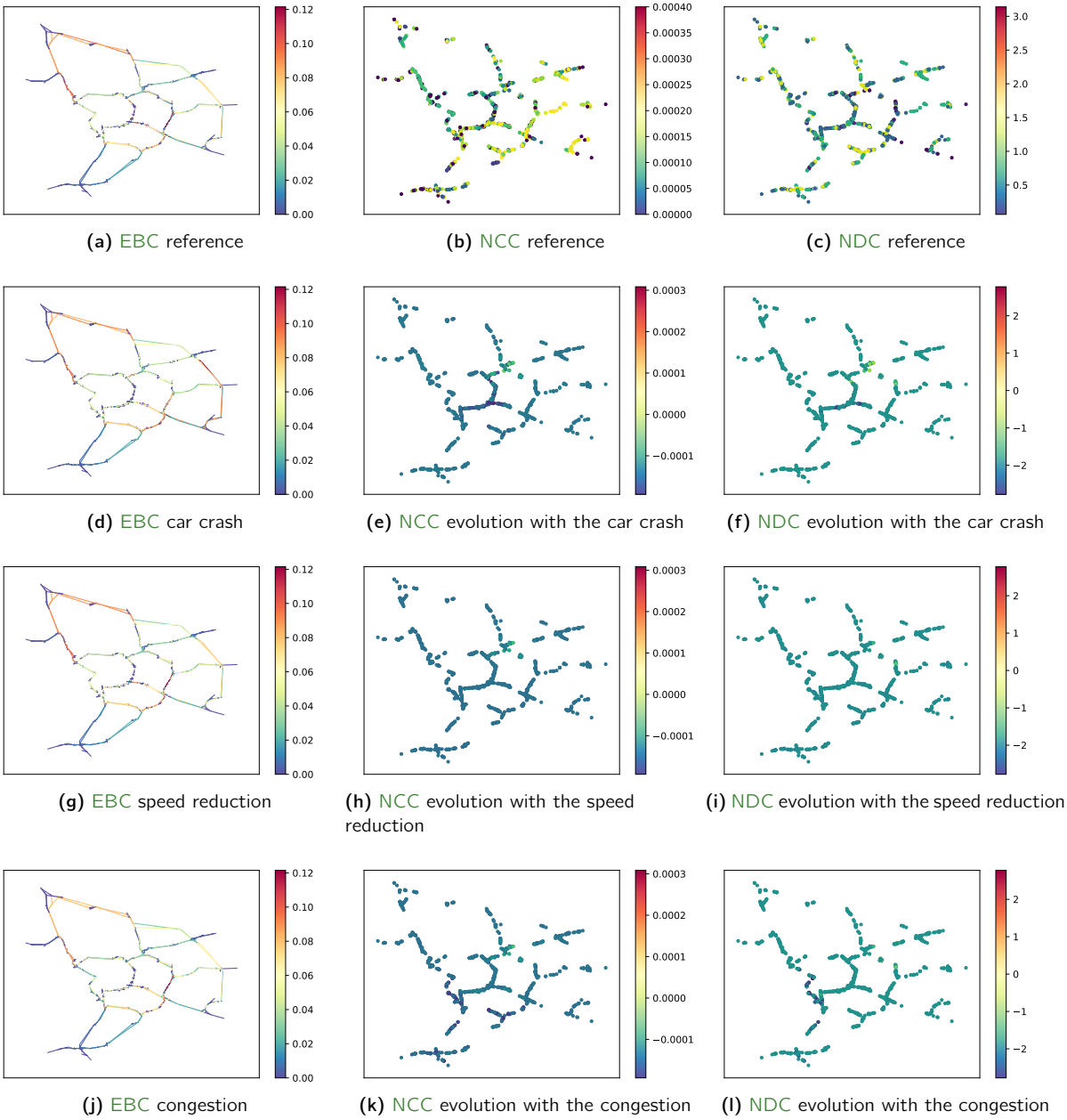

(a) EBC reference **(b)** NCC reference **(c)** NDC reference

(d) EBC car crash **(e)** NCC evolution with the car crash **(f)** NDC evolution with the car crash

(g) EBC speed reduction **(h)** NCC evolution with the speed reduction **(i)** NDC evolution with the speed reduction

(j) EBC congestion **(k)** NCC evolution with the congestion **(l)** NDC evolution with the congestion

Figure 3.17: Spatial evolution of the EBC, the NCC, and the NDC under normal conditions and in presence of three simulated disruptions at 9 : 30 am. For the sake of readability, we plot the difference in NCC and NDC between the normal and the disrupted situations.

Figure 3.17 presents the spatial distribution of the EBC, the NCC, and the NDC under normal conditions (Figure 3.17a-Figure 3.17c), in presence of a car crash (Figure 3.17d), with a speed reduction (Figure 3.17g-Figure 3.17i) and during a strong congestion (Figure 3.17j-Figure 3.17l) at 9 : 30 am, when the impact is the worth (Figure 3.15b and Figure 3.15c). With the car crash, the EBC (Figure 3.17d) of the peripheral road, as well as the EBC of *N*356 (Figure 3.2a), are reduced a lot on North-South direction. Indeed, the shortest paths no longer cross the peripheral road where the car crash is localized. These paths are deviated to the highway *A*432, as shown by the huge value of EBC compared to the normal traffic conditions. The NCC (Figure 3.17e) is reduced for the nodes located close to the incident, as well as the NDC (Figure 3.17f).

Indeed, due to the closure of a lane over the peripheral road, the travel times over the peripheral road are reduced, implying a reduction in the accessibility of these nodes and consequently, a decrease of the NCC. In presence of the speed reduction, which uniformly impacts the whole network, the EBC distribution is almost unchanged (Figure 3.17g) compared to the initial conditions, although the global analysis proves the reduction in EBC values (Figure 3.16a and Figure 3.16d). Indeed, all the shortest paths are longer, degrading the traffic conditions (Figure 3.15), but the distribution of them is the same. Regarding the NCC (Figure 3.17h) a similar trend is observed. The speed reduction has a lower impact on the nodes located at the junction between the highways *A*46, *A*42 and the *N*346. The NDC (Figure 3.17i), is uniformly reduced over the nodes. Finally, the congestion of the *A*7 on South-North direction mainly impacts the EBC of the highways *A*6 and *A*46 which are reduced (Figure 3.17j). The reachability of the nodes located on the highway *A*7 is penalized, with a reduction of their NCC during the congestion. Specifically, the nodes located at the junction between the peripheral road and the highway *A*7 are the most impacted one with a reduction of both NCC (Figure 3.17k) and NDC (Figure 3.17l).

Finally, we combine the three disrupted events, the speed reduction implied by the weather conditions, the car crash, and the congestion. Figure 3.18 presents the global evolution of the speed, the flow, and the AE under normal conditions and in presence of the three previously described disruptions, occurring simultaneously. The impact is stronger with a lowest average speed value equal to 63 km/h at 9 : 30 am (Figure 3.18a). The flow is reduced with a stronger impact between 8 : 30 am and 10 : 00 am due to the car crash (Figure 3.18b). As expected, the AE is lower in presence of the disruptions (Figure 3.18c). In accordance with both the speed and the flow evolution, the impact is worst until 8 : 30 am because of the car crash and the beginning of the congestion.

The EBC is highly impact by this combination of disruptions (Figure 3.19a). Indeed, because of the car crash, the EBC of the *A*432 is increased, contrary to the ones of the peripheral road as well as the one of the *N*356, and due to the congestion on the *A*7, the EBC of the corresponding edge is close to 0. In accordance

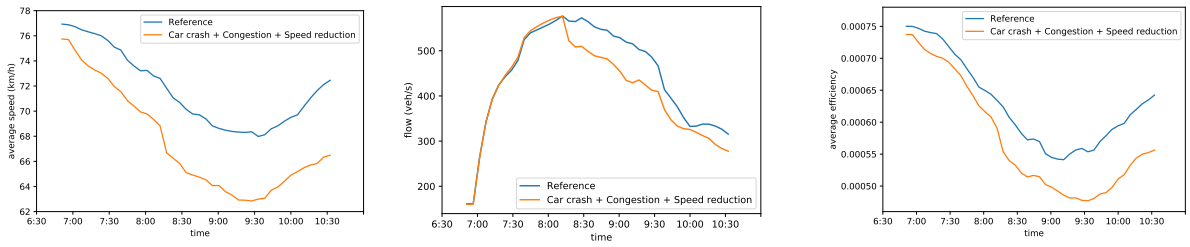

(a) Average speed **(b)** Flow **(c)** AE

Figure 3.18: Global evolution of the average speed (a), the flow of vehicles (b), and the AE under normal conditions and in presence of the three previously described disruptions at the same time.

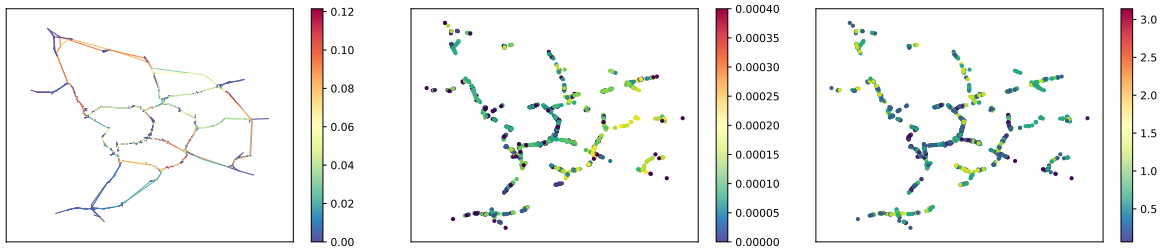

(a) EBC **(b)** NCC **(c)** NDC

Figure 3.19: Spatial distribution of the EBC, the NCC, and the NDC at 9 : 30 am in presence of the three disruptions at the same time.

with the degraded traffic conditions, most of the nodes have a reduced NCC value (Figure 3.19b), compared to the normal conditions (Figure 3.17b), expect for the ones belonging to the *D*302. Regarding the NDC (Figure 3.19c), the impacts are more localized to the event places (Figure 3.15a), *i.e.*, on the peripheral road and on the *A*7 highway.

Such results prove the ability of the CM to capture the impact of disruptions. Such an analysis aims at improving the knowledge of the network, crucial in the improvement of the resilience. Moreover, the CM capture the impacted areas as a consequence of a stress that becomes vulnerable. This is particularly the case of a non-robust network which is unable to evenly absorb the shock as the CM seem to prove.

3.4 Demand-Sensitive Centrality Measures

In this section, we introduce the demand in the CM computation. Such consideration aims at considering another aspect of the traffic conditions in the transport network resilience characterization and the merging of both topological and dynamics approaches. Section 3.4.1 focuses on the observation of the impact induced by the demand consideration in the EBC (Demand-Sensitive Edge Betweenness Centrality (DSEBC) (2.14)) computation over the peri-urban transport network of Lyon (Figure 3.2a) (Section 3.1.2). A spatio-temporal correlation analysis between the EBC and the flow is lead in Section 3.4.2 over the urban transport network of Lyon (Figure 3.1a) (Section 3.1.1) in order to characterize the ability of such measure to capture and anticipate the evolution of congestion.

3.4.1 Demand-Sensitive Edge Betweenness Centrality: the Peri-Urban Transport Network Use Case

We aim at observing the impact of the demand consideration in the DSEBC computed over the peri-urban of Lyon (Figure 3.2a) (Section 3.1.2). The demand is recorded at 7 : 30 am and 9 : 30 am over the peri-urban network of Lyon. Figure 3.20 presents the per-node demand extracted from the OD matrix used in the HubSim simulator, corresponding to the sum of the in- and out-going demand for a specific node. We represent the demand per-node for a sake of simplicity and readability, although we use the demand between the pairs of nodes. The demand is defined between a set of nodes but not all of them. For this reason, we compute the EBC only for this set of nodes. Along the simulation, the demand globally decreases as noticed by the difference in the demand between 9 : 30 am and 7 : 30 am (Figure 3.20c), in accordance with the evolution of the flow of vehicles (Figure 3.2b) which reaches its maximum at 8 : 00 am and then begins to decrease.

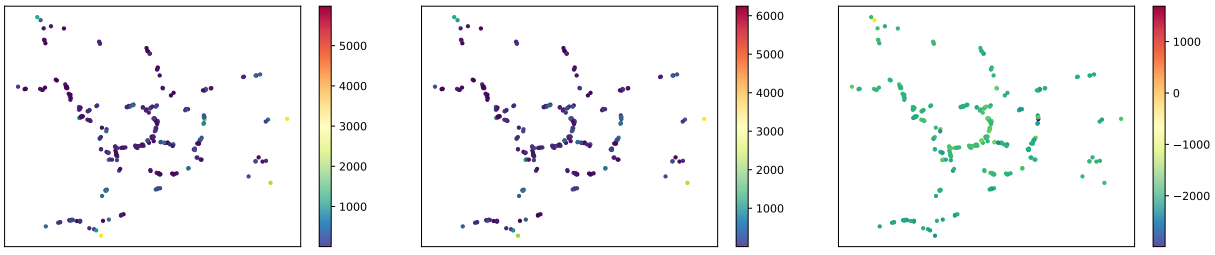

(a) Demand (7 : 30) **(b)** Demand (9 : 30) **(c)** Demand difference (9 : 30 - 7 : 30)

Figure 3.20: Demand spatial distribution at 7 : 30 am (a) and at 9 : 30 am (b)and the difference between 9 : 30 am and 7 : 30 am (c).

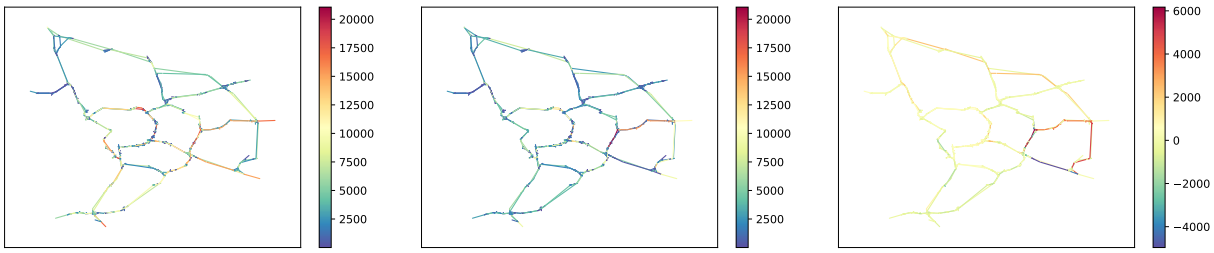

(a) DSEBC (7 : 30) **(b)** DSEBC (9 : 30) **(c)** DSEBC difference (9 : 30 - 7 : 30)

Figure 3.21: DSEBC distribution at 7 : 30 am (a), at 9 : 30 am (b) and the difference between 9 : 30 am and 7 : 30 am (c).

Figure 3.21 shows the spatial distribution of the DSEBC at 7 : 30 am (Figure 3.21a) and at 9 : 30 am (Figure 3.21b). Compared to the EBC results (Figure 3.9), we notice that the edges with the higher values of DSEBC now belong to the *D*302 rather than the *A*6 and the *A*46. This is in accordance with both the demand (Figure 3.20) and the travel time (Figure 3.2g) evolution. Because of the presence of a congestion over the *A*43, the shortest paths are deviated to the *D*302 as observed with the demand-unsensitive EBC (Figure 3.9). All the south of the network edges presents a diminution in the DSEBC results (Figure 3.21) such as the corresponding nodes demand (Figure 3.20).

3.4.2 Correlation between the Edge Betweenness Centrality and the flow: the Urban Transport Network Case

As a second step, we aim at analyzing the ability of the CM to be Demand-Sensitive (DS) by comparing the EBC with the traffic flow. The aim is to discover correlations between the CM and vehicle flows, both in space and in time. We start our analysis by considering classical EBC computed on unweighted graphs moving towards the more informed EBC metrics that consider network demand and travel times, by adopting the definitions previously reported. To analyze the correlation between traffic flow and EBC (2.4a), we consider multiple variants of EBC and especially by modifying the traditional definition to include the demand in the Demand-Sensitive Edge Betweenness Centrality (DSEBC) (2.14) (Section 2.2.3). The spatio-temporal correlation analysis is performed via simulation on the urban road network of Lyon and Villeurbanne, France (Figure 3.1a). To generate realistic traffic flows and get insights on the different EBC metrics, SymuVia (Section 3.1.1) has been exploited to obtain: *i)* travel time data, used to weight the graph; *ii)* hourly flows of vehicles, used in the correlation analysis with respect to different EBC metrics. In our analyses, both metrics EBC and DSEBC have been applied to different graph configurations, with or without the traffic conditions consideration (Section 3.2): Unweighted (U), *statically weighted* with Free-Flow (FF) Travel Times, *dynamically weighted* with average Travel Times (TT), entries-exits (EE) filtering in shortest path computation to only consider those pairs of nodes that mainly originate or absorb traffic. For this measure we consider the same metric as from (2.4a) but picking nodes i and j for shortest path computation from two subsets of the network nodes, respectively the entries (*i.e.*, traffic sources) and the exits (*i.e.*, traffic sinks). Entry and exit nodes are usually introduced in traffic simulation to identify the specific points of the network where vehicles are to be injected or absorbed, respectively and usually exploited also in the definition of the OD matrix in order to couple the demand to the defined sources and sinks. Therefore, we consider different EBC variants depending on both the EBC formula and the nature of the graph, reported in Table 3.1.

Weight	Unweighted (U)		Free-Flow (FF) Travel Times		Average Travel Times (TT)	
Demand-Sensitivity	NO	YES	NO	YES	NO	YES
All pairs	UEBC	DSUEBC	FFEBC	DSFFEBC	TTEBC	DSTTEBC
Entry-Exit (EE)	EEUEBC	DSEEUEBC	EEFFEBC	DSEEFFEBC	EETTEBC	DSEETTEBC

Table 3.1: Different variants of EBC (table of the abbreviations)

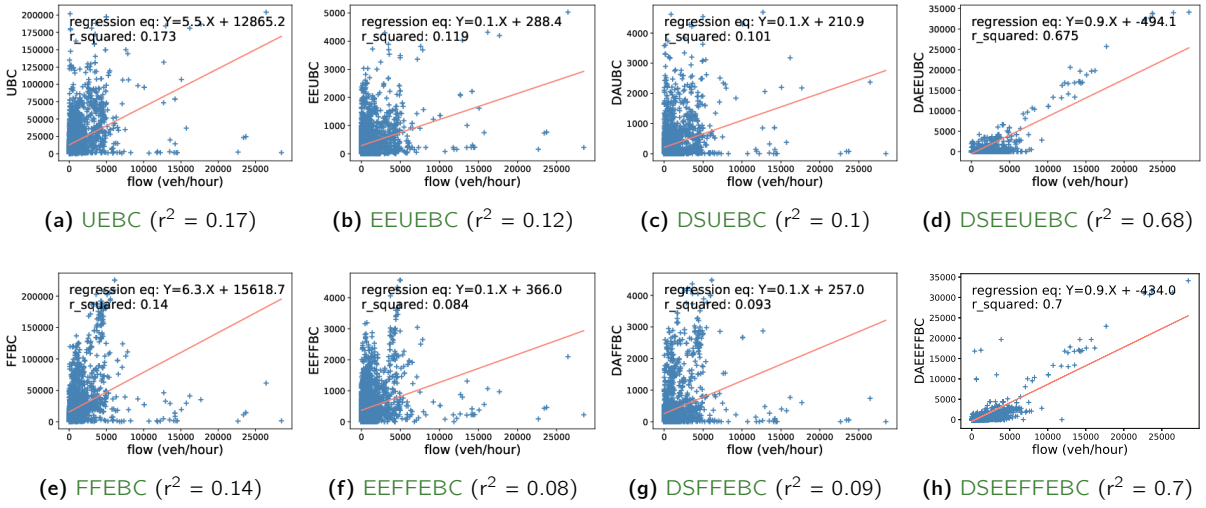

(a) UEBC (r^2 = 0.17) **(b)** EEUEBC (r^2 = 0.12) **(c)** DSUEBC (r^2 = 0.1) **(d)** DSEEUEBC (r^2 = 0.68)

(e) FFEBC (r^2 = 0.14) **(f)** EEFFEBC (r^2 = 0.08) **(g)** DSFFEBC (r^2 = 0.09) **(h)** DSEEFFEBC (r^2 = 0.7)

Figure 3.22: Correlation of per-edge traffic flow and different EBC metrics (on the unweighted simulated network (a)-(d) and free-flow travel time weighted graph (e)-(h)). The highest correlation is achieved when using demand-sensitivity in combination with entry-exit computation of shortest paths (on both unweighted and free-flow travel time weighted graphs).

3.4.2.1 Traffic Flow Static Correlation Analysis

This analysis aims to verify, in a controlled simulated environment, the capability and limitations of traditional static EBC metrics to identify the edges of a transportation network that are most subject to high traffic flow, thus potentially representing critical edges of the urban network deserving monitoring and proper maintenance. In Figure 3.22, we present the results of multiple linear least squares regressions computed between several EBC metrics and the hourly flows observed on network edges. In all the subplots of the figure, each point corresponds to an edge with associated values of the hourly flow (on the x-axis) and the edge's value of EBC (on the y-axis). As an example, Figure 3.22a graphically shows each edge e of the network as a point with coordinates (UEBC(e), $flow(e)$), where UEBC(e) represents the value of UEBC for edge e, computed as from (2.4a) on the unweighted graph, while $flow(e)$ is the corresponding value of hourly flow observed between 6 : 30 am and 13 : 30 am (*i.e.*, average hourly traffic flow observed over the edge during the entire simulation). The subplots also report the square of the Pearson correlation coefficient (*i.e.*, r^2) as well as the regression line coefficients. We call this kind of correlation *spatial* as it covers the totality of network edges and does not consider any temporal information (*i.e.*, flows are aggregated over the whole duration of the simulations and the graph is either static or weighted via free-flow travel times). The scatter plots of Figure 3.22a-Figure 3.22d report the spatial correlation analysis for the EBC variants computed on the unweighted simulated graph (UEBC, EEUEBC, DSUEBC,DSEEUEBC, respectively), while those in Figure 3.22e-Figure 3.22h are related to the free-flow travel time weighted simulated graph (FFEBC, EEFFEBC, DSFFEBC,DSEEFFEBC, respectively).

The first interesting conclusion that we can draw from Figure 3.22a-Figure 3.22d is in line with the previous work on EBC with unweighted graphs (Altshuler et al., 2011; Leung et al., 2011; Akbarzadeh et al., 2019): UEBC could be a good static indicator of flow. In other words, edges with higher UEBC can be expected to be highly attractive in terms of typical traffic flow, especially if EBC is corrected with information on travel demand and simulation-related settings (traffic entries/exits), as suggested by the higher r^2 score, which is equal to 0.68 in Figure 3.22d, in the case of the DSEEUEBC metric. Higher-EBC edges are crucial edges that connect areas of the transport network via (topologically) shortest paths. Therefore, these edges are statistically crossed by a larger number of vehicles as they are along the only (or preferred) routes available for drivers to travel from multiple origins to multiple destinations, even in the presence of congestion along such paths. Similar observations apply when considering graphs that are weighted via free-flow travel times. Such kind of (static) weights does not appear to provide any significantly relevant additional information with respect to unweighted graphs that can be related to traffic flows, as only a slight improvement in the correlation coefficients can be observed with respect to DSEEUEBC (the DSEEFFEBC variant allows achieving a 0.7 value of r^2 instead of a 0.68 of the DSEEUEBC, (Fig 3.22h and Fig 3.22d) on the simulated scenario.

To summarize, the spatial correlation between static EBC and flow (in the variants that consider both the demand and the sources and sinks of traffic) confirms that EBC is a useful metric to understand how vehicles distribute themselves in the network. The free-flow travel time edges weighting, modifying the temporal shortest paths computation in EBC evaluation data does not improve significantly the correlation of EBC with flow information. Finally, as traffic flow is a dynamic information that can exhibit very different behaviors depending on the moment of the day (peak hours vs non-rush hours), the specific nature of the edge (*e.g.*, highways vs. urban roads) as well as the risk of hardly-predictable events (*e.g.*, accidents, gatherings, etc.), it appears relevant to investigate whether the computation of EBC on a dynamically (travel-time) weighted graph can provide deeper insights on flow dynamics observed over smaller time windows (*e.g.*, 30 minutes, 1 hour, etc.). This last point is the focus of our dynamic correlation analysis.

3.4.2.2 Traffic Flow Dynamic Correlation Analysis

Motivated by the considerations above, we move in this subsection to a more dynamic analysis of EBC centered on the DSEETTEBC metric (Figure 3.23). We decided to focus on this metric because both in the unweighted and in the free-flow previous spatial correlation analyses higher scores have been observed when considering demand and entry/exit-sensitivity during computation of EBC. To compute DSEETTEBC in dynamic settings, we consider multiple graphs that are topologically equivalent but associated to different weight configurations, each related to one of the eight time slots reported at the end of Section 3.1.1. We

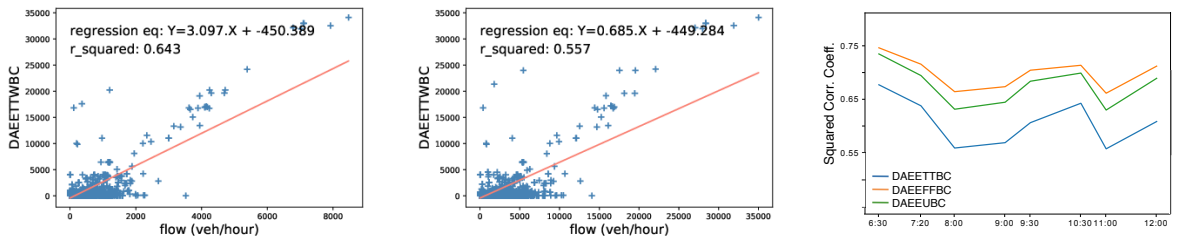

(a) Correlation between DSEETTEBC and Flow for the interval 10:30-11:00 (r^2 = 0.64)

(b) Correlation between DSEETTEBC and Flow for the interval 11:00-12:00 (r^2 = 0.56)

(c) Evolution of the spatial correlation r^2 score over different time slots

Figure 3.23: Correlation between DSEETTEBC and Flow during specific simulation time slots (a) and (b), and along all the simulation period.

select these temporal windows as our granularity level in the study of dynamic EBC metrics. In fact, we assume these slots to be representative both of relevant changes in the travel demand (Figure 3.1b) and of variations of the ways drivers select the alternative routes for their movements (*i.e.*, different assignment coefficients are associated to alternative paths over these time slots in our simulations). Hence, for a given simulation time slot t (*e.g.*, t = {6:30-7:15}), we produce a graph whose edge weights correspond to the average travel times observed during t. We use the travel time weights to compute DSEETTEBC(e) and retrieve the flow information (*veh/h*) on e during time slot t for every edge e of the graph. We repeat the process for every time slot t.

Figure 3.23a reports on the spatial correlation analysis of DSEETTEBC in t_1 = {10:30-11:00}, while Figure 3.23b is related to time slot t_2 = {11:00-12:00}. For the sake of comparison, it has to be highlighted that the per-edge flow values considered in the spatial correlation diagrams are related to the specific time slot t which the average travel-time weighted graph refers to, and not to the typical flow observed on the edge over the whole simulation duration. These figures show comparable, but slightly lower, spatial correlation scores r^2 with respect to the cases of DSEEUEBC and DSEEFFEBC from Figure 3.22. To shed some light on the reasons behind these slightly lower spatial correlations, we plot in Figure 3.23c the temporal evolution over the complete set of simulation time slots of the r^2 score in the cases of DSEEUEBC, DSEEFFEBC and DSEETTEBC, obtained by correlating the per-edge EBC values to the flow values observed along the edges during the different time slots. It is worth remarking that both DSEEUEBC and DSEEFFEBC obviously do not depend on time as the graph is either unweighted or weighted by free-flow travel times, respectively. Thus, the variations of the r^2 score are to be imputed only to the dynamics of the flow during the different considered slots for the cases of DSEEUEBC, DSEEFFEBC. Conversely, it has to be remarked that DSEETTEBC changes in time as the average travel times variate during different simulation slots and are exploited to compute the temporal shortest paths DSEETTEBC depends on. As a first insight, it appears interesting to observe how the spatial correlation score is affected by the presence of higher flows during peak hours in all the considered variants of EBC. Concerning the unweighted and the free-flow static scenarios, it appears evident that flow increases negatively impact correlation (the r^2 score decreases in correspondence of peak hours), thus showing an important limitation of both DSEEUEBC and DSEEFFEBC: such a metrics have no possibility to follow, estimate or anticipate any kind of flow variation in time, but they may only provide generic statistical indications about expected flows (*e.g.*, higher EBC means higher expected flow on the edge) as anticipated in the previous subsection (Sec.3.4.2.1). To better grasp instead the dynamic properties of DSEETTEBC, we move now to analyzing the relationships that exist between variations of observed flows and variations of DSEETTEBC in time over the different graph edges.

First of all, Figure 3.24b spatially depicts the standard deviation of the flow on each edge of the network over the simulation time slots, while Figure 3.24a graphically presents the absolute values of the flow in the time slot {7:15-8:00}. To mitigate the effect of network charging at the beginning of the simulation, the figure excludes the first time slot {6:30-7:15} in the computation of the standard deviation. These two figures, if considered together, provide an idea of the entity of flow variation in relation to the highest ranges of flows observed in the network. They clearly indicate that the most evident flow variations (in the range [200, 600] veh/hour) are relatively low but definitely not negligible, if considered with respect to the extremely high values of flow that are observed on the city ring road (the red edges in Figure 3.24a correspond to flows that are larger than 5000 veh/hours). Having proved the existence of significant flow variation on a subset of network edges, we move to analyzing the impact of such variation on the DSEETTEBC, by means of another kind of linear correlation that we call *per-edge temporal correlation*. This correlation is computed by considering, for a given edge e of the graph, the vector corresponding to the DSEETTEBC values over the eight simulation time slots and the vector of the corresponding observed vehicle flows (measured as veh/hour). Hence, we calculate the linear correlation score (which can be either positive or negative) for each edge e of the network. The edge temporal correlation values are spatially visualized in Figure 3.24c. In the figure, highly anti-correlated edges can be easily spotted (blue/green edges) from the positively-correlated ones (orange/red edges), while yellow edges correspond to weakly-correlated edges.

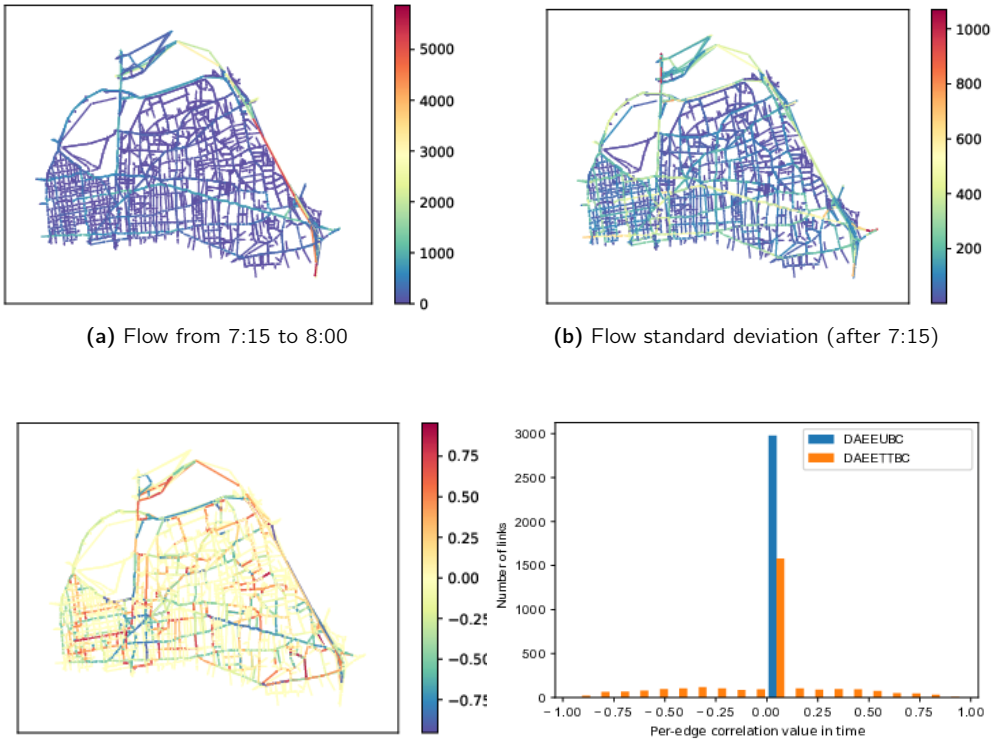

(a) Flow from 7:15 to 8:00

(b) Flow standard deviation (after 7:15)

(c) Per-edge temporal correlation

(d) Distribution of the per-edge temporal correlation

Figure 3.24: Spatial representation of flow at 7 : 15 am (a), the flow variability after 7 : 15 am (b), distribution of per-edge temporal correlation between EBC and flow (c) and distribution of the temporal correlation coefficient for the DSUEBC and the DSTTEBC (d).

Figure 3.24d represents instead the distribution of the temporal correlation score (as an histogram) for DSEETTEBC (in orange). The distribution is also shown (in blue) for the case of DSEEUEBC, but, as expected, the latter is fully located on the 0 value (no correlation) due to the time-independent (*i.e.*, constant) nature of such metric. The Pearson correlation coefficient is undefined when one of the two variables is a constant. For the sake of simplicity, we represent this situation with a 0 (null) value in our figures. The comparison between the two distributions reported in Figure 3.24d provides interesting insights about the more dynamic nature of DSEETTEBC. Firstly, it can be noted that only a portion (approximately around the half) of the network edges have a constant DSEETTEBC. This confirms the fact that DSEETTEBC conveys dynamic information on traffic flows that is inevitably neglected when considering centrality metrics on static graphs (*i.e.*, UEBC or FFEBC). Also, we state that the dynamic nature of the DSEETTEBC, which exhibits both positive or negative time correlation with flow for different edges, could be the reason of the lower spatial correlation observed in Figure 3.23c: certain edges are characterized by a DSEETTEBC that changes in time according to an opposite trend with respect to flow, thus contributing to lower the global (spatial) correlation with the typical flow at a network scale. Secondly, a very low temporal correlation between the DSEETTEBC and flow vectors for a given edge can be explained by the fact that these edges are traversed by a high number of shortest paths (therefore showing high EBC), when they have either high or low flows (and therefore can be either severely congested or in free-flow). In other words, we can speculate that, in such cases, drivers choose these edges according to a mainly static, geometric knowledge of the road network or that a low number of alternative shortest paths is available to traverse these segments. Thirdly, a non-null correlation in time means that EBC and flow are either having similar trends (which corresponds to positive correlation, *i.e.*, the relative number of shortest paths traversing the edge

varies in time as the flow) or opposite tendency (which corresponds to negative correlation, *i.e.*, the relative number of shortest paths traversing the edge varies in time with a similar shape with respect to the flow but with a delay). In the first case (positive temporal correlation on an edge), increasing (respectively decreasing) flows are almost instantaneously followed by increases (respectively decreases) of EBC. This situation may happen because neighboring zones (previously including most of the shortest paths) become congested (respectively fluid) thus potentially becoming less (respectively more) attractive than the considered edge. We can therefore speculate that, when we observe non-null correlation on an edge, drivers may be choosing these edges by considering also dynamic information about traffic. Specifically, negative high correlation on an edge could be interpreted as a consequence of the fact that vehicles start preferring the edge (that is along multiple alternatives routes for OD traffic re-distribution) during congested states of surrounding edges (that are instead preferred in presence of low congestion), by possibly considering information on traffic conditions. Conversely, in case of positive high correlation, vehicles choose the paths considering their static initial knowledge and there is generally low congestion in the network. Finally, positive or negative medium/low correlation can be seen as an indicator of vehicles behaving in different ways. Some vehicles are forced to follow some paths due to some constraints; other vehicles adapt their choices based on the available resources by selecting the paths with lower traffic.

To summarize, a spatial analysis of the flow standard deviation of timed samples for each edge can show useful properties of the road network. A spatial analysis of the temporal correlation of DSEETTEBC and flows can therefore unveil whether correlation is negative or not, so better highlighting the properties of the dynamic urban system. This study is then extended on real data to confirm these observations in Section 4.4.2.

3.5 Concluding Remarks and Discussions

The consideration in the CM computation of both traffic conditions, through graph weighting, and/or travel demand, by modifying the formula, relevant to capture both static and dynamic resilience properties (Chapter 2). By computing the CM over the travel time weighted graph of the peri-urban (Figure 3.2a) (Section 3.1.2) and a part of the urban (Figure 3.1a) (Section 3.1.1) of Lyon, we observe their sensitivity to the traffic conditions.

At the global scale, whereas the GEBC rises (Figure 3.6 and Figure 3.8a) in presence of a travel time increase, the AE (Figure 3.10 and Figure 3.11a) and the $\langle NDC \rangle$ (Figure 3.13a) decrease. Because of the appearance of slowdowns, the shortest paths are deviated to longer ones to get around the more impacted edges, significantly increasing the EBC of some specific edges which are interesting both in terms of travel times and topology. Moreover, by being deviated, the shortest paths are usually longer in terms of travel times as well as crossed edges which will increase the global measure by rising the EBC of these specific edges. Regarding the AE, the metric decreases (Figure 3.11a) with travel time augmentation. The degradation of the traffic conditions implies a travel time increase for most of the network paths, especially for the shortest paths. By being longer, the shortest paths modifications induce a reduction of the AE. The network performances, computed by the AE, are negatively impacted with the rise of the distance between the nodes. At the end of the simulation, the metrics rise again with the travel time decrease. Finally, the $\langle NDC \rangle$, dependent of the level of services due to the graph weighting, decreases wile the travel time increases (Figure 3.13a). Because the weights describe how effectively the edge connects nodes by considering the actual traffic conditions, a travel time increase caused by congestion phenomena or perturbations on one edge will imply a reduction in adjacent nodes' weighted NDC, as noticed in the metric distribution (Figure 3.13b). Indeed, we assume that in free flow conditions, all nodes are connected at the best possible level, *i.e.*, all edges have a weight equal to one. When travel time increases, we assume edge weight progressively decreases to zero, with zero corresponding to the case of a completely congested edge, *i.e.*, a road segment where vehicles are completely stuck.

At local scale, all the studied metrics (EBC, NCC and NDC) present a change in their spatial distribution due to the traffic conditions evolution. A localized reduction in both metrics is related to the travel time evolution and the appearance of congestion or slowdowns over specific edges. The travel time increase degrades both the connectivity of the nodes, thus reducing their NDC, and the accessibility, thus reducing their NCC. While the NDC characterizes the graph connectivity, the NCC and the EBC, based on the shortest paths computation, quantify the network efficiency considering the network redundancy. All these aspects are essential for the resilience characterization. Regarding the EBC, we notice a difference in its spatial distribution because of the modification of the shortest paths induced by the traffic conditions evolution. Because its computation is based on the number of shortest paths (2.4a), we introduce a weight discretization process. By discretizing the weights, we observe an increase of shortest path alternatives (Figure 3.4b) over the urban network of Lyon (Figure 3.1a) (Section 3.1.1), contrary to the peri-urban network which is not sufficiently meshed (Figure 3.2a) (Section 3.1.2). Such discretization process ensures a better representation of the users' behavior. Because the travel time is not the only variable entering in the route choice decision and because of the bounded rationality, it is better to consider a set of alternatives paths in the analysis of resilience rather than a unique one.

Finally, we notice that the addition of the travel demand consideration in the CM formula aims at providing more accurate results in the vulnerability characterisation of the network by being consistent with the users' behavior, in terms of road use. We begin by observing the impact of the demand consideration with the DSEBC compared to the demand-unsensitive EBC over the periurban transport network Lyon (Section 3.4.1). The spatial distribution of the DSEBC (Figure 3.21) change to the EBC one (Figure 3.9) by being influenced by the travel demand (Figure 3.20). Then, we lead a spatio-temporal correlation analysis between the DSEBC and the flow of vehicles over the urban transport network of Lyon (Section 3.4). The spatial correlation, consisting in the correlation of the indicator of resilience and the flow for all the edges at a given time step, confirms the results issued from the literature (Altshuler et al., 2011; Puzis et al., 2013; Akbarzadeh et al., 2017) with a better correlation once the traffic conditions are considered through the graph weighting, and demonstrate the interest of dynamically analyzing these variables because of the traffic dynamicity. The temporal correlation between the EBC variants and the traffic flow, consisting in correlating the evolution of both variables per edge, provides different behaviors (negative, null or positive) depending on the network properties and topology.

Chapter 4

Disruptions Impact Quantification on the Network Resilience

This chapter aims at validating on real data our findings regarding the simulation-based characterization of resilience (Chapter 3) using hybrid approaches (Section 1.3 and Section 2.2.3).

Two datasets are used in this chapter: Floating Car Data (FCD) (Section 4.1.1) and a combination of Loop and Taxi trip data (Section 4.1.2). In the first dataset, a set of adverse weather situations as well as incidents events were recorded (Section 4.1.1): a snowfall, a strike, a tunnel closure and a subway failure.

By computing the network indicators over the corresponding dynamically weighted graph, we analyze the network performances and characterize resilience considering both the traffic conditions and network topology. First, the impact of the disurptions, recorded in the FCD, is quantified using the NDC and some global indicators, derived from its distribution (H, S and $\langle NDC \rangle$) (Section 4.2). Then we characterize the efficiency of the network under normal and disrupted conditions using the NCC (Section 4.3) and the EBC (Section 4.4.1). The ability of this last metric to capture the traffic conditions is analyzed through the extension of the work initiated in Section 3.4, by correlating it with purely traffic indicators (Section 4.4.2).

This chapter contributes to the state of the art by supporting the results issued from the simulated data-based analysis with historical data. The ability of the CM to both capture traffic and disruptions impact is analyzed, as well as the correlation between such measures and the traffic flow. Through the temporal correlation between the EBC and the flow, we prove the dependence of such resilience metric to route choices from travellers and on the evolution of congestion.

Section 4.2 is an updated and enhanced version of the paper Henry et al. (2021a), and Section 4.4.2 is an updated version of the conference paper Henry et al. (2019a).

Contents

4.1 Actual Data

In this chapter we analyze transport network resilience using historical data, issued from Floating Car Data (FCD) (Section 4.1.1) and a combination of Loop data and Taxi Trip data recorded over a same period (Section 4.1.2). With the FCD, we aim at proving the ability of the NDC, the NCC, and the EBC to capture the traffic dynamics and characterize the network resilience in time and in presence of disruption. With the two last dataset (Loop and Taxi Trip data), we pursue the correlation analysis between the traffic flow, as issued from the Loop data, and the traffic conditions-sensitive EBC, as computed over a dynamic travel time weighted graph with the Taxi Trip data (Section 3.4.2).

4.1.1 Floating Car Data

To demonstrate the ability of the CM to capture traffic dynamics, we use FCD. These data were recorded, by BeMobile[1] (BeMobile), a provider of real-time traffic and mobility information services, from October 2017 to September 2018, in the Rhône-Alpes region, France. Nonetheless, we reduce the studied area to the Lyon Metropolitan area, divided into 21 sub-areas, corresponding to the districts of Lyon and neighboring cities (Figure 4.1), to keep a reasonable graph size and guarantee a large availability of traffic information on the retained edges. The GPS positions of tracked vehicles have been map-matched to the closest edge of the road network. Finally, in order to produce a topologically reliable graph, we have pre-processed the graph by only retaining the nodes that represent road intersections. This step is essential because of the high dependency of the NDC to network topology. At the end, we obtain a graph composed of 13 090 nodes and 27 618 edges (Figure 4.1). In order to produce the per-edge average speed variable with a given periodicity over a sufficiently large portion of edges for computing a reliable average speed, we aggregate the available speed raw data in 30 minutes slots. This choice permits to increase the number of speed samples from the data.

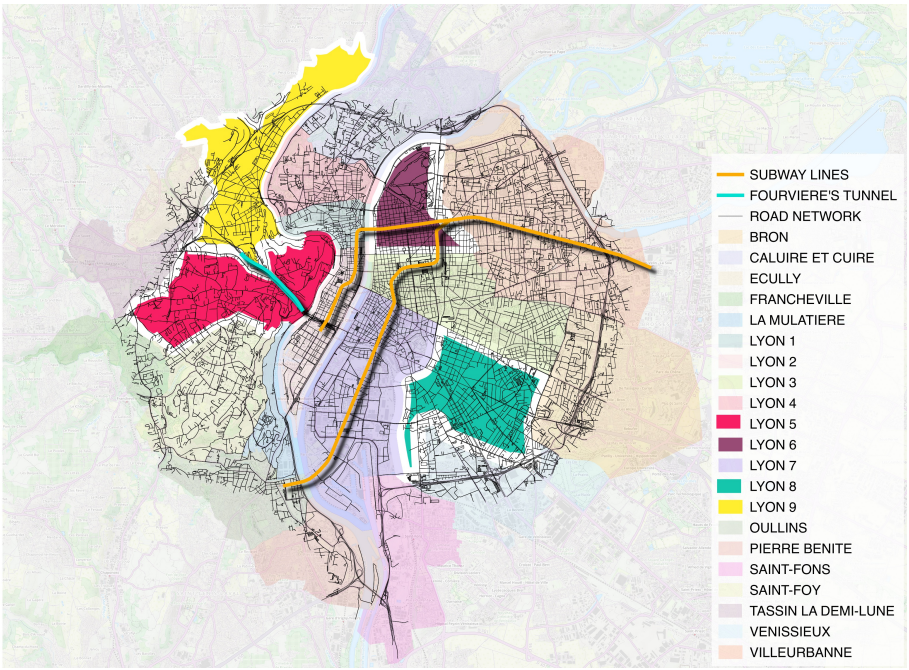

Figure 4.1: Urban network of Lyon and its neighborhoods on which FCD are available with the details of Lyon's boroughs and some part of the network impacted by the recorded disruptions.

[1] http://www.be-mobile.com/

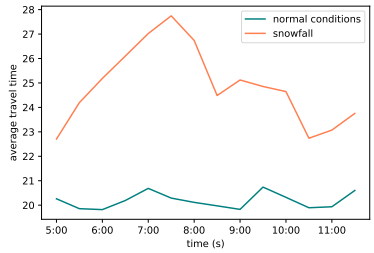

(a) Average travel time evolution under normal conditions and in presence of disruption

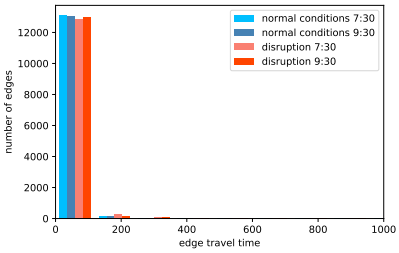

(b) Travel time distributions

(c) Reduced graph of Lyon

Figure 4.2: (a) Evolution of the average travel time and (b) its distribution between both 7 : 30 am and 9 : 30 am and under normal and disrupted conditions. (c) Reduced graph of Lyon.

To reduce the computational time, we compute the NCC and the EBC on the reduced road transport network of Lyon (Figure 4.2c), composed of 13 269 edges and 6 398 nodes and weighted using FCD (Section 4.1.1). The travel time evolution of this network is reported in Figure 4.2. The difference in the travel time values distribution between 7 : 30 am and 9 : 30 am is highlighted in Figure 4.2b. Under disrupted conditions at 7 : 30 am, when the impact of the snowfall is the strongest (Figure 4.3a and Figure 4.2a), the number of edges with a travel time lower than 200 seconds is the lowest.

Using the FCD we aim at identifying both typical and unusual situations of the network in order to understand the sensitivity of the proposed resilience indicators to disruptions. After extracting the typical speed profile, obtained by averaging data over twenty days, for all the edges of the network from 5 : 00 am to 10 : 00 pm, with a 30-minutes periodicity, which are not affected by any special event or perturbation (Figure 4.5a), we focus on unusual speed profiles issued from different specific days presenting a disruption (Figure 4.3). By relying on information from national weather and local newspapers, we identified specific events, that took place in the observed region and which impacted traffic conditions. The speed information is not always available for all the network because the number of observed vehicles in the FCD is limited.

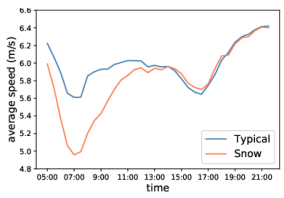

(a) December 18th

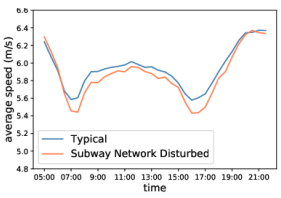

(b) December 19th

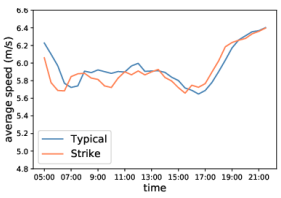

(c) March 4th

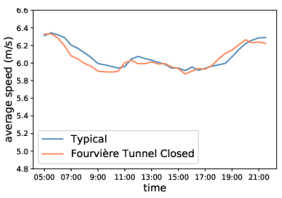

(d) June 2nd

Figure 4.3: (Average speed profiles (blue) and speed profile in presence of the four recorded disruptions (orange): (a) the snowfall, (b) the subway disruption, (c) the strike, and (d) the tunnel closure.

For these edges with a missing travel time information, either in the case of typical or for abnormal days, we assume a free flow condition. The data issued from abnormal day are on average available for 35% of the 27 618 edges but this percentage is obviously higher for the typical day, obtained with the aggregation of multiple days and related speed observations. Four different disruptions recorded during the period in which data are available are considered:

- A heavy snowfall on Monday, December 18th, 2017, which fully disturbed the road network; (Figure 4.3a)
- A subway service failure (Figure 4.1 (orange lines)) from 7 : 30 am to 4 : 15 pm, on Tuesday (Figure 4.3b) where the impact of the potential modal shift may have changed the road network dynamics;
- An impact of protesters which partially blocked the circulation over a part of the road network on Wednesday, April 4th, 2018 (Figure 4.3c);
- An important tunnel of the city, called Fourviere tunnel (Figure 4.1 (blue line) and crossed by more than 100 000 vehicles per day, was closed in the north-south direction for renovations for three days (Figure 4.3d).

While some of the disruptions, as the snowfall, impacted the whole network, some others, as the tunnel closure, were localized in specific areas of the city.

4.1.2 Loop Data and Taxi Trip Data

To extend the EBC correlation with the traffic flow analysis based on simulated data (Section 3.4.2), we use two different datasets. First, we use loop detector data collected from January 2007 to January 2015. These data report on the flow for several edges of the road network. Second, we use taxi GPS data recorded on week days for 9 weeks from March to May 2011 for the city of Lyon, France. We removed trajectories with a duration lower than 60 seconds and anomalous sequences of GPS points whose average speed is higher than 130km/h. Hence, we obtain 103 639 taxi trips containing 5 581 590 taxi records providing the origin, the destination, the distance, the duration and the taxi speed. Taxi trips and loop detectors have been map-matched to the edges belonging to the road network graph, composed of 248 337 links and 117 605 nodes (Figure 4.4).

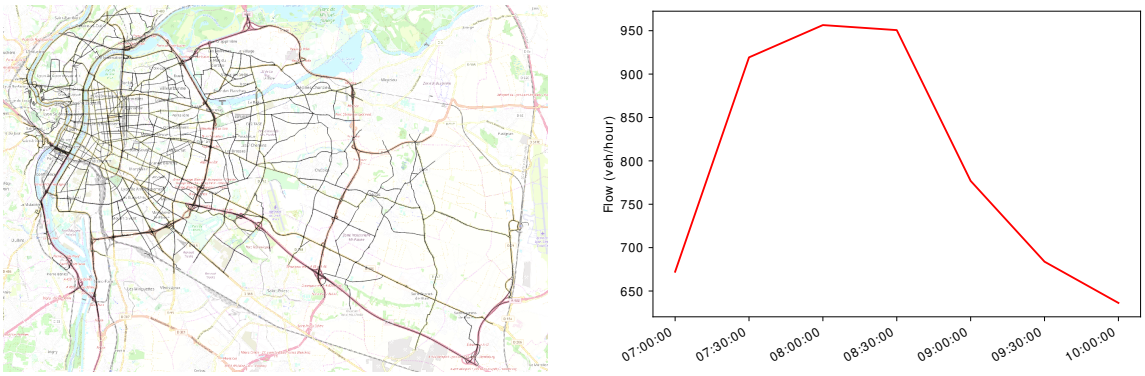

(a) Network topology **(b)** Average flow

Figure 4.4: The simplified real network (a) and the average flow (b).

4.1.3 Construction of a Dynamic Graph

To introduce traffic dynamics in the Centrality Measures (CM) computation, with the aim of combining topological and dynamic approaches, the first step consists in obtaining a graph whose weights describe the traffic conditions, as we did for the simulated data (Section 3.1.3). The road network is represented as a weighted, directed graph, whose nodes N correspond to road intersections and edges E correspond to road segments. The edge weights, which evolve with a given frequency, represent the dynamic traffic conditions, using the average speeds or the travel times on the corresponding road segments. By studying the characteristics of such a dynamic network, via a travel-time dependent weighted graph, we ensure and confirm, as presented in the previous Chapter 3, that the proposed combination of dynamic, weighted network indicators are sensitive to disruptions and can be effectively exploited to characterize resilience of large-scale networks.

4.1.3.1 Graph Weighting with the Floating Car Data

To introduce traffic dynamics in the NDC (Figure 4.5b), we assume that in free flow conditions (Figure 4.5a) the nodes are connected at the best possible level, *i.e.*, all edges have a weight equal to one. When travel time increases,edge weight progressively decreases to zero, with zero corresponding to the case of a completely congested edge, *i.e.*, a road segment where vehicles are completely stuck. By considering the principle of bounded rationality for modelling drivers' behaviors (Jones, 1999; Sivak, 2002), we assume that a small travel time increase should produce a negligible impact on the edge weight (Figure 4.5c). Finally, we adopt a discretization process in order to improve the relevance of the edge weights and to consider a group of edges equivalent when traffic conditions (travel time) are similar, but not necessarily equal. We assume that a travel time increase lower than a free flow travel time fraction (*i.e.*, $\alpha \cdot fftt$) has no impact on the drivers' route choice decisions. We choose $\alpha = 0.2$. In our analysis, the longer per-edge free flow travel time is of 12 minutes. In this case, a travel time of 14.4 minutes ($(1+\alpha) \cdot fftt$) is considered as recorded in free flow conditions. In general, for a given edge, its weight is assumed to be constant at its highest possible value of 1 for an observed travel time in the range $[0, fftt + \alpha \cdot fftt]$ (Figure 4.5c). Beyond this limit, we impose a progressive decrease of the weight value on the edge, as a step-wise hyperbolic function of the observed travel time. In Figure 4.5c, the orange curve represents the ratio between the free flow travel time and the observed travel time. The blue curve is the discretized travel-time ratio which considers the drivers' bounded rationality principle. The blue curve is the one used to determine the edge weight in a given time slot. In other words, by the proposed discrete function, we can model the level of service on each road link, by also taking into account the impact of the (bounded rational) driver's route choice process. An edge with a larger

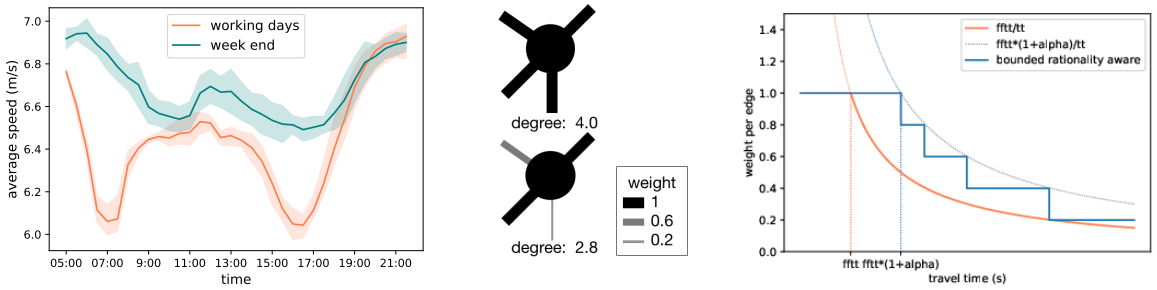

(a) Average Speeds **(b)** Weighted NDC **(c)** Weight distribution

Figure 4.5: (a) Average speed profiles for the week days (orange) and the week ends (blue). (b) Computation of a node's unweighted (top) and weighted (bottom) NDC. (c) Attribution of a weight to an edge based on observed travel time (in a given time slot) and free-flow travel time.

weight (closer to 1) represents a road segment with close-to-free-flow conditions, while lower-weight edges represent less likely preferable alternatives for drivers, exposed to higher congestion or disruption, that are working at a reduced level of service. With this method, only significant travel time variations can actually impact the ability of an edge to connect nodes.

4.1.3.2 Graph Weighting with the Loop and Taxi Trip Data

Regarding the loop and taxi trip data, we consider a graph weighted by the average taxi travel times. However, the map-matched taxi data do not cover all the edges of the whole Rhône-Alpes region's graph homogeneously. For instance, the main urban roads and commuting areas, such as the rail-station or airport, are much better covered by the taxi data than minor roads. Thus, we filter the initial road network to obtain a relevant sub-graph of the road network and properly capture traffic conditions via the available data, several modelling choices were performed. Because of the constraint amount of data, we decided to use an average day (instead of a specific day), built on the aggregation of several days, focusing our analysis on the part of the day when we have more data, i.e., the morning peak hour 07:00-10:30, during which we observe the average hourly flow reported in Figure 4.4b. Finally, we selected a time period of 30 minutes for our dynamic analysis (large enough to have statistically significant average taxi travel time computed via the available samples). Based on these choices, our methodology to compute the graph used for the analysis is based on three steps: (1), we retain only the links of the original Rhône-Alpes graph on which we can assume average taxi travel time is statistically significant (at least 5 samples of travel time available per edge and time slot). This step reduces the size of the original graph to only 1 703 links. The retained edges create a highly disconnected sub-graph; (2), we complete the sub-graph by concatenating the retained edges via selected links from the original Rhône-Alpes graph that correspond to primary (*i.e.*, highways) and secondary (*i.e.*, main urban roads) segments of the road network. We compute the largest weakly connected component of the previous graph. The resulting graph is composed of 7 867 nodes and 12 406 edges; (3), we assign a travel time to all the links of the graph as a weight for each time slot. To that purpose, we divide the links in three categories: *i) observed links* (1 395 in total) for which the weight is computed as the average travel time directly estimated from the available samples (average of at least 5 travel times per slot); *ii) partially observed links* (9 071 in total) for which some samples of travel time exist but in a number insufficient for defining the link as relevant. We assume these links to have a constant travel time over the different slots (which we label as free-flow travel time) and compute it by averaging the travel time samples available over all the observed time periods; *iii) unobserved links* (1 940 in total) that are not covered at all by taxi data (no sample available) and for which we assign a free-flow travel time computed via speed limit and length of the link. The final reconstructed graph is shown in Figure 4.4a.

4.2 Traffic Condition-Sensitive Node Degree Centrality

In this section, we focus on the global characterization of the network resilience. Based on Gao et al. (2013) analysis (Section 2.2.2.2), we aim at quantifying the impact of a disruption using a NDC-based approach considering the network Heterogenity (H). We aim at defining how effectively the edge connects nodes by taking into account the actual traffic conditions in the NDC computation. As a reminder, Gao et al. (2013) characterizes resilience of ecological networks by first describing the system through the self-dynamics of each component as well as their interactions, and second by defining the transition state between normal and disturbed conditions.

4.2.1 Node Degree Centrality Distribution Shifting

As a consequence of the assumption described in the previous section, a travel time increase (caused by congestion phenomena or perturbations) on one edge will imply a reduction in adjacent nodes' weighted NDC (Figure 4.5b). By generalizing such reasoning to the whole network, we suppose that in presence of a disturbance, the NDC distribution is shifted toward the zero value. This phenomenon is amplified with the disruption intensity and, particularly, in the case of weak-resilient networks. On the contrary, when the offset towards zero of the NDC distribution is negligible in presence of major disruption affecting the whole network, we can assume the network has higher resilience, by being able to maintain a good level of connection among its nodes. However, it is worth noting that, in presence of localized disturbances, the shift of the NDC distributions towards zero could be weak at a global scale (i.e., the whole network), whereas some local areas could be nonetheless strongly impacted. Hence the interest to study the NDC distribution also at a local scale, in order to analyze resilience of the different areas of the network. To that purpose, we always extract the NDC values over the whole network to take into account the actual traffic dynamics and to preserve network connectivity. However, we analyze and compare both the NDC distribution at network scale (*i.e.*, all nodes) and the distribution of the centrality values for a subset of nodes localized around the area mostly impacted by the perturbation. Moreover, to quantify the offset in NDC distributions, we compute the curves of the average NDC (known as Network Density ($\langle NDC \rangle$)) over time under normal conditions and in presence of disturbance. Then, we measure the area between the curves. As for the NDC distribution offset, the gap between the curves depends on the network resilience and the disruption intensity.

4.2.1.1 Global Scale

First, we focus on the typical average speed represented by the blue curves of Figure 4.3a-Figure 4.3d. We notice a lower typical average speed for the first three scenarios (Figure 4.3a-Figure 4.3c) than for the last typical one (Figure 4.3d). Whereas the three first typical days are working ones, respectively Monday, Tuesday and Wednesday, the last one takes place during a weekend, specifically on a Saturday with different operating conditions in terms of traffic loads. This explains the difference in typical speed profiles computed under normal conditions. The same trend is noticeable in the NDC distributions computed for the speeds of the typical days, displayed in blue (Figure 4.6a-Figure 4.6d). Under normal conditions, we notice a larger number of nodes possessing high NDC values (between 6.0 and 6.2) for the typical Saturday (Figure 4.6d) than for the other days (Figure 4.6a-Figure 4.6c). We plot the NDC distributions at $7:30$ am because we consistently noticed a major change between the typical and the observed average speed profiles at this specific time slot (Figure 4.3a-Figure 4.3d). For all the studied cases (Figure 4.6a-4.6d), a higher number of nodes, possessing a NDC value between 6.0 and 6.2, is observed for the typical distribution than for the disrupted one. This observation is true for the intervals with high NDC values. On the contrary, for the ranges grouping small NDC values, lower than 3.0, the trend is reversed: there is a larger number of nodes for such NDC values in the deteriorated situation than in the normal one. Therefore, in the presence of disruptions, the NDC distributions appear to be shifted to the left, *i.e.*, towards zero. This aspect is exacerbated for the first disruption (Figure 4.6a), presenting the most relevant impact on the average speed profile (Figure 4.3a). The comparison of the gap between the two curves, representing the average NDC, corroborates the impression. Whereas the area between the curves is equal to 5.24 for the first disruption (Figure 4.6e), for the second one it is only equal to 4.31 (Figure 4.6f). For any specific case, when computed in disrupted conditions, the average NDC is always lower than the one measured under normal conditions (Figure 4.6g and Figure 4.6h) on the same day of the week. The fact that we consider bounded rationality in the graph weighting process (Section 4.1.3.1) contributes to determine more evident variations (*i.e.*, decrease) of the average NDC, with respect to those observable on the average speed profiles. Finally, the visualisation of the relative error between the weighted NDC (Figure 4.6i and Figure 4.6j), issued from the typical and abnormal speed profiles, provides information about the spatial localization of the disturbance at $7:30$ am. We notice a stronger impact for the snowfall scenario than for the tunnel closure. There are

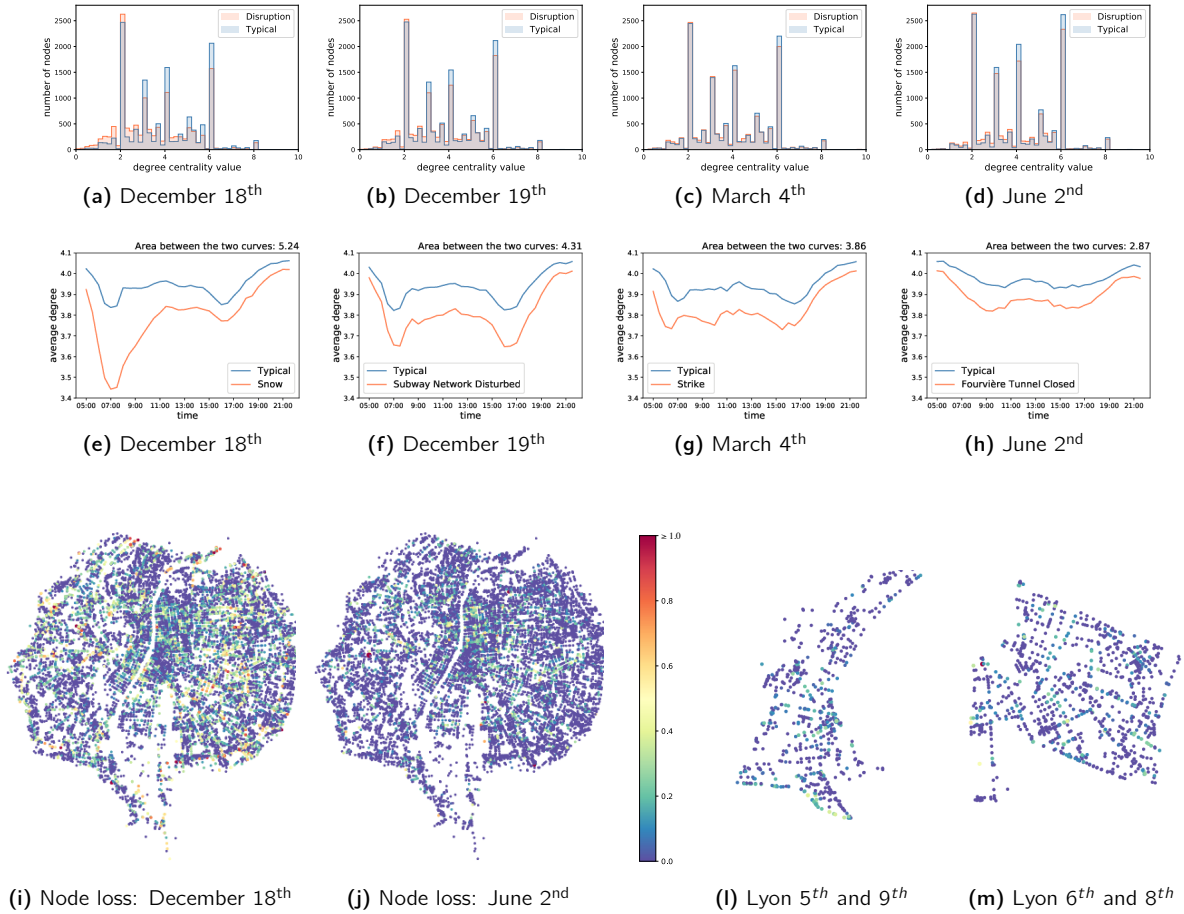

(a) December 18th **(b)** December 19th **(c)** March 4th **(d)** June 2nd

(e) December 18th **(f)** December 19th **(g)** March 4th **(h)** June 2nd

(i) Node loss: December 18th **(j)** Node loss: June 2nd **(l)** Lyon 5^{th} and 9^{th} **(m)** Lyon 6^{th} and 8^{th}

Figure 4.6: The NDC distribution (a)-(d) and the average NDC (e)-(h) are plotted for the four disrupted situations. The NDC distribution is computed at 7 : 30 am as well as the relative error of the NDC in typical and disturbed situations observed per node at global scale (i),(j) and by zooming over the areas that are closer (k) or less close (l) to the closed tunnel.

more nodes with a high relative error on Monday, December 18th (Figure 4.6i), where non-zero values are more dispersed on the network, than for Saturday, June 2nd (Figure 4.6j). By zooming on the studied areas on June 2nd, we notice a higher proportion of nodes with a deteriorated level of service in the districts close to the tunnel than for the other studied ones. In Lyon 5^{th} and Lyon 9^{th} (Figure 4.6l), 44% of nodes have a lower level of service with the tunnel closure, against 26% of nodes in Lyon 6^{th} and Lyon 8^{th} (Figure 4.6m).

4.2.1.2 Local Scale

We focus now on the impact of the tunnel closure and the snowfall at local scale by observing the behavior of the network locally. We focus on four areas: Lyon 5^{th} and Lyon 9^{th}, localized around the Fourvière tunnel, more likely to be disturbed, and Lyon 6^{th} and Lyon 8^{th} farther from the tunnel. First, one can notice a stronger change in the NDC distribution for the districts including and surrounding the tunnel (Figure 4.7e and 4.7f). The decrease of the number of nodes with NDC value between 6.0 and 6.2 is more important for these areas than for the two other ones (Figure 4.7g and 4.7h). The average NDC gap, assessed by computing the area between the curves, confirms the observation. We notice a greater reduction in the average NDC for Lyon 5^{th} and 9^{th}, with an area between the two curves respectively equal to 5.56 and

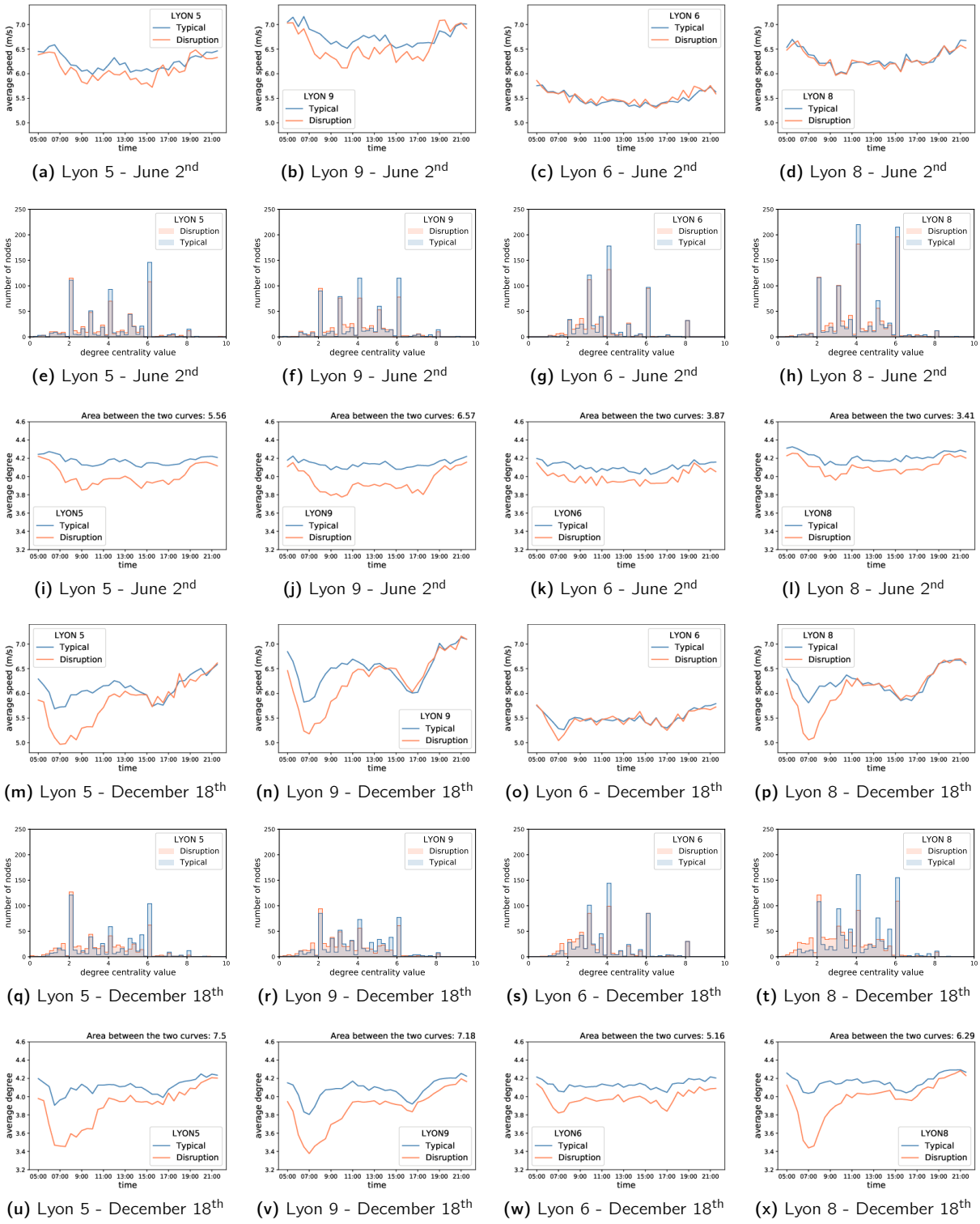

(a) Lyon 5 - June 2nd **(b)** Lyon 9 - June 2nd **(c)** Lyon 6 - June 2nd **(d)** Lyon 8 - June 2nd

(e) Lyon 5 - June 2nd **(f)** Lyon 9 - June 2nd **(g)** Lyon 6 - June 2nd **(h)** Lyon 8 - June 2nd

(i) Lyon 5 - June 2nd **(j)** Lyon 9 - June 2nd **(k)** Lyon 6 - June 2nd **(l)** Lyon 8 - June 2nd

(m) Lyon 5 - December 18th **(n)** Lyon 9 - December 18th **(o)** Lyon 6 - December 18th **(p)** Lyon 8 - December 18th

(q) Lyon 5 - December 18th **(r)** Lyon 9 - December 18th **(s)** Lyon 6 - December 18th **(t)** Lyon 8 - December 18th

(u) Lyon 5 - December 18th **(v)** Lyon 9 - December 18th **(w)** Lyon 6 - December 18th **(x)** Lyon 8 - December 18th

Figure 4.7: The average speed, the NDC distribution and the average NDC are plotted for the north-south direction tunnel closure(a)-(l) and the snowfall (m)-(x) for different districts: 5^{th}, 6^{th}, 8^{th} and 9^{th} districts of Lyon. The NDC distributions (e)-(h) and (q)-(t) are computed at 7 : 30 am.

6.57 (Figure 4.7i and Figure 4.7j), than for Lyon 6^{th} and 8^{th} (Figure 4.7k and Figure 4.7l). These districts, far from the disruption, present an area between the two curves of around 3.50. These observations are in accordance with the respective average speed evolution (Figure 4.7a-Figure 4.7d). The second scenario, related to snowfall, strongly impacts most of the considered areas. The 6^{th} district of Lyon is the only one which conserves a similar behavior in both conditions (typical and disrupted). In this neighborhood, the NDC distribution is not modified for the highest NDC values (Figure 4.7s). Compared to the typical situation, the reduction of the NDC occurrence only happens between 3.0 and 4.2. Such an offset has a limited impact on the average NDC. Here also, the conclusions on NDC distributions and the average NDC profiles are in accordance with the average speed evolution (Figure 4.7m-Figure 4.7p). The comparison of the results obtained in the two studied scenarios also provides insights about the road network and associated traffic dynamics. We notice a lower proportion of nodes with high NDC values (between 6.0 and 6.2) in Lyon 5^{th} during the typical Monday than during the typical Saturday. A similar trend is observed for the 9^{th} and the 8^{th} districts of Lyon, where this phenomenon is amplified. These results are in accordance with the average speed difference between the working days and the weekend (Figure 4.5a, Figure 4.7a-Figure 4.7d and Figure 4.7m-Figure 4.7p). Lyon 6^{th} conserves similar NDC distributions and similar average NDC in both studied scenarios, although the area between the curves is a bit higher with the snowfall than for the Fourvière tunnel closure. For the other areas, the results indicate an impact over the traffic conditions due to disruptions. Regarding our assumption, the 6^{th} district of Lyon is the most resilient one. This could be explained by a lower typical average speed. Consequently, the gap with the average speed in presence of disruption will be smaller.

Having studied the weighted NDC behaviors, we focus on the previously presented metrics ((2.8), (2.9) and (2.10a)) although the network $\langle NDC \rangle$, *i.e.* the average NDC, had already been under consideration. The combination of the three indicators will allow us to characterize the network state under different traffic conditions in a spatio-temporal way (Gao and Albert-László Barabási, 2016) (Section 2.2.2.2).

4.2.2 Heterogeneity Analysis

Besides characterizing the impact of perturbations through the NDC distribution shifting, we globally study network resilience by measuring its H (2.9), $\langle NDC \rangle$ (2.8) and S (2.10a) properties. In that sense, we follow an approach similar to the one proposed by Gao and Albert-László Barabási (2016) to determine resilience of ecological networks (Section 2.2.2.2). Based on the weighted in- and out-NDC, these measures become sensitive to the traffic conditions. The NDC (resp. in-NDC, out-NDC) of a node, used to compute the three indicators, is thus equal to the sum of the level of service of the connected links (resp. entering links, outgoing links) A spatio-temporal analysis, led by first computing the metrics per areas and then observing their evolution in time, provides interesting insights on the network characteristics and performances. Such an analysis allows to have a deep understanding of the network behavior. The comparison of the measures computed under both normal and disrupted conditions is realized in time or at a given time step, for the whole network or by focusing on different areas. Like for the NDC distribution shifting analysis, for this spatial analysis, we compute the weighted NDC over the whole graph and then extract the NDC values of the nodes surrounding the area interested by the perturbation.

By comparing the values of H, $\langle NDC \rangle$ and S in normal and disturbed conditions, at global scale, we aim at characterizing the magnitude of a speed reduction over the network. We conduct both temporal and spatial analysis. Firstly, we perform a temporal analysis by plotting the network characteristics from 5:00am to 9 : 00 pm, every two hours. Secondly, we quantify the local impact of disruptions by computing the metrics through the NDC distributions of the nodes included in the studied areas. This local analysis also allows to detect localized events hardly detectable at the global scale, but it also provides information on resilience of specific sub-networks. As an indicator of the impact of the disruption over the metrics, we compute the Euclidean distance between the points determined by the three measures computed in different situations.

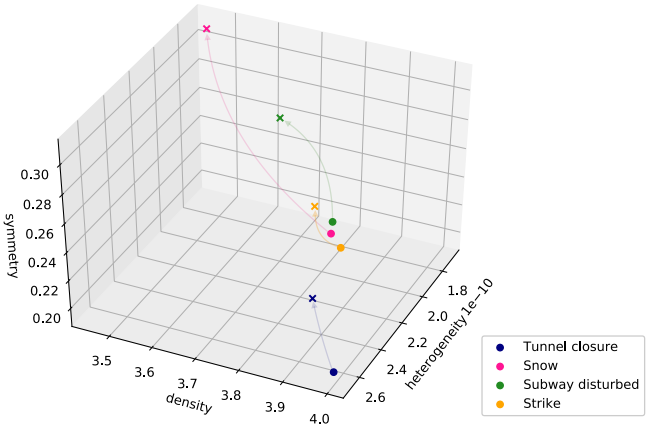

(a) Several disruptions at 7 : 30 am

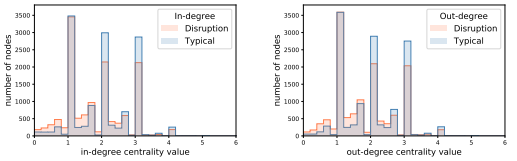

(b) Evolution of in-NDC and out-NDC in presence or not of snow (18/12/2017) at 7 : 30 am

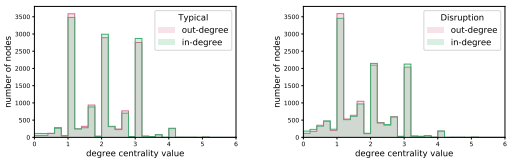

(c) Overlay of in-NDC and out-NDC in presence or not of snow (18/12/2017) at 7 : 30 am

Figure 4.8: The Heterogenity (H), the Symmetry (S) and the Network Density ($\langle NDC \rangle$) for the whole network are plotted under normal conditions (•) and in presence of disruptions (×) in (a) at 7 : 30 am. The distributions in (b) correspond to the in- and out-NDC under normal condition and in presence of the snowfall at 7 : 30 am. The histograms overlay the in- and out-NDC distributions in a typical situation (c) and in the presence of the snowfall (d) at 7 : 30 am.

For the spatial analysis, all the metrics are computed at 7 : 30 am, where the impacts of disruptions are the strongest ones regarding the average speed profiles (Figure 4.5a). In the presence of the disruption (×), the graph $\langle NDC \rangle$ and its H decrease whereas the S grows comparing to the reference situations (•). In Section 4.2.1, we notice the NDC distribution shifting toward zero inducing the reduction of the network $\langle NDC \rangle$ (Figure 4.7). Therefore, the decline in H (2.9) is due to the diminution of the standard deviation of the in-NDC and out-NDC distributions. The rise of the S value reflects an increase in in-NDC and out-NDC correlation coefficient. When a disruption occurs, both in-NDC and out-NDC distributions move to zero, diminishing the corresponding average NDC. Nonetheless, this reduction is accompanied by a stronger decrease of the distribution standard deviation, hence the increase of the S. Figure 4.8b illustrates the difference of the in-NDC (left) and out-NDC (right) under normal or abnormal conditions. The Figure 4.8c shows a better overlay between the in-NDC and the out-NDC without disruption (left) or with (right). The correlation coefficient is thus higher in this second case. The evolution of these three topological indicators, dependent on the traffic dynamics, provides information about the traffic conditions. The lower the values of $\langle NDC \rangle$ and H the higher the value of S, with worse traffic conditions. The impact of disruptions (×) differs in intensity. The effect of the snowfall (red symbols) is stronger than all other considered scenarios: the corresponding cross and circle marks are the furthest apart, with an Euclidean distance of 0.40. This assumption is confirmed by the average speed evolution (Figure 4.5a) and the NDC shifting (Figure 4.6), which present the largest variations for such disruption. On the contrary, the smaller incidence is the one induced by the protesters (yellow symbols), with a distance between the reference and the disrupted situations of only 0.09. The disruption of the subway network (green symbols) and the tunnel closure (blue symbols) present moderate impacts with Euclidean distances respectively equal to 0.19 and 0.12. By comparing the four reference situations (•) computed over typical days, we notice a huge difference between the one corresponding to the tunnel closure and the other disruptions. Whereas the first disturbance occurs on a Saturday, all others happen during week days where typical travel times are lower (Figure 4.5a), explaining the difference in network states.

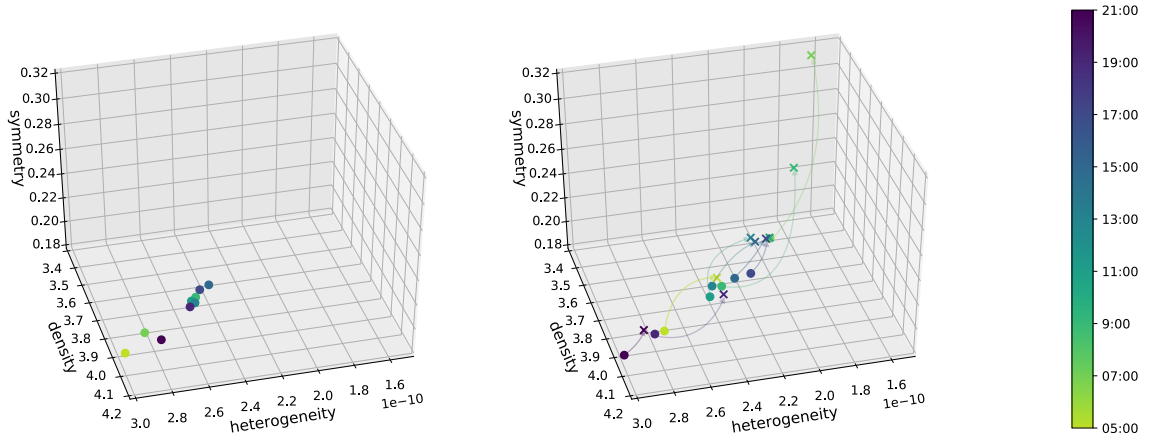

(a) June 2nd **(b)** December 18th

Figure 4.9: The H, the S and the network $\langle NDC \rangle$ of the global network are plotted under normal conditions on typical Saturday (a) and on typical Monday (b) (•) and in presence of the snowfall (×) in (b) each two hours, from 5:00am to 9 : 00 pm.

4.2.2.1 Global Scale - Temporal Analysis

Due to the dynamic nature of traffic conditions, we expect a time-dependent evolution of the network states also in presence of disruptions. To explore this aspect, we plot the indicators (S, $\langle NDC \rangle$ and H) for the typical Saturday (Figure 4.9a) and the typical Monday, as well as in the disturbed scenario of the snowfall (Figure 4.9b) from 5:00am to 9 : 00 pm, with a two-hours time granularity for the sake of readability. By leveraging a dynamic graph, we can characterize the time-dependent network state through the three indicators. In both situations, corresponding to a typical Saturday (Figure 4.9a) and a typical Monday (Figure 4.9b), the H and the $\langle NDC \rangle$ are the highest ones with the smallest S value for non-peak-hours slots (5:00am and 9 : 00 pm), when traffic conditions are better than during the day. Regarding the typical Saturday (Figure 4.9a), there are also good traffic conditions at 7 : 00 am, regarding the position of the corresponding point in the 3D-map. This statement is confirmed by the weekend speed with the shifting of the first reduction from 7 : 00 am to 9 : 00 am (Figure 4.5a). On the contrary, on a typical Monday (Figure 4.9b) we have the worst traffic conditions at 7 : 00 am due to the morning peak-hour. Nonetheless, we have good traffic conditions at 7 : 00 pm, in accordance with the speed profile of the working days (Figure 4.5a). In Figure 4.9b, we plot the network state when disrupted by the snowfall. The highest change between the typical situation and the disrupted one happens at 7 : 00 am and 9 : 00 am (Figure 4.9b), in accordance with the evolution of the speed profile (Figure 4.3a).

4.2.2.2 Local Scale - Spatial Analysis

To perform the spatial analysis, the metrics are computed for the four studied districts at the same time, 7 : 30 am. Figure 4.10a presents network $\langle NDC \rangle$, H and S on Saturday, June 2nd, 2018 when the north-south direction of the Fourvière tunnel was closed. Figure 4.10b illustrates the same metrics for the same districts impacted by a snowfall on December 18th. The impact over the 5^{th} and 9^{th} districts is stronger for the tunnel closure (Figure 4.10a) casthan for the two other areas. Indeed, the Euclidean distance between the point and the corresponding cross for the 5^{th} and 9^{th} districts of Lyon are respectively equal to 0.25 and 0.29, against 0.17 for the 6^{th} district and 0.16 for the 8^{th}. This trend was already observed with the average speed profiles evolution (Figure 4.7a-Figure 4.7d) and the NDC shifting (Figure 4.7e-Figure 4.7h).

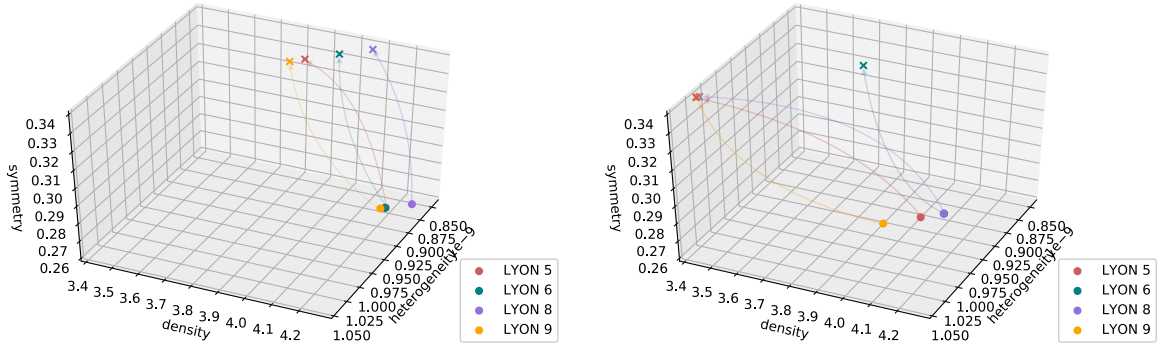

(a) June 2nd at 7 : 30 am

(b) December 18th at 7 : 30 am

Figure 4.10: The local H, the local S and the local network $\langle NDC \rangle$, are plotted under normal conditions (•) and in presence of the tunnel closure (×) in (a) and the snowfall (×) in (b) at 7 : 30 am for four districts.

Regarding the second disrupted situation (Figure 4.10b), the districts are similarly impacted, except the 6^{th}. We already observed this specific behavior with the NDC distribution translation analysis (Figure 4.7o, 4.7s and 4.7w). In any scenario, the Euclidean distances between reference situations and disrupted ones are larger for the snowfall than for the tunnel closure: respectively 0.54, 0.23, 0.60 and 0.44 for the 5^{th}, the 6^{th}, the 8^{th} and the 9^{th} districts. We notice a different behavior for the areas in terms of resilience. The network states, characterized by the observed measures of H, $\langle NDC \rangle$ and S, are close, even superimposed, for the 6^{th} and the 8^{th} districts for the typical Monday whereas in presence of the snowfall affecting both areas (Figure 4.10b), their corresponding parameters are far from each other. On the typical Saturday, the 8^{th} district has a different behavior under normal conditions (Figure 4.10a). This could be explained by the higher number of nodes. Moreover, in this area, there is a large amount of high NDC value. This could be caused by (i) a better topological node connection or (ii) a higher amount of nodes presenting free flow conditions. By computing the topological average NDC, we can affirm we are in the second case. Indeed, the average topological NDC is higher for the 6^{th} district than for the 8^{th}. The NDC distribution observed for the typical Saturday (Figure 4.7d) also shows this distinction by presenting a higher number of nodes with a large value than in other areas. Regarding the other districts (Figure 4.10a), the 9^{th} has a typical behavior close to the 5^{th} and the 6^{th} with a similar average speed profile (Figure 4.7a-Figure 4.7c). The trend changes during the working day (Figure 4.10b), where the area average speed profile is higher for 9^{th} district than the two other ones (Figure 4.7m-Figure 4.7o).

To summarize, by computing the NDC and other global metrics based on its distribution (H, S and $\langle NDC \rangle$) over a dynamically weighted graph, we consider static and dynamic aspects of a transport network and quantify resilience considering the topological vulnerabilities and the traffic conditions. The translation of the NDC distribution (Section 4.2.1) evolution has proved to be sensitive to disruptions, confirming our initial assumption. This change in NDC implies a modification in H, $\langle NDC \rangle$ and S used to compute the network state in the 3D-figure as performed Gao and Albert-László Barabási (2016). We notice a reduction in H and $\langle NDC \rangle$, associated with the increase of the S, as due to the presence of disruptions. The more intense the impact, the more amplified this behavior. Whereas the global scale results quickly provide an indication of the global resilience (Figure 4.9)), those related to a more local scale permit to precisely identify the areas more exposed to disruptions. A reduction in the global measures should be therefore analyzed also on a local basis, in order to properly react to the disruption. Indeed, we notice that some areas (6^{th} neighborhood of Lyon (Figure 4.10)) can maintain an acceptable level of service even in the presence of disruptions.

4.3 Traffic Condition-Sensitive Node Closeness Centrality

After computing the NDC over a dynamically weighted road network using FCD, we aim at characterizing the shortest paths evolution induced by the change in traffic conditions. First, we focus on the NCC metric. As noticed in Section 4.1.1, to compute the NCC, we use the reduced graph of Lyon (Figure 4.2c) weighted by the per 30 minutes averaged travel time from 5 : 00 am to 11 : 30 am, issued from the FCD. This time period is chosen regarding the traffic conditions (Figure 4.3a and Figure 4.2a). Indeed, we notice a huge decrease (resp.increase) of the speed (resp. travel time) at the beginning of the time period from 5 : 00 am to 7 : 00 am which corresponds to the morning peak hour. Then, the speed (resp. travel time) increases (resp. decreases) until the end of the time period. Regarding the disrupted scenario, traffic conditions are degraded with a huge difference in traffic conditions around 7 : 00 am between normal and disrupted conditions.

At global scale, Figure 4.11a presents the AE evolution under normal conditions (blue curve) and in presence of the snowfall which occurs on 18^{th} Decembre 2017 (red curve) (Figure 4.3a) (Section 4.1.1). The huge decrease of the metric, for both traffic conditions, from 5 : 30 am to 7 : 30 am, is related to the speed (Figure 4.3a) and travel time (Figure 4.2a) evolution during the same period, corresponding to the morning peak hour. With the snowfall, the AE is always lower than under normal conditions. Because the average travel time in presence of disruption is higher than under normal conditions (Figure 4.2a), the network performances are degraded, reducing the reachability between the nodes of the network. Figure 4.11b shows the NCC distributions at both 7 : 30 am and 9 : 30 am under normal conditions. We notice that at 7 : 30 am, the NCC distribution is shifted to the 0-values compared to the NCC distribution at 9 : 30 am, in accordance with the AE evolution which is higher at 9 : 30 am ($2.06e^{-3}$) than at 7 : 30 am ($1.83e^{-3}$). Because the travel time is higher at 7 : 30 am (Figure 4.2a), the nodes are further from each other and it is longer to join the different places of the network. In presence of the snowfall, the NCC distribution (Figure 4.11c) presents a similar trend: at 7 : 30 am, when the traffic conditions are degraded (Figure 4.3a), the distribution is shifted to the 0-values, as the NDC. In such situation also, the AE evolution which is higher at 9 : 30 am ($1.83e^{-3}$) than at 7 : 30 am ($1.51e^{-3}$). The reachability of the nodes is reduced due to the travel time increase. As observed with the AE evolution, we notice that under normal traffic conditions the NCC distributions present higher values than in presence of disruption. Indeed, at 9 : 30 am under normal conditions, about 300 nodes present NCC values higher than $2.00e^{-3}$ whereas in presence of the snowfall, no edge has such a value. At 7 : 30 am, the difference is stronger. Whereas in presence of disruption, no node has a NCC greater than $1.50e^{-3}$, under normal conditions about 1 500 nodes have such NCC values.

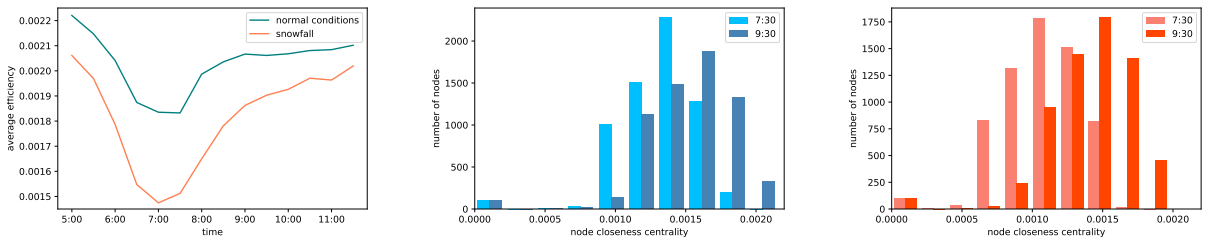

(a) AE under normal conditions and in presence of a snowfall **(b)** NCC evolution under normal conditions **(c)** NCC evolution in presence of disruption

Figure 4.11: Evolution of the AE under normal conditions and in presence of disruption (a), and difference in NCC distribution between 9 : 30 am and 7 : 30 am under normal conditions (b) and in presence of disruption (c).

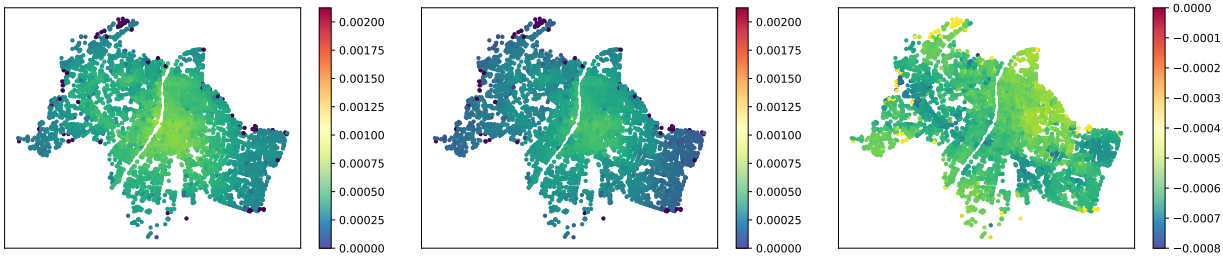

(a) NCC under normal conditions (7 : 30) **(b)** NCC in presence of disruption (7 : 30) **(c)** Spatial NCC difference between disrupted and normal conditions (7 : 30)

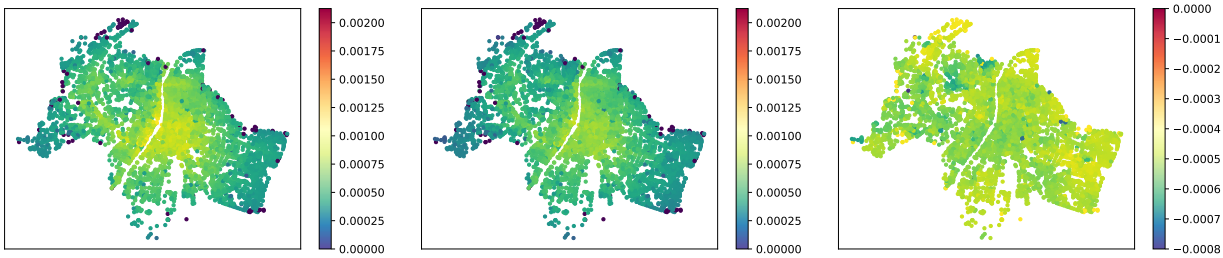

(d) NCC under normal conditions (9 : 30) **(e)** NCC in presence of disruption (9 : 30) **(f)** Spatial NCC difference between disrupted and normal conditions (9 : 30)

Figure 4.12: NCC spatial distribution under normal conditions (a)(d) or in presence of disruption (b)(e) and the difference in values distribution between both situations (c)(f) at 7 : 30 and at 9 : 30 am.

The spatial impact of the disruption over the NCC is analyzed in Figure 4.12. At 7 : 30 am, the nodes located in the city center, under normal conditions (Figure 4.12a), are better connected than the ones in the periphery. Such an observation is amplified by the side-effect which artificially reduced the reachability of the nodes located at the graph extremities. At 9 : 30 am, the spatial distribution of the NCC is similar but the reachability is globally increased with higher NCC values (Figure 4.12d), which is in accordance with the AE evolution (Figure 4.11a) related to the travel time decreases (Figure 4.2a). In presence of the snowfall, the network performances are also better at 9 : 30 am (Figure 4.12e) than at 7 : 30 am (Figure 4.12a) and the central nodes are the more accessible ones, by being closer to each other in terms of travel time, as proved the NCC. Regarding the impact of the snowfall, we notice a reduction in the NCC, meaning that the nodes are less accessible than under normal conditions. At 9 : 30 am, the spatial distributions in presence of disruption is closer to the one recorded under normal conditions, with a NCC reduction which does not exceed $-0.4e^{-3}$ (Figure 4.12f), contrary to the NCC reduction observed at 7 : 30 am which reaches $-0.8e^{-3}$. This is in accordance with the travel time evolution which highlights a stronger impact at 7 : 30 am than at 9 : 30 am.

Such results are in accordance with the conclusions found with the simulated data-based analysis (Section 3.2.3. Computed over a dynamically weighted graph, the AE and the NCC can capture the traffic dynamics, modifying the reachability of the nodes depending on the travel time evolution. The impact of a disruption is also visible with both metrics which is essential in resilience characterization.

4.4 Traffic Condition-Sensitive Edge Betweenness Centrality

As a first step, we observe the ability of the EBC to capture both the traffic dynamics and the disruption impact when computed over a dynamically weighted graph (Section 4.4.1). Such an analysis is led with FCD, on the reduced graph of Lyon (Figure 4.2c) (Section 4.1.1). As a second step, we pursue the correlation analysis began with simulated data (Section 3.4). We extend the analysis with real data to understand the distinction between the correlated, the anti-correlated and the non-correlated EBC and flow edges behavior (Section 4.4.2). Such an analysis is led with the combination of both Loop and Taxi Trip data (Figure 4.4) (Section 4.1.2).

4.4.1 Weight Discretization and Disruption Impacts

Similarly to the NCC computation, we focus the analysis over the reduced road network of Lyon (Figure 4.2), weighted by the per 30 minutes averaged travel time, using the FCD (Section 4.1.1). As for the simulated data-based analysis (Section 3.2.2), we compute the GEBC which is the sum of all the EBC, to observe the metric evolution at global scale. The impact of the discretization, which leads to reproduce the drivers' behavior more accurately by considering the bounded rationality, is also analyzed. To do so, we discretized the travel time by assuming that the drivers consider equal paths whose increase does not exceed 0.2 times, the initial travel time: $t \equiv \frac{t' \times (1+\alpha) - t'}{2}$ for $t \in [t', t' \times (1+\alpha)]$ with $\alpha = 0.2$.

The evolution of the GEBC, follows the traffic conditions (Figure 4.13a). A travel time increase implies a GEBC rise. The impact of the disruption is identified with the huge increase of the GEBC from 5 : 30 am to 7 : 30 am, going from 5.45 to 5.9, which corresponds to the time period where the disruption presents the strongest impact (Figure 4.3a and Figure 4.2a). The real data-based analysis supports the conclusions issued from the simulated data-based analysis (Section 3.2.2), ensuring that the EBC is dependent to the traffic conditions when computed over a dynamically weighted graph (Section 3.2.2). The discretization has no significant impact on the GEBC (Figure 4.13), expect during the morning peak hour, around 7 : 00 am, under normal conditions and in presence of the snowfall, from 5 : 30 am to 8 : 00 am, corresponding to the time period with the worst traffic conditions (Figure 4.2a). Indeed, at this time, with the discretization of the weights, the GEBC is slightly reduced compared to the one computed with undiscretized travel times. Regarding the EBC distribution, at 7 : 30 am and 9 : 30 am, under normal conditions (Figure 4.13b) and in presence of disruption (Figure 4.13c), we observe the same trend: at 9 : 30 am, the distribution is a bit shifted to the 0-values. The number of edges with an EBC higher or equal than 0.2 is larger in presence of disruption whatever the time stamp. More edges become critical in terms of EBC due to the larger set of crossed edges by the shortest paths induced by the traffic conditions and the involved, necessary, bypasses.

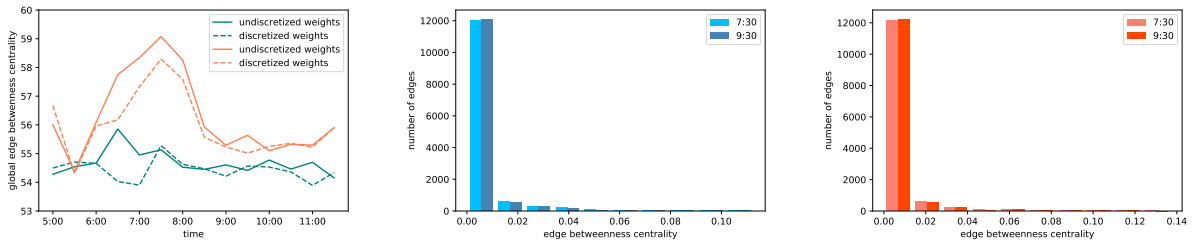

(a) GEBC under normal and disrupted conditions

(b) EBC distribution under normal conditions at 7 : 30 am and 9 : 30 am

(c) EBC distribution in presence of disruption at 7 : 30 am and 9 : 30 am

Figure 4.13: Impact of the weight discretization (dark green: undiscretized, green: discretized) at global scale under normal conditions or in presence of a snowfall (a) and evolution in the EBC distribution between 7 : 30 am and 9 : 30 am under normal (b) and disrupted (c) conditions.

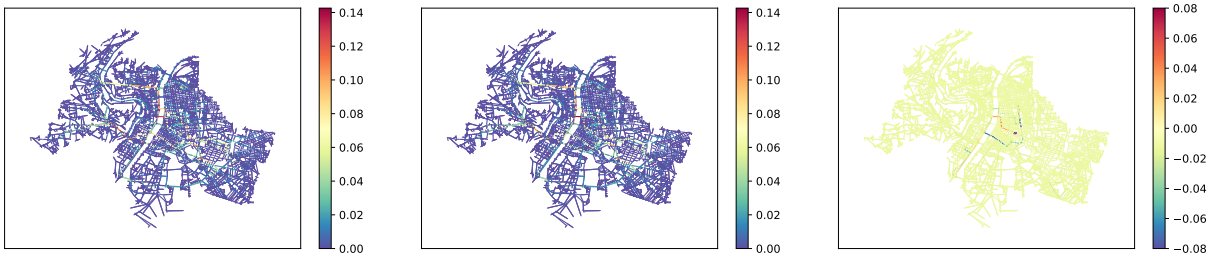

(a) EBC in presence of the snowfall with undiscretized weights (7 : 30)

(b) EBC in presence of the snowfall with discretized weights (7 : 30)

(c) Spatial EBC difference between discretized and undiscretized weights (7 : 30)

Figure 4.14: EBC distribution in presence of a snowfall at 7 : 30 am with undiscretized (a) and discretized (b) weights. The difference in the EBC distribution between discretized a undiscretized weights (c).

Figure 4.14 presents the spatial distribution of the EBC computed with discretized weights at both 7 : 30 am (Figure 4.14b) and 9 : 30 am (Figure 4.14b). The impact of the weight discretization, compared to the EBC computed with undiscretized weights, is presented at 7 : 30 am in Figure 4.14c in presence of a snowfall. At global scale (Figure 4.13a), we notice a modification in the GEBC between discretized and undiscretized weights at these time stamps with a lower value of GEBC with the weight discretization. Regarding the spatial distribution of the EBC, we notice that the weight discretization hugely impact a small set of edges. Indeed, we observe a huge increase in the EBC (+0.08) (Figure 4.14c), compared to the metric obtained with the undiscretized weights, on the Wilson bridge (Figure 4.2c (yellow)) and an equivalent reduction of the EBC (−0.08) over the close Université bridge (Figure 4.2c (blue)). With the weight discretization, the Wilson bridge appears as an attractive path by being part of a huge amount of shortest paths, increasing its EBC. On the contrary, Université bridge which is no longer the unique shortest path, lose its initial attractiveness with a reduction of the EBC. For most of the edges, the EBC is reduced (−0.01) with the weight discretization due to the increase of shortest paths alternatives. The EBC values is modified when computed with discretized (Figure 4.14b) and undiscretized (Figure 4.14a) weights which is in accordance to the GEBC diminution (Figure 4.13a).

Figure 4.15 highlights the impact of a snowfall at 7 : 30 am and 9 : 30 am over the spatial distribution of the EBC, which is modified (Figure 4.15c and Figure 4.15f). Indeed, the shortest paths are modified implying a reduction of the EBC for the edges belonging to the initial shortest paths, recorded under normal conditions, and an increase of the EBC for the edges belonging to the new shortest paths, observed in presence of the snowfall. These modifications mostly impact the city center of Lyon. In accordance with the speed and travel time profiles (Figure 4.3a and Figures 4.2a), the change in the EBC results are strongly impacted at 7 : 30 am, where we observe a larger set of colored (blue or red) edges (Figure 4.15c) than at 9 : 30 am (Figure 4.15f). Because of the bad traffic conditions, the shortest paths change and cross other edges, impacting the edge criticality recorded with the EBC. For instance, at bot 7 : 30 am and 9 : 30 am, the Wilson bridge, as the path allowing to reach Cours Gambetta (extension of Cours Albert Thomas (Figure 4.2c (orange))) via Avenue Marechal Saxe (Figure 4.2c (green)), is more critical (+0.08 at 7 : 30 am and +0.06 at 9 : 30 am) in presence of the snowfall by being crossed by a larger set of shortest paths. This path permits to bypass the southern bridges which presents a reduction in EBC value. Some of the major arterial roads at the east of the city (Avenue Lacassagne (Figure 4.2c (purple)) and Cours Albert Thomas) highlights a decrease of the EBC. The shortest paths no longer cross these roads but prefer the smaller road around to avoid the congestion.

These results prove the ability of the EBC to be sensitive to traffic dynamics. The analysis of the weight discretization impact proves the importance of considering the bounded rationality in the graph weighting to compute the EBC. Finally, we observe the impact of a snowfall recorded with the EBC.

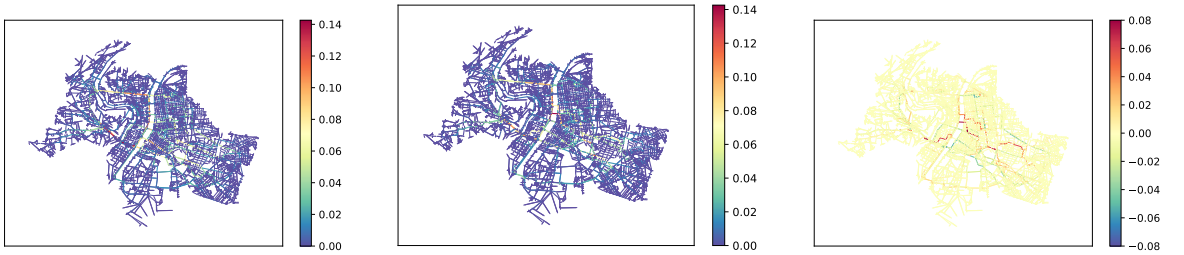

(a) EBC under normal conditions with discretized weights (7 : 30)

(b) EBC in presence of the snowfall with discretized weights (7 : 30)

(c) Spatial EBC difference between disrupted and normal conditions (7 : 30)

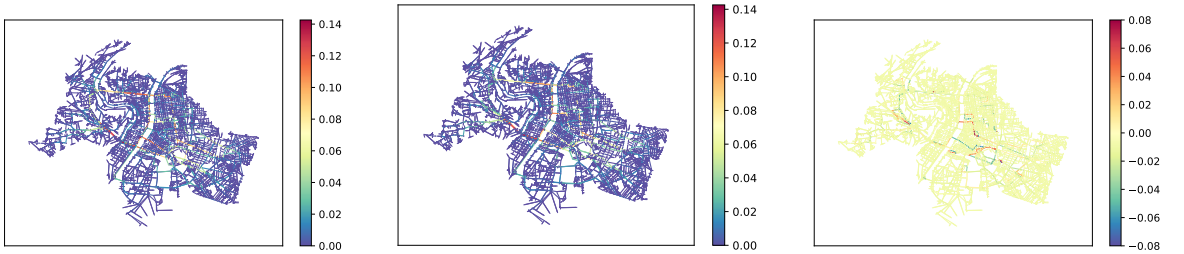

(d) EBC under normal conditions with discretized weights (9 : 30)

(e) EBC in presence of the snowfall with discretized weights (9 : 30)

(f) Spatial EBC difference between disrupted and normal conditions (9 : 30)

Figure 4.15: EBC distribution in presence of a snowfall with discretized weights at 7 : 30 am (a) and at 9 : 30 am (d) with the spatial distribution difference compared to normal conditions (b)(e). The difference in the EBC distribution under normal conditions and in presence of a snowfall (c)(f).

4.4.2 Correlation Between the Edge Betweenness Centrality and the Flow

To complete the simulation-based analysis (Section 3.4), we performed a second set of analyses based on multi-source real data from the city of Lyon. We study spatio-temporal correlations by leveraging travel time data (estimated from GPS taxi logs (Section 4.1.2)) to dynamically weight our graph and compute shortest paths. The computed EBC values are then correlated to flow values observed, via loops detectors, on the edges.

4.4.2.1 Static Correlation Analysis

Due to the unavailability of entry-exit and complete demand data for the whole network reported in Figure 4.4a, we were not able to compute the DS and entry-exit variants of EBC in the real data case. Moreover the demand data used in the simulated analysis (Chapter 3) are not available on the entire Lyon's transport network. We restrict therefore the real-data analysis to the following metrics: UEBC, FFEBC and TTEBC (Tab. 3.1). In Figure 4.16a and Figure 4.16b, we present the results of the linear least squares regressions performed between the selected EBC metrics (computed on a static graph) and the hourly flows observed on network edges. The results show a 0.34 value of r^2 for UEBC and a 0.40 value of r^2 for FFEBC, validating the capability of static EBC metrics to explain flow distribution on the network. This result, already claimed in the literature and in the previous section, is validated in a real case study. As in our previous simulation-driven analysis (Section 3.4.2.1), we report in Figure 4.16c the evolution of the correlation between flow and three metrics: the static (UEBC and FFEBC) and the dynamic (TTEBC) ones, the latter computed using average taxi travel times. Consistently with our previous simulation-based analysis, we can observe that TTEBC is sensitive to traffic dynamics. Indeed, we observe an important drop of correlation during rush hours 07:30-09:00 for TTEBC whereas FFEBC remains constant.

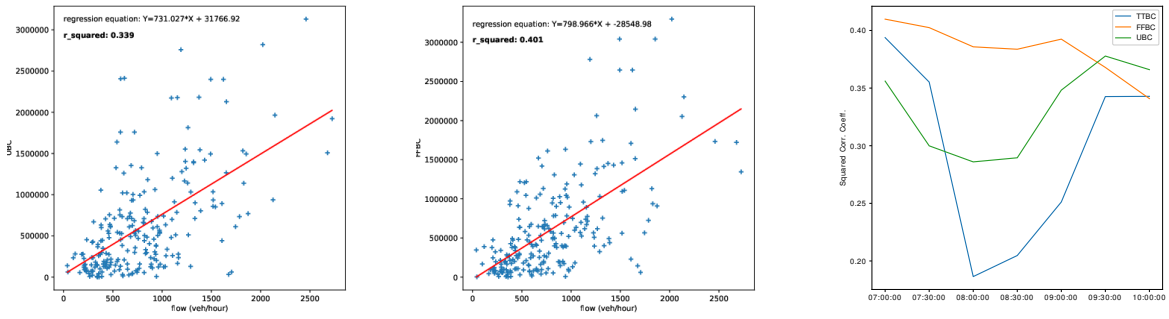

(a) UEBC (r^2 = 0.34) **(b)** FFEBC (r^2 = 0.40) **(c)** Evolution of r^2 over time

Figure 4.16: Correlation of per-edge average traffic flow and different EBC metrics (UEBC, FFEBC). Correlation between different metrics (UEBC, FFEBC, TTEBC) and Flow during all the period

4.4.2.2 Dynamic Correlation Analysis

In order to have a deeper understanding of the interactions between TTEBC and traffics dynamics, we have studied the per-edge temporal correlation. The spatial map reported in Figure 4.17a highlights the H of this correlation. To simplify the analysis, we classify links in three categories. The first one represents *highly* anti-correlated links, that is edges with negative correlation (r value in the range [-1, -0.4]). The second category refers to *positively* correlated links (r value in the range [0,4 to 1]). The third one includes *neutral* links with either a low positive or a low negative correlation (r value in the range [-0.4 to -0.4]). According to the boxplots shown in Figure 4.18, these three categories have different characteristics. The first boxplot (Figure 4.18a) is related to a congestion indicator calculated as the average relative difference between the observed and free-flow speed. The higher this indicator, the more congestion on a link. We observe that anti-correlated links are globally more congested (critical flow) than the positively correlated ones (free-flow). It is worth noting that in our network there is no link with very high congestion, which can contribute to high positive correlations. This behavior is also confirmed by the fact that the average link flow and FFEBC are higher for anti-correlated links than correlated ones as show in Figure 4.18b and Figure 4.18c. We analyze the detail of these dynamics (related to TTEBC and flows) by focusing on a specific region of the analyzed graph including two roads with a mirror behavior in terms of temporal correlation, *i.e.*, Quai Dr. Gailleton (QDG) and Quai Claude Bernard (QCB). Since FFEBC of QDG is much higher than FFEBC of QCB (see values reported in Figure 4.17b), QDG should typically attract larger flow than QCB, as confirmed by the observed average flow of QDG equals to 2 679 veh/hour, significantly higher than the one observed on QCB (967 veh/hour). A high FFEBC combined with a high average flow suggests that the link is slightly congested (*i.e.*, close to critical flow). Indeed, we confirm from the available speed data that congestion is actually observed on QDG at 2 different time slots, *i.e.*, 08:00 and 08:30. Our data also indicates that when congestion happens on this link, an increase of travel time is also observed on the link. This is coupled to a decrease of TTEBC, which exhibits therefore an anti-correlation behavior. Conversely, the QCB link, which is characterized by a lower demand, appears to be in free-flow conditions during the whole observed time period. As travel time is high for QDG in congestion period, QCB becomes then a viable alternative for drivers to avoid congestion on QDG. Consequently, we observe that TTEBC increases as well as its flow. This explains why the QCB edge exhibits a highly positive temporal correlation. After the congestion phase (08:00 and 08:30), the flow globally decreases in the area. As QDG becomes more and more fluid, the corresponding travel time decreases to free-flow travel time and TTEBC increases, *i.e.*, thus again maintaining an anti-correlated tendency. Contextually, QCB appears to lose its attractiveness compared to QDG as the flow decreases on this edge. TTEBC decreases as well confirming the positively

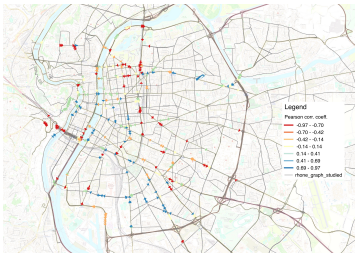

(a) Per-edge temporal correlation (only edges equipped with loop detectors have a non-null value)

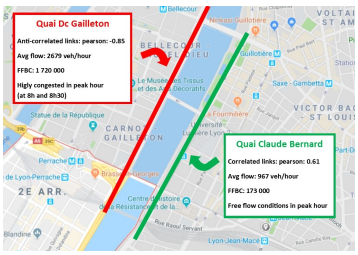

(b) Zoom on an area with two roads: QDG and QCB

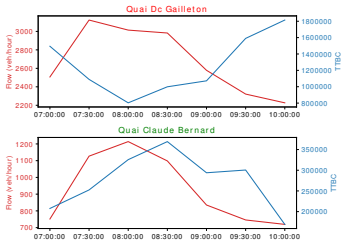

(c) Evolution of the TTEBC and flow on the road: QDG and QCB

Figure 4.17: Per-edge temporal correlation between EBC and flow (a) and zoom on a specific region (b,c).

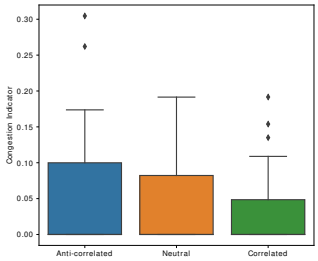

(a) Congestion indicator

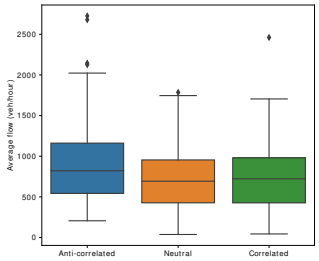

(b) Average flow

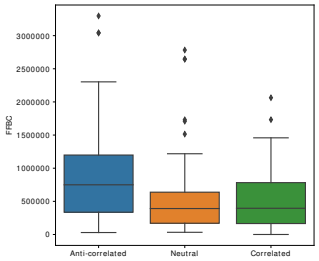

(c) FFEBC

Figure 4.18: Boxplots of congestion indicator (a), average flow (b), and FFEBC (c) for anti-correlated, neutral and correlated links.

correlated trend. The analysis is confirmed by the evolution of the flow and the TTEBC, which are known from the available data for both QDG and QCB as reported in Figure 4.17c.

To summarize, FFEBC gives information on critical edges, *i.e.*, road segments on which a high flow and possible congestion should be expected. Then, by studying the dynamic behavior of TTEBC, we highlight different types of edges. On the one hand, anti-correlated edges seem to be critical by nature (higher FFEBC) and even if a high congestion is observed on these links, the flow will be high whereas TTEBC low. On the other hand, there are correlated edges which are dynamically viable in term of travel time only when nearby roads are congested and then attract flows. In an intermediate situation, there are *neutral* edges (low correlation) which are characterized by either low or medium/high demand and the edge is able to dispatch such a flow, without becoming congested.

4.5 Concluding Remarks and Discussions

As noticed in Chapter 3, weighting the graph by the dynamic traffic conditions aims at considering them in the CM computation. This aims at combining the traditional topological and dynamic approaches to characterize transport network resilience and thus to have a global overview of the network performances.

First, we prove the NDC and the associated global metrics derived from its distribution (H, S and $\langle NDC \rangle$) ability to capture traffic dynamics (Section 4.2). By transposing the methodology developed by Gao et al.

(2013) (Section 2.2.2.2) to the transportation field, we characterize resilience with such measures considering both the topological vulnerabilities and the traffic conditions. We extend the simulated data-based analysis lead with the NCC and the AE (Section 3.2.3), as well as the GEBC and the EBC (Section 3.2.2), with FCD in the city of Lyon (Figure 4.2c). The evolution of the measures in time and when submitted to a disruption prove their traffic conditions sensitivity (Section 4.3 and Section 4.4.1). The importance of the faithful drivers' behavior, considering the bounded rationality with the weights discretization is highlighted for the EBC computation (Section 4.4.1).

Second, we confirm the observation lead with simulated data about the flow and EBC correlation (Section 3.4.2). The spatial correlation proves the sensitivity of the TTEBC to traffic dynamics (Section 4.4.2.1). By extending the correlation analysis between the flow of vehicles and the EBC (Section 4.4.2.2) using real data, we better understand the properties of the dynamic urban system highlighted by the spatial analysis of the temporal correlation of DSEETTEBC and flows (Figure 3.24). The anti-correlated edges seem to be critical by nature (higher FFEBC), the neutral edges are either topologically critical or uninteresting for the network with a null flow and the correlated edges are dynamically viable in term of travel time only when nearby roads are congested and then attract flows. We have shown that on critical edges characterized by high flows, dynamic EBC could be a predictor of traffic flow at a following time step, so motivating the need for a fast algorithm to compute dynamic EBC in order to follow the network dynamics and to predict possible future critical conditions. The analysis has shown also that to understand the behavior of an edge from its dynamic EBC, three aspects should be investigated: *(i)* TTEBC temporal deviation from FFEBC, *(ii)* connectivity NDC and *(iii)* EBC distribution of the graph regions around the considered edge, which we plan to explore in future work.

Chapter 5

Resilience-Oriented Multimodal Network Design

This chapter illustrates the methodologies developed with the aim of improving the network performances. An overview of the existing strategies to enhance resilience is presented in Section 5.1, with a distinction between pre-disaster strategies (Section 5.1.1) which precede and anticipate the disturbance, and post-disaster ones (Section 5.1.2) which aims at maintaining an acceptable level of performances (Section 5.1.2.1) and regaining the initial level of performances as soon as possible (Section 5.1.2.2). Section 5.1.3 will provide a brief description of some international projects aiming at resilience improvement.

Two strategies were developed during the thesis. On the one hand, the REINFORCE (Rapid augmentation of large-scale multi-modal transport networks for resilience enhancement) methodology (Section 5.2) aims at prioritizing the construction of multiple, already designed transport lines or modes, based on the quantification of the performance improvement that derives from the addition of the considered transport lines. The methodology also aims at ranking alternatives for deploying an emergency transport service, such as a dynamic ensemble of bus lines explicitly designed for managing an unforeseen hazardous event that might disrupt the transport network. After modelling a macro multimodal network, necessary for the quick computation, the increase of performances, computed using traffic conditions-sensitive metrics and the travel demand in the network performances computation.The gain of the dynamic approach proposed is highlighted by observing the impact of a special event on the line addition. On the other hand, the deployment of a Park-and-Ride (P&R) system (Section 5.3), adapted to recurrent disruptions and combined with an existing transport network, aims at reinforcing the existing transport network and thus enhancing its resilience. Two models are proposed. In the first formulation (Section 5.3.1) the goal is to determine the facility locations, respecting budget and time constraints, in order to maximize the ridership computed using a market share model based on the logit formula. By being attractive even in presence of recurrent disruptions, the P&R system competes the use of personal vehicles implying some modal shifts and thus a reduction of the traffic congestion with a decrease of vehicles number. To solve such problem over the large scale network of Lyon, a Lagrangian Relaxation Algorithm (LA) is formulated. The second formulation (Section 5.3.2), defines the facility locations and adapts the vehicle fleet according to the number of passengers taking the route. The purpose of this model is to minimize the facilities construction costs, the shuttle fleet costs and the travel costs by optimally distributing passengers on the paths joining the pick ups and the drop offs. Such problem is solved on a toy network.

This chapter contributes to the state of the art by proposing the two previously described strategies which enhance transport network resilience. The addition of new transport modes, maximizing the network performances and/or adapted to disruptions, increases the redundancy, as well as the efficiency of the transport network.

Section 5.2 is an updated version of the conference paper Henry et al. (2020) extended in Henry et al. (2021b), Section 5.3.1 is under review process for a publication in the Transport Research Part E Henry et al. (2022), and Section 5.3.2 is inspired from the conference paper Henry et al. (2021c).

Contents

5.1 Overview of Resilience Improvement Strategies

Jin et al. (2014) distinguish two resilience improvement strategies: before and after the disruption. According to Peeta et al. (2010), "disaster management is a multi-stage process that starts with pre-disaster mitigation and preparedness that focus on long-term measures for reducing or eliminating risk, and extends to post-disaster response, recovery and re-construction". On the one hand, the pre-disruption, seen as the preparedness, aims at preparing some strategies before the occurrence of a disruption. On the other hand, the post-disruption phase, which encompasses the response and the recovery phases, aims at developing some strategies to alleviate the transportation system disruption consequences.

5.1.1 Pre-Disaster Planning

The pre-disaster phase includes the preparedness and the mitigation stages. Whereas the preparedness stage aims at taking actions ahead of time to be ready for an emergency, the mitigation one focuses on the prevention of future emergencies and the minimization their effects. This phase involves awareness about emergency exercises, training in various methods of responding to the disturbance, planning to respond immediately as well as, thinking about the minimization of the effect induced by probable disasters in the future.

To improve the pre-disaster resilience, some articles focus on the allocation of limited renovation resources over transport networks with the objective of improving its resilience and robustness in such a way that potential disruptions incur minimal negative impact (Jin et al., 2014). Liu et al. (2009) study the improvement of resilience and robustness of transportation systems over multiple highway bridges, minimizing future seismic losses at the same time. The renovation goal of Du and Peeta (2014) is to enhance network survivability and minimize the expected post-disaster response time. Chu et al. (2015) propose a model to identify an optimal protection plan to maximize connectivity reliability for highway networks. Peeta et al. (2010) develop a pre-disaster planning problem with the goal of maximizing post-disaster network connectivity and minimizing network travel time. Yan et al. (2017) tend to minimize the expected railway system service loss subject to earthquake hazard. Zhou et al. (2019) analyze pre-disaster renovation decisions for sustainable transportation systems in urban areas. As the optimization goal, pre-disaster renovation costs and post-disaster restoration costs under constraints of post-disaster system connectivity, travel time reliability, and post-disaster link capacity are considered to build the model.

By redesigning a transport network with the aim of maximizing its resilience, the impact of disruptions should be mitigated. Vajanapoom K Tipper D (2010) propose three new risk management based approaches for survivable network design. The authors try to minimize the damage/risk from the worst case failure scenario, by both minimizing the maximum damage that could occur in the network and the maximum risk in the network, but also the variability of damage across all failure scenarios, by minimizing the root mean squared damage. Liu et al. (2011) develop a genetic algorithm to optimize airline routes in terms of the network properties, with the ultimate goal to increase the reliability of airspace systems. Dunn and Wilkinson (2016) modify the topology of the European air traffic network to increase its resilience by limiting the maximum number of air routes that can be connected to an airport to decrease the impact caused by its closure. Zhang and Wang (2016) present a decision methodology to select optimal solutions among possible alternatives of new construction to improve resilience of the network by altering its existing topology. The objective is to maximize the network performance and, simultaneously, to minimize the associated cost. By evaluating and comparing alternative risk mitigation strategies, using their own reliability based measure, the authors define the best choice from a set of candidate links. Edrisi and Askari (2019) enhance the network performance by improving the overall travel time of the transportation network in the day-to-day conditions, and by decreasing fatalities of the disaster by stabilizing the infrastructure to improve the network resiliency. Regarding the public transport network, Andersson et al. (2013) tend to decrease the sensitivity to disruptions

by increasing timetable robustness. Increasing the timetable resilience and robustness is crucial for the public transport network functioning, to prevent or reduce secondary delays which occur if a given delay exceeds the buffer time between two train paths at a critical block section with the aim of being insensitive to delays and minor perturbations (Goverde and Hansen, 2013). In the context of graph augmentation and centrality improvement, Crescenzi et al. (2016) optimally improve node accessibility, by maximizing the NCC, with the addition of a limited set of edges, thus reducing the distance between the nodes. Bergamini et al. (2018) and Angelo et al. (2016) develop optimization models aiming at maximizing EBC with the creation of a limited set of edges. Nonetheless, such approaches are extremely time consuming and therefore hardly apply to large scale transport networks.

Some strategies such as the elaboration of a on-demand vehicle system could be seen as both long and short-term strategies. Indeed, the on-demand vehicle fleet allocation could be adapted to some disruptions in real time to improve the short-term transport network resilience whereas the construction of some transit stop or car park as it is needed in a Park-and-Ride (P&R) system depends on a long-term strategy. By increasing the public transport network and thus the network redundancy, Jenelius and Cats (2015) notice a greater resistance to system failure, as a result of an improvement of the transport network resilience. Using shared mobility aims to maximize the utilization of the mobility resources that are available to the society (Machado et al., 2018). To be efficient, P&R must be attractive by optimally locating the car parks regarding some constraints such as the travel time minimization. By modelling transit service frequency and considering the user equilibrium in the optimization of the location and capacity of P&R facilities, Song et al. (2017) aim at minimizing the travel time and the expected waiting time experienced by transit users. Another optimization constraint for locating the facilities should be to maximize the ridership of P&R systems. Farhan and Murray (2008) aim at maximizing P&R demand coverage, as well as both accessibility and integration with the existing transport network by minimizing the park distance to the major roads of the network. Aros-Vera et al. (2013) propose to maximize the ridership, capturing via a logit model wherein users disutilities represent their generalized travel costs via the designed P&R system and private vehicles, within a P&R system by optimally locating a given number of parks used to access a shared mobility service. Cheng et al. (2021) aim to estimate quantitatively the potential of bike sharing to promote transport resilience. They find that bike sharing acts as a supplementary mode to enhance urban transport resilience in the case of complete transit closure, given its flexibility and various social, environmental, and economic benefits, and the proximity of bike sharing docks to metro stations. Nonetheless, extreme weather, which negatively impacts transport networks, is one of major barriers to bicycling as the distance and the security.

5.1.2 Post-Disaster Restoration

The post-disaster phase is distinguished into sub-phases according to the timing, status and role of the network (Iida et al., 2000): during or shortly after the disaster which is the response phase and after the disaster which corresponds to the recovery phase. The response phase focuses on addressing immediate threats to people, property and business whose safety largely depends on the preparedness phase, before the disaster. The recovery phase is the restoration of the transport network following any impact from a disaster.

5.1.2.1 Short-Term Strategies

Many works in the literature address decision-making to support emergency management for post-disaster applications or address optimal allocation of resources specifically for post-disaster repair. Yi and Özdamar (2007) and Özdamar et al. (2004) propose models, based on network flow routing formulation, to locate the emergency services with the aim of maximizing response service level by enabling fast relief access to affected areas and locating temporary emergency units in appropriate sites. Guo Jingni et al. (2021) focus their study to improve resilience of multimodal transport network by optimizing the location selection strategy of

emergency rescue facilities by maximizing the utility of construction costs, the coverage of the demand, and by minimizing the total travel time to reach the emergency rescue facilities. Because restoration activities may take a long time to complete, some temporary solutions, analyzed in the evacuation optimization problem, have to be employed to maintain a minimum level of performance. Xie et al. (2010) discuss a dynamic evacuation network optimization problem that incorporates lane reversal and crossing elimination strategies. These two lane-based planning strategies complement one another by increasing capacity in specific directions through the evacuation network. Kepaptsoglou et al. (2014) plan highway operations in the response period using a network design model and implement temporary remedial actions to manage traffic, maximize performance, and even restore the connectivity of the network: redistribution of lanes in each direction and shoulder use. Al-Zinati and Zalila-Wenkstern (2018) propose a resilient agent-based re-organizing traffic model for urban evacuations to implement effective traffic road reversals. Directly after a major disruption, particularly in the case of an earthquake, roads could be blocked by some debris which must be removed. Tuzun Aksu and Ozdamar (2014) focus on the road restoration efforts during disaster response by maximizing the network accessibility for all locations in the area during the restoration process to evacuate survivors and remove road side debris as soon as possible. Ulusan and Ergun (2018) propose a model to schedule the roads cleaning with the limited resources and the aim of maximizing the satisfied demand over time.

The rerouting of vehicles could be a solution in the emergency phase management to mitigate the disruption. Besides that, drivers increasingly use navigation applications for avoiding traffic congestion and routing to unfamiliar destinations (Yamsaengsung and Papasratorn, 2017). Hu and Sun (2012) develop a knowledge-based modelling method, which combines the knowledge of experienced schedulers with the operations research knowledge, to support the disruption management process in real time in urban distribution. In their analysis, Dunn and Wilkinson (2016) propose an adaptive strategy to redirect air routes from disturbed airports to their closest operational airport respecting a surplus capacity constraint. Regarding the public transport networks, in presence of a disruption, it is necessary in real time to reschedule the timetable and the vehicles. Cacchiani et al. (2014) propose an overview of recovery models and algorithms for real-time railway disturbance and disruption management. D'ariano et al. (2007) formulate an algorithm to compute a conflict-free train timetable compatible with the actual status of the railway network with the aim of minimizing the global delay. Mannino and Mascis (2009) implement an exact algorithm to route and schedule trains in real time in metro stations. Nielsen et al. (2012) deal with real-time disruption management of railway rolling stock by adjusting the original scheduled rolling stock to keep the circulation feasible and minimize the train cancellation. Yap et al. (2021) also formulate a problem to reschedule the train of the public transport in presence of disruption to minimize the travel time variations (waiting time, journey time, costs).

5.1.2.2 Long-Term Strategies

The long-term post-disaster strategies aim at re-building the transport network in order to regain the initial level of performances. Chen and Tzeng (2000) propose a simulation model to find the optimal reconstruction order of each damage point in a post-earthquake road network with the aim of minimizing the travel time, to optimally reconstruct a road network after an earthquake. Matisziw et al. (2010) aim at both minimizing the system cost and maximizing the system flow in the network restoration. Rey and Bar-Gera (2020) address the problem of scheduling reconstruction efforts in a transport network struck by a disaster with the aim of minimizing the total network delay, determined by the user-equilibrium based traffic flow pattern for the current state, under the recovery resource availability constraint. Merschman et al. (2020) propose an optimization formulation aiming at optimally planning the bridge reconstruction by considering the change in total travel distance and total travel time, the importance of the bridge in the network connectivity modeled in terms of the number of shortest paths passing through each bridge, and the access to healthcare facilities measured by the change in travel time to an emergency facility. Zhou et al. (2021) introduce four different restoration prioritization strategies on the US airport network, which help to consider the combined impacts

of network load dynamics and network dependency on catastrophic failures. The first restoration strategy is the *random* repair one and consists in repairing the disrupted nodes in random order, the second one *high degree first* consists in targeting for the repair order assigned according to the degree of failed nodes, the third one *short time first* aims at involving the repair order assigned based on the required repair time of failed nodes and the last one *high load first* prioritizes repair according to the amount of load carried by the failed nodes. The authors find that the most effective recovery of network connectivity can be achieved by applying *short time first* strategy, while the expected system restoration time is longer. The degree- and load-based strategies are the choices if shorter system restoration time is preferred with an acceptable resiliency loss. Sohouenou and Neves (2021) also analyze different link-repair strategies across different scenarios of disruption: repair the links in a random order, repair the links with highest traffic flow under normal conditions, repair the links which minimizes the disruption consequences over the recovery process, and repair the links whose individual failure results in the highest impacts on the system performance first. The choice of the strategy, crucial when several links are affected, depends on the traffic conditions. In presence of a reduced number of impacted links, robustness is a good equivalence for network resilience. Numerous additional works consider the ordering of infrastructure repair operations and assignment of tasks to crews for civil infrastructure maintenance (Camahan et al., 1987; Chen and Tzeng, 1999; Childress and Durango-Cohen, 2005; Durango-Cohen and Sarutipand, 2009).

5.1.3 International Projects and State of Practice

To reduce transport network vulnerability, many operational projects exist and aim at improving critical transport network infrastructures resilience. For instance, Sevilla et al. (2018) present the European project PANOPTIS whose main target is to improve the resilience of the road infrastructures and to ensure reliable network availability under unfavourable conditions through the combination of climate change scenarios with structural simulation tools and with actual data from a multi-sensor network. The final goal is to provide the operators with an integrated tool able to support more effective management of their infrastructures at planning, maintenance and operation level. The goal of the INFRARISK (Novel Indicators for Identifying Critical INFRAstructure at RISK from Natural Hazards) (INFRARISK) project is to develop tools and methodologies to assess the impact of extreme, low probability natural hazard events on critical transport infrastructure networks, in order to enable infrastructure managers and owners to perform stress tests for critical networks to determine their resilience to low probability, extreme natural hazard events and, consequently, to assist in the decision-making process with regard to the protection of critical infrastructure networks (Connolly, 2018). The RAIN (Risk Analysis of Infrastructure Networks in Response to Extreme Weather) (RAIN Project) project aims at quantifying the complex interaction of infrastructure systems and their interrelated damage potential in the event of specific extreme weather events. The intent is to improve the robustness of the critical infrastructures networks in order to avoid disproportionate damage or disruption due to extreme weather events. This involved increasing the level of redundancy in the infrastructure networks at critical nodes, improving the performance of key infrastructures and developing detailed plans for a range of potential emergency scenarios (Connolly, 2018). Other projects that can be mentioned include RESOLUTE (RESilience management guidelines and Operationalization appLied to Urban Transport Environment) (RESOLUTE consortium) which also focuses on the critical transport infrastructure resilience improvement, HAZUS (HAZards US) (FEMA), governed by FEMA, which estimates the risks from earthquakes, floods, tsunamis, and hurricanes to increase community resilience, etc.

5.2 REINFORCE: Rapid Augmentation of Large-scale Multimodal Transport Networks for Resilience Enhancement

This section proposes a quick-to-compute methodology, called REINFORCE (Rapid augmentation of large-scale multi-modal transport networks for resilience enhancement), which aims at prioritizing the deployment of the multiple lines or modes that a transport operator might want to propose to increase its offer. In a development of the urban transport network context, REINFORCE prioritizes the order of construction of the lines of a newly designed transport mode by maximizing the network performance gain, as described by complex networks metrics and in a resilience context, REINFORCE could also be helpful to support the rapid and quick response to disruptions by setting up or reinforcing an adapted emergency transport line (*e.g.*, bus service) over a set of predefined itineraries. For these reasons, the methodology works as a long-term strategy as well as a short-term one. The addition of multimodal transport lines, modeled by edges, improves the network redundancy by enlarging the transport offer, enhancing transport network resilience. To that purpose, REINFORCE adopts a multilayer graph modelling of the urban multimodal transport network and a set of global and local metrics to quantify the performance improvement. In order to apply REINFORCE to large-scale transport networks and to maintain the quick computation, incompatible for certain graph metrics such as EBC, we propose an approach to simplify the graph by producing a macroscopic graph, which we call *macro-graph* in the following, that constitutes an aggregate, simplified and unified abstraction of the whole multimodal urban mobility system, based on the mono-modal transport networks, modeled as simple directed graphs (*e.g.*, road network, bus lines, subway lines, etc.) (Section 1.5). For road networks, the road intersections are represented by the nodes and the road segments with edges, for the public transport networks, the nodes corresponds to the transit stops and the edges to the lines.

To build the macro-graph, we divide the network coverage into areas $\mathcal{A}$ whose spatial extent can be covered on foot, such hexagon area with a maximal length of 1 km and each node of the macro-graph is located at the centroid c_i of each of the areas $A_i \in \mathcal{A}$. After the creation of the macro-nodes, REINFORCE creates a layer l for each transport mode and an inter-layer edge $e^l \in E_l$ between any two areas (A_i, A_j) if at least one edge exists among any pair (v_i^l, v_j^l) of nodes from the initial fine-grained graph representation of transport mode l, where v_i^l is selected from the set of nodes belonging to area A_i and v_j^l is selected from those related to area A_j, in order to preserve an accurate connectivity in the multilayer simplified abstraction. Based on this approach, we consider two cases, both presented In Figure 5.1a. In the first cases, no direct edge joining area A_1 to area A_3 exists. Thus, no edge is created in the macro-graph between these two areas for the specific analyzed mode. In the second cases, a connection exists because of the presence of the direct edge connecting the blue nodes in areas A_1 and A_3 from the fine-grained underlying graph. For each transport mode we follow the same approach to simplify the corresponding fine-grained graph. To consider the traffic conditions in the network performance characterization, we weight each intra-layer edge of the macro-graph with the free-flow travel time. Consequently, edge weights are static and the impact of traffic dynamics as well as users route choices are not taken into account in this study. This could represent a limitation of the present study which is currently unable to address complex (dynamic) scenarios (*e.g.*, Braess's paradox (Braess et al., 2005)). Regarding the demand-sensitive metrics based on shortest path computation (DSAE, DSEBC and DSNCC), we compute, for all the transport mode network layers, the weight associated to the edge connecting any two centroids c_i and c_j of areas A_i and A_j by averaging the length of the shortest paths computed over the free-flow weighted sub-graph $G[A_i, A_j]$ induced on the original, fine-grained modal graph by the subset of nodes included in both areas A_i and A_j (Figure 5.1a), i.e.:

$$\forall A_i, A_j \in \mathcal{A} \times \mathcal{A}, \quad \text{if } P_{A_i A_j} \neq \emptyset, \quad w_{c_i c_j}^{mode} = \frac{1}{|P_{A_i A_j}|} \sum_{p \in P_{A_i A_j}} f(p) \tag{5.1}$$

where $\mathcal{A}$ is the set of hexagon areas, c_k the centroid of the area A_k, $P_{A_i A_j}$ the set of the shortest paths of

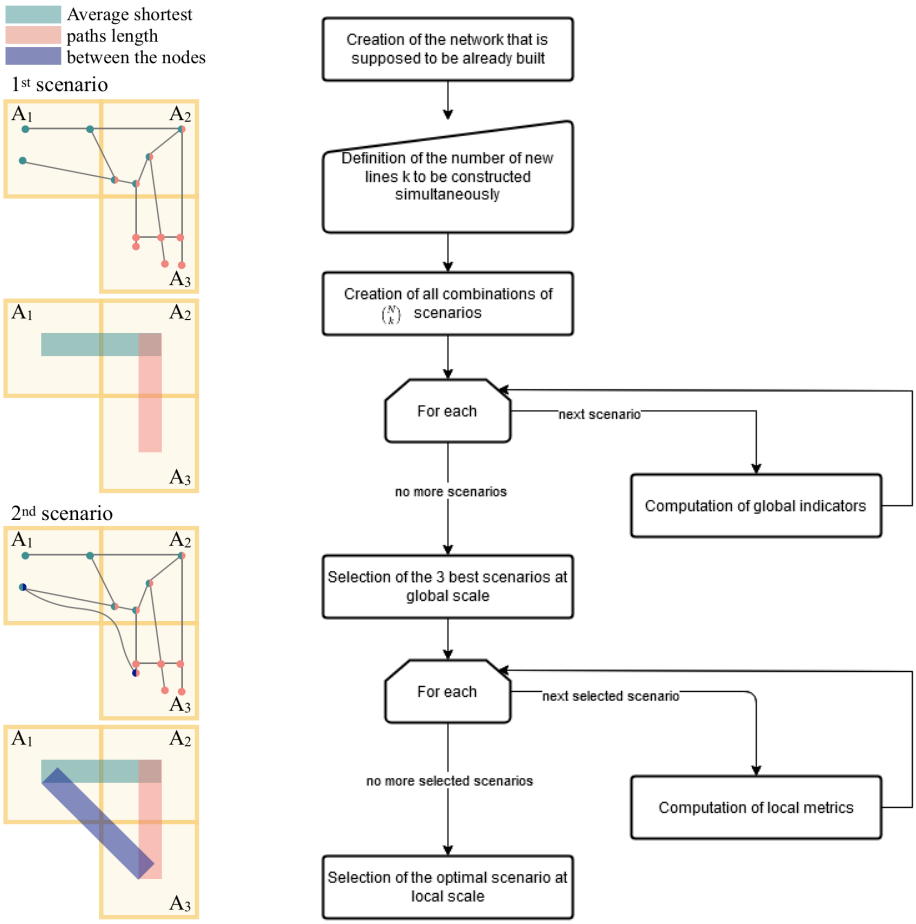

(a) Macro-graph modelling **(b)** Global REINFORCE methodology

Figure 5.1: Description of the REINFORCE methodology including the macro-layer modelling.

the sub-graph $G[A_i, A_j]$, $|P_{A_iA_j}|$ the cardinality of the set $P_{A_iA_j}$ and $p \mapsto f(p)$ the function which computes the free flow travel time of path p. We assume the subway network free flow speed to be about 40km/h, and the tramway one to be about 30km/h (Hitge and Vanderschuren, 2015).

Regarding inter-layer connectivity, modelling inter-modal transitions that can be available to travellers in a given area of the city, inter-layer edges are created between replicas of the centroid node corresponding to the considered area. These inter-layers edges can only exist if at least two transport modes are present in the area.The weights of the inter-layer edges are determined based on the specific features of the transport mode transitions that are possible in each specific area. Specifically, we define inter-layer weights in terms of *the average area walking time*, *i.e.*, the mean pair-wise walking travel time computed according to a walking speed of 1.5 m/s. The pair-wise walking travel times within an area are computed between each road intersection and public transport stops of the given area, as well as between the transit stops belonging to the subway or the tramway networks. The inter-layer weight in an area providing access to multiple transport modes thus depends on the specific features of the area and, particularly, on the density of the transport network inside it: the proposed procedure to define an inter-layer weight allows considering the (average) walking time necessary to perform a modal shift inside each area. In addition, concerning modal changes related to the private vehicle mode, we penalize more the inter-layer edges within areas that do not include dedicated car parks for mode change to transit (*i.e.*, park-and-ride stations).

Once the weights have been assigned to the macro-graph, shortest paths can be computed between macro-graph nodes (area centroids) to calculate the metrics in their traditional nature (AE, NDC, NCC and EBC) and in their demand-sensitive adaptation (DSAE, DSNDC, DSNCCand DSEBC) under normal conditions and during the Festival of Lights.

Lastly, concerning our main objective of prioritizing the construction of multiple transport lines, we select the best combinations by computing the selected network performance metrics for each possible scenario of joint construction. As reported in Figure 5.1b, we first create the set S of all the $\binom{N}{k}$ considered scenarios, where N is the total number of new transport lines designed to be built and $k \leq N$ is the number of lines that we allow to be jointly constructed. This number k could be determined by considering budget constraints, roadworks space consuming, the available labor, etc. Because of the large number of combinations, we aim at first computing, for all scenarios, the global indicators DSAE and $\langle DSNDC \rangle$ (Section 2.2.2.2), not time-consuming, atop the newly computed macro-graph that includes any pre-existing transport line or mode, plus all the new lines to be built for a given scenario s. After computing DSAE and $\langle NDC \rangle$ on the graph induced by each scenario s, it is possible to sort scenarios with respect to a given metric $m \in \{DSAE, \langle DSNDC \rangle\}$, and compute the ranking $rank_m(s)$ of s among all considered scenarios, with respect to the given metric m Thus, we are able to select the most interesting scenario via the objective function: $argmin_{s \in S}(rank_{DSAE}(s) + rank_{\langle DASDC \rangle}(s))$. In addition to the most interesting scenario, *i.e.*, the one that minimizes the aforementioned objective function, we also consider the second- and third-best scenarios for our local analysis. The global characterization of the scenarios is crucial to reduce the number of scenarios to be analyzed at local scale. Then, we focus on the local indicators (DSEBC and DSNCC) (Section 2.2.2.1) for the reduced set of three best scenarios because of the complexity in computing such indicators. Nonetheless, such indicators are essential to observe the spatial impact of adding new transport lines.

5.2.1 REINFORCE Implementation on Lyon Metropolitan Network

We apply the REINFORCE methodology on the transportation network of Lyon, France (Figure 5.2a), composed of 7 tramway lines (Figure 5.2e) (progressively numbered from 0 to 6 as reported in Figure 5.2a) and 5 subway lines (Figure 5.2d) (labelled with letters A, B, C, D, E, F1, F2, as from Figure 5.2a). Although our study focuses on the spatial area delimited by the extent of the subway and tramway networks, to mitigate the border effect on the CM Porta et al. (2006) computed on the macro-graph, we also consider a buffer area around the two studied public transport networks that only includes portions of the road network. This permits to include potential road paths joining pairs of areas more efficiently than the public transports in the computation of the metrics. Because REINFORCE aims at prioritizing the construction of a transport mode, we assume that the public transport (tramway and subway) networks are not constructed. Such an assumption is motivated by the desire to evaluate the applicability of our approach on a large network. Regarding the second point, we succinctly explore such an application of REINFORCE by considering the prioritization of line construction during a special event. To model the macro-graph we use 324 hexagon area with a maximal length of 1km, which was found to be a good compromise between computing time and graph accuracy. The scenario including all the public transport lines is seen as the optimal one. The resulting corresponding macro-graph (Figure 5.2) is composed of 407 nodes and 1 986 edges of which 1 606 belong to the road network (Figure 5.2c), 70 to the subway one (Figure 5.2d) and 110 to the tramway one (Figure 5.2e). 200 edges permit to transit from a transport mode to another one at the centroid of the areas. Longer road edges (Figure 5.2c) represent highways or peripheral roads which directly join farther areas of the city.

Whereas the intra-layer edges weight represent the free flow travel time needed to join two areas with the corresponding transport mode, the values of the inter-layer edges weight correspond to the mean pair-wise walking travel time computed according to a walking speed and are comprised between 3.8 minutes and 8.7 minutes for modal shifts between the road network to a public transport mode, and between 0.0 and

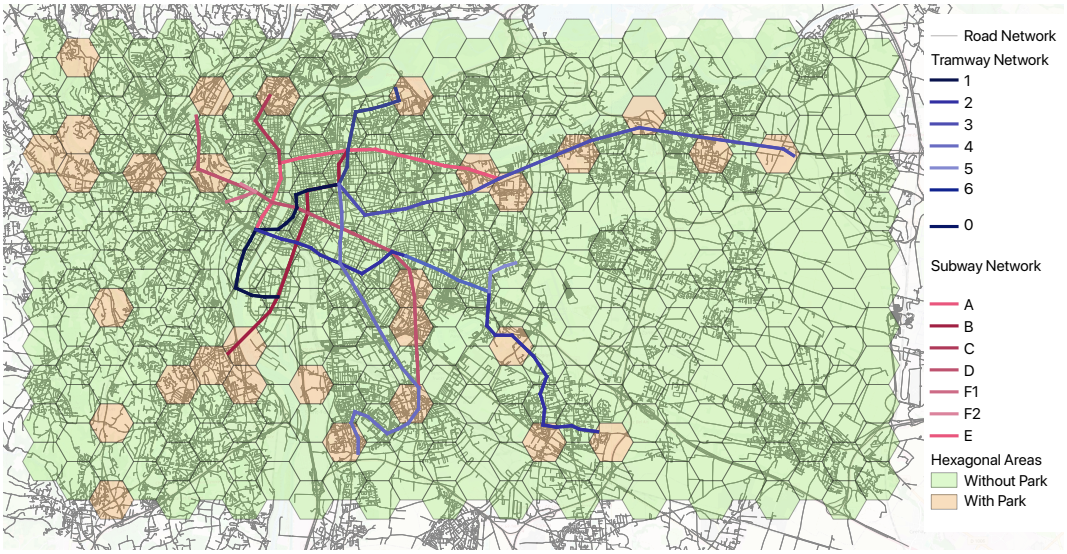

(a) Real Transport network with the hexagon areas used for the macro-graph construction. The orange areas are those where a car park dedicated for modal change exist.

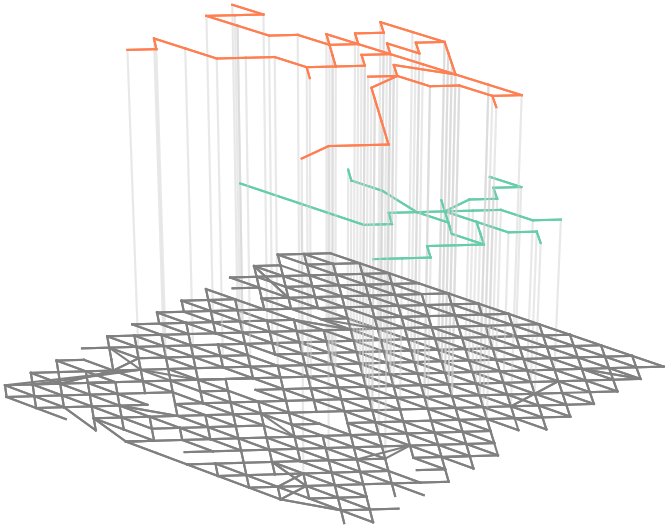

(b) Multilayer Transport network with the road network (c), the subway one (d) and the tramway one (e) with the intra-layer edges in light grey.

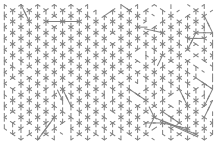

(c) Road

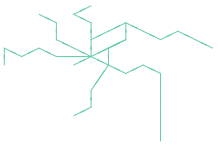

(d) Subway

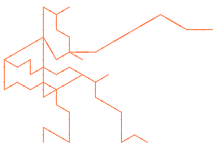

(e) Tramway

Figure 5.2: The real transport network of Lyon and its hexagon tessellation (a). The simplified macro-graph (b) when all public transport lines are constructed, with its road network (c), subway network (d) and tramway network (e) layers.

10.1 minutes for modal shifts on the public transit system of the city (Figure 5.3). To penalize the changes related to the private vehicle mode, we increase the weight of 3.5 minutes for the inter-layer edges related to the road-transit, when there is no park-and-ride station in the associated area in order to model the delay necessary to find a parking space. As observed Lefauconnier (2005), in the city of Lyon, people spent in average 11.8 minutes per day to find a car park and 3.3 displacements are realized in average per day (Sytral, 2015).

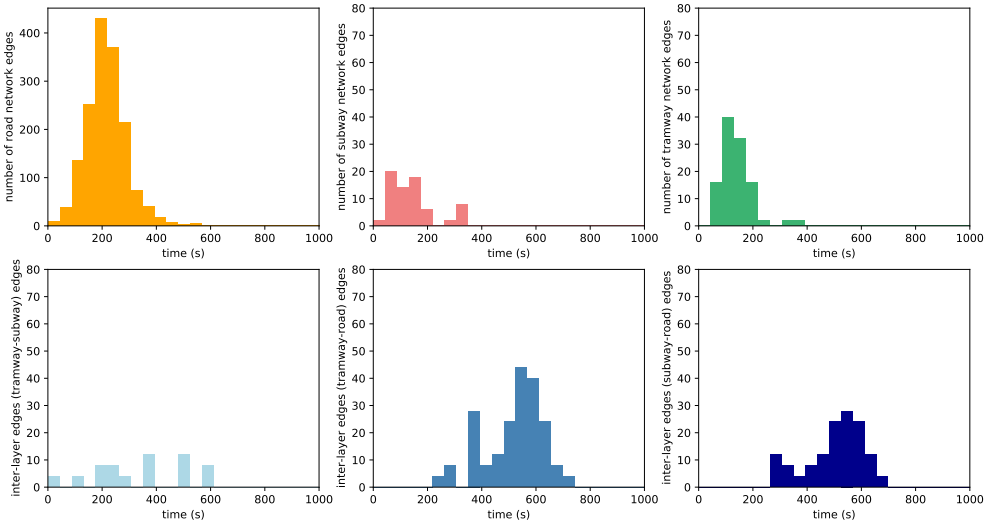

Figure 5.3: Edge travel time distribution for the road network (orange), the tramway network (pink), the subway network (green) and for the different inter-mode changes (light blue, blue, and dark blue).

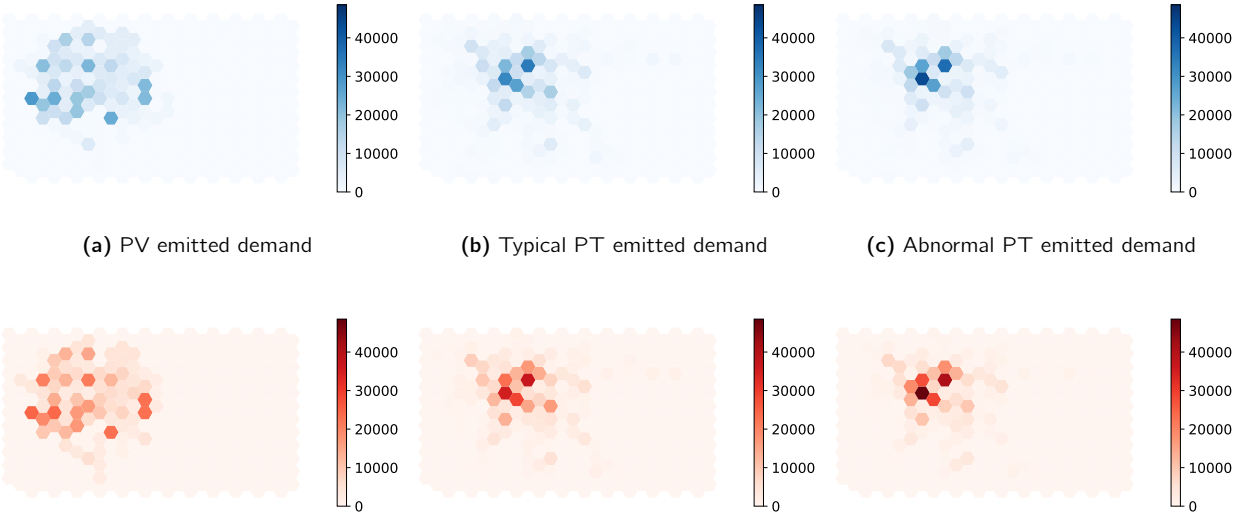

(a) PV emitted demand **(b)** Typical PT emitted demand **(c)** Abnormal PT emitted demand

(d) PV attracted demand **(e)** Typical PT attracted demand **(f)** Abnormal PT attracted demand

Figure 5.4: Typical private vehicle travel demand emitted (blue) (a) and attracted (red) (d) by the areas. Typical emitted (blue) (b) attracted (red) (e) the areas and abnormal emitted (blue) (c) attracted (red) (f) the areas public transport travel demand.

To infer travel demand coefficients, we use two datasets. The first one provides private vehicles' demand whereas the second one is related to the public transport demand. For both datasets travel demand is provided at the level of the finer-grained graphs used as inputs for the construction of the macro-graph. More specifically, we consider that a path whose origin and destination belong to the road network only serves road users' demand. Otherwise, we consider that the demand served by the path is the sum of two contributions, *i.e.*, the road part and the public transport one. Therefore, we have adapted such a data to our simplified representation: the demand associated to a given pair of hexagon areas (A_i, A_j) has been obtained by summing up the demands related to all pairs of nodes (v_k, v_l) from the initial finer-grained graph where $v_k \in A_i$ and $v_l \in A_j$.

To explore the ability of REINFORCE to capture traffic conditions, we analyze the impact of a large increase of the public transport demand over the selected lines. In our experiments, we assume that 3 out of 12 lines are built simultaneously, meaning that 3 subaway or tramway lines will be constructed at the same time, which corresponds to $x = \binom{12}{3} = 220$ scenarios. As explained in the REINFORCE methodology description, we first compute the global indicators for the 220 line combinations before analyzing the impact of a reduced set of scenarios at local scale. The computational time related to the first step does not exceed 4 minutes. We present the results obtained in our experimentation when using both global and local metrics in their demand-sensitive adaptation described in Section 2.2.3 and introduced to account for the impact that travel demand might have in the construction of new transport lines. By using such metrics, the importance of a line depends not only on the amount of travel time it permits to save, but also on the amount of travel demand it can serve. When a line is not present in a given construction scenario, we adopt the simplifying assumption to remove the associated demand, without reassigning it over other existing lines. By this approach, a public transport line is considered more attractive if it allows to connect areas more rapidly than the road network and the associated demand is significant. As a first dataset, we observe the ability of our methodology to capture travel demand information for the prioritization of line construction scenarios under normal conditions. As a second dataset, we analyze the impact of the 2017 Lyon Festival of Lights, a very popular event that attracted 1.8 billions of visitors that strongly solicited the transport network of the city. We use the specific public transport travel demand observed during these days rather than a typical one. Such analysis aims at confirming the ability of the methodology to capture travel demand information, and aims to show an example in which the methodology could be helpful to dynamically reconfigure the transport network. The idea is to compute, the best combination of newly designed transport lines to be deployed in order to handle an exceptional situation that might significantly disrupt the quality of the transport offer of a city.

5.2.1.1 Traditional (demand-unsensitive) Metrics

First, we study the impact of adding new public transport lines by quantifying their impact through traditional metrics that do not consider the demand in their computation. We thus compute the $\langle NDC \rangle$ and the AE to select the three best scenarios at global scale and then analyze the local impact by computing the NCC and the EBC. In Figure 5.5, we plot the values of AE (Figure 5.5a) and $\langle NDC \rangle$ (Figure 5.5b) for all the 220 scenarios corresponding to the construction of three public transport lines. We also plot the values of these metrics for the two reference scenarios where: *i)* there is no public transport lines (light pink bottom line in Figure 5.5a and 5.5b); *ii)* all the 5 subway and 7 tramway lines (dark pink line in Figure 5.5a and 5.5b) are considered as constructed. Higher AE values indicate that the addition of the transport lines significantly improves the efficiency of the network with respect to the reference scenario with no public transport line, by reducing on average the travel time of the shortest paths. In other words, it is quicker to reach the different areas of the graph thanks to the presence of the additional public transport (subway and tramway) lines. An increase of $\langle NDC \rangle$ corresponds to the addition of new connections between the different nodes of the network. The original network (only including roads) is almost a 12-regular graph. Each area is connected to its neighbors by in-going and out-going edges. Therefore, an increase of the density is the result of the creation of alternative paths using public transport modes. Scenarios are sorted by computing a score which is equal to the sum of their rank for both global metrics (AE and $\langle NDC \rangle$), as detailed in the introduction of the section. The scenarios corresponding to smaller scores indicate that both AE and $\langle NDC \rangle$ are higher. We select the three scenarios with the smallest scores. Then, such scenarios are analyzed at local scale to provide a description of the geographical impact of the construction of the selected lines. Due to computational limitations, it is essential to reduce the set of selected scenarios before starting the local analysis. In free flow conditions and without considering the travel demand, the three best combinations of lines to be built, according to the global indicators, are the joint creation of lines {2, 4, D} (Figure 5.5c), {2, 4, A} (Figure 5.5d) and {2, 3, 4} (Figure 5.5e).

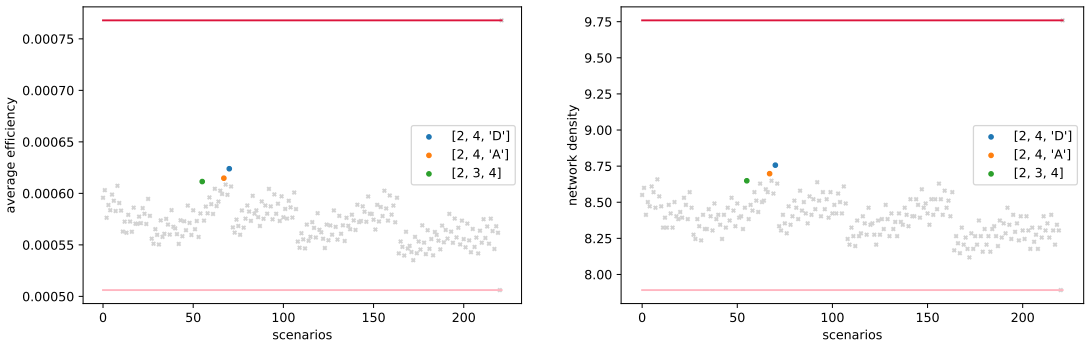

(a) AE **(b)** $\langle NDC \rangle$

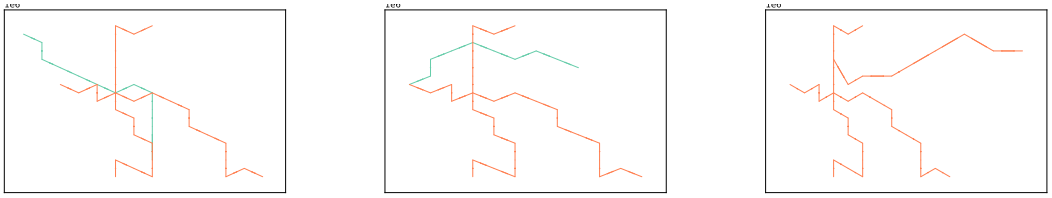

(c) Network - lines 2, 4, D **(d)** Network - lines 2, 4, A **(e)** Network - lines 2, 3, 4

Figure 5.5: Global indicators AE and $\langle NDC \rangle$ for all the scenarios consisting in adding three new transport mode lines

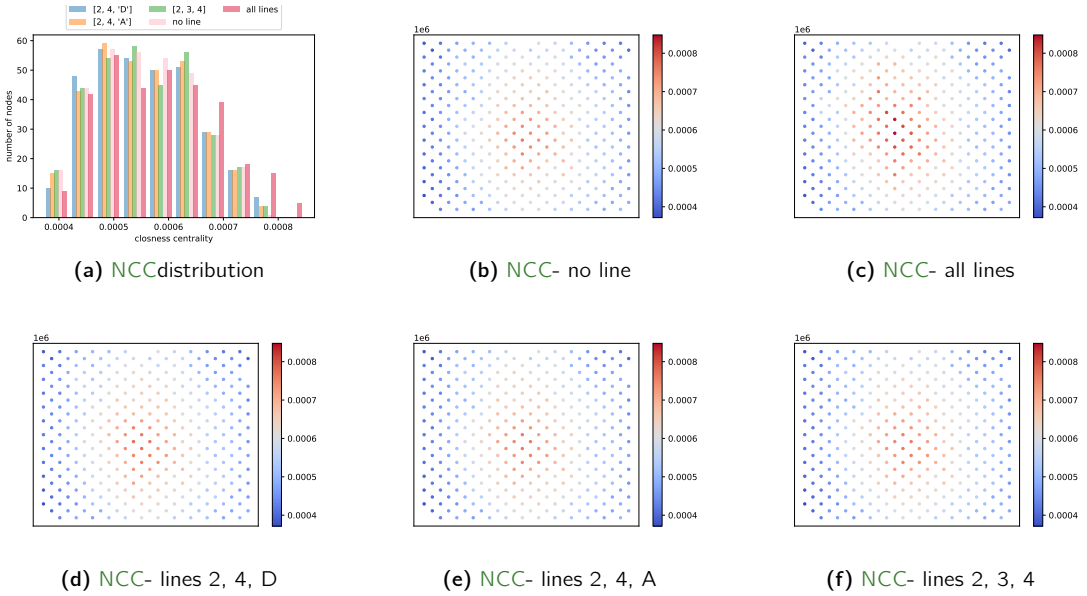

(a) NCCdistribution **(b)** NCC- no line **(c)** NCC- all lines

(d) NCC- lines 2, 4, D **(e)** NCC- lines 2, 4, A **(f)** NCC- lines 2, 3, 4

Figure 5.6: Histogram of node closeness centrality and its spatial distribution in the studied scenario.

Figure 5.6 summarizes the impact on NCC (2.6) induced by the three selected construction scenarios and the two reference ones. The improvement on the network efficiency induced by the public transport lines construction is noticeable in the reported plot of the distribution of the NCC metric (Figure 5.6a). The NCC distribution shifting to higher values (with respect to the baseline scenario with no public transport) confirms an increase of the number of nodes with high NCC, meaning that macro-graph nodes are globally

closer to each other, generally improving the characteristics of the transport network in terms of shortest paths: it is easier and quicker to reach an area from all the other ones. The light pink scenario, with no public transport line, has the leftmost skewed distribution, whereas the dark pink scenario, where all the public transport lines are constructed, has the rightmost one. Both observations are in accordance with Figure 5.6b, where the vast majority of nodes exhibits lower NCC values with respect to Figure 5.6c, related to all lines built, which, unsurprisingly, denotes significantly higher values of NCC, especially in city center areas. Concerning the three selected construction scenarios, we observe a higher number of nodes with high NCC in scenario {2, 4, D} (see Figure 5.5c) as denoted in Figure 5.6a. For the two remaining scenarios, the construction of lines {2, 3, 4} (Figure 5.5e) appears as the least attractive in terms of NCC. Indeed, the distribution of NCC is more shifted to lower values than scenario {2, 4, A}(Figure 5.5d).

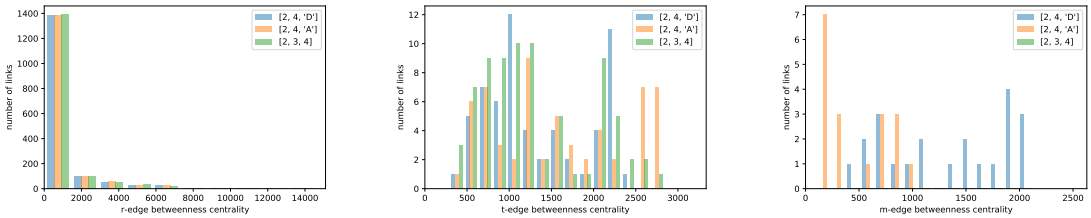

(a) EBC - road network **(b)** EBC - tramway network **(c)** EBC - subway network

Figure 5.7: Histogram per transport mode of the EBC in the studied scenarios.

Figure 5.7 presents the distribution of the EBC (2.4a) per transport mode in each of the studied scenario. The more the EBC distribution is shifted to the right, the more links tend to be crossed by a high fraction of shortest paths per pairs of origin/destinations. Independently of the scenario, we observe that the majority of road network edges have very low values of EBC (Figure 5.7a). This means that most of these edges are crossed by a small fraction of shortest paths or none at all. This trend is similar in all of the three selected scenarios concerning road network edges. However, concerning the tramway lines (Figure 5.5e), we observe in scenario {2, 3, 4} a larger set of edges with EBC close to 0 than in the two other scenarios (Figure 5.7b). Indeed, 17 edges have a quasi-null EBC in this scenario, against 13 in scenario {2, 4, A} (Figure 5.5d) and 12 for the scenario {2, 4, D} (Figure 5.5c). A similar trend can be observed for the subway network (Figure 5.7c). Whereas in scenario {2, 4, A} (Figure 5.5d) 12 edges of the A-line are almost never crossed by shortest paths, almost all D-line edges in scenario {2, 4, D} make the transport network more efficient by being crossed by a large number of shortest paths.

5.2.1.2 Demand-Sensitive Metrics

When sorting all the possible scenarios based on the ranks of demand-sensitive global metrics (DSAE and $\langle DSNDC \rangle$), we find lines {1, B, D} (Figure 5.8e), {1, A, D} (Figure 5.8f) and {1, A, B} (Figure 5.8g) to be the three best alternatives under normal conditions and during the Festival of Lights. These results are in accordance with the emitted (Figure 5.4b and Figure 5.4c) and the attracted (Figure 5.4e and Figure 5.4f) public transport travel demands. Nonetheless, during the Festival of Lights, scenario {1, A, D} (Figure 5.8f) becomes more interesting than the {1, B, D} one (Figure 5.8e). This is legitimated by the fact that, during this event some subway stations covered by line A (*e.g.*, Bellecour square, Hotel de Ville, Cordeliers) and line D (*e.g.*, Bellecour square) are the most impacted one. In fact, these areas attract a larger than usual demand (Figure 5.4c and Figure 5.4f), especially due to visitors wanting to participate to light spectacles taking place at such city-center zones. Under normal conditions, the westernmost darker-blue area in Figure 5.4b (corresponding to the westernmost darker-red one in Figure 5.4e) presents the highest emitted (respectively attracted) demand of the city and it is reachable with the A and the D subway lines, as well as via the 1 tramway line. Likewise, concerning the northernmost darker-blue (Figure 5.4b) and darker-red

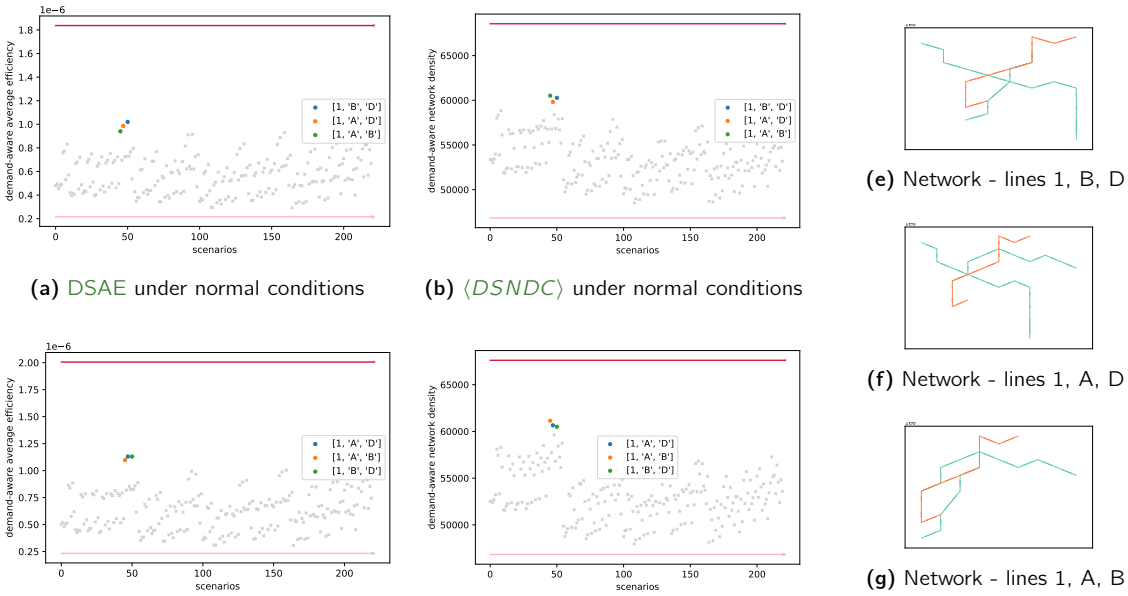

(a) DSAE under normal conditions

(b) $\langle DSNDC \rangle$ under normal conditions

(e) Network - lines 1, B, D

(f) Network - lines 1, A, D

(g) Network - lines 1, A, B

(c) DSAE during the Festival of Lights

(d) $\langle DSNDC \rangle$ during the Festival of Lights

Figure 5.8: Global indicators DSAE and $\langle DSNDC \rangle$ for all the scenarios consisting in adding three new transport mode lines under normal conditions and during the Festival of Lights.

(Figure 5.4e) areas, lines 1, 4, A and 3 allow to reach such high-demand zones of the city. Regarding the southernmost darker-blue and darker-red areas, the B-line serves them to reach the north of the network by also crossing the darker-blue and darker-red central zone (Figure 5.4b and 5.4e) which corresponds to an important transit hub of the city of Lyon. It appears therefore consistent to observe the aforementioned scenarios (*i.e.*, {1, B, D}, {1, A, D} and {1, A, B}) as the best results when using demand-sensitive global metrics with the REINFORCE methodology (Figure 5.2).

When considering demand-sensitive local metrics under normal conditions, we first notice that the DSNCC distribution (Figure 5.9a) with all public transport lines, the distribution is shifted to the right, meaning that more nodes have higher values of DSNCC and thus a better reachability by having a larger set of nodes closer to the other ones, in terms of free flow travel time, and attracting a huge part of the demand. Similar conclusions can be drawn for the three best selected scenarios with this demand-sensitive local metric. The accessibility of some nodes is improved as demonstrated by the increase of the number of nodes with values of DSNCC, higher than 200 with respect to the reference scenario without any public transport line. The two first scenarios {1, B, D} (Figure 5.9d) and {1, A, D} (Figure 5.9e) improve the reachability of the center-southern part of the network via the construction of the D-line, whereas concerning scenario {1, A, B} (Figure 5.9f), an improvement can be identified for the center-northern part of the city. Nonetheless, we notice that the improvement induced by this scenario is mild compared to the other two, as also highlight by the distribution of the metric, slightly skewed to the left compared to the other two, reported in Figure 5.9a. During the Festival of Lights, the shape DSNCC distribution (Figure 5.9h) does not change significantly from the one observed with typical public transport demand (Figure 5.9b), although the values are impacted by the change of the demand. Nonetheless, the spatial distribution of the metric over the areas is modified and this change is more visible when all the public transport lines are built. The DSNCCof the two areas with the highest demand is high (Figure 5.9i). In this case also, the D-line improves the reachability of the south of the network in scenarios {1, A, D} and {1, B, D}.

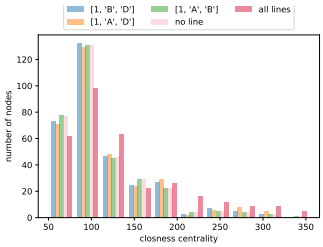

(a) DSNCC distribution under normal conditions

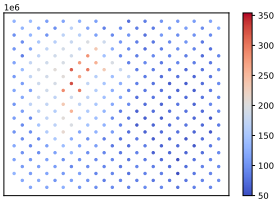

(b) DSNCC - no line under normal conditions

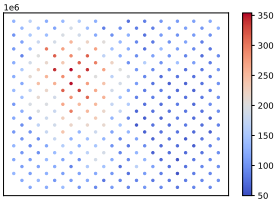

(c) DSNCC - all lines under normal conditions

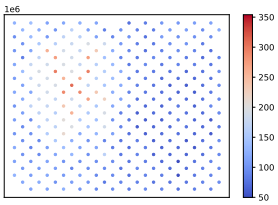

(d) DSNCC - 1, B, D under normal conditions

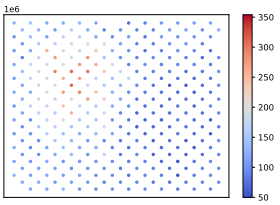

(e) DSNCC - 1, A, D under normal conditions

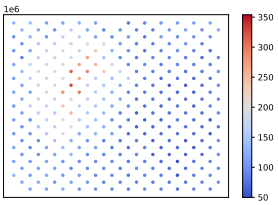

(f) DSNCC - 1, A, B under normal conditions

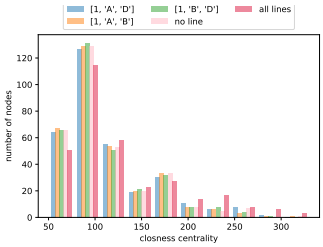

(g) DSNCC distribution during the Festival of Lights

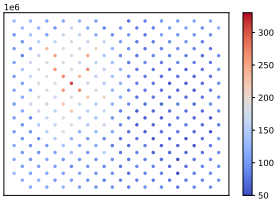

(h) DSNCC - no line during the Festival of Lights

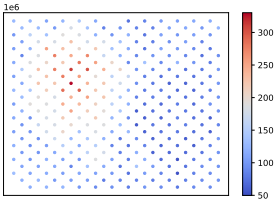

(i) DSNCC - all lines during the Festival of Lights

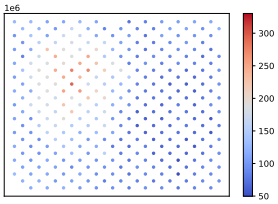

(j) DSNCC - 1, A, D during the Festival of Lights

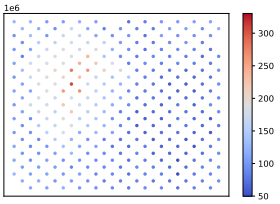

(k) DSNCC - 1, A, B during the Festival of Lights

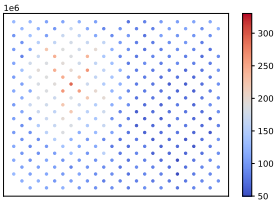

(l) DSNCC - 1, B, D during the Festival of Lights

Figure 5.9: Histogram of DSNCCand its spatial distribution in the studied scenarios under normal conditions and during the Festival of Lights.

Figure 5.10 present the distribution of the DSEBC under normal conditions and during the Festival of Lights. Under normal conditions as during the Festival of Lights, a large set of the road network (Figure 5.10a and Figure 5.10d) edges is crossed by a very small amount of shortest paths. Around 200 road-network edges presents an advantage in the multi-layer network performance by being crossed by a huge amount of shortest paths (DSEBC $>$ 2000) (Figure 5.10a and Figure 5.10d). During the Festival of Lights, the distribution of the DSEBC values for scenario {1, A, D} presents a slightly lower number of quasi-zero DSEBC than the two other scenarios. Regarding the tramway network, in all the selected scenarios and in both traffic conditions (normal conditions (Figure 5.10b) and during the Festival of Lights (Figure 5.10e)) the DSEBC of the edges belonging to the 1-line, have a similar trend. Whereas 11 edges of the 1-line have very marginal influence on the network performance by presenting a DSEBC close to 0, 9 edges of this line

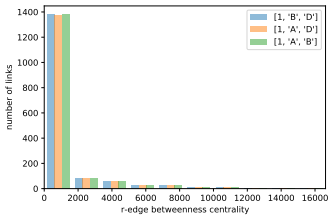

(a) DSEBC - road network under normal conditions

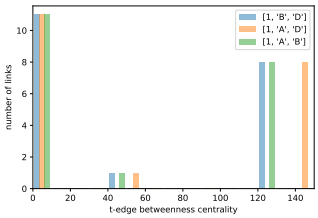

(b) DSEBC - tramway network under normal conditions

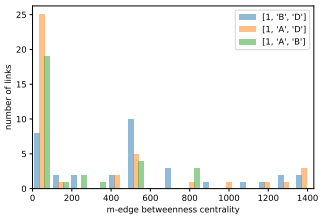

(c) DSEBC - subway network under normal conditions

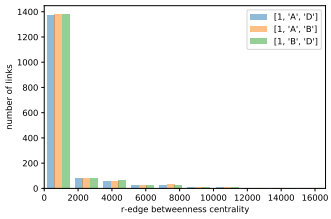

(d) DSEBC - road network during the Festival of Lights

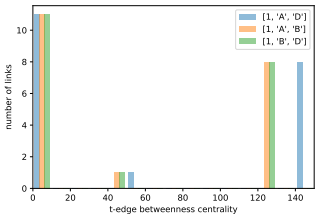

(e) DSEBC - tramway network during the Festival of Lights

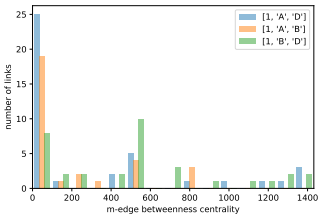

(f) DSEBC - subway network during the Festival of Lights

Figure 5.10: Histogram per transport mode of DSEBC in the studied scenarios.

still presents an interest, with one edge having a DSEBC comprised between 40 and 60, depending on the studied scenario, while 8 other edges of the 1-line are crossed by a much larger amount of shortest paths, *i.e.*, DSEBC presents values larger than 120. In particular, the second scenario, {1, A, D}, (Figure 5.8f) presents even higher values of DSEBC. Indeed, the 8 most attractive edges of the 1-line present DSEBC values higher than 140, against values comprised between 120 and 130 for the 8 same edges in the two other scenarios. This means that the line is more used in the scenario {1, A, D} when the B-line is not built. During the festival of Lights, the interest of 1-line in the scenario {1, A, D} is slightly reduced (Figure 5.10e) compared to the normal conditions (Figure 5.10b) with a reduction from 140 to 120 for the 8 more interesting edges in terms of DSEBC. On the contrary, in the scenario {1, B, D}, the tramway edges belonging to the 1-line better improve the transport network performances. Finally, concerning the subway network under normal conditions (Figure 5.10c), only 26 edges have a non-zero DSEBC in scenario {1, B, D} (Figure 5.8e) against 15 edges in scenario {1, A, D} and 11 edges in scenario {1, A, B}. The scenario {1, A, B} presents the less attractive distribution, by having a largest set of quasi-zero DSEBC and being shifted ti the left compared to the two others scenarios. During the Festival of Lights, for the subway network (Figure 5.10f), scenario {1, A, D} presents 25 quasi-zero DSEBC edges against 19 for scenario {1, A, B} and 8 for scenario {1, B, D}. In this last scenario, more edges are interesting in terms of transport network performance by attracting a higher demand over the shortest paths crossing these subway lines, according to the DSEBC distribution, which appears shifted to the right.

The REINFORCE methodology is suitable for quick augmentation of large multimodal transport networks, easily adaptable to any city for which the actual transport network offer is known, jointly with a plan of the new transport lines/modes to be built. The proposed solution can be also useful for the optimal deployment of public transport alternatives (such as a temporary bus line) when a disruptive event occurs on the network. By defining a set of alternative lines as an input, it is possible to find the bus routes which will provide the best network performances despite the disturbance. By quantifying the network performance and by taking both transport mode shift time into account for shortest path computation, using well-known resilience indicators and a suitable graph modelling, we ensure to propose the best lines combinations to be constructed in terms of efficiency and robustness. The redundancy is characterized by the NDC and the $\langle NDC \rangle$, while the efficiency by the AE, NCC and the EBC. The consideration of the travel demand in the selected metrics permits to assign more importance to specific transport lines or modes that serve a larger amount of trips. This conveys additional realism and accuracy to the REINFORCE methodology.

5.3 Optimization of a Disruption-sensitive Park-and-Ride System

In this chapter, we develop a Park-and-Ride (P&R) system adapted to recurrent disruptions and combined with an existing transport network. Two models are developed in this context. The first one aims at maximizing the ridership to reach city hype-center from the rest of the city and its neighborhoods whereas the second one aims at optimizing both the park locations and the deployment of an on-demand vehicle fleet by being attractive in terms of construction, operational and travel costs.

Both formulations are stochastic problems, allowing to make a resilient-aware P&R design, which aims at considering a set Ω of different scenariosω with a probability of occurrence p^{ω}, representing both normal conditions or recurrent disruptions, in the optimization of the P&R system in an existing transport network. Such existing network is represented by a graph whose nodes N correspond to the road intersections and the edges E to the road segments. Note that the scenario-dependency of the variables and parameters will be noted with a superscript $^{\omega}$. In each scenario we determine the set of the OD pairs (r, s) with a non-zeros total travel demand $W^{\omega} = \{(r, s) : d^{\omega}_{rs} > 0, r \in N, s \in N\}$ and for each OD pair, we determine the sets of the accessible pick ups i and drop offs j. To be attractive, the potential pick ups of the P&R has to be reached from the origin r in a reasonable time t^{ω}_{ri} lower than t^{access} as the destination s must be reached from the drop off j in a given time t^{ω}_{js} lower than t^{egress}. The travel times t^{ω}_{ri} correspond to the shortest travel time between the origin r and the pick up i of our road network (respectively the drop off j and the destinations s) fixed both t^{access} and t^{egress}. At the end we obtain the set of the potential pick ups $P^{\omega}_{r} = \{i \in P : t^{\omega}_{ri} \leq t^{\text{access}}\}$ among all the pick ups P and the set of potential drop offs $D^{\omega}_{s} = \{j \in D : t^{\omega}_{js} \leq t^{\text{egress}}\}$ among all the drop offs D. The set $\Sigma^{\omega}_{rs} = \{(i, j) : i \in P^{\omega}_{r}, j \in D^{\omega}_{s}, (r, s) \in W^{\omega}\}$ corresponds to the P&R possible combinations of pick ups and drop offs at each OD pair.

A notation table, for both formulation, is available at the end of the manuscript in Table 14 (Appendix C) and summarizes the parameters and variables names used in both models.

5.3.1 Ridership Maximization

First, we aim at proposing a model maximizing the ridership of the on-demand P&R system, which is a shared mobility system, in the presence of recurrent disruptions, with the goal of reducing the personal vehicle users whatever the traffic conditions or the external events. With the establishment of such a new public transport mode we reduce the number of vehicles over the network by capturing a part of the demand with the P&R system which is expected to improve resilience of the mobility network to recurrent traffic disruptions. A budget B is allowed to the construction of the pick ups and the drop offs whose costs $\boldsymbol{c}^{\text{loc}}_{i}$ depends on the nature of the facility. Because we focus the analysis on the morning peak hour, from the neighborhood to the city center, the pick ups are the places where the P&R users park their private vehicles to take the shuttles and the drop offs are the locations where the P&R users leave the shuttle to reach the destination on foot. For this reason, car parks need to be built for the pick ups whereas transit stop are sufficient for the drop offs. We define a binary decision variable $y_i \in \{0, 1\}$ indicating the facility locations by being equal to one when a park is open. To determine the mode choice we use a market share model based on the logit formula, widely used in transportation field (Aros-Vera et al. (2013), Chen et al. (2016), Huang et al. (2018), Jian et al. (2019)). The probability of choosing a transport mode for a specific itinerary is equal to the ratio of the utility of this transport mode and the sum of the utilities for all the others transport mode. It is important to notice that in our model, each combination of pick up and drop off to realize the itinerary is a possible choice for the transport mode. The utility function is thus $-\theta g^{\omega}_{rijs}$ where θ represents users sensitivity to the generalized cost g^{ω}_{rijs}. The higher θ is, the more people are sensitive to the generalized cost and will chose the transport mode with the lower cost. The generalized cost g^{ω}_{rijs} for each itinerary corresponds to the travel cost between the three parts of the path: from the origin to the pick up $c^{\mathrm{R}_{rs},\omega}_{ri}$, from the pick up to the drop off $c^{\text{route},\omega}_{ij}$ and from the drop off to the destination c^{walk}_{js} that we consider

equal to the travel time. When using the private vehicle, called reserve mode, this travel cost corresponds to the travel time from the origin to the destination $c_{rs}^{R_{rs},\omega}$. We define the decision variable $x_{rijs}^{\omega} \in \mathbb{R}^{+}$ as the flow which determine the part of the demand d_{rs}^{ω} using our P&R system on the OD pair (r,s) by using the pick up i and the drop off j. The decision variable $x_{rs}^{\omega,R_{rs}}$ defines the part of the users taking the reserve mode on the OD pair (r,s). As Aros-Vera et al. (2013) pointed out, we must adapt the logit model to consider all the possible pick ups and drop offs combinations while we do not know which are open before the solution. For a sake of simplicity in the implementation of the model, we considered $x_{rs}^{\omega,R_{rs}}$ and x_{rijs}^{ω} as a unique variable where i and j could take the value R_{rs}, symbolizing the use of the reserve mode to realize the entire itinerary. The corresponding decision variable $y_{R_{rs}}$ is always equal to 1 meaning that this transport mode is always available to assess the path and the corresponding construction cost $c_{R_{rs}}$ is null. We finally obtained a unique variable $x_{rijs}^{\omega}, \forall \omega \in \Omega, \forall (r,s) \in W^{\omega}, \forall (i,j) \in P_r^{omega} \times D_s^{omega} \cup \{R_{rs}\}$.

5.3.1.1 Problem Formulation

5.3.1.1.1 Mode-choice model: The mode-choice behaviour and the route choice are emulated by means of a market share model based on a logit formulation, widely used in the field of transportation (Aros-Vera et al., 2013; Chen et al., 2016; Huang et al., 2018; Jian et al., 2019). The probability of choosing a transport mode for a specific itinerary is equal to the ratio of the exponential of the utility $e^{-\theta g_{rijs}^{\omega}}$ of this transport mode and the sum of the utilities for all the other transport mode. It is important to notice that in our model, each combination of pick up and drop off available to realize the itinerary is a possible choice for the transport mode. At the end, the different transport mode are the reserve mode and the shuttle service of the proposed P&R from all accessible pick ups i to all accessible drop offs j. As Aros-Vera et al. (2013) pointed out, we do not know which pick ups or drop offs are open before the solution of the model. For this reason, we adapt the logit formulation to consider all the transport mode alternative possibilities (reserve mode and different P&R choices between the accessible pick ups and drop offs). Because both pick up and drop off have to be opened to be considered as an option in the mode choice, the exponential of the utility for all the transport mode possibilities are multiplied by the pick up and the drop off location decision variables y_i and y_j. The closure of a pick up, a drop off or both will remove the consideration of the associated transport modes in the logit computation. For the sake of simplicity, in the implementation of the model, we consider $x_{rs}^{\omega,R_{rs}}$ and x_{rijs}^{ω} as a unique variable where i and j could take the value R_{rs}, symbolizing the use of the reserve mode to realize the entire itinerary. At the end, the probability that users choose the pair i and j of the P&R system is:

$$x_{rijs}^{\omega} \equiv \frac{y_i y_j e^{-\theta g_{rijs}^{\omega}}}{\sum\limits_{(m,n) \in \Sigma_{rs}^{\omega} \cup \{R_{rs}\}} y_m y_n e^{-\theta g_{rmns}^{\omega}}} \quad \forall (r,s) \in W, \forall (i,j) \in \Sigma_{rs}^{\omega} \cup \{R_{rs}\} \tag{5.2}$$

Variable x_{rijs}^{ω} represents the probability of using the reserve mode between the OD pair (r,s), when i and j are equal to R_{rs}, as well as the probability of using the proposed P&R system by using a shuttle joining the pick up i to the drop off j for the OD pair (r,s). The consideration of the possible use of a pick up and a drop off depends on the opening of both locations, *i.e.*, $y_i = 1$ *and* $y_j = 1$. If the pick up i or the drop off j or both are not located (*i.e.*, $y_i = 0$, $y_j = 0$ or $y_i = 0$ *and* $y_j = 0$) the probability of using this transport mode is null. The reserve mode, conversely, is always a possible alternative to perform a trip between an origin r and a destination s, as $y_{R_{rs}}$ is always equal to one. It is worth to recall that θ symbolizes the users' sensitivity to the generalized costs $g_{rs}^{R_{rs}}$, which corresponds to the travel time between r and s using the reserve mode and the parameter g_{rijs}^{ω} (respectively g_{rmns}^{ω}) corresponds to the travel time between r and s using the P&R system from the pick up i (respectively m) to the drop off j (respectively n) for the path going from the origin r to the destination s.

5.3.1.1.2 Flow and linking constraints: The linearization of the market share equation given by the logit model (5.2) is essential to consider the mode choice in our Mixed-Integer Linear Programming (MILP) problem. The combination of the following equations (5.3a), (5.3b), (5.3c) and (5.3d), based on the ones proposed by Aros-Vera et al. (2013), reproduce the logit formulation and represents the proportion of the users for each mobility alternative. The first constraint (5.3a) ensures that the whole demand is served for each origin-destination pair. Users must perform these trips through the P&R system or using the reserve mode. The second constraint (5.3b) requires that the flow share of each mobility alternative obey to a logit model. For each OD pair, this choice is governed by the utility of mobility alternatives through the P&R system which is function of opened P&R facilities and of that of the reserve mode. For a given P&R path (r, i, j, s), if the pick up location y_i or the drop off location y_j or both are closed, the constraint is inactive due to linking constraints (5.3c) and (5.3d), forcing the flow share to be lower than one when parks are open, and zero otherwise. For a given OD pair (r, s), it is only possible to have a non zero portion of users use path (r, i, j, s) if and only if $y_i = y_j = 1$. The decision variable representing the portion of users going from the origin r to the destination s through the pick up i and the drop off j, x^{ω}_{rijs}, must be positive (5.3e). Constraints (5.3f) and (5.3g) set the domain of binary variables y_i and fix all such variables to one for the mobility alternative corresponding to the reserve mode. The following result is an extension of the result of Aros-Vera et al. (2013) for three-link trip chains.

$$\sum_{(i,j)\in\Sigma^{\omega}_{rs}\cup\{\mathrm{R}_{rs}\}} x^{\omega}_{rijs} = 1 \qquad \forall\omega\in\Omega, \forall(r,s)\in W^{\omega} \tag{5.3a}$$

$$x^{\omega}_{rijs} \leq x^{\omega}_{rmns}\frac{e^{-\theta g^{\omega}_{rijs}}}{e^{-\theta g^{\omega}_{rmns}}} + (2 - y_m - y_n) \qquad \forall\omega\in\Omega, \forall(r,s)\in W^{\omega}, \forall(m,n),(i,j)\in\Sigma^{\omega}_{rs}\cup\{\mathrm{R}_{rs}\}: \forall(m,n),(i,j)\in\Sigma^{\omega}_{rs}\cup\{\mathrm{R}_{rs}\}:(i,j)\neq(m,n) \tag{5.3b}$$

$$x^{\omega}_{rijs} \leq y_i \qquad \forall\omega\in\Omega, \forall(r,s)\in W^{\omega}, \forall(i,j)\in\Sigma^{\omega}_{rs} \tag{5.3c}$$

$$x^{\omega}_{rijs} \leq y_j \qquad \forall\omega\in\Omega, \forall(r,s)\in W^{\omega}, \forall(i,j)\in\Sigma^{\omega}_{rs} \tag{5.3d}$$

$$x^{\omega}_{rijs} \geq 0 \qquad \forall\omega\in\Omega, \forall(r,s)\in W^{\omega}, \forall(i,j)\in\Sigma^{\omega}_{rs}\cup\{\mathrm{R}_{rs}\} \tag{5.3e}$$

$$y_{\mathrm{R}_{rs}} = 1 \qquad \forall\omega\in\Omega, \forall(r,s)\in W^{\omega} \tag{5.3f}$$

$$y_i \in \{0,1\} \qquad \forall i\in P\cup D \tag{5.3g}$$

5.3.1.1.3 Budget constraint: The P&R model aims at maximizing the part of users of the P&R system, by opening some facility locations, within a set of candidates, accessible from the users' origin and destination. The determination of the scenario-dependent flow per pick up/drop off path insights about the fleet sizing needed for a specific event. In the proposed P&R model, the facility location variable is binary due to the two potential state of the parks (closed or open) and is constrained by the park construction cost c^{loc}_i and the global allocated budget B. The budget constraint (5.3) determines the ability of building the facilities by satisfying the global cost of the open parks.

$$\sum_{i\in P\cup D} c^{\mathrm{loc}}_i y_i \leq B \tag{5.3}$$

5.3.1.1.4 Formulation: The resulting P&R facility location formulation summarized in (5.4) is a MILP. By maximizing the objective function (5.4a), the solution increases for all the OD pairs (r, s) the portion x^{ω}_{rijs} of the demand d^{ω}_{rs} using our P&R system whatever the chosen pick up i and drop off j in each scenario ω. The higher the probability p^{ω} related to the occurrence of an event is, the more the system will fit it.

By being attractive in terms of travel time with the car parks and transit stops opening, the P&R system helps to reduce the private vehicle circulation in the city center of the cities and increase its resilience with respect to recurrent disruptive scenarios by providing an alternative transport mode. The complexity of the problem highly increases with the graph size due to the number of variables, as detailed in the sensitivity analysis (Section 5.3.1.4): for the small network composed of 59 nodes used in our numerical experiments, the formulation corresponds to 267 000 constraints and 15 000 variables; the problem grows to 15 000 000 constraints and 270 000 variables for the larger one, composed of 135 nodes. We thus propose, in the next Section 5.3.1.2, a scalable approach that can accommodate large mobility networks.

$$\max \quad \sum_{\omega\in\Omega} p^{\omega} \sum_{(r,s)\in W^{\omega}} d^{\omega}_{rs} \sum_{(i,j)\in\Sigma^{\omega}_{rs}} x^{\omega}_{rijs} \tag{5.4a}$$

$$\text{s.t.} \sum_{i\in P\cup D} c^{\text{loc}}_i y_i \leq B \tag{5.4b}$$

$$\sum_{(i,j)\in\Sigma^{\omega}_{rs}\cup\{\text{R}_{rs}\}} x^{\omega}_{rijs} = 1 \qquad \forall\omega\in\Omega, \forall(r,s)\in W^{\omega} \tag{5.4c}$$

$$x^{\omega}_{rijs} \leq x^{\omega}_{rmns} \frac{e^{-\theta g^{\omega}_{rijs}}}{e^{-\theta g^{\omega}_{rmns}}} + (2 - y_m - y_n) \qquad \forall\omega\in\Omega, \forall(r,s)\in W^{\omega}, \forall(m,n),(i,j)\in\Sigma^{\omega}_{rs}\cup\{\text{R}_{rs}\} : (i,j)\neq(m,n) \tag{5.4d}$$

$$x^{\omega}_{rijs} \leq y_i \qquad \forall\omega\in\Omega, \forall(r,s)\in W^{\omega}, \forall(i,j)\in\Sigma^{\omega}_{rs} \tag{5.4e}$$

$$x^{\omega}_{rijs} \leq y_j \qquad \forall\omega\in\Omega, \forall(r,s)\in W^{\omega}, \forall(i,j)\in\Sigma^{\omega}_{rs} \tag{5.4f}$$

$$y_{\text{R}_{rs}} = 1 \qquad \forall\omega\in\Omega, \forall(r,s)\in W^{\omega} \tag{5.4g}$$

$$x^{\omega}_{rijs} \geq 0 \qquad \forall\omega\in\Omega, \forall(r,s)\in W^{\omega}, \forall(i,j)\in\Sigma^{\omega}_{rs} \tag{5.4h}$$

$$y_i \in \{0,1\} \qquad \forall i\in P\cup D \tag{5.4i}$$

5.3.1.2 Lagrangian Relaxation Algorithm

To solve the proposed P&R facility location problem (5.4) over large scale networks, we adopt a decomposition approach based on the Lagrangian Relaxation (LR) (5.5) and (5.6) which approximates a difficult problem of constrained optimization by a simpler problem. The solution of the LR formulation provides upper bounds on the original problem objective function (5.4a). To iteratively generate lower bounds during the solution of the LR problem, we define a customized heuristic algorithm. In the Lagrangian function $L(\boldsymbol{\pi},\boldsymbol{\delta},\boldsymbol{\lambda})$, we dualize constraints (5.4d), (5.4e) and (5.4f) which contain both flow variables (x_{rijs}) and location variables (y_i), and we associate Lagrange Multipliers (LM), vectors of positive values, to the relaxed constraints. ($\lambda^{\omega}_{rijmns}$ for constraint (5.4d), π^{ω}_{rijs} for constraint (5.4e), and δ^{ω}_{rijs} for constraint (5.4f)). The aim of LR is to find the LM $\boldsymbol{\pi}^{\star}$, $\boldsymbol{\delta}^{\star}$ and $\boldsymbol{\lambda}^{\star}$ which maximize $L(\boldsymbol{\pi},\boldsymbol{\delta},\boldsymbol{\lambda})$ so that the lower bound is as tight as possible, ideally equal, to the optimal objective value. Moreover, by relaxing the constraints involving both variables x^{ω}_{rijs} and y_i, *i.e.*, (5.4e), (5.4f) and (5.4d), we can separate the LR into two sub-problems: a linear assignment problem which distributes users within paths of the P&R system or their reserve mode (5.5), a facility location problem which is an easier integer-linear problem (5.6) than (5.4). $L_{\boldsymbol{x}}(\boldsymbol{\pi},\boldsymbol{\delta},\boldsymbol{\lambda})$ is the part of $L(\boldsymbol{\pi},\boldsymbol{\delta},\boldsymbol{\lambda})$ which contains exclusively terms depending on the scenario-based flow variables and $L_{\boldsymbol{y}}(\boldsymbol{\pi},\boldsymbol{\delta},\boldsymbol{\lambda})$ the part of $L(\boldsymbol{\pi},\boldsymbol{\delta},\boldsymbol{\lambda})$ which contains exclusively terms related to the facility location variables. The Lagrangian sub-problem (5.5) depends on the flow variable and can be decomposed into scenario-based sub-problems by separating flows variables x^{ω}_{rijs} corresponding to each scenario $\omega\in\Omega$. At the end, we obtain $L_{\boldsymbol{x}}(\boldsymbol{\pi},\boldsymbol{\delta},\boldsymbol{\lambda}) = \sum_{\omega\in\Omega} L_{\boldsymbol{x},\omega}(\boldsymbol{\pi},\boldsymbol{\delta},\boldsymbol{\lambda})$.

$$L_{\boldsymbol{x}}(\boldsymbol{\pi},\boldsymbol{\delta},\boldsymbol{\lambda}) = \max \sum_{\omega\in\Omega} p^{\omega} \sum_{(r,s)\in W^{\omega}} d^{\omega}_{rs} \sum_{(i,j)\in\Sigma^{\omega}_{rs}} x^{\omega}_{rijs} - \sum_{\omega\in\Omega}\sum_{(r,s)\in W^{\omega}}\sum_{(i,j)\in\Sigma^{\omega}_{rs}} (\pi^{\omega}_{rijs}+\delta^{\omega}_{rijs})x^{\omega}_{rijs}$$
$$+ \sum_{\omega\in\Omega}\sum_{(r,s)\in W^{\omega}}\sum_{(i,j)\in\Sigma^{\omega}_{rs}\cup\{\mathsf{R}_{rs}\}}\sum_{\substack{(m,n)\in\Sigma^{\omega}_{rs}\cup\{\mathsf{R}_{rs}\},\\(m,n)\neq(i,j)}} \lambda^{\omega}_{rijmns}\left(x^{\omega}_{rmns}\frac{e^{-\theta g^{\omega}_{rijs}}}{e^{-\theta g^{\omega}_{rmns}}} - x^{\omega}_{rijs}\right) \tag{5.5a}$$

$$\text{s.t.} \sum_{(i,j)\in\Sigma^{\omega}_{rs}\cup\{\mathsf{R}_{rs}\}} x^{\omega}_{rijs} = 1 \qquad \forall\omega\in\Omega, \forall(r,s)\in W^{\omega} \tag{5.5b}$$

$$x^{\omega}_{rijs} \geq 0 \qquad \forall\omega\in\Omega, \forall(r,s)\in W^{\omega}, \forall(i,j)\in\Sigma^{\omega}_{rs}\cup\{\mathsf{R}_{rs}\} \tag{5.5c}$$

The Lagrangian sub-problem (5.6) depends on the facility location variable.

$$L_{\boldsymbol{y}}(\boldsymbol{\pi},\boldsymbol{\delta},\boldsymbol{\lambda}) = \max \sum_{\omega\in\Omega}\sum_{(r,s)\in W^{\omega}}\sum_{(i,j)\in\Sigma^{\omega}_{rs}} (\pi^{\omega}_{rijs}y_i + \delta^{\omega}_{rijs}y_j)$$
$$+ \sum_{\omega\in\Omega}\sum_{(r,s)\in W^{\omega}}\sum_{(i,j)\in\Sigma^{\omega}_{rs}\cup\{\mathsf{R}_{rs}\}}\sum_{\substack{(m,n)\in\Sigma^{\omega}_{rs}\cup\{\mathsf{R}_{rs}\},\\(m,n)\neq(i,j)}} \lambda^{\omega}_{rijmns}(2-y_m-y_n) \tag{5.6a}$$

$$\text{s.t.} \sum_{i\in P\cup D} c^{\text{loc}}_i y_i \leq B \tag{5.6b}$$

$$y_{\mathsf{R}_{rs}} = 1 \qquad \forall\omega\in\Omega, \forall(r,s)\in W^{\omega} \tag{5.6c}$$

$$y_i \in \{0,1\} \qquad \forall i\in P\cup D \tag{5.6d}$$

To implement the LR, we develop a Lagrangian Relaxation Algorithm (LA). The proposed LA, which aims at solving both $L_{\boldsymbol{x}}(\boldsymbol{\pi},\boldsymbol{\delta},\boldsymbol{\lambda})$ and $L_{\boldsymbol{y}}(\boldsymbol{\pi},\boldsymbol{\delta},\boldsymbol{\lambda})$ to compute the UB and at computing some heuristics to compute feasible solutions corresponding to the LB, is presented in the Algorithm 1. In the following, $\boldsymbol{x}$ corresponds to the vector of the scenario-based flow variables and $\boldsymbol{y}$ the vector of the facility location variables.

The proposed LA is presented in Algorithm 1. As a first step of the LA, we initialize the LM and the iteration counter. A first lower bound LB^0, issued from the constructed vectors $\hat{\boldsymbol{x}}^0$ and $\hat{\boldsymbol{y}}^0$, is computed using the heuristic described in Algorithm 2, before beginning the iterations. Such step could help the proposed LA to converge if this LB^0 is better than the lower bound issued from the iterations, especially when the problem complexity limits the number of iterations in a given time. Although simplistic, the heuristic provides more accurate results, with a higher lower bound and a lower gap between the lower and the upper bounds, for large-scale instances than the one obtained in a very small set of iterations of the proposed LA. In this heuristic we first open all the locations y_i to compute the feasible flow x^{ω}_{rijs} (Algorithm 3), with the market share model issued from the logit formula (5.2), for each scenario, each origin/destination pair and each pick up/drop off or reserve mode of the P&R model, in order to know the flow crossing each location. After sorting the decision variable y_i, depending on the ratio of the construction cost over the part of the flow of users crossing each facility, then we close the car park and/or transit stop with the higher ratio, while the budget constraint is respected. The new corresponding flow is computed using the logit formulation (Algorithm 3). As a final step, the lower bound is computed, issued from the objective function. The combination of this heuristic (Algorithm 2) with the LA ensures a reduced gap between the lower and the upper bounds especially for large scale instance.

Algorithm 1: Lagrangian Relaxation Algorithm Overview

Input: ϵ, TL^{glob}, TL^{heur}
Output: LB, UB, $\boldsymbol{x}$, $\boldsymbol{y}$
/* Initialization of bounds, LM and parameters */
1 Gap $\leftarrow +\infty$
2 UB $\leftarrow +\infty$
3 LB $\leftarrow$ Algorithm 2 // Construct initial feasible solution
4 $\boldsymbol{\pi}, \boldsymbol{\delta}, \boldsymbol{\lambda} \leftarrow \mathbf{0}$
5 $\mathsf{TL}^{glob} \leftarrow 0$
6 $n \leftarrow 0$
/* Main loop */
7 **while** Gap $> \epsilon$ **or** $\mathsf{Timer}^{glob} \leq \mathsf{TL}^{glob}$ **do**
8 **for** $\omega \in \Omega$ **do**
9 $\boldsymbol{x}^{\omega,n} \leftarrow$ Solve $L_{\boldsymbol{x},\omega}(\boldsymbol{\pi}, \boldsymbol{\delta}, \boldsymbol{\lambda})$
10 $L_{\boldsymbol{x}}(\boldsymbol{\pi}, \boldsymbol{\delta}, \boldsymbol{\lambda}) \leftarrow \sum_{\omega \in \Omega} L_{\boldsymbol{x},\omega}(\boldsymbol{\pi}, \boldsymbol{\delta}, \boldsymbol{\lambda})$
11 $\boldsymbol{x}^n \leftarrow [\boldsymbol{x}^{\omega,n}]_{\omega \in \Omega}$
12 $\hat{\boldsymbol{y}}^n, \boldsymbol{x}'^n, \mathsf{LB}^n_{L_{\boldsymbol{x}}} \leftarrow$Algorithm 4 $(\boldsymbol{x}^n)$ // Construct feasible solution from $\boldsymbol{x}$
13 $\boldsymbol{y}^n \leftarrow$ Solve $L_{\boldsymbol{y}}(\boldsymbol{\pi}, \boldsymbol{\delta}, \boldsymbol{\lambda})$
14 $\hat{\boldsymbol{x}}^n, \mathsf{LB}^n_{L_{\boldsymbol{y}}} \leftarrow$Algorithm 5 $(\boldsymbol{y}^n)$ // Construct feasible solution from $\boldsymbol{y}$
15 $\mathsf{LB}^n \leftarrow \max\{\mathsf{LB}^n_{L_{\boldsymbol{x}}}, \mathsf{LB}^n_{L_{\boldsymbol{y}}}\}$
16 **if** $\mathsf{LB}^n_{L_{\boldsymbol{x}}} \geq \mathsf{LB}^n_{L_{\boldsymbol{y}}}$ **then**
17 $(\boldsymbol{x}^{*,n}, \boldsymbol{y}^{*,n}) \leftarrow (\boldsymbol{x}'^n, \hat{\boldsymbol{y}}^n)$
18 **else**
19 $(\boldsymbol{x}^{*,n}, \boldsymbol{y}^{*,n}) \leftarrow (\hat{\boldsymbol{x}}^n, \boldsymbol{y}^n)$
20 $\mathsf{TL}^{heur} \leftarrow 0$
/* Local search loop */
21 **while** LB^n *improved by the local search* **and** $\mathsf{Timer}^{heur} \leq \mathsf{TL}^{heur}$ **do**
22 $\mathsf{LB}^n, \boldsymbol{x}^{*,n}, \boldsymbol{y}^{*,n} \leftarrow$ Algorithm 6 $(\mathsf{LB}^n, \boldsymbol{y}^{*,n})$ // 1-distance local search on $\boldsymbol{y}$
23 $\mathsf{LB}^n, \boldsymbol{x}^{*,n}, \boldsymbol{y}^{*,n} \leftarrow$ Algorithm 7 $(\mathsf{LB}^n, \boldsymbol{y}^{*,n})$ // Swap local search on $\boldsymbol{y}$
24 Update Timer^{heur}
25 **if** $\mathsf{LB}^n \geq \mathsf{LB}$ **then**
26 $\mathsf{LB} \leftarrow \mathsf{LB}^n$ $(\boldsymbol{x}, \boldsymbol{y}) \leftarrow (\boldsymbol{x}^{*,n}, \boldsymbol{y}^{*,n})$
27 $\mathsf{UB} \leftarrow \min\{\mathsf{UB}, L_{\boldsymbol{x}}(\boldsymbol{\pi}, \boldsymbol{\delta}, \boldsymbol{\lambda}) + L_{\boldsymbol{y}}(\boldsymbol{\pi}, \boldsymbol{\delta}, \boldsymbol{\lambda})\}$
28 $\mathsf{Gap} \leftarrow \frac{\mathsf{UB}-\mathsf{LB}}{\mathsf{UB}}$
29 Update LM using (5.7)
30 Update Timer^{glob}

After initializing the parameters and computing a first lower bound, we begin the LR (Algorithm 1, line 1 to line 5). At each iteration n we repeat the same steps. First, we compute the optimal solution for of sub-problems $L_{\boldsymbol{x}}(\boldsymbol{\pi}, \boldsymbol{\delta}, \boldsymbol{\lambda})$ and $L_{\boldsymbol{y}}(\boldsymbol{\pi}, \boldsymbol{\delta}, \boldsymbol{\lambda})$. The first sub-problem $L_{\boldsymbol{x}}(\boldsymbol{\pi}, \boldsymbol{\delta}, \boldsymbol{\lambda})$ provides a vector $\boldsymbol{x}^n$ (Algorithm 1, line 8 to line 11) which may not be feasible. To obtain a feasible solution from this vector, we build a feasible vector $\hat{\boldsymbol{y}}^n$ from $\boldsymbol{x}^n$ (Algorithm 1, line 12). To that purpose, we open all the parks crossed by a non zero flow. If opening all these parks violates the budget constraint, we close the pick up and/or drop off whose ratio of construction cost over the crossing flow is the highest, until the budget constraint is satisfied. Finally, we recompute the flow $\boldsymbol{x}'^n$ corresponding to the P&R design $\hat{\boldsymbol{y}}^n$ (Algorithm 4).

Algorithm 2: First LB computation

Input:
Output: $\boldsymbol{x}^0$, $\boldsymbol{y}^0$, LB^0

for $i \in P \cup D$ **do**
  $\hat{y}_i^0 \leftarrow 1$ $f_i \leftarrow$ Sum of the flows $\boldsymbol{x}^0$ crossing i
$S_{\hat{\boldsymbol{y}}^0} \leftarrow$ Sort $\hat{\boldsymbol{y}}^0$ increasingly by $\boldsymbol{c}_i^{\mathsf{loc}}/f_i$
for $i \in S_{\hat{\boldsymbol{y}}^0}$ **do**
  while $\sum_{j \in P \cup D} \boldsymbol{c}_j^{loc} y_j \geq B$ **do**
    $\hat{y}_i^0 \leftarrow 0$
$\hat{\boldsymbol{x}}^0 \leftarrow$ Feasible flow for the park design $\hat{\boldsymbol{y}}^0$ according to Eq. (5.2) using Algorithm 3
$\mathsf{LB}^0 \leftarrow$ Compute objective function (5.4a) for $(\hat{\boldsymbol{x}}^0, \hat{\boldsymbol{y}}^0)$ **while** LB^0 *improved by the local search* **and** $\mathsf{Timer}^{heur} \leq \mathsf{TL}^{heur}$ **do**
  $\mathsf{LB}^0, \hat{\boldsymbol{x}}^0, \hat{\boldsymbol{y}}^0 \leftarrow$ Algorithm 6 $(\mathsf{LB}^0, \hat{\boldsymbol{y}}^0)$ `// 1-distance local search on` $\boldsymbol{y}$
  $\mathsf{LB}^0, \hat{\boldsymbol{x}}^0, \leftarrow$ Algorithm 7 $(\mathsf{LB}^0, \hat{\boldsymbol{y}}^0)$ `// Swap local search on` $\boldsymbol{y}$
  Update Timer^{heur}

Algorithm 3: Feasible flow computation

Input: $\boldsymbol{x}$
Output: $\boldsymbol{y}$

for $\omega \in \Omega$ **do**
  for $(r,s) \in W^\omega$ **do**
    for $(i,j) \in \Sigma_{rs}^\omega$ **do**
      $x_{rijs}^\omega \leftarrow \frac{y_i y_j e^{-\theta g_{rijs}^\omega}}{\sum_{(m,n) \in \Sigma_{rs}^\omega \cup \{\mathsf{Rrs}\}} y_m y_n e^{-\theta g_{rmns}^\omega}}$

Algorithm 4: Construction of a feasible solution from $L_{\boldsymbol{x}}$

Input: $\boldsymbol{x}^n$
Output: $\hat{\boldsymbol{y}}^n$, $\boldsymbol{x}'^n$, $\mathsf{LB}_{L_{\boldsymbol{x}}}^n$

for $(i,j) \in \Sigma_{rs}^\omega$ **do**
  if $x_{rijs}^\omega \neq 0$ **then**
    $(\hat{y_i}^n, \hat{y_j}^n) \leftarrow (1,1)$
$f_i \leftarrow$ Sum of the flows $\boldsymbol{x}^n$ crossing i
$S_{\hat{\boldsymbol{y}}^n} \leftarrow$ Sort $\boldsymbol{y}$ by increasing $\boldsymbol{c}_i^{\mathsf{loc}}/f_i$
for $i \in S_{\hat{\boldsymbol{y}}^n}$ **do**
  while $\sum_{j \in P \cup D} \boldsymbol{c}_j^{loc} y_j \geq B$ **do**
    $\hat{y}_i^n \leftarrow 0$
$\boldsymbol{x}'^n \leftarrow$ Feasible flow for the park design $\hat{\boldsymbol{y}}^n$ (5.2)
$\mathsf{LB}_{L_{\boldsymbol{x}}}^n \leftarrow$ Compute the objective function for $(\boldsymbol{x}^n, \hat{\boldsymbol{y}}^n)$ (5.4a) Algorithm 3

The second sub-problem $L_{\boldsymbol{y}}(\boldsymbol{\pi}, \boldsymbol{\delta}, \boldsymbol{\lambda})$ gives a solution $\boldsymbol{y}^n$ (Algorithm 1, line 13). We use the logit formula to obtain a feasible flow pattern $\hat{\boldsymbol{x}}^n$ corresponding to this P&R design solution (Algorithm 5) (Algorithm 1, line 14). Once the two feasible solutions are established $(\boldsymbol{x}^n, \hat{\boldsymbol{y}}^n)$ and $(\hat{\boldsymbol{x}}^n, \boldsymbol{y}^n)$ we are able to compute both corresponding lower bounds $\mathsf{LB}_{L_{\boldsymbol{x}}}^n$ and $\mathsf{LB}_{L_{\boldsymbol{y}}}^n$ respectively issued from $L_{\boldsymbol{x}}(\boldsymbol{\pi}, \boldsymbol{\delta}, \boldsymbol{\lambda})$ and $L_{\boldsymbol{y}}(\boldsymbol{\pi}, \boldsymbol{\delta}, \boldsymbol{\lambda})$. The higher of the two is conserved as a local lower bound LB^n and the couple of vectors $(\boldsymbol{x}^{*,n}, \boldsymbol{y}^{*,n})$ corresponding

to the best vectors combination, maximizing the lower bound, $(\boldsymbol{x}^n, \hat{\boldsymbol{y}}^n)$ or $(\hat{\boldsymbol{x}}^n, \boldsymbol{y}^n)$ is defined (Algorithm 1, line 15 to line 19). The global lower bound LB, which corresponds to the highest lower bound obtained since the beginning of the LA, including the first lower bound LB^0, is updated, as well as the couple of vectors $(\boldsymbol{x}, \boldsymbol{y})$, if and only if the local lower bound LB^n exceeds the global one.

Algorithm 5: Construction of a feasible solution from $L_{\boldsymbol{y}}$

Input: $\boldsymbol{y}^n$
Output: $\hat{\boldsymbol{x}}^n$, $\mathsf{LB}^n_{L_{\boldsymbol{y}}}$
1 $\hat{\boldsymbol{x}}^n \leftarrow$ Feasible flow for the park design $\boldsymbol{y}^n$ using the logit formula Eq. (5.2) Algorithm 3
2 $\mathsf{LB}^n_{L_{\boldsymbol{y}}} \leftarrow$ Compute the objective function for $(\hat{\boldsymbol{x}}^n, \boldsymbol{y}^n)$ (5.4a)

Algorithm 6: One distance neighborhood search

Input: LB^n, $\boldsymbol{y}^{*,n}$
Output: LB^n, $\boldsymbol{x}^{*,n}$, $\boldsymbol{y}^{*,n}$, $\boldsymbol{x}$, $\boldsymbol{y}$
1 `update` $\leftarrow$ `True`
2 **while** `update = True` **do**
3 `update` $\leftarrow$ `False`
4 **for** $i \in P \cup D$ **do**
5 $\overline{\boldsymbol{y}} \leftarrow \boldsymbol{y}^{*,n}$
6 **if** $y_i^{*,n} = 1$ **then**
7 $\overline{y_i} \leftarrow 0$
8 **else**
9 $\overline{y_i} \leftarrow 1$
10 $\overline{\boldsymbol{x}} \leftarrow$ Feasible flow for the park design $\overline{\boldsymbol{y}}$ (5.2) Algorithm 3
11 $\overline{\mathsf{LB}} \leftarrow$ Compute the objective function for $(\overline{\boldsymbol{x}}, \overline{\boldsymbol{y}})$ (5.4a)
12 **if** $\overline{\mathsf{LB}} \geq \mathsf{LB}^n$ **then**
13 $\mathsf{LB}^n \leftarrow \overline{\mathsf{LB}}$
14 $(\boldsymbol{x}^{*,n}, \boldsymbol{y}^{*,n}) \leftarrow (\overline{\boldsymbol{x}}, \overline{\boldsymbol{y}})$
15 `update` $\leftarrow$ `True`
16 **break**

To improve the performance of our heuristic, we apply local search algorithms for the solutions with the aim to further increase the previously discussed lower bound. To this purpose, we alternate between a neighborhood search and swap moves until there is no improvement in the lower bound or all the local combinations have been explored. We also use a time limit constraint to avoid spending excessive computation time in the search procedure for local improvement of a given iteration of theLR (Algorithm 1, line 21 to line 24). In our neighborhood exploration (Algorithm 6), we sequentially set binary facility variables of the current best solution $\hat{\boldsymbol{y}}^n$ to their complementary value, *i.e.*, open parks that are closed and close parks that are open, provided that the budget constraint remains satisfied. For each solution in the neighborhood of the current best solution, we recalculate the flow assignment $\boldsymbol{x}$ (Algorithm 3) and determine the corresponding objective value which will replace the local lower bound LB^n if the result is higher. The global lower bound LB should also be replaced by this solution if LB is lower.

We apply a second local search which swaps pairs of open and closed parks (Algorithm 7). Contrary to the neighborhood local search, the $\boldsymbol{y}$ vector is modified in a way that a park opening is combined with a park closure and a park closure is paired with a park opening based on the respective park construction costs. We also recalculate the flow assignment $\boldsymbol{x}$ and modify the LB^n if the solution improves.

Algorithm 7: Swap search

Input: LB^n, $\boldsymbol{y}^{*,n}$
Output: LB^n, $\boldsymbol{x}^{*,n}$, $\boldsymbol{y}^{*,n}$, $\boldsymbol{x}$, $\boldsymbol{y}$

```
update ← True
while update = True do
    update ← False
    for i ∈ P ∪ D do
        ȳ ← y^{*,n}
        if y_i^{*,n} = 1 then
            ȳ_i ← 0
            for j ∈ P ∪ D do
                if y_j^{*,n} = 0  &  c_j^{loc} < c_i^{loc} then
                    ȳ_j ← 1
        else
            ȳ_i ← 1
            for j ∈ P ∪ D do
                if y_j^{*,n} = 1 then
                    ȳ_j ← 0
        x̄ ← Feasible flow for the park design ȳ (5.2) Algorithm 3
        LB̄ ← Compute the objective function for (x̄, ȳ) (5.4a)
        if LB̄ ≥ LB^n then
            LB^n ← LB̄
            (x^{*,n}, y^{*,n}) ← (x̄, ȳ)
            update ← True
            break
```

$$\pi_{rijs}^{\omega,n+1} = max\left(\pi_{rijs}^{\omega,n} + \gamma^n\left(x_{rijs}^{\omega,n} - y_i^n\right), 0\right) \qquad \forall\omega \in \Omega, \forall(r,s) \in W^\omega, \forall(i,j) \in \Sigma_{rs}^\omega \quad (5.7a)$$

$$\delta_{rijs}^{\omega,n+1} = max\left(\delta_{rijs}^{\omega,n} + \gamma^n\left(x_{rijs}^{\omega,n} - y_j^n\right), 0\right) \qquad \forall\omega \in \Omega, \forall(r,s) \in W^\omega, \forall(i,j) \in \Sigma_{rs}^\omega \quad (5.7b)$$

$$\lambda_{rijmns}^{\omega,n+1} = max\left(\lambda_{rijmns}^{\omega,n} + \gamma^n\left(x_{rmns}^\omega \frac{e^{-\theta g_{rijs}^\omega}}{e^{-\theta g_{rmns}^\omega}} + 2 - y_m - y_n - x_{rijs}^\omega\right), 0\right) \qquad \forall\omega \in \Omega, \forall(r,s) \in W^\omega, \forall(i,j) \in \Sigma_{rs}^\omega, \forall(m,n) \in \Sigma_{rs}^\omega : (i,j) \neq (m,n) \quad (5.7c)$$

LM are updated at the end of each iteration of the main while loop using (5.7) (Algorithm 1, line 29). To update the LM, we use a classical formulation (Fisher, 2004). If the constraint (2b), (2c) or (2d) are not respected, the corresponding LM are updated λ_{rijmns}^ω, π_{rijs}^ω or δ_{rijs}^ω and become greater than 0. Indeed, if a flow share x_{rijs}^ω crosses a closed park y_i (respectively y_j), the LM π_{rijs}^ω (respectively δ_{rijs}^ω) will increase to incentivize the constraint to be respected in the next iterations. Regarding λ_{rijmns}^ω, the LM increases if the flow share does not follow the used market share model which is the logit formuLA. Because we aim at

maximizing the ridership, and because the LM are deducted from the objective function, such update will incentivize the constraint to be respected. To compute the step-size γ^n, we use the traditional formulation (Fisher, 2004).

$$\gamma^n = \alpha^n \frac{L(\boldsymbol{\pi}, \boldsymbol{\delta}, \boldsymbol{\lambda}) - \text{LB}}{\left\| x^{\omega,n}_{rijs} - y^n_i \right\|_2 + \left\| x^{\omega,n}_{rijs} - y^n_j \right\|_2 + \left\| x^{\omega,n}_{rijs} - x^{\omega,n}_{rmns} \frac{e^{-\theta g^\omega_{rijs}}}{e^{-\theta g^\omega_{rmns}}} - 1 + y^n_{mn} \right\|_2} \tag{5.8a}$$

$$\left\| x^{\omega,n}_{rijs} - y^n_i \right\|_2 = \sum_{\omega \in \Omega} \sum_{(r,s) \in W^\omega} \sum_{(i,j) \in \Sigma^\omega_{rs}} \left(x^{\omega,n}_{rijs} - y^n_i \right)^2 \tag{5.8b}$$

$$\left\| x^{\omega,n}_{rijs} - y^n_j \right\|_2 = \sum_{\omega \in \Omega} \sum_{(r,s) \in W^\omega} \sum_{(i,j) \in \Sigma^\omega_{rs}} \left(x^{\omega,n}_{rijs} - y^n_j \right)^2 \tag{5.8c}$$

$$\left\| x^{\omega,n}_{rijs} - x^{\omega,n}_{rmns} \frac{e^{-\theta g^\omega_{rijs}}}{e^{-\theta g^\omega_{rmns}}} - 1 + y^n_{mn} \right\|_2 = \sum_{(r,s) \in W^\omega} \sum_{(i,j) \in \Sigma^\omega_{rs}} \sum_{(m,n) \in \Sigma^\omega_{rs}} \left(x^{\omega,n}_{rijs} - x^{\omega,n}_{rmns} \frac{e^{-\theta g^\omega_{rijs}}}{e^{-\theta g^\omega_{rmns}}} - 1 + y^n_{mn} \right)^2 \tag{5.8d}$$

5.3.1.3 Case Study

For our case study, we use the road network of Lyon, France, composed of 10 905 nodes N and 19 703 edges E. The geography of the city constructed around a peninsula makes the center sensitive to disturbances due to the relatively weak number of alternative paths. The city center is also the location where most events take place and where businesses are attracting most people. Finally, the pedestrianisation of Lyon's peninsula is currently an active topic of discussion in the city (Justin Boche, 2019). For these reasons, we investigate the potential of an alternative, on-demand transport mode to improve accessibility and reduce the use of private vehicles. We focus on trips from outside the peninsula to the peninsula. All the destinations which are supposed to be potential drop offs area (j), are located in the 1^{st} and the 2^{nd} neighborhoods of Lyon which form the peninsula, whereas all the origins and potential pick ups (i) are sited in the rest of the city. Observe that the roles of pick up and drop off nodes is only indicative. In principle, a P&R transit stop can serve both purposes, *i.e.* pick up or drop off. Indeed, we only consider the morning peak hour. For the evening commute, the sets of pick ups and drop offs will be reversed.

	Small (S)	Medium (M)	Large (L)	Real areas
Origins	53	83	121	745
Pick ups (P)	53	83	121	155
Destinations	6	10	14	171
Drop offs (D)	6	10	14	25

Table 5.1: Graph sizes

For the sensitivity analysis, we consider three graph sizes: a small graph (S) composed of 59 nodes, which represents both potential pick ups and potential drop offs, a medium graph (M) composed of 93 nodes and a large graph (L) composed of 135 nodes (Table 5.1). We aim at considering a restricted number of nodes of the road network, evenly distributed in Lyon. Therefore, we divide Lyon in equal areas using a spatial clustering methOD and assume that there is a unique origin (respectively destination) in each area which acts as a potential pick up (respectively drop off) based on its location in Lyon. For this instance

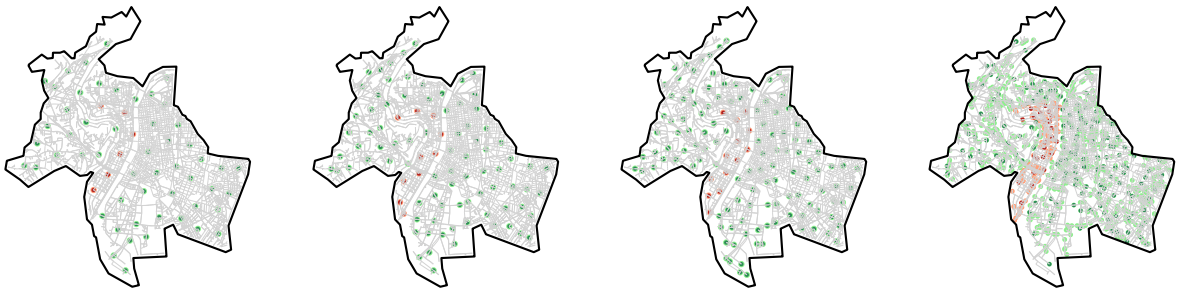

(a) 60 nodes **(b)** 100 nodes **(c)** 140 nodes **(d)** Real graph

Figure 5.11: Reduced graphs with a given number of nodes where the green nodes are origins (potential pick ups) and the red nodes are the destinations (potential drop offs). Real graph has a set of pick ups in dark green (respectively drop offs in dark red) different from the set of origins in light green (respectively destinations in light red).

(Figure 5.11a-5.11c), the set of origins (respectively destinations) is equal to the set of the potential pick ups P (respectively drop offs D). The green nodes represent the origins and the potential pick ups whereas the red nodes correspond to the destinations and the potential drop offs. For the realistic case study, we assume that the set of origins (respectively destinations) differs from the set of potential pick ups (respectively drop offs) (Figure 5.11d). We use a segmentation of the city into zones, called Iris sectors, developed by the French Institute of Statistics. Iris sectors divide the conurbation of Lyon into small geographical areas, each grouping approximately 2 000 inhabitants (Insee, 2016). These areas are thus used to uniformly distribute the sets of potential pick ups and drop offs nodes in the graph. We assume that there is a unique potential pick up (respectively drop off) per Iris sector, which is the closest node to the centroid of the area. Concerning origin and destination nodes, they correspond to a tenth of the road intersection nodes of the real road network of Lyon, and they are uniformly distributed over the Lyon's city network.

Road travel times are determined using Floating Car Data (FCD) (Section 4.1.1). This provides the travel cost, equal to the recorded travel time, for the proposed P&R system between the origin and the pick up $c_{ri}^{\mathsf{R}_{rs},\omega}$ and between the pick up and the drop off $c_{ij}^{\text{route},\omega}$. The travel cost between the drop off and the destination c_{js}^{walk} corresponds to the walking travel time and is computed through the road network using a walking speed of $1.5m/s$. The travel cost between the origin and the destination using the reserve mode $c_{rs}^{\mathsf{R}_{rs},\omega}$ corresponds to the travel time of the shortest path between the origin and the destination, recorded through the FCD. We do not consider the additional costs associated to the reserve transport mode (*e.g.*, fuel, parking, congestion, pollution) in accordance with the simplistic representation but the generalized cost computation could be improved in the future in accordance with the existing literature (Aros-Vera et al., 2013; Hitge and Vanderschuren, 2015). As noticed in Section 4.1.1, during the recorded period, many events of different nature perturbing traffic conditions occurred such as snowfall, strike, road works or public transport disruptions, corresponding to recurrent disturbances. By selecting the recurrent abnormal traffic conditions in the FCD, as well as the baseline one, we build a first instance with four stochastic scenarios. These four scenarios have their own travel cost, recorded during different days whereas the construction cost is defined once and for all. For the realistic analysis (Section 5.3.1.5), the scenarios are recorded at 7 : 30 am: *i)* during a snowfall, *ii)* with a public transport disruption where two subway lines were stopped, *iii)* during a normal week day, and *iv)* during a normal week end day. Each scenario presents a different speed profile representative of the disruption (Figure 4.3). The probability depends on the scenario. We assumed the snowfall has similar impact to a rainfall and fix the probability of occurrence of 35%. The subway disruption could model more generally a public transport failure, which is a rather regular event. We fix the probability to 30%. Finally, the probability for the normal week day (respectively week end day) is set

to 25% (respectively 10%).

Regarding the demand d_{rs}^{ω}, we use realistic data reconstructed by Krug et al. (2021) by relying on a methodology combining survey-based information, simulations and measures of flows collected via loop detectors installed in the city of Lyon. Moreover, demand data have been properly adapted, via an aggregation procedure, to the specific graph sizes considered in our evaluation (Section 5.3.1.4). The construction cost c_i^{loc} for the pick up nodes corresponds to the cost that is required for a car park to be built, whereas the construction cost for drop off nodes corresponds to that of a transit stop. Hence, in our numerical experiments the construction cost of pick up nodes is chosen about ten times greater than that of drop off nodes. The budget allocated to the facility location construction B, is defined as a percentage of the total cost corresponding to the opening of all the facility locations. In both sensitivity and real analysis, we use four different budget corresponding to 20%, 40%, 60% or 80% of the global construction cost.

We implement the proposed P&R facility location formulations to instances based on the city of Lyon. We conduct two analyses: a sensitivity analysis to measure the performance of the proposed LA approach versus a direct MILP approach, and a real case study analysis to illustrate the behavior of the proposed P&R system in an operative context. We only consider the morning peak hour by analyzing the paths going to the city center. For the evening commute, the sets of pick ups and drop offs will be reversed. The proposed formulations and algorithms are implemented in Python on a machine with 16 Gb of RAM and a CPU of 4.20GHz (Intel(R) Core(TM) i7-7700K). All mixed-integer and/or linear programs are solved using CPLEX's Python API. We conduct numerical experiments to explore the behavior of the proposed P&R facility location formulation and compare the performance of the proposed Lagrangian Relaxation Algorithm (LA) with a direct MILP approach.

5.3.1.4 Sensitivity Analysis

The following results aim to showcase the ability of the proposed LA to provide results that are superior to those obtained using a direct MILP solver for solving (5.4). We first examine the influence of the graph size (S, M, L) and the budget B (20%, 40%, 60%, 80%) on both solution methods. In a second analysis, we explore the impact of the access time t^{access} and the egress time t^{egress} which determine the set of accessible pick ups from the origins and the set of drop offs allowing to access the destinations, respectively. Finally, we observe the impact of the waiting time related to our P&R on the ridership. These parameters directly impact the number of constraints in the formulations and may thus significantly influence the computational performance of the solution methods tested. To perform our sensitivity analyses, we use a time limit of one hour. The analyzed instance I, is built on the construction cost randomly defined in the range of a car park construction or the transit stop installation, the travel time recorded in the FCD and the demand modified in accordance with the travel time variations during four specific days to define our four different stochastic scenarios: one Sunday, one Saturday, Christmas day and one Thursday. For the purpose of the sensitivity analysis, we decided to assign an equal probability of occurrence to each scenario.

To analyze the impact of the graph size on the performance of the solution methods, we set t^{access} and t^{egress} to 3 minutes and 10 minutes, respectively. This means that the pick up must be reachable within a travel time of 3 minutes by a car from its origin and the drop off must be within a distance of 900 meters from the destination, to respect a maximum walking time constraint of 10 minutes. With such parameters, (5.4) leads to a problem with, on average, 267 000 constraints and 15 000 variables (binary and continuous) for the small graph size S, 2 000 000 constraints and 67 000 variables for the medium one M, and 15 000 000 constraints and 270 000 variables on the large graph size L.

Table 5.2 summarizes the results obtained using the MILP approach and the proposed LA algorithm for instance I. We compute the LA-gap as the relative gap between the upper and the lower bounds. Notably, the gap obtained using LA is for some instances greater than the MILP gap even though both methods found comparable solutions in terms of objective value. This is because the Lagrangian relaxation duality

gap cannot be guaranteed to be zero (Fisher, 2004). This occurs especially for the small graph size S where our lower bound often exceeds the best bound of the MILP approach. Conversely, we occasionally observe a lower MILP gap compared to the LA gap but the MILP solution has a lower objective value than the best LB found using LA. To compare the obtained feasible solutions, most of time sub-optimal, using the MILP approach and the LA, we compute the gain as the relative gap between both solutions. Note that the optimality gaps of both methods (MILP and LA) may not reflect accurately the quality of the solutions obtained. A positive gain means that our lower bound is higher than the MILP solution. In this case, the gain is written in green and prove the ability of the proposed LA to provide a better solution. Else, the gain is written in red. On the small graph S, the proposed LA is less efficient than the direct MILP approach (Table 5.2): the gain is negative for the instance and ranges from -5.2% for a budget of 20% to -0.2% for the larger budget 80%. We find that the proposed LA is not particularly efficient for the small graph S and the lower budget 20% with a gap between the upper and the lower bounds of 25.2%. Nonetheless, for the medium M and the large L graph sizes, the proposed LA is competitive relative to the MILP approach. For instance I (Table 5.2), the gain is positive for all the budgets except for the one of 40% (I^M) for the medium graph size M. Moreover, this gain is very high, 88.7% for I^M and the lower budget of 20%. For the large graph size L, the gain is positive for the budget going from 20% to 60%. The MILP approach is unable to provide a solution in one hour for 40% and 60% budgets tested. Regardless of the graph size (S, M, L), the lower the budget, the higher the LA gap due to the complexity of the problem. For all the graph sizes (S, M, L), we obtained a gap greater than 10.0% which is not particularly conclusive, although this is due to the slow reduction of the upper bound. Using a greater budget (40%, 60%, 80%) tends to reduce the optimality gap of the proposed LA. This behavior can be explained by the fact that the initial upper bound, which is mostly the better one due to the slow even non-existent decrease during the one-hour allowed runtime, is equal to the portion of passengers using the P&R system when all the pick ups and drop offs are open. With a larger budget, more and more locations are open and the P&R ridership rises, thus reducing the LA gap with the upper bound.

			Parameters	CPLEX solution		LA solution		
Instance	t^{access}	t^{egress}	Budget (%)	Solution	Gap (%)	LB	Gap (%)	Gain (%)
I^S	3	10	20	1 053.850	4.6	1 001.849	25.2	-5.2
			40	1 189.682	3.8	1 181.146	12.4	-0.7
			60	1 241.595	1.5	1 235.390	9.6	-0.5
			80	1 259.218	0.0	1 257.202	8.1	-0.2
I^M	3	10	20	137.546	100.0	1 219.896	13.4	88.7
			40	1 257.042	6.3	1 289.893	8.4	2.5
			60	1 319.766	1.3	1 315.126	6.6	-0.3
			80	1 331.724	0.4	1 333.122	5.4	0.1
I^L	3	10	20	405.012	100.0	1 329.833	12.2	69.5
			40	-	-	1 400.280	7.6	-
			60	-	-	1 435.024	5.3	-
			80	1 455.080	0.3	1 450.163	4.3	-0.3

Table 5.2: sensitivity analysis results after 1 hour running for the I.

	I^S				I^M				I^L			
Waiting time	20%	40%	60%	80%	20%	40%	60%	80%	20%	40%	60%	80%
0min	66.9	78.1	84.6	86.7	78.8	86.6	90.2	91.7	84.9	92.2	93.0	95.8
+5min	66.0	78.6	82.4	86.7	72.6	84.0	87.6	91.7	82.6	92.1	93.3	95.4
+10min	66.2	77.8	80.9	86.3	77.8	75.7	87.3	91.3	85.0	91.9	93.1	95.2
+15min	64.7	70.8	81.5	86.3	75.8	76.2	87.0	91.3	84.7	91.7	92.8	95.4

Table 5.3: Sensitivity analysis on the waiting time of P&R mobility alternatives (% of flow share).

We next conduct a sensitivity analysis on the attractiveness of P&R mobility alternatives by incorporating user waiting time within the corresponding generalized costs. Specifically, we inflate the generalized costs of P&R alternatives by adding a waiting time ranging from 5 to 15 minutes. The results of this analysis are summarized in Table 5.3. As expected, a longer waiting time lowers the percentage of users choosing the P&R system. Nonetheless, the differences are very marginal, with the only exception of the case where the budget is fixed to 40% of the maximal one between both extreme waiting times (0 minute and +15 minutes): in this case, the reduction of users is about 7.3% for the small graph size, 10.4% for the medium one, and only 0.4% for the large one. For all the other budgets and graph sizes, the difference induced by the waiting time increase is always lower, not exceeding 4% between both extreme waiting times (0 minute and +15 minutes).

The modification of t^{access} and t^{egress} highly influences the complexity of the problem by significantly increasing the number of constraints and decision variables of the model. Compared to the previous configuration ($t^{\text{access}} = 3$ minutes and $t^{\text{egress}} = 10$ minutes), with the small graph size S, the number of constraints increases of 1 500% and the number of variables rises of 450%. For the medium graph size M, the number of constraints increases of 1 750% and the number of variables rises also by 450%. For the large graph size L the direct MILP approach fails to be successfully implemented and CPLEX is unable to provide the number of constraints and variables for this instance. Table 5.4 presents the results obtained using the MILP approach and the proposed LA with t^{access} equal to 5 minutes and t^{egress} equal to 15 minutes for the first instance I and Contrary to the results for t^{access} and t^{egress} respectively equal to 3 and 10 minutes (Table 5.2), even for the small graph size S, the proposed LA exhibits a better performance relatively to

			Parameters	CPLEX solution		LA solution		
Instance	t^{access}	t^{egress}	Budget (%)	Solution	Gap (%)	LB	Gap (%)	Gain (%)
I^S	5	15	20	1 213.533	13.4	1 312.649	6.6	7.5
			40	1 351.306	1.8	1 355.782	3.5	0.3
			60	1 367.905	0.6	1 368.623	2.6	0.0
			80	1 374.490	0.1	1 372.509	2.3	-0.1
I^M	5	15	20	-	-	1 362.338	3.3	-
			40	-	-	1 379.385	2.1	-
			60	-	-	1 386.546	1.6	-
			80	-	-	1 390.005	1.3	-
I^L	5	15	20	-	-	1 478.955	-	-
			40	-	-	1 493.202	-	-
			60	-	-	1 496.828	-	-
			80	-	-	1 498.430	-	-

Table 5.4: sensitivity analysis results after 1 hour running for the I.

the MILP approach for a budget of 20%. Because of the complexity of the problem with the one-hour time constraints and the large graph size L, we are unable to solve (5.4) using a direct MILP. Solving the Lagrangian relaxation formulations (5.5) or (5.6) is also impossible in the one-hour time constraints for the large graph size. Nonetheless, the first heuristic (Algorithm 2) developed in the LA successes to provide a lower bound to the problem which is a feasible solution. The quality of this solution cannot be assessed due to the lack of an upper bound. For the medium graph size M (Table 5.1), the direct MILP approach is unable to find a feasible solution, whereas the LA provides a solution whose gaps do not exceed 5.0% for all the considered budget values.

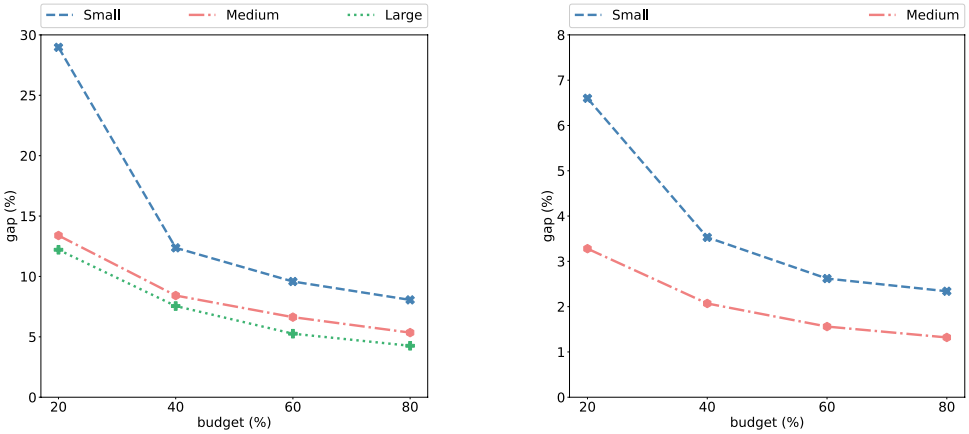

(a) 1^{st} instance I **(b)** 1^{st} instance I

Figure 5.12: Evolution of the gap between the Upper and Lower Bounds (UB and LB) computed with our Lagrangian Relaxation Algorithm (LA) regarding the graph size and the park construction cost budget for one hour running. The results are computed for the first instance I over the two smaller studied graph sizes (S, M) and for the four different considered budgets (20%, 40%, 60%, 80%). In this computation, we accept an accessible travel time from the origin to the pick up of 3 minutes (respectively 5 minutes) and an egress time from the drop off to the final destination of 10 minutes (respectively 15 minutes) (a) (respectively (b)).

Figure 5.12a confirms these observed results and claims. The gap between the proposed LA based lower and upper bounds is larger when the budget is 20% for all the graph sizes (S, M, L). The curves decrease significantly when the budget is equal to 40% and again when it is equal to 60%. Between 60% and 80% the decrease becomes steadier. Figure 5.12b provides insights about the accuracy of our algorithm. Regarding these results, we can conclude that except for a budget of 20% computed with the small graph size S (I^S), the gap between the bounds is globally lower than 5.0% and thus truly close to the optimal solution.

5.3.1.5 Real Case Study

In this section, we present results computed on a realistic graph size (R) composed of 746 origins and 171 destinations with 155 potential pick ups and 25 potential drop offs. The set of potential pick ups and drop offs is uniformly distributed across the network geography and the population spreading. Specifically, we determine a potential pick up or drop off per Iris area (Section 5.3.1.3). The access and egress times are respectively fixed at $t^{\text{access}} = 2$ minutes and $t^{\text{egress}} = 8$ minutes. Such problem is composed of about 9 062 000 variables and induced around 77 000 constraints. We customize the proposed LA in order to balance the time assigned to the local search heuristics and the number of realized iterations in one hour of runtime. The time dedicated to the local search heuristics (Algorithm 6 and Algorithm 7) is fixed at 20 minutes per iteration rather than 10 minutes per iteration in the sensitivity analysis (Section 5.3.1.4).

			Parameters		MILP		LRA	
Instance	t^{access}	t^{egress}	Budget (%)	Objective	Gap (%)	LB	Gap (%)	Gain (%)
I^R	2	8	5	287.956	2.9	902.346	51.5	68.1
			10	1 156.906	0.3	1 352.844	27.3	14.4
			15	1 408.596	0.2	1 534.226	17.6	8.1
			20	1 618.571	0.0	1 618.593	13.0	0.0

Table 5.5: Real instance results after 1 hour running for the first instance I with an heuristic time constraint of 20 minutes and with the first lower bound LB^0 computation (Algorithm 2). The access time t^{access} and the egress time t^{egress} are fixed to 2 and 8 minutes and the generalized cost sensitivity θ is set to 0.1.

		Scenario	P&R flow share			
Index	Description	Prob.	Budget 5%	Budget 10%	Budget 15%	Budget 20%
0	Snowfall impact	0.35	42.6%	67.4%	76.8%	86.3%
1	Public transport disruption	0.30	46.9%	75.7%	82.7%	86.9%
2	Week day	0.25	54.8%	72.0%	86.2%	88.9%
3	Week-end	0.1	44.3%	69.5%	78.6%	82.7%

Table 5.6: Flow share distribution for the different scenarios and the different budget with the following parameters: $\theta = 0.1$, $t^{access} = 2$ minutes, $t^{egress} = 8$ minutes

Table 5.5 summarize the results obtained with the realistic instance for access times fixed to 2 minutes and egress times equal to 8 minutes. The sensitivity parameter to the generalized cost θ is equal to 0.1 as in the sensitivity analysis. Whatever the allocated budget (5%, 10%, 15% and 20%), the LA always exceeds the MILP approach performances by always providing a higher feasible solutions. For the smallest budget, the gain between both solutions even exceeds 50%. Although the gap of the LA is important due to the small reduction of the upper bound, the lower bound, representing the best found feasible solution, is very interesting to solve the complex problem of allocating P&R, respecting a market share model, on a large-scale network.

Table 5.6 summarizes the flow shares using the P&R for an access time fixed at 2 minutes and an egress time set to 8 minutes, depending on the allocated budget to the facilities construction and the scenario. The higher the budget, the more people use the P&R due to the increase of possible path alternatives induced by the rise of the open pick ups and drop offs (Figure 5.13), reducing the travel cost of the P&R mode by being closer to both origin and destination. We notice the P&R is fitted to recurrent disruptions by being highly attractive even in presence of snowfall or public transport disruption. Although the flow share is not equal for all the scenarios, the order of magnitude remains the same.

An increase of acces and egress times leads to a rise of the attractiveness for the P&R by serving a larger part of the demand for the same allocated budgets. This observation has been confirmed for and egress times respectively fixed to 3 and 10 minutes. Whereas, for a construction budget of 5% (respectively 20%), in average 47.91% (respectively 86.25%) of users choose the P&R system with and egress times fixed at 2 and 8 minutes, 61.73% (respectively 92.71%) of people use the P&R system for and egress times set to 3 and 10 minutes. By being larger, the access and egress times make P&R alternatives accessible to more origins and more destinations increasing the part of the demand served by the transport service with a similar number of opened pick ups and drop offs. For this greater pair of access and egress time, the MILP approach is unable to provide solution contrary to our LA.

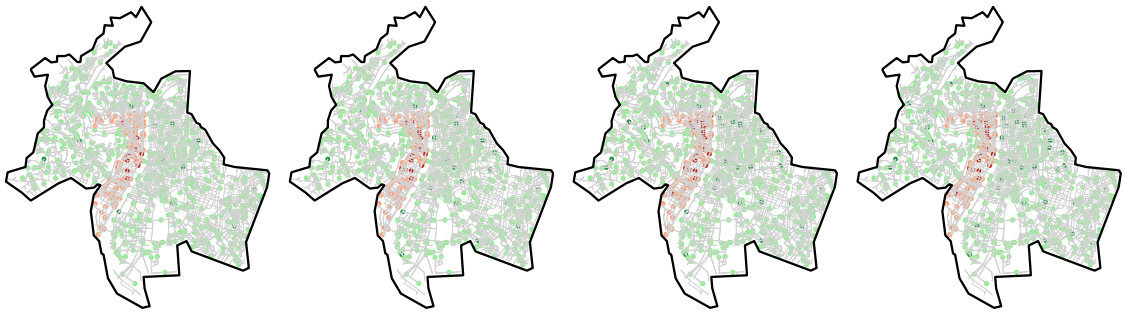

(a) 5%: 12 P and 10 D **(b)** 10%: 20 P and 15 D **(c)** 15%: 29 P and 20 D **(d)** 20%: 37 P and 20 D

Figure 5.13: Real instance with a given number of nodes where the green nodes are origins (potential pick ups) and the red nodes are the destinations (potential drop offs) for an access time fixed at 2 minutes and an egress one set to 8 minutes with $\theta = 0.1$.

The proposed formulation aims to find optimal location for pick up and drop off facilities. These P&R facilities are used to provide on-demand mobility services that complement the existing transport network. Users trips in the P&R system are modeled as three-link chains, *i.e.*, from origin to pick up, drop off and destination. Users modal shift from reserve travel modes to the proposed P&R mobility service is modeled using a logit choice model and the goal is to maximize the expected ridership in the P&R system under varying traffic conditions. Specifically, we propose a stochastic programming approach where a set of finite scenarios is considered, which may represent both regular traffic conditions and recurrent disruptions in the network. The resulting P&R facility location formulation is a challenging MILP problem with a large number of decision variables. We develop a LR approach to solve large-scale instances. We decompose the relaxed formulation into sub-problems that can be solved efficiently and propose local-search algorithms to find competitive solutions along the search. Across our numerical experiments, we observe that the LA provides better feasible solution than the MILP approach when computed over complex instances, *i.e.*, larger graph size and smaller allocated budget for opening facilities in the P&R system. Indeed, these two variables hugely impact the complexity of the problem. The application of the LA on the realistic instance (Section 5.3.1.5) proves the ability of the algorithm to provide the facility locations and to distribute the flow over the P&R alternatives and the reserve mode over the transport network, considering recurrent disruptions in a large-scale network. For larger budgets, the number of opened pick up and drop off facilities increases significantly. This leads to an increase in the number of feasible transit routes in the P&R system which results in relatively large flow shares for this mobility option compared to the reserve mode. While flow shares of this magnitude may be unrealistically high, this can be explained by the fact that only a single concurrent mobility mode is considered, the reserve mode, which may not be sufficient to fully capture competition effects across travel options in an urban multi-modal transportation network. Since the focus of our study is on developing optimization methods, we leave the detailed modelling of such mobility alternatives for future research.

5.3.2 Costs Minimization

Second, we present a model for optimal deployment and dimensioning of an *on-demand vehicle fleet* (*e.g.*, classical/automated shuttles, ride-sharing services) that could integrate regular public transportation and circulation of non-restricted vehicles. The deployed fleet, accessible by travellers via re-configurable P&R facilities, shall allow for properly serving a restricted-access urban area by satisfying the same travel demand that could be directed towards the restricted zone in normal operational conditions. We next present the proposed two-stage stochastic MILP formulation before illustrating the model on an artificial case study.

The following formulation aims to optimize P&R systems to reduce traffic emissions in urban transport networks. One of the applications of this model is to design P&R systems when certain classes of vehicles have restricted access to some areas of the network. For instance, such policies are routinely implemented during pollution peaks in city centres. We focus on two features of P&R systems: facility location and fleet-sizing. P&R facilities aims to provide user access to dedicated public transport or ridesharing services that can reach restricted areas of the network. Upon reaching a P&R facility, users are expected to leave their vehicle at dedicated parking spots and use existing mobility services to reach the closest transit stops and arrive at their destination on foot. To ensure that sufficient mobility resources are provided to P&R users, transit vehicles are then deployed to accommodate this demand. P&R travel demand and routing costs are modeled as uncertain data. This is motivated by the observation that the proportion of origin-destination (OD) demands that will opt for a P&R solution may depend on unobserved data at the time of decision. For instance, the P&R travel demand may be influenced by meteorological conditions, day-of-week, and the availability of alternative mobility solutions. These external factors may also affect traffic conditions and thus routing costs, which typically represent a combination of travel time and travel cost. For these reasons, we still propose a stochastic model to adapt the P&R system to a set of some extreme events Ω. In this model, two main decisions are considered. In a first stage, a strategic decision is made to optimize placement of P&R facilities, still modeled using binary variables $y_i \in \{0,1\}$ for each node $i \in P \cup D$. In a second stage, a tactical decision is made based on the realization of travel demand and routing costs, and shared mobility vehicles are allocated to trips between P&R facilities and drop-off destinations. The flow share distribution is still represented by the decision variable $x^{\omega}_{rijs} \geq 0$ which is the proportion of the travel demand for OD pair $(r,s) \in W^{\omega}$ for a scenario $\omega \in \Omega$ which transits through P&R facility $i \in P_r$ and drop-off location $j \in D_s$. To determine the number of shared mobility vehicles required to accommodate the demand, we assume the existence of an unlimited fleet of vehicles from different class $k \in K$ with their own capacity q_k. The number of vehicles of class $k \in K$ required to accommodate the demand travelling from $i \in P$ to $j \in D$ in scenario $\omega \in \Omega$ is represented by the decision variable $z^{\omega}_{ijk} \in \mathbb{Z}^+$. In this model, we propose to optimize three components of the proposed P&R system: routing costs, facility location costs and fleet-sizing costs. Recall that $c^{\text{route},\omega}_{ij}$ is the unit routing cost corresponding to travel between $i \in P$ and $j \in D$ with the P&R system. The construction cost Let c^{loc}_i be the cost corresponding to opening a P&R facility at $i \in P$ or using location $i \in D$ for drop-off. Finally, let c^{fleet}_k be the unit cost of using a vehicle of class $k \in K$.

5.3.2.1 Problem Formulation

5.3.2.1.1 Flow and Linking Constraints: As for the previous model (Section 5.3.1), the flow distribution must respect some constraints. First (5.9a), all the demand must be served the P&R system for all the scenarios and the OD pairs. Contrary to the first model where all the demand was considered (Section 5.3.1), in this second model the demand only represents to the P&R users. Second, the allocation of a flow over a path (r,i,j,s) is only possible if both the pick up i (5.9b) and the drop off j are open (5.9c).

$$\sum_{i \in P_r} \sum_{j \in D_s} x^{\omega}_{rijs} = 1 \qquad \forall \omega \in \Omega, \forall (r,s) \in W^{\omega} \tag{5.9a}$$

$$x^{\omega}_{rijs} \leq y_i \qquad \forall \omega \in \Omega, \forall (r,s) \in W, \forall i \in P_r, \forall j \in D_s \tag{5.9b}$$

$$x^{\omega}_{rijs} \leq y_j \qquad \forall \omega \in \Omega, \forall (r,s) \in W, \forall i \in P_r, \forall j \in D_s \tag{5.9c}$$

$$\tag{5.9d}$$

5.3.2.1.2 Fleet sizing constraint: To satisfy the P&R users, we require that the fleet servicing segment (i, j) supplies enough capacity to accommodate the total demand traveling on this segment (5.10) in each stochastic scenario for all the scenarios and the OD pairs.

$$\sum_{(r,s)\in W_{ij}^{\omega}} x_{rijs}^{\omega} d_{rs}^{\omega} \leq \sum_{k\in K} z_{ijk}^{\omega} q_k \qquad \forall \omega \in \Omega, \forall i \in P, \forall j \in D \tag{5.10a}$$

(5.10b)

5.3.2.1.3 Formulation: This two-stage stochastic MILP can be formulated as a deterministic equivalent MILP as summarized in (5.11). This formulation is a MILP which can be solved by commercial optimization software. By minimizing the objective function (5.11a), the construction cost c_i^{loc}, the travel costs $c_{ri}^{\text{R}_{rs},\omega}$, $c_{ij}^{\text{route},\omega}$ and c_{js}^{walk} between the origin r and the destination s using the available P&R alternatives for most of the users $d_{rs}^{\omega} \cdot x_{rijs}^{\omega}$, and the cost related to the deployment of the vehicle fleet c_k^{fleet},

$$\min \sum_{i\in P\cup D} c_i^{\text{loc}} y_i + \sum_{\omega\in\Omega} p^{\omega} \left(\sum_{i\in P} \sum_{j\in D} \sum_{(r,s)\in W_{ij}^{\omega}} d_{rs}^{\omega} x_{rijs}^{\omega} (c_{ri}^{\text{R}_{rs},\omega} + c_{ij}^{\text{route},\omega} + c_{js}^{\text{walk}}) + \sum_{i\in P} \sum_{j\in D} \sum_{k\in K} c_k^{\text{fleet}} z_{ijk}^{\omega} \right) \tag{5.11a}$$

$$\text{s.t.} \sum_{i\in P_r} \sum_{j\in D_s} x_{rijs}^{\omega} = 1 \qquad \forall \omega \in \Omega, \forall (r,s) \in W^{\omega} \tag{5.11b}$$

$$\sum_{(r,s)\in W_{ij}^{\omega}} x_{rijs}^{\omega} d_{rs}^{\omega} \leq \sum_{k\in K} z_{ijk}^{\omega} q_k \qquad \forall \omega \in \Omega, \forall i \in P, \forall j \in D \tag{5.11c}$$

$$x_{rijs}^{\omega} \leq y_i \qquad \forall \omega \in \Omega, \forall (r,s) \in W, \forall i \in P_r, \forall j \in D_s \tag{5.11d}$$

$$x_{rijs}^{\omega} \leq y_j \qquad \forall \omega \in \Omega, \forall (r,s) \in W, \forall i \in P_r, \forall j \in D_s \tag{5.11e}$$

$$x_{rijs}^{\omega} \geq 0 \qquad \forall \omega \in \Omega, \forall (r,s) \in W, \forall i \in P_r, \forall j \in D_s \tag{5.11f}$$

$$z_{ijk}^{\omega} \in \mathbb{Z}_+ \qquad \forall \omega \in \Omega, \forall k \in K, \forall i \in P, \forall j \in D \tag{5.11g}$$

$$y_i \in \{0,1\} \qquad \forall i \in P \cup D \tag{5.11h}$$

5.3.3 Case Study

To validate our approach, we apply the formulation (5.11) on a simple network representing a small-size city. We implemented the proposed two-stage stochastic integer program using CPLEX's Python API with a time limit of one hour. The MILP solver finds an integer solution with a gap of 0.19%. In Figure 5.2, orange nodes represent the access-restricted city center. Light-blue nodes fall in the outskirts of our city, where transit is authorized to all vehicles and P&R pick-ups can potentially be located. The network is an undirected weighted graph, composed of 36 nodes and 60 edges. Three different classes of vehicles have been considered, each with specific q_k capacity constraints and c_k^{fleet} deployment costs (Figure 5.14b). In our setup, we assume that constructing a parking facility implies higher costs than planning an additional drop-off location in the city center. Thus, as reported in Figure 5.14c, facility location costs (c_i^{loc}) are assumed to be higher (random values in the range [2 000€, 4 000€]) in the outskirts than in the city center (where

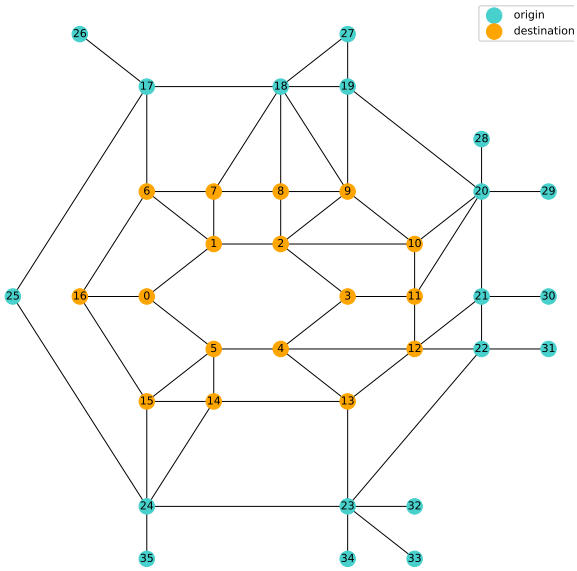

(a) Small-city Graph

	Capacity	Cost
Small	5 passengers	60 €
Medium	10 passengers	100 €
Large	40 passengers	300 €

(b) Cost and capacity of the vehicle classes

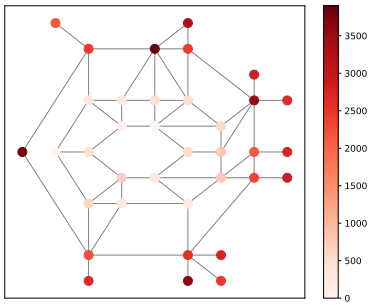

(c) Cost of pick-up and drop-off facilities (in €)

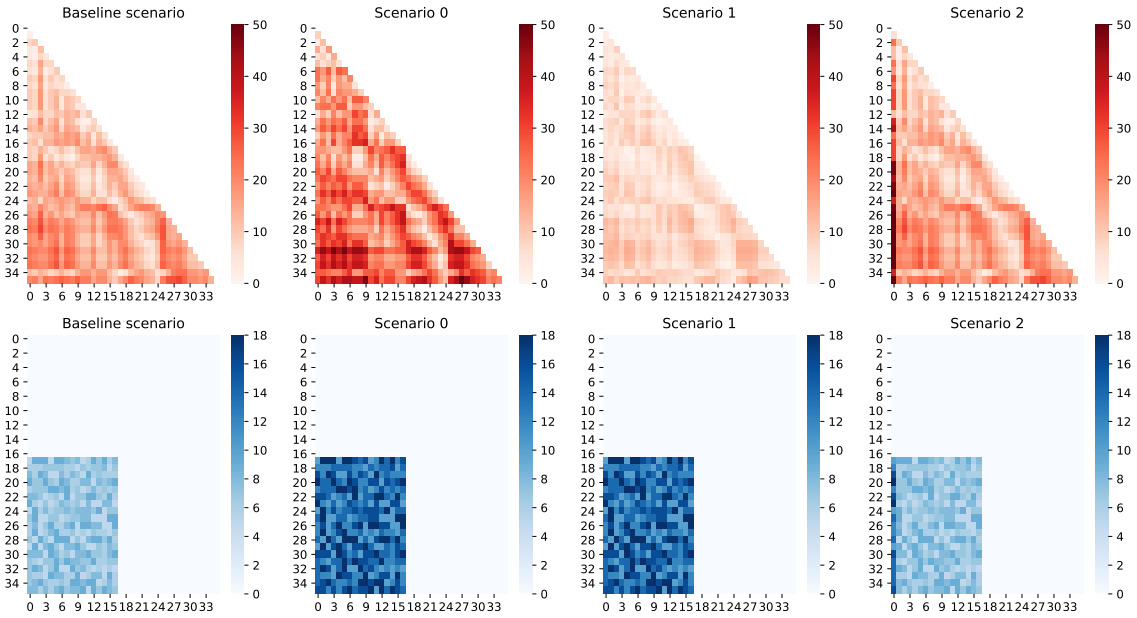

(d) Demand and routing costs for the baseline scenario and the three disrupted ones used to solve the problem

Figure 5.14: Simple network with a vehicle-restricted area (orange nodes) in the center and a peripheral area (light-blue nodes) (a) with the cost and the capacity for the different vehicle classes (b), the construction cost of the different facilities (c), and three equally-likely stochastic scenarios with their own routing cost and demand (d): scenario 1 relates to adverse weather, scenario 2 deals with emission reduction and scenario 3 concerns a localised special event.

random values in the range [1€, 1 000€] have been selected). Concerning the other variables, routing costs $c_{ij}^{route,\omega}$ and demand d_{rs}^{ω} both depend on the specific ω scenario, as detailed in the following. To evaluate our stochastic model, firstly, we define a reference scenario (Figure 5.14d), with given routing costs and demand. We use the latter as a baseline to derive three equally-likely stochastic scenarios, corresponding to situations of reduced accessibility to the city center, for which we aim at planning an optimal P&R deployment. The first stochastic scenario models a situation where the demand towards the city center is uniformly higher than in the baseline scenario, due to the shift from active travel modes (walking, biking, etc.) to motorized ones, *e.g.*, in response to adverse weather conditions. Routing costs are assumed to raise due to the increased demand and perturbed driving conditions. In the second scenario, we consider a situation where the demand towards the city center is uniformly higher, as in the previous scenario, but routing costs towards the city center are lower, *e.g.*, due to transit restrictions applied to highly-polluting vehicles. Finally, in the third scenario, we consider a localised increase of both demand and routing costs towards a specific zone of the city center (*i.e.*, node 0 in Figure 5.2), due to a special event happening in this area. In this situation, we assume higher demand and routing costs from all origins to this specific destination. A value of 12 time units is considered in all scenarios for the t^{egress} and t^{access} parameters. It is worth to highlight that the three considered stochastic scenarios only represent a simplified modelling of a potentially much larger set of alternative configurations of demand and routing costs, with a known probability distribution, that a transport provider could be interested in studying to find the optimal P&R deployment for an elastic adaptation of its mobility offer to different possible expected configurations.

5.3.4 Results

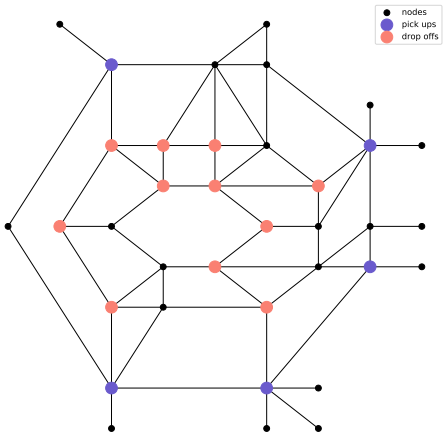

Figure 5.15: Optimal pick-up and drop-off locations in the network.

In Figure 5.15, we report the solution found with the basic formulation (5.11) aiming at minimizing the travel, the construction, and the operational costs (Section 5.3.2), which suggests the localisation of 5 pick-ups and 14 drop-offs facilities. The significant number of opened drop offs, compared to the number of opened pick ups, is due to the construction costs. Indeed, it is less expensive to open a drop off than a pick up, and it is less expensive to open a drop off rather than increasing the travel cost with a cost between the drop off and the destination. We recall that facility location variables are first-stage ones, and thus remain the same for all possible realization of the uncertain data. Conversely, the flow distribution x_{rijs}^{ω} and the size of the P&R fleet z_{ijk}^{ω} depends on the specific traffic conditions (road cost c_{ij}^{road} and demand d_{rs}) related to the stochastic scenario ω.

We assume the P&R shuttles use the shortest paths to join the drop-off from the pick-up, as represented in Figure 5.16a, 5.16b and 5.16c for the different scenarios, with a color and a width proportional to the fleet size, independently of the chosen vehicle class. The number of per-class vehicles for all the scenarios is

	Scenario 1			Scenario 2			Scenario 3		
	Class 0	Class 1	Class 2	Class 0	Class 1	Class 2	Class 0	Class 1	Class 2
# of vehs	2	11	111	1	2	113	1	0	60

Table 5.7: Number of vehicles per-class and per-scenario.

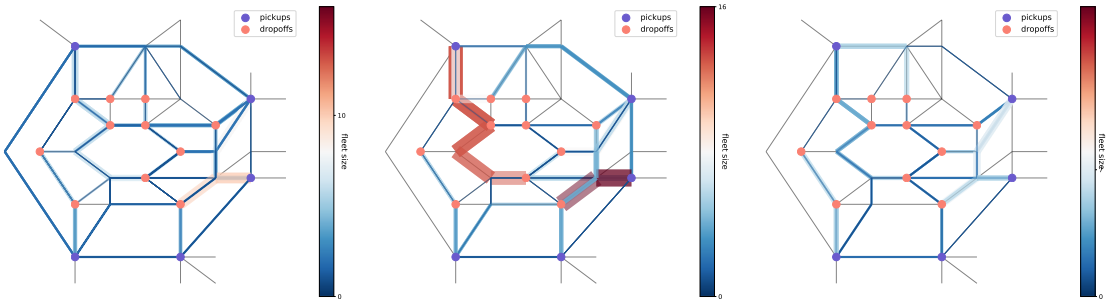

(a) Scenario 1 **(b)** Scenario 2 **(c)** Scenario 3

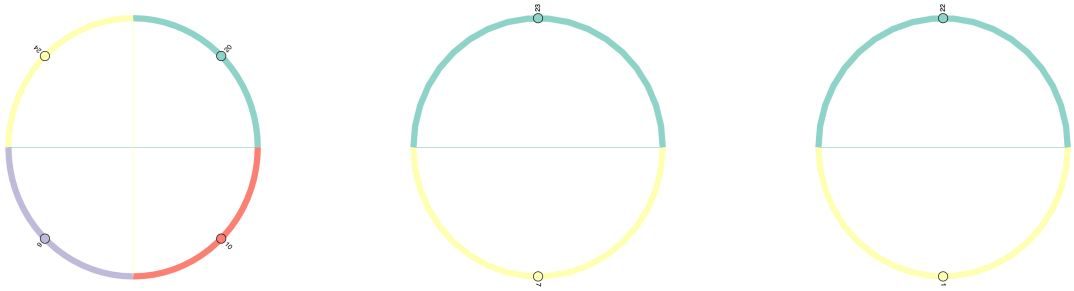

(d) Scenario 1 - Small vehicles **(e)** Scenario 2 - Small vehicles **(f)** Scenario 3 - Small vehicles

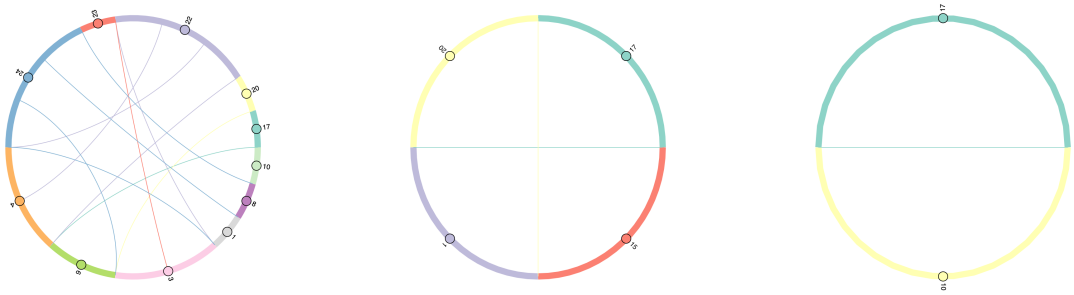

(g) Scenario 1 - Medium vehicles **(h)** Scenario 2 - Medium vehicles **(i)** Scenario 3 - Medium vehicles

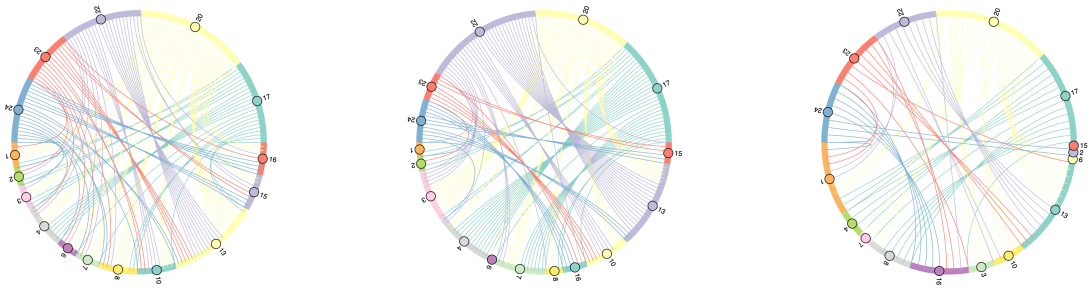

(j) Scenario 1 - Large vehicles **(k)** Scenario 2 - Large vehicles **(l)** Scenario 3 - Large vehicles

Figure 5.16: Fleet size and its distribution (z^{ω}_{ijk}) between optimal pick-ups (purple nodes/labels) and drop-offs (light-red nodes/labels) for the 3 stochastic scenarios.

detailed in Table 5.7. The chord diagrams in Figure 5.16d, 5.16e and 5.16f illustrate the number of small-size shuttles (unused in the first and the third scenarios) going from a specific pick-up to a specific drop-off, the chord diagrams in Figure 5.16g, 5.16h and 5.16i represent the number of medium-size shuttles, and the chord diagrams in Figure 5.16j, 5.16k and 5.16l represent the number of large-size shuttles. In both cases, each chord of the diagram represents the trajectory (*i.e.*, the pick-up/drop-off pair) of each shuttle allocated in the model solution, using the color of the pick-up node to represent the chord. Whereas the first and the second scenarios have the same demand (Figure 5.14d), we notice a different distribution of the vehicle fleet (Figure 5.16a and 5.16b). Because of lower routing costs in the second scenario (Figure 5.14d), people can reach pick-up locations further away from their origins. Thus, in the second scenario, larger fleets and a smaller set of pick-up/drop-off pairs are preferred (Figure 5.16d-Figure 5.16j versus Figure 5.16e-Figure 5.16k). Indeed, whereas 2 small-size vehicles (respectively 11 medium-size vehicles) are employed in the first scenario, only 1 (respectively 2) is used in the second scenario. On the contrary, 2 more large-size vehicle are requisitioned in the second scenario compared to the first one. Regarding the paths, two of them are mainly used in the second scenarios with more than 10 allocated vehicles. Specifically, 13 large-size vehicles are deployed from the pick up 17 to the drop off 4, and 16 large-size vehicles are allocated to the path joining the pick up 22 to the drop off 13. In the first scenario, the vehicles are more distributed across the network with a fleet more fitted to the demand and their itinerary. In other words, the solution for the second scenario groups many travellers at the same pick-up locations and transfer them to the same drop-off, by means of a larger fleet of vehicles over the corresponding paths. The reduction of pick-up/drop-off pairs minimizes the second term of objective function (5.11a) by diminishing the number of traversed edges, which influences the result via the decision variable x^{ω}_{rijs}. Regarding the third scenario (Figure 5.16l), the proportion of vehicles going to the drop-off nodes 1 and 16, which allow to join the relevant node 0, is higher than for the two first scenario (Figure 5.16j and Figure 5.16k). This is consistent with the demand distribution, which is spatially non-uniform (*i.e.*, higher demand from all origins to node 0). Indeed, 11 (respectively 9) large-size vehicle reaches the node 1 (respectively 16), against 4 (respectively 7) in the second scenario and 7 (respectively 9) in the first one. Although the demand is globally lower over the network, the number of vehicles joining these nodes is higher to satisfy the demand related to the event.

The results prove the ability of the model (5.11) to optimally deploy a P&R system with minimum travel, construction, and operational costs, adapted to some disruptions. The solution provides the location for building the parks once and for all considering different traffic conditions and distributing the passengers over the P&R, as well as deploying an adapted fleet of vehicles, depending on the occurring event.

5.3.5 Extension

In order to increase the attractiveness of the P&R system, whatever the happening traffic conditions, we decide to add a constraint ensuring a minimum level of services. Indeed, (5.12a) imposes that for each scenario, the proportion of the cost due to routing and fleet sizing is not greater than M^{ω}.

$$\sum_{i\in P}\sum_{j\in D}\sum_{(r,s)\in W^{\omega}_{ij}} d^{\omega}_{rs}x^{\omega}_{rijs}(c^{\mathrm{R}_{rs},\omega}_{ri}+c^{\mathrm{route},\omega}_{ij}+c^{\mathrm{walk}}_{js})+\sum_{i\in P}\sum_{j\in D}\sum_{k\in K}c^{\mathrm{fleet}}_{k}z^{\omega}_{ijk}\leq M^{\omega} \qquad \forall\omega\in\Omega \qquad (5.12a)$$

To observe the impact of the addition of such a constraint, we apply the formulation (5.11) with the consideration of the constraint (5.12a) on the previously described case study (Figure 5.14) (Section 5.3.3), with two different vectors for the maximum cost M^{ω} related to the fleet sizing z^{ω}_{ijk} and the flow distribution x^{ω}_{rijs} to be respected per-scenario. In the first vector M^{ω}_{1}, we assume that the maximum cost for the first scenario is higher than the two others because of the catastrophic traffic conditions (high demand and high routing cost) (Figure 5.14d). We fix the value to $M^{1}_{1}=1.6e^{6}$, knowing that the objective value of the basic problem (5.11) is equal to 114 695. For the second scenario, the value is fixed to $M^{2}_{1}=1.0e^{6}$

	Scenario 1			Scenario 2			Scenario 3		
	Class 0	Class 1	Class 2	Class 0	Class 1	Class 2	Class 0	Class 1	Class 2
M^1	0	12	111	0	0	114	1	0	60
M^2	2	11	111	0	0	114	1	0	60

Table 5.8: Number of vehicle per-class and per-scenario for the extended problem formulation, with the consideration of the constraint (5.12a), with two different vectors of M.

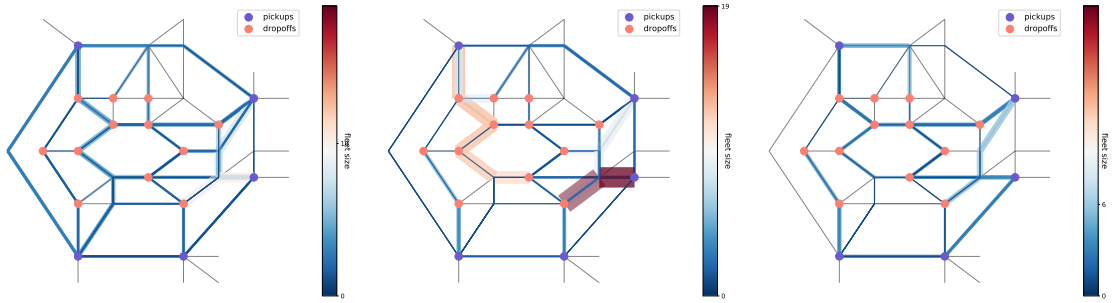

(a) M_1^1 **(b)** M_1^2 **(c)** M_1^3

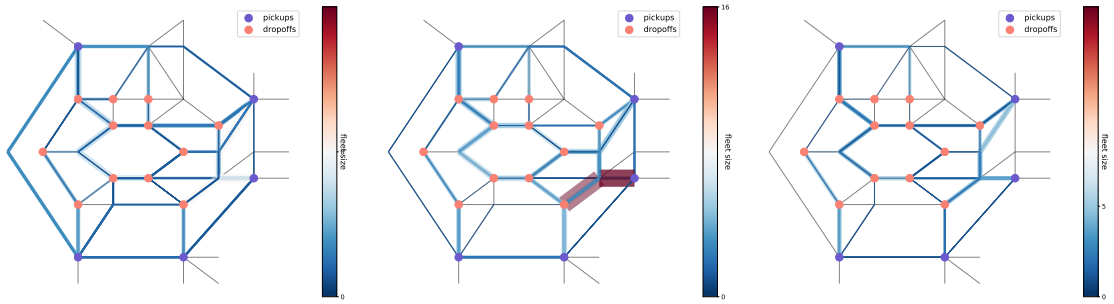

(d) M_2^1 **(e)** M_2^2 **(f)** M_2^3

Figure 5.17: Fleet of vehicle of class 0, 1 and 2 for the Scenario 0 per-couple of pick ups and drop offs, without and with the consideration of the constrains (5.12a), for two different M values.

because of the low routing cost induced by the low use of the road network due to the pollution restrictions. In the third scenario, the maximum allocated cost for the fleet sizing and the travel cost is set up to $M_1^3 = 0.6e^6$. Regarding the second vector M_2^ω, we suppose that the maximum cost per-scenario is always equal to $M_2^\omega = 1.6e^6, \forall \omega \in \Omega$. We solved the extended MILP, for two different M^ω values, using CPLEX's Python API with a time limit of two hours which provided solutions with a gap of 0.41% (M_1) and 0.35% (M_2). With such a constraint, the problem is not guaranteed to be feasible if the M^ω is too restrictive. For instance with $M^\omega = 1.4e^6, \forall \omega \in \Omega$, the problem does not solve successfully.

Table 5.8 summarizes the number of needed vehicles per-class and per-scenario for the extended formulation (5.11) with the consideration of the constraint (5.12a), and two different sets of values allocated to the maximum cost per-scenario M_1^ω and M_2^ω. Although close to the basic formulation results (Table 5.7), the number of vehicles per-class and per-scenario is different.

As we can observe in Figure 5.17, the open parks y_i without and with the consideration of the new constraint (5.12a) are modified. More specifically, the change concerns the drop offs opening, less expensive than the pick ups. We have 12 drop offs open against 11 with the basic formulation (5.11), with the consideration of M_1 as a maximum cost per-scenario, the new drop off is located at 0, while withe M_2 as a

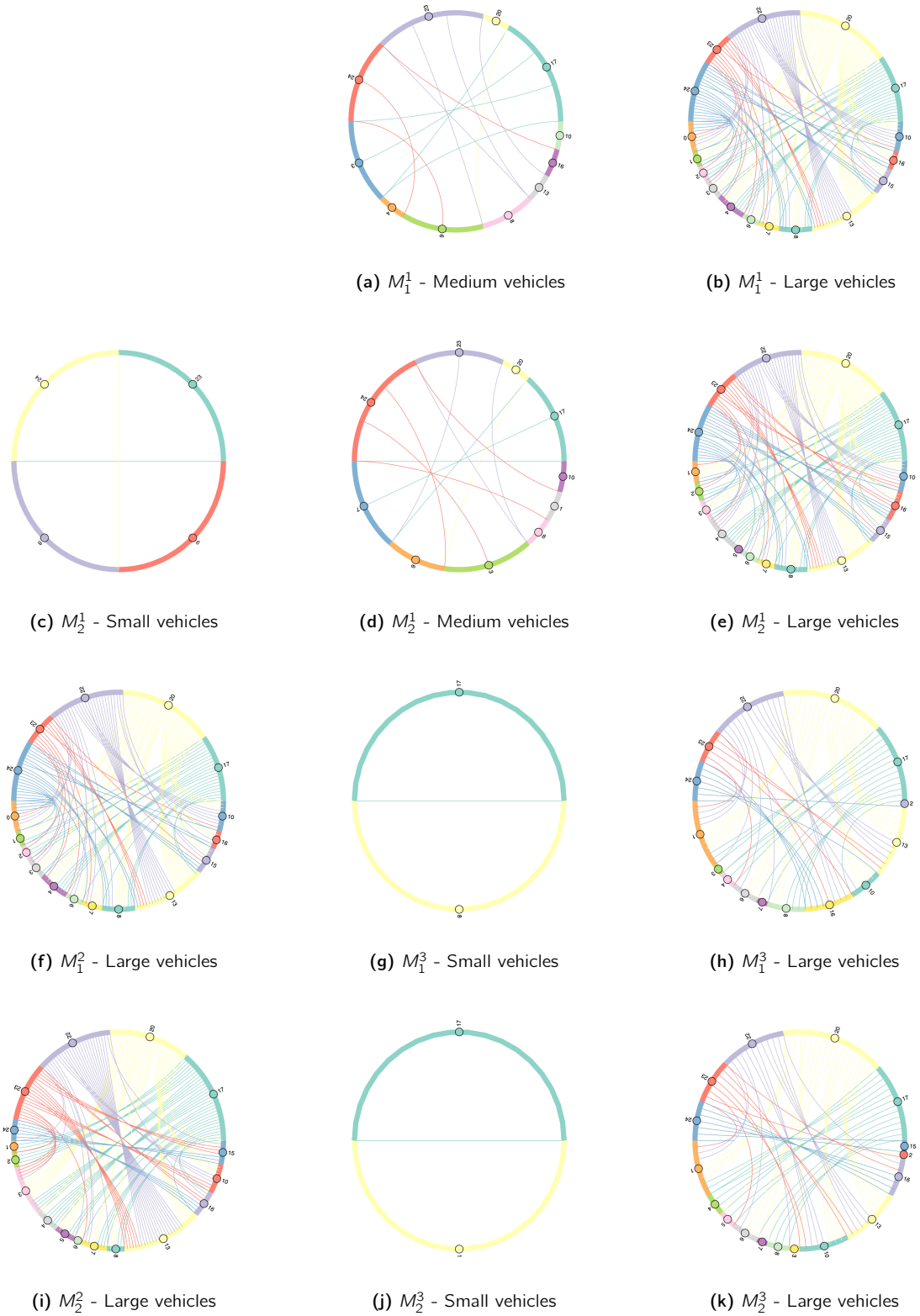

(a) M_1^1 - Medium vehicles

(b) M_1^1 - Large vehicles

(c) M_2^1 - Small vehicles

(d) M_2^1 - Medium vehicles

(e) M_2^1 - Large vehicles

(f) M_1^2 - Large vehicles

(g) M_1^3 - Small vehicles

(h) M_1^3 - Large vehicles

(i) M_2^2 - Large vehicles

(j) M_2^3 - Small vehicles

(k) M_2^3 - Large vehicles

Figure 5.18: Fleet composition (z_{ijk}^{ω}) for the first scenario ((a)-(f)), for the second (g) and (j), and the third scenario (h), (i), (k) and (l) with the constraint (5.12a).

maximum cost, this drop off this located at 5. Such a result supposes that the opening of a drop off, not so expensive, permits to respect the constraint (5.12a), ensuring that the P&R will not exceed a certain travel cost and operational cost whatever the happening scenario. The flow distribution x^{ω}_{rijs} as well as the fleet sizing z^{ω}_{ijk} are also impacted.

The first scenario (Figure 5.18a-Figure 5.18e) is constrained by the same value of $1.6e^6$ for the two different values M^1_1 and M^1_2. Nonetheless, the flow distribution is modified due to the difference in the open parks. For the first scenario, with M^1_1, no small-size vehicle is used, while with M^1_2 (Figure 5.18c), the paths between the pick up 23 (respectively 24) and the drop off 8 (respectively 6) are realized, among other vehicles, by small-size one. Regarding the medium-size vehicles (Figure 5.18a and Figure 5.18d) Finally, the large-size vehicles distribution between the different couple of pick ups and drop offs is slightly change (Figure 5.18b and Figure 5.18e) with more accessible drop offs from the pick ups 20, 22 and 24 with the maximum cost of M^2_1, while the pick ups 17 and 23 present higher set of destinations with the maximum cost of M^2_2. In the second scenario, the only used class of vehicles is the largest one (Figure 5.18f and Figure 5.18i). As for the basic formulation, such a scenario is characterized by a huge demand and a low routing cost (Figure 5.14d). The cost $c^{\mathsf{R}_{rs},\omega}_{ri}$, $c^{\mathsf{route},\omega}_{ij}$ and c^{walk}_{js} are thus hugely reduced in the objective function (5.11a). It is cheaper to gather people over the same paths using the large-size vehicles, despite the increasing time between the origin and the pick up $c^{\mathsf{R}_{rs},\omega}_{ri}$, as well as the distance between the drop off and the destination c^{walk}_{js}. Indeed, the cost per passenger is reduced with the rise of the vehicle size. We notice a difference in the flow distribution and the fleet allocation, especially on the path joining the pick up 17 to the drop off 4. More generally, with the maximum cost M^2_2 (Figure 5.18i), the number of vehicles departing from the pick up 17 is larger than for the cost M^2_1 (Figure 5.18f) with two more larger vehicles in the second situation. The increase of the cost from $1.0e^6$ to $1.6e^6$ tend to gather the passengers, rather than distribute them over more suitable paths, with pick ups closer to their origins and destinations, closer to their drop offs. The fleet distribution in the third scenario (Figure 5.18g, Figure 5.18j, Figure 5.18h and Figure 5.18k) is not so impacted by the cost restriction increase from $0.6e^6$ to $1.6e^6$. Indeed, the results (Figure 5.17c, Figure 5.17f and Table 5.8) are very similar even with the one issued from the basic formulation (Figure 5.16c and Table 5.7).

The addition of the constraint (5.12a) hugely enriches the initial formulation and ensures a minimum level of P&R performances whatever the considered event rather than ensuring in average a good level of P&R performances.

5.4 Concluding Remarks and Discussions

Section 5.1.1 and Section 5.1.2 detail existing strategies to reduce the impact of disruptions or disasters over transport networks. Several transport network dimensions have to be improved in order to increase its resilience. Namely, *i)* the *robustness* and the *redundancy* of the network which absorb chocs generated by a given disruption; *ii)* the *reactivity* to manage effectively the consequences of the disruption in order to accelerate performance recovery by facilitating the emergency access, the evacuations, as well as the removing of potential debris; *iii)* the *recovery* of the network through the reconstruction of transport network infrastructure to regain the initial level of performances. The existence of projects, presented in Section 5.1.3), focusing on the improvement of transport network resilience confirm the relevance of such issues.

The developed methodologies aim at proposing new strategies to improve transport network resilience with the addition of new transport modes through a resilience-oriented (multimodal) network design. The first method (Section 5.2), quick-to-compute, focuses on the creation of the most suitable new public transport mode (metro, tramway, etc.) on large urban areas, as well as the deployment of the best bus lines in presence of disruptions, with the objective of maximizing the gain of performance. The consideration of traffic conditions and travel demand in the performances quantification influences the set of lines to be

constructed to maximize the performance gain. It is thus essential to include such traffic dynamics in the computation of the metrics.

The second method (Section 5.3) provides two different stochastic formulations to optimally deploy the P&R system. The proposed system is adapted to disruptions, and maximize the ridership while minimizing operational costs. The proposed framework aims to enhance resilience by increasing the attractiveness of public transit services which is widely acknowledged Mohring (1972); Lee and Vuchic (2005); Jenelius and Cats (2015) as a proxy for resilience.

The application of such formulation on large urban area is possible for the ridership maximization with the development of a LA which proves its efficiency compared to the existing MILP solver CPLEX. Nonetheless, we haven't developed yet an algorithm to solve the second formulation on large scale problems, *e.g.* the column generation process. Such an approach is a promising perspective that will be explored in future work.

Conclusions and Future Work

The subject of this dissertation was motivated by the importance of characterizing and improving transport network in order to maintain an acceptable level of performances whatever the traffic conditions and the disruption occurrence. After focusing on the research synthesis, limitations and future works are presented.

Conclusion

First, we focus on the characterization of resilience leading the analyses both on simulated and real data. Related works mostly investigate separately the topological and the dynamic aspects resilience despite their complementarity, which justifies the deployment of a hybrid approach. In our work, we aim at analyzing the ability of the proposed hybrid approach (Section 1.3) to characterize the transport network performances using extended metrics issued from graph theory and traditionally based on network topology, to consider traffic dynamics as well (Section 2.2.3). Second, we develop resilience-oriented network design strategies. Whereas the REINFORCE methodology (Section 5.4) aims at supporting a new transport mode construction, or a quick deployment of an emergency bus line to limit a disruption impact (Section 5.4), the second proposed solution aims at deploying a P&R system, adapted to disruptions, (Section 5.4) by either maximizing the ridership or minimizing the construction, travel and operational costs.

Resilience Characterization

We propose contributions to network resilience modeling and analysis by enhancing classical topological metrics with the integration of traffic dynamics via a simulation-based and real data-based approaches in our hybrid solution (Section 1.3 and Section 2.2.3). For the record, the topological approach (Section 1.1 and Section 2.2.2), based on graph theory, focuses on the characterization of the topological resilience and is mostly dependent on the network redundancy and connectivity, while the dynamic one (Section 1.2 and Section 2.2.1) is interested in the variation of some traffic indicators to characterize the transport network resilience. By means of a dynamically weighted graph (Chapter 1), using traffic conditions, we relate both traditional topological and dynamic approaches, used in the transport network resilience characterization. The network performance, computed with the weight-dependent CM over such a graph, is thus dependent on both network topology and traffic dynamics. We lead analysis both with simulated (Chapter 3) and real (Chapter 4) data.

The analysis proves the ability of the CM to capture traffic dynamics when computed over a travel time/level of service weighted graph. Indeed, we notice that NDC, characterizing the graph connectivity, is degraded in presence of a congestion. By diminishing the level of service of the congested edges, we can emulate the traffic conditions which negatively impact the connectivity of the transport network. Our results confirm these observations with a global reduction of the $\langle NDC \rangle$ and a modification of the NDC distribution, mostly diminished, during the morning peak hour or in presence of disruptions. Regarding, both

NCC and EBC, based on the shortest paths computation, we observe that the results evolve in accordance with the traffic conditions. By being modified, the travel time, used to weight the graph, changes the shortest paths which become aware of the traffic dynamics. Because the EBC depends on the number of shortest paths, we discretized the weights to consider a set of paths, considered equivalent in terms of travel time, rather than a unique shortest path. Indeed, the drivers not only chose the shortest path due to their numerous decision variables in the route choice (*e.g.*, memory, habit, familiarity, travel time, safety, etc.) as well as their limited information processing resources. With such a discretization, we can consider the bounded rationality. Such a weight modification hugely impacts the metric distribution in urban areas, due to the huge number of alternative paths (contrary to peri-urban areas) increasing the interest to accurately reproduce the driver behaviors.

The correlation between EBC, which could be modified in DSEBC to consider the travel demand in its computation, and the traffic flow confirms the potential of such a CM to capture the traffic dynamics. With the spatial correlation, focusing on the analysis of the flows and the EBC for all the edges at a given time stamp, we find the same conclusion as in the literature review. The graph weighting which provides traffic condition information in EBC computation gives a better correlation coefficient value, even better with the travel demand consideration in the DSEBC. When temporally correlated, the analysis focuses on both the flow and the EBC evolution for a unique edge, we observe that *i)* the anti-correlated edges are globally closer to their critical flow, *ii)* the non-correlated edges correspond either to unused edges with a 0-flow or the topologically vulnerable edges such as bridges which are still crossed by shortest paths whatever the travel time increase, *iii)* the correlated edges mostly present a free-flow state with an attractive travel time.

Resilience-oriented Network Design

Within the thesis, we developed two main strategies in order to improve transport network resilience through the development of new transport modes, supporting the existing one. First, we proposed a methodology which aims at prioritizing the construction, in a transport mode creation context, or the deployment, in an emergency context, of a transport line with the objective of improving the network performance as much as possible. Second, we formulated two models which aim at optimally locating the facilities of a P&R system, using stochastic formulations to make it adapted to disturbed situations, with the objective of first maximizing the ridership and second minimizing the costs.

REINFORCE Methodology

First, we proposed the REINFORCE methodology for a quick augmentation of large multimodal transport networks, as well as the optimal deployment of public transport alternatives in presence of disruptions, easily adaptable to any city for which the actual transport network offer is known, jointly with a plan of the new transport lines/modes to be built. By quantifying the network performance, using well-known resilience indicators, we ensure to propose the best lines combinations to be constructed in terms of efficiency and robustness. Indeed, the redundancy is characterized by the NDC as well as the $\langle NDC \rangle$ and the efficiency by the AE, the NCC, and the EBC. Through the consideration of the transport mode shift time for shortest path computation, and the consideration of the travel demand in the selected metrics, which permits to assign more importance to specific transport lines or modes that serve a larger amount of trips, we convey realism and accuracy to the REINFORCE methodology. By applying the REINFORCE methodology both on normal and disturbed travel demand, we highlight the ability of the methodology to prioritize the transport line choice in accordance with the traffic conditions.

Park-and-Ride System Deployment

We proposed two new models for locating P&R facilities to enhance the resilience of urban mobility networks. On the one hand, the first model distributes the flow between the P&R alternatives and the private vehicles, following a market share model based on the logit formulation, and locates the pick ups and the drop offs with the objective of maximizing the P&R ridership. On the other hand, the second model distributes the P&R-related flow over the alternatives, locates the pick ups and the drop offs, and provides the adapted fleet size with the objective of minimizing the costs.

The first study, focusing on the design of P&R systems when maximizing the ridership, aims to improve the resilience of urban mobility networks in presence of recurrent disruptions. However, the proposed facility location approach can be generalized beyond P&R systems to the design of flexible multimodal and on-demand mobility networks. Indeed, the proposed framework could be used to model three-link trip chains in a generic context. The sensitivity analysis (section 5.3.1.4) proves that compared to the direct MILP approach, the proposed LA is more scalable and capable to generate feasible solutions with large-size instances. Although the optimality gap of the LA is sometimes higher than that of the MILP approach, the LA often finds better feasible solutions. The results obtained on the realistic instance (Section 5.3.1.5) prove the ability of the proposed LA to provide information about the implementation of a budget constrained optimized P&R system adapted to the recurrent disruptions in a large-scale network, as well as the flow share distribution between the reserve mode and the P&R for a given allocated budget. The development of the LA permits to solve the problem over large-scale instances and could be easily applied in other large urban areas.

The second model is very promising to adapt an on-demand fleet vehicle to a specific event in order to maintain an acceptable transport system. The problem solution (Section 5.3.4) provides the optimal facility locations, as well as the flow distribution and the fleet sizing between the different pick ups and drop offs, for a minimal cost (travel, construction and operational costs). The addition of the robust constraint (Section 5.3.5) ensures a maximum cost per scenario and thus increases the attractiveness of the P&R in presence of disruption as well as under normal conditions, rather than being attractive in average whatever the traffic conditions. Nonetheless, some efficient operational research methods have to be developed to solve the problem on large-scale graph. The application of the LR, usually used to solve facility location problems, has failed, due to the extremely large size of the flow share variables x^{ω}_{rijs}, too big to solve the problem of computing time.

Future works

Perspectives of the presented research are numerous and can be listed according to the two main topics which are the resilience characterization and the resilience-oriented network design.

Resilience Characterization

Future works on the characterization of resilience must pursue the combination of both the static and the dynamic approaches mainly used to study the transport network resilience. Such works include the extension of the NDC distribution analysis, based on Gao and Albert-László Barabási (2016) works (Section 4.2). By defining a traffic model equation, the delimitation between the resilient and the non-resilient states would be determined and would improve the knowledge issued from the CM. Moreover, the consideration of the multimodality through the use of a multilayer graph should be extended, although we prove the ability of the measures to capture the impact of a transport line addition. Finally, others metrics such as the A, quickly discussed in Appendix A, should be studied to deepen the knowledge of the transport network behavior under

normal and disturbed conditions to better characterize its resilience, again with the objective of combining the topological and dynamic approaches.

Resilience-oriented Network Design

Future works are also numerous for the resilience-oriented network design. First, in our two proposed strategies aiming at increasing the transport network resilience through the addition of a new public transport mode, some improvements should be done. Second, the proposition of new optimization problem formulations should be proposed for the creation and the improvement of new transport networks.

Regarding the REINFORCE methodology, we aim at *i)* using the approach to plan the construction of non-existing transport lines or for the post-disaster reconstruction of transport lines; *ii)* using this approach for the emergency planning of temporary transport lines for resilience enhancement and short-term disaster response. By dynamically compute the metrics used in the REINFORCE methodology, the evolution of traffic conditions over time will be considered. Such an improvement should allow to adapt the prioritization of the line construction for the morning and the evening peak hours when the public transports are usually widely used. Regarding the emergency planning of transport lines, the dynamic computation of the metrics will help to suit the evolution of the disruption in order to provide the best temporary alternatives. Additionally, other kinds of metrics, such as road or train capacity, or construction costs for additional transport segments are expected to improve the definition of the edge weights and further refine our methodology.

Regarding the Park-and-Ride system deployment, the second proposed formulation which aims at minimizing the construction, the operational, and the travel costs, has to be extended to be applied on large scale urban network. The column generation which is efficient in handling big variables dimension, should be applied to our problem. The principle consists in solving the initial problem with this subset of variables x^{ω}_{rijs}, solving the pricing problem dependent on the constraints of the initial problem to find the negative reduced costs for x^{ω}_{rijs}, adding theses variables x^{ω}_{rijs} with negative reduced costs in the initial subset, and iterating these three steps until there is no variable x^{ω}_{rijs} with negative reduced cost, ensuring that we have an optimal solution to the initial problem.

Next models of P&R system should focus on merging both proposed approaches in order to both maximize the ridership and minimize the travel, exploitation and construction costs. Because the addition of the P&R system may influence transit flows and subsequently traffic congestion in the network, the incorporation of congestion effects in the proposed framework may be achieved by incorporating a traffic and/or transit assignment. Such extensions of the proposed formulation should be explored in future works. Finally, the possibility of applying a variant of the proposed model to support people evacuation for disaster management might be a powerful strategy for the reaction phase, directly after the disruption.

Finally, others optimization formulations should be developed to improve the transport network resilience. The Covid-19 has a huge impact on our societies and also over the transport networks. Although the recurrent disruptions such as the congestion were reduced during the lockdowns, other kind of issues happened with the social distancing. In this sense, we though to an interesting and actual work consisting in proposing an optimal distribution of the passengers over a public transport network to reduce the capacity of passengers per public transport lines while maintaining an acceptable travel time for the users.

Appendices

A. Accessibility

This appendix is an updated version of the conference paper Henry et al. (2021a).

Accessibility (A) represents the ultimate goal of most transportation activity (Litman, 2008), *i.e.*, the ease of reaching a destination (Hansen, 1959) from different areas of a city. A is strongly influenced by several mobility characteristics, such as the travel demand, transport mode or travel time, but also depends on network topology. It thus appears as a relevant candidate to consider the two major existing approaches for resilience/vulnerability analysis. In the literature, different equations are provided to compute A, including travel cost. Most of them are derived from the Hansen integral index (13) (Hansen, 1959), which defines A on a per-origin basis, by considering the distances of destination zones from the given city area origin, weighted by the attractiveness of the destination areas, measured in terms of presence of Points Of Interest (POIs).

$$A_s = \sum_{r \in Z} \frac{\omega_r}{c_{rs}} \tag{13}$$

where ω_r is the attractiveness of the area r and $\frac{1}{c_{rs}}$ is the impedance function, often equal to the reciprocal of network travel distance.

A large majority of works focuses on the computation of the A for a specific transport mode. Chen et al. (2007a) propose a method for evaluating the impact of link failure on the road network by analyzing the change in the A weighted by the socioeconomic activities. The used metric depends on the random utility of the different alternative paths, which is consistent with the combined travel demand based on utility maximization with budget constraints. They conclude that their metric can quantify the consequences of both demand and supply changes due to the presence of a disruption. Taylor et al. (2006) propose an A and remoteness index, called ARIA, for studying the impact of degradation on some vulnerable sections of the Australian highway network. The ARIA index is based on the computation of road distance measurements from populated locations. Lu and Lin (2019) focus instead on the A of the urban rail transit network. Their A metric is defined on a per-station basis, by measuring the impact of disruptions as the capability to provide an alternative mode (*e.g.*, additional buses with a specific capacity) to reach the destinations from the disrupted station. Nonetheless, the study is limited because it focuses only on the computation of A per one single transport mode (*i.e.*, metro transit system). Biazzo et al. (2019) characterize the A through two scores: the velocity one and the sociality one. Whereas the first score measures how fast it is possible to reach any point from any other point in the city, the second one measures the amount of population that it is possible to reach from any point in the city. Travençolo et al. (2008) assume that the diversity entropy, similar to the network heterogeneity (Section 2.2.2.2), can also be used to derive an estimation of the relative frequency of access effectively received and made by a particular node. This can be accomplished by a simple normalization, yielding the concept of node A. More specifically,the outward A quantifies the potential that a specific node has in accessing the other nodes of the network. In an analogous fashion, the inward A quantifies the frequency of the visits to each node of self-avoiding walks departing from all other nodes.

Chen et al. (2015) modified the Accessibility (A) to consider the impact of floods on different travel modes. The authors compare the Hansen index (Hansen, 1959) with their proposed metric. Similarly, Miao and Ni (2019) focus on the multimodal A of a city. They analyze the impact of disruption over the intercity transportation network of Yangtze River Delta, which includes bus, car and train alternatives. The disrupted scenarios consist in removing one or two road nodes or rail stations. Miao and Ni (2019), define the A as follows (14):

$$A_s = \omega_s^a \sum_{\substack{r \in Z \\ r \neq s}} \omega_r^g \left[(1-\beta) \sum_{l \in M} \left(p_{lrs} \frac{c'_{lrs}}{c_{lrs}} \right) + \beta \frac{s_{lrs}}{s'_{lrs}} \right]^{-\alpha} \tag{14}$$

where ω_r^g (respectively ω_s^a) represents the travel generation weights of the departure area r (respectively travel attraction weights of the destination area s) and Z the set of areas; β ($0 \leq \beta \leq 1$) is a coefficient weighting the impact of the level of service; p_{lrs} is the probability to choose transport mode l to travel from r to s and M is the set of all the transport mode; c_{lrs} (respectively c'_{lrs}) is the travel cost from r to s with transport mode l under normal conditions (respectively disturbed conditions); s_{lrs} (respectively s'_{lrs}) is the level of service of transport mode l when travelling from r to s under normal conditions (respectively disturbed conditions); and α represents a travel cost decay parameter, greater than zero, allowing to control the weight of the travel cost ratio.

The following study aims at characterizing the spatio-temporal evolution of the Accessibility (A) (14) for an urban multimodal transport network to quantify the impact of a disruption both in time and space. The area generation weights ω_r^g and the area attraction ones ω_s^a are defined by counting the number of POIs included in the areas and their nature. We assume that a touristic point attracts and generates more travel demand than *e.g.*, a school, which interests a smaller part of the population. In this paper, for simplicity reasons, we fix the parameter β equal to 0. The metric does not include therefore the disruption impacts on the level of transportation service s_{lrs} caused by the reduction of available travel alternatives. Based on such assumptions, the A metric only depends on travel cost dynamics, expressed via travel cost under normal c_{lrs} and disrupted c'_{lrs} conditions for each available transport mode l, from departure area r to the arrival one s, which is equal to the travel time. The final simplified definition of A, based on (14) is the following:

$$A_s = \omega_s^a \sum_{\substack{r \in Z \\ r \neq s}} \omega_r^g \frac{1}{\sum_{l \in M} p_{lrs} \frac{c'_{lrs}}{c_{lrs}}} \tag{15}$$

By computing the A (15) over the network under normal conditions and in the presence of a snowfall, we want to observe the ability of the studied metric to capture the vulnerability of the urban multimodal transport network. While for personal cars, the corresponding graph is weighted via average travel time information, computed from FCD, for public transport modes (bus, subway and tramway), we do not have access to actual travel time data. We weight the graph with a fixed travel time computed according to an average bus speed of 20km/h, to consider the waiting time at bus stop. For the tramway and the subway sub-networks, we adopt a similar approach, by considering a fixed travel time with average speeds equal to 30km/h and 40km/h, respectively (Hitge and Vanderschuren, 2015). These speeds are assumed to be higher because such modes are composed of completely dedicated lanes and a lower number of stops exists compared to buses. Finally, we consider a walking graph, weighted by a walking speed of 4 km/h, composed of non-directed road network edges, connecting all the remaining areas of the city.

Without disruption, under normal conditions, the A only depends on the area attraction and generation weights. Indeed, in such conditions, the ratio of travel costs is equal to one for every transport mode. With such definition, the central area presents the highest A because of the presence of many points of interests (Figure 19a). Under such conditions, the global A, which is the sum of all areas A, is equal to

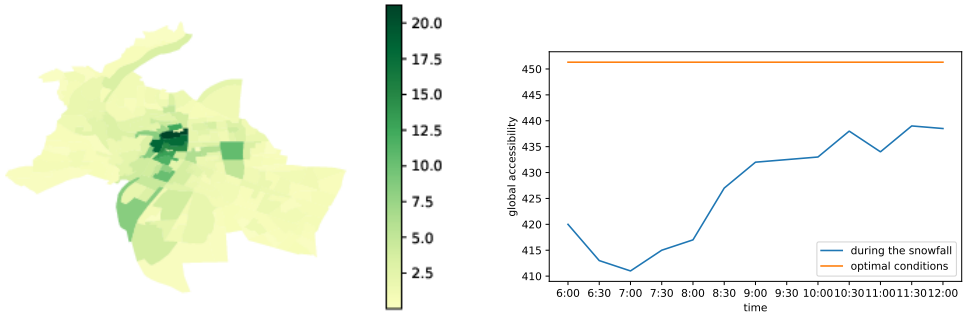

(a) Optimal A **(b)** Global A

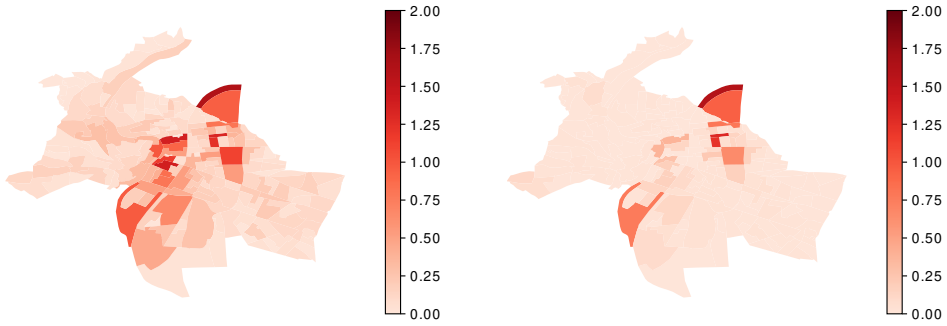

(c) Loss of A at 7 : 00 am **(d)** Loss of A at 11 : 30 am

Figure 19: A recorded under normal conditions (a) and in presence of a snowfall on 18th December, 2017. The temporal impact is presented in (b) and the spatial one is observed at both at 7 : 00am in (c) and at 11 : 30am in (d).

451.31. Based on such reference value, we can study the temporal evolution of global A in time in presence of disruption, thus providing insights on the network state. The temporal impact of the snowfall (Section 4.1.1) (Figure 4.2), induced only by the car travel time increase, is analyzed in Figure 19b) while the spatial impact is observed at 7 : 00 am (Figure 19c) and 11 : 30 am (Figure 19d), for the extreme values of A. The reduction per area is stronger at 11:30am as recorded in Figure 19b and in accordance with the travel times evolution under normal conditions and in presence of disruption. The loss of A is higher for the central areas. We notice that A strictly follows the variations of travel times (Figure 4.2). The more travel time increases in presence of disruption, compared to normal conditions, the lower A is. The spatial distribution of the metric shows that the central areas are the most impacted by the snowfall (Figure 19c). Nonetheless, by analyzing the spatial distribution of the A, the evolution of the metric is more evident without the public transport disruption (Figure 19c).

We prove that the A provides interesting insights on network vulnerability in the presence of daily or heavy disruptions that cause slowdowns or public transport delays. The measure depends on traffic conditions and appears thus to be sensitive to the dynamic nature of the disruption. Nonetheless, A presents two major limits. Such measure is not appropriate to capture the impact caused by the total removal of a public transport mode without supposing people will realize their path by walk (or other slower mode), which is a strong assumption. Otherwise, area A will be equal to 0 whereas other transport modes still allow moving in the network. Another limit results in the negative impact of the boarding effect on the measure. Indeed, we notice a huge reduction of A for the bordering areas because of the weak presence of paths going to them. It is thus not possible to study the areas at the extremities of the graph, implying the necessity to broaden the study perimeter.

B. State-of-the-Art Resilience Summary

The following tables summarized a set of articles dealing with network resilience since 2002. The analyzed transport mode is specified, as well as the used approach which could be topological, dynamic or both. A presentation of the major measures applied to characterize resilience is done with a distinction between the Centrality Measures (CM), issued from graph theory, the Demand- / Capacity-based Indicators (DCI) and the Travel time-based Indicators (TTI). Finally, the methodology employed to simulate the disruptions is detailed.

Article	Network			Approaches			Metrics			Disruptions				
				Topo		Dyna								
	RN	PTN	MMN	U	W		CM	DCI	TTI	R	CR	MC	HD	Stress tests
Chen et al. (2002)	×					×		✱	◀		×			
Immers et al. (2004)	×					×			▶		×			
Dall'Asta et al. (2006)					×		▲ ■ ×			×				
Crucitti et al. (2006)	×			×			▲ ▼ ● ×							
Scott et al. (2006)	×			×	×	×	×	▶	×	×				
Murray-Tuite (2006)	×					×		▶	◀✿					
Al-Deek and Emam (2006)						×	✱	◀		×				
Taylor and D'Este (2007)	×					×		×	◀					
Scheurer et al. (2007)		×		×			▲ ▼ ■ ●							
Erath et al. (2009)	×					×			◀✿	×				
Berche et al. (2009)		×		×			▲ ▼ ■ ◆ ×			×				
Sullivan et al. (2010)	×					×			◀		×			
Opsahl et al. (2010)					×		▲ ▼ ■							
Soh et al. (2010)		×			×		▼ ×	✖						
Leu et al. (2010)	×	×		×		×	▲ ▼ ◆		✿	×				
Zhang et al. (2011)	×			×			▲ ▼ ■							
Porta Sergio et al. (2009) Porta et al. (2012)	×			×			▲ ▼ ×							
Jenelius and Mattsson (2012)	×					×		×	◀✶◗	×				
Freckleton et al. (2012)	×					×		✱	◀✿				×	

Table 9: Literature review summarize (2002-2012): some studies analyze the Road Network (RN) or the Public Transport Network (PTN) which could be formed by the bus network or the subway network or both using Multi-Modal Network (MMN) with a ✈ to represent the airlines networks. The network could be model using an Unweighted (U) graph (UW) or a Weighted (W) graph. Two major approaches are used in the resilience analysis: the topological one (Topo) or the dynamic one (Dyna). Both approaches could be hybrid to be more consistent with the transport network. Some measures are frequently employed such asCentrality Measures (CM) (▲: EBC, ▼: NCC, ■: NDC, ●: efficiency / AE, ◆: GCC, ×: others) issued from graph theory and knowing that they become aware of the traffic conditions when computed over a W graph, Demand- / Capacity-based Indicators (DCI) (✖: DSCM, ✱: flow variation, ✚: # trip variation, ▶: V/C) or Travel time-based Indicators (TTI) (◀: travel time variation / delay, ✿: length variation, ✶: I, ◗: E). The disruption modelling could be done through a node or edge Removal (R), a edge Capacity Reduction (CR), the catastrophe and traffic simulations Model Coupling (MC) or using Historical Data (HD).

Article	Network			Approaches			Metrics			Disruptions				
				Topo		Dyna								
	RN	PTN	MMN	U	W		CM	DCI	TTI	R	CR	MC	HD	Stress tests
Altshuler et al. (2011) Puzis et al. (2013)	×				×	×	▲	✖ ✱						
Cardillo et al. (2013)			×	×		×	■	✱		×				
Lhomme et al. (2013)	×			×			×							
Cheng et al. (2013)		×			×		▲ ▼ ■	✖						
Chen and Hero (2013)				×			▲ ■ ◆			×				
Kuang et al. (2013)	×					×		✱	◀		×			
Rodríguez-Núñez and García-Palomares (2014)		×		×		×	■	✚	✿	×				
Oliveira et al. (2014)	×					×		▶	◀					
De Domenico et al. (2014)			×		×		×			×				
Cats and Jenelius (2014)		×			×	×		✱ ✚	◀	×				×
Jin et al. (2014)		×				×		✱	◀	×				×
Stamos et al. (2015)	×	×				×			◀				×	
Janić (2015)		✈				×		✚					×	
Wang (2015)	×			×			▲ ▼ ■ ◆			×				
Freiria et al. (2015)	×				×		▲ ■ ×		✿	×				
Cheng et al. (2015)		×		×		×	▲ ▼ ■	✱	◀					
Bíl et al. (2015)	×			×			●	×	✿	×			×	
Soltani-Sobh et al. (2015)						×		✱	◀		×			

Table 10: Literature review summarize (2013-2015): some studies analyze the Road Network (RN) or the Public Transport Network (PTN) which could be formed by the bus network or the subway network or both using Multi-Modal Network (MMN) with a ✈ to represent the airlines networks. The network could be model using an Unweighted (U) graph (UW) or a Weighted (W) graph. Two major approaches are used in the resilience analysis: the topological one (Topo) or the dynamic one (Dyna). Both approaches could be hybrid to be more consistent with the transport network. Some measures are frequently employed such asCentrality Measures (CM) (▲: EBC, ▼: NCC, ■: NDC, ●: efficiency / AE, ◆: GCC, ×: others) issued from graph theory and knowing that they become aware of the traffic conditions when computed over a W graph, Demand- / Capacity-based Indicators (DCI) (✖: DSCM, ✱: flow variation, ✚: # trip variation, ▶: V/C) or Travel time-based Indicators (TTI) (◀: travel time variation / delay, ✿: length variation, ✶: I, ◗: E). The disruption modelling could be done through a node or edge Removal (R), a edge Capacity Reduction (CR), the catastrophe and traffic simulations Model Coupling (MC) or using Historical Data (HD).

Article	Network			Approaches			Metrics			Disruptions				
				Topo		Dyna								
	RN	PTN	MMN	U	W		CM	DCI	TTI	R	CR	MC	HD	Stress tests
Pokharel and Ieda (2016)	×				×	×			×				×	
El-Rashidy and Grant-Muller (2016)	×			×		×	×	✱▶						
Yoo and Yeo (2016)		✈			×		■	✖		×				
Martinez-Pastor et al. (2016)	×					×			×				×	
Dunn and Wilkinson (2016)		✈		×		×	■●	✚		×				
Adjetey-Bahun et al. (2016)		×				×		✱	◀	×				×
Kim and Yeo (2016)	×					×			MFD	×				
Pitilakis et al. (2016)	×			×	×		×	✚		×				×
Du et al. (2016)			✈	×			▼◆			×				
Pregnolato et al. (2016)	×				×	×	▲	✱				×		
Shalaby et al. (2016)		×		×			▲●	×	✶◗	×				
Lu et al. (2016)		👣				×		✱✆					×	
Zhu et al. (2016) Zhu et al. (2017)	×					×		✚					×	
Pregnolato et al. (2017)	×					×			◀			×		
Yin et al. (2017)	×				×	×	emergency response (SP)					×		×
Danczyk et al. (2017)	×					×		✱	◀				×	
Donovan and Work (2017)	×					×			◀				×	
Aleta et al. (2017)			×		×	×	■	×	◀✿	×				

Table 11: Literature review summarize (2016-2017): some studies analyze the Road Network (RN) or the Public Transport Network (PTN) which could be formed by the bus network or the subway network or both using Multi-Modal Network (MMN) with a ✈ to represent the airlines networks. The network could be model using an Unweighted (U) graph (UW) or a Weighted (W) graph. Two major approaches are used in the resilience analysis: the topological one (Topo) or the dynamic one (Dyna). Both approaches could be hybrid to be more consistent with the transport network. Some measures are frequently employed such asCentrality Measures (CM) (▲: EBC, ▼: NCC, ■: NDC, ●: efficiency / AE, ◆: GCC, ×: others) issued from graph theory and knowing that they become aware of the traffic conditions when computed over a W graph, Demand- / Capacity-based Indicators (DCI) (✖: DSCM, ✱: flow variation, ✚: # trip variation, ▶: V/C) or Travel time-based Indicators (TTI) (◀: travel time variation / delay, ✿: length variation, ✶: I, ◗: E). The disruption modelling could be done through a node or edge Removal (R), a edge Capacity Reduction (CR), the catastrophe and traffic simulations Model Coupling (MC) or using Historical Data (HD).

Article	Network			Approaches			Metrics			Disruptions				
				Topo		Dyna								
	RN	PTN	MMN	U	W		CM	DCI	TTI	R	CR	MC	HD	Stress tests
Zhou and Wang (2018)	×					×			◀		×			
Aydin et al. (2018)	×			×			▲●◆			×				
Lam et al. (2018)	×					×		✚	◀			×		×
Zhang et al. (2018b)		×			×		▲■●			×				
Gauthier et al. (2018)	×			×	×	×	▲		◀	×	×			×
Cats and Jenelius (2018)		×				×			×		×			×
Akbarzadeh and Estrada (2018)	×				×		×							
Silver et al. (2018)	×			×		×	▲▼■◆×	✚×			×			
Tang and Heinimann (2018)	×					×		✱▶	◀					
Calvert and Snelder (2018)	×					×			◀×					
Chandramouleeswaran and Tran (2018)		✈				×		✚	◀				×	
Balal et al. (2019)	×					×			◀✿	×				
Xu et al. (2019)	×				×	×	▲×	✱						
Hassan et al. (2019)		×			×		▲■●×			×				
Marra et al. (2019)		×			×	×	▲▼■		◀				×	
Akbarzadeh et al. (2019)	×				×		▲■●◆	×			×			
Ilbeigi (2019)	×				×	×	▼						×	
Gecchele et al. (2019)	×					×			◀✶×	×				
Suryani (2019)	×					×		▶	▶					

Table 12: Literature review summarize (2018-2019): some studies analyze the Road Network (RN) or the Public Transport Network (PTN) which could be formed by the bus network or the subway network or both using Multi-Modal Network (MMN) with a ✈ to represent the airlines networks. The network could be model using an Unweighted (U) graph (UW) or a Weighted (W) graph. Two major approaches are used in the resilience analysis: the topological one (Topo) or the dynamic one (Dyna). Both approaches could be hybrid to be more consistent with the transport network. Some measures are frequently employed such asCentrality Measures (CM) (▲: EBC, ▼: NCC, ■: NDC, ●: efficiency / AE, ◆: GCC, ×: others) issued from graph theory and knowing that they become aware of the traffic conditions when computed over a W graph, Demand- / Capacity-based Indicators (DCI) (✖: DSCM, ✱: flow variation, ✚: # trip variation, ▶: V/C) or Travel time-based Indicators (TTI) (◀: travel time (cost) variation / delay, ✿: length variation, ✶: I, ◗: E). The disruption modelling could be done through a node or edge Removal (R), a edge Capacity Reduction (CR), the catastrophe and traffic simulations Model Coupling (MC) or using Historical Data (HD).

Article	Network			Approaches			Metrics			Disruptions				
				Topo		Dyna								
	RN	PTN	MMN	U	W		CM	DCI	TTI	R	CR	MC	HD	Stress tests
Cats and Krishnakumari (2020)		×		×			▲ ■			×				
Jiao et al. (2020)		×			×		●			×				×
Shang et al. (2020a)						×		✱	◀		×			×
Wang et al. (2020)		✈			×		▲ ■ ● ◆ ×	✖		×				
Shang et al. (2020b)	×				×	×	▲ ▼ ■ ● ×		◀	×				
Jafino et al. (2020)		×		×	×	×	▲ ■ ● ×	✱	◀◗					
Morelli and Cunha (2020)	×				×	×	×		✿			×		×
Gu et al. (2020)	×					×	×	×	◀	×	×			×
Li et al. (2020)	×					×			◀				×	
Mahdavi et al. (2020)		×				×		▶				×	×	
Yap et al. (2021)		×				×			◀		×			
Cheng et al. (2021)		🚲				×		✚					×	
Guo Jingni et al. (2021)			×			×		✱	◀					
Martín et al. (2021)	×					×		✱	◀	×				
He et al. (2021)			×		×	×	▲ ▼ ■		◀	×	×			
Zhang and Ng (2021)		×			×		▲ ▼ ■ ● ◆ ×			×				×
Malandri et al. (2021)		×				×			◀	×				
Nawod Kalpana et al. (2021)	×				×		▲ ▼					×		
Aghababaei et al. (2021)	×					×		✚	◀				×	
Janić (2021)	×	×				×		✱✚	◀				×	

Table 13: Literature review summarize (2020-2021): some studies analyze the Road Network (RN) or the Public Transport Network (PTN) which could be formed by the bus network or the subway network or both using Multi-Modal Network (MMN) with a ✈ to represent the airlines networks. The network could be model using an Unweighted (U) graph (UW) or a Weighted (W) graph. Two major approaches are used in the resilience analysis: the topological one (Topo) or the dynamic one (Dyna). Both approaches could be hybrid to be more consistent with the transport network. Some measures are frequently employed such asCentrality Measures (CM) (▲: EBC, ▼: NCC, ■: NDC, ●: efficiency / AE, ◆: GCC, ×: others) issued from graph theory and knowing that they become aware of the traffic conditions when computed over a W graph, Demand- / Capacity-based Indicators (DCI) (✖: DSCM, ✱: flow variation, ✚: # trip variation, ▶: V/C) or Travel time-based Indicators (TTI) (◀: travel time variation / delay, ✿: length variation, ✶: I, ◗: E). The disruption modelling could be done through a node or edge Removal (R), a edge Capacity Reduction (CR), the catastrophe and traffic simulations Model Coupling (MC) or using Historical Data (HD).

C. Table of Notations

The following table summarizes the notations used for the elaboration of the Park-and-Ride (P&R) systems, presented in Chapter 5.3. The sets, the parameters, and the decision variables, mostly common to both formulations are detailed.

Sets	**Definition**
Ω	Set of stochastic scenarios
N	Set of nodes in the network
E	Set of edges in the network
$W^\omega \subset N \times N$	Set of OD pairs in scenario $\omega \in \Omega$.
$P \subset N$	Set of pick up nodes.
$P_r^\omega \subset P$	Set of accessible pick ups nodes from the origin node $r \in N$ in scenario $\omega \in \Omega$.
$D \subset N$	Set of drop off nodes.
$D_s^\omega \subset D$	set of accessible drop offs nodes from the destination node $s \in N$ in scenario $\omega \in \Omega$.
$\Sigma_{rs}^\omega \subset N \times N$	Set of P&R paths in scenario $\omega \in \Omega$ for OD $(r,s) \in W^\omega$. Each element $(i,j) \in \Sigma_{rs}^\omega$ corresponds to the path (r,i,j,s) in the P&R system.
K	Set of the different vehicle classes k.
Parameters	
p^ω	Probability of the scenario $\omega \in \Omega$.
d_{rs}^ω	Travel demand in scenario $\omega \in \Omega$ for OD pair $(r,s) \in W^\omega$.
q_k	Capacity of the vehicle of class k.
c_k^{fleet}	Unit cost for the vehicle of class k.
c_i^{loc}	Construction cost of a pick up (car park) or a drop off (transit stop) at node $i \in P \cup D$.
B	Budget available for the construction of pick up and drop off nodes
$c_{ri}^{\text{R}_{rs},\omega}$	Travel time by the reserve mode allowing to reach the pick up i from the origin r
$c_{ij}^{\text{route},\omega}$	Travel time from pick up $i \in P$ to drop off $j \in D$ through the P&R system.
c_{js}^{walk}	Travel time from drop off $j \in D$ to destination $s \in N$ (assumed to be walking).
g_{rijs}^ω	Generalized cost of path (r,i,j,s) in the P&R system.
θ	Parameter in the logit model representing users' sensitivity to the generalized cost.
Decision variables	
$x_{rijs}^\omega \in [0,1]$	Proportion of users in scenario $w \in \Omega$ on OD $(r,s) \in W^\omega$ using the P&R system via path (r,i,j,s).
$x_{\text{R}_{rs}}^\omega \in [0,1]$	Proportion of users using the reserve mode in scenario $w \in \Omega$ on OD $(r,s) \in W^\omega$.
$y_i \in \{0,1\}$	Decision to open a pick up or drop off facility at node $i \in P \cup D$.
$z_{ijk}^\omega \in \mathbb{Z}_+$	Number of vehicle of class k needed between the pick up i and the drop off j in the scenario ω.

Table 14: Notation table

Bibliography

Adebisi, A., 2017. A review of the difference among macroscopic, microscopic and mesoscopic traffic models. Technical Report. Florida A&M University. doi:10.13140/RG.2.2.11508.65929.

Adjetey-Bahun, K., Birregah, B., Châtelet, E., Planchet, J.L., 2016. A model to quantify the resilience of mass railway transportation systems. Reliability Engineering & System Safety 153, 1–14. doi:10.1016/J.RESS.2016.03.015.

Afrin, T., Yodo, N., 2020. A Survey of Road Traffic Congestion Measures towards a Sustainable and Resilient Transportation System. Sustainability 12, 4660. doi:10.3390/su12114660.

Aghababaei, M.T.S., Costello, S.B., Ranjitkar, P., 2021. Measures to evaluate post-disaster trip resilience on road networks. Journal of Transport Geography 95, 103154. doi:10.1016/J.JTRANGEO.2021.103154.

Akbarzadeh, M., Estrada, E., 2018. Communicability geometry captures traffic flows in cities. doi:10.1038/s41562-018-0407-3.

Akbarzadeh, M., Memarmontazerin, S., Derrible, S., Salehi Reihani, S.F., 2017. The role of travel demand and network centrality on the connectivity and resilience of an urban street system. Transportation , 1–15doi:10.1007/s11116-017-9814-y.

Akbarzadeh, M., Salehi Reihani, S.F., Samani, K.A., 2019. Detecting critical links of urban networks using cluster detection methods. Physica A: Statistical Mechanics and its Applications 515, 288–298. doi:10.1016/j.physa.2018.09.170.

Al-Deek, H., Emam, E.B., 2006. New Methodology for Estimating Reliability in Transportation Networks with Degraded Link Capacities. Journal of Intelligent Transportation Systems 10, 117–129. doi:10.1080/15472450600793586.

Al-Zinati, M., Zalila-Wenkstern, R., 2018. A Resilient Agent-Based Re-organizing Traffic Network for Urban Evacuations, in: International Conference on Practical Applications of Agents and Multi-Agent Systems, Springer, Cham. pp. 42–58. doi:10.1007/978-3-319-94580-4{_}4.

Aldagheiri, M., 2009. The role of the transport road network in the economic development of Saudi Arabia. Urban transport doi:10.2495/UT090251.

Alessandretti, L., Karsai, M., Gauvin, L., 2016. User-based representation of time-resolved multimodal public transportation networks. Royal Society Open Science 3. doi:10.1098/rsos.160156.

Aleta, A., Meloni, S., Moreno, Y., 2017. A Multilayer perspective for the analysis of urban transportation systems. Scientific Reports doi:10.1038/srep44359.

Aliakbary, S., Habibi, J., Movaghar, A., 2018. Quantification and Comparison of Degree Distributions in Complex Networks, in: 7th International Symposium on Telecommunications (IST), Teheran. pp. 464–469.

Altshuler, Y., Puzis, R., Elovici, Y., Bekhor, S., Pentland, A., 2011. Augmented Betweenness Centrality for Mobility Prediction in Transportation Networks. Securing Transportation Systems, Protecting Critical Infrastructures Series .

Amini, S., Tilg, G., Busch, F., 2018. Evaluating the impact of real-time traffic control measures on the resilience of urban road networks, in: 21st International Conference on Intelligent Transportation Systems (ITSC), IEEE. pp. 519–524. doi:10.1109/ITSC.2018.8569678.

Andersson, E.V., Peterson, A., Krasemann, J.T., 2013. Quantifying railway timetable robustness in critical points. Journal of Rail Transport Planning & Management doi:10.1016/j.jrtpm.2013.12.002.

Angelo, G.D.., Severini, L., Velaj, Y., 2016. On the Maximum Betweenness Improvement Problem. Electronic Notes in Theoretical Computer Science 322, 153–168. doi:10.1016/j.entcs.2016.03.011.

Aros-Vera, F., Marianov, V., Mitchell, J.E., 2013. p-Hub approach for the optimal park-and-ride facility location problem. European Journal of Operational Research 226, 277–285. doi:10.1016/j.ejor.2012.11.006.

Aydin, N.Y., Heinimann, H.R., Duzgun, H.S., Wenzel, F., 2018. Integration of stress testing with graph theory to assess the resilience of urban road networks under seismic hazards. Natural Hazards 91, 37–68. doi:10.1007/s11069-017-3112-z.

Balakrishnan, A., Mirchandani, P., Prasad Natarajan, H., 2009. Connectivity Upgrade Models for Survivable Network Design. Operations Research 57, 170–186. doi:10.1287/opre.1080.0579.

Balal, E., Valdez, G., Miramontes, J., Long Cheu, R., 2019. Comparative evaluation of measures for urban highwaynetwork resilience due to traffic incidents. International journal of transportation science and technology .

Bankes, S., 2010. Robustness, Adaptivity, and Resiliency Analysis, in: AAAI Fall Symposium: Complex Adaptative Systems, pp. 1–6.

Barabási, A.L., Albert, R., 1999. Emergence of Scaling in Random Networks. Science .

Barcelo, J., Casas, J., García, D., Perarnau, J., 2007. A Methodological Approach Combining Macro, Meso and Micro Simulation Models for Transportation Analysis, in: 11th World Conference on Transport Research, pp. 1–40.

Barigozzi, M., Fagiolo, G., Garlaschelli, D., 2010. Multinetwork of International Trade: A Commodity-Specific Analysis. Physic Review .

Barrat, A., Barthé Lemy †, M., Pastor-Satorras, R., Vespignani, A., 2004. The architecture of complex weighted networks, in: Proceedings of national Academy of Sciences of the United States of America, pp. 3747–3752.

Barthélemy, M., 2011. Spatial networks. Physics Reports 499, 1–101. doi:10.1016/J.PHYSREP.2010.11.002.

Barwaldt, M.S., Franzin, R.d.F., Casarin, V.A., Santos, A.V.d., 2014. Using the Theory of Graphs on the Implementation of Bike Lane in Small Towns. Procedia - Social and Behavioral Sciences doi:10.1016/j.sbspro.2014.12.216.

Battiston, F., Nicosia, V., Latora, V., 2014. Metrics for the analysis of multiplex networks. Physical Review E .

Battiston, S., Mandel, A., Monasterolo, I., Schütze, F., Visentin, G., 2017. A climate stress-test of the financial system. Nature climate change doi:10.1038/NCLIMATE3255.

BBC, 2021a. France wildfire: Thousands evacuated as blaze rages near Riviera.

BBC, 2021b. Germany floods: 'My city looks like a battlefield'.

Bell, M.G.H., 2000. A game theory approach to measuring the performance reliability of transport networks. Transportation Research Part B: Methodological 34, 533–545. doi:10.1016/S0191-2615(99)00042-9.

Bell, M.G.H., Schmöcker, J.D., 2002. Network Reliability: Topological Effects and the Importance of Information, in: ICTT, Guilin. pp. 1–8.

BeMobile, . BeMobile Web Page.

Berche, B., Von Ferber, C., Holovatch, T., Holovatch, Y., 2009. Resilience of public transport networks against attacks. Eur. Phys. J. B 71, 125–137. doi:10.1140/epjb/e2009-00291-3.

Berdica, K., 2002. An introduction to road vulnerability: what has been done, is done and should be done. Transport Policy 9, 117–127. doi:10.1016/S0967-070X(02)00011-2.

Bergamini, E., Meyerhenke, H., Crescenzi, P., 2018. Improving the Betweenness Centrality of a Node by Adding Links. Journal of Experimental Algorithmics 23.

Berkeley, A.R., Wallace, M., 2010. A Framework for Establishing Critical Infrastructure Resilience Goals Final Report and Recommendations by the Council. National Infrastructure Advisory Council .

Bettilyon, T.E., 2019. What Is A Graph.

Bhouri, N., Aron, M., Kauppila, J., 2012. Relevance of Travel Time Reliability Indicators: A Managed Lanes Case Study. Procedia - Social and Behavioral Sciences 54, 450–459. doi:10.1016/J.SBSPRO.2012.09.763.

Bianconi, G., 2013. Statistical Mechanics of Multiplex Ensembles: Entropy and Overlap. Physic Review .

Biazzo, I., Monechi, B., Loreto, V., 2019. General scores for accessibility and inequality measures in urban areas. royal society open science doi:10.1098/rsos.190979.

Bíl, M., Vodák, R., Kubeček, J., Bílová, M., Sedoník, J., 2015. Evaluating road network damage caused by natural disasters in the Czech Republic between 1997 and 2010. Transportation Research Part A: Policy and Practice 80, 90–103. doi:10.1016/J.TRA.2015.07.006.

Blaschke, W., Jones, M.T., Majnoni, G., Peria, S.M., Johnston, R.B., Ize, A., Johnston, B., Kupiec, P., Laurin, A., Madrid, P., Morales, A., Promisel, L., Ulgenerk, F.E., 2001. Stress Testing of Financial Systems: An Overview of Issues, Methodologies, and FSAP. International Monetary Fund .

Boldi, P., Rosa, M., Vigna, S., 2013. Robustness of social and web graphs to node removal. Social Network Analysis and Mining 3, 829–842. doi:10.1007/s13278-013-0096-x.

Bondy, J.A., Murty, U.S.R., 1976. Graph theory with applications. North holland ed.

Boulmakoul, B., Besri, Z., Karim, L., Boulmakoul, A., Lbath, A., 2017. Combinatorial connectivity and spectral graph analytics for urban public transportation system. Transportation Research Procedia 27, 1154–1162. doi:10.1016/j.trpro.2017.12.019.

Braess, D., Nagurney, A., Wakolbinger, T., 2005. On a Paradox of Traffic Planning. Transportation science 39. doi:10.1287/trsc.1050.0127.

Brandes, U., Borgatti, S.P., Freeman, L.C., 2016. Maintaining the duality of closeness and betweenness centrality. Social Networks 44, 153–159. doi:10.1016/J.SOCNET.2015.08.003.

Brandes, U., Fleischer, D., 2005. Centrality Measures Based on Current Flow, in: Proceedings of the 22nd Symposium Theorical Aspects of Computer Science, pp. 533–544.

Bródka, P., Kazienko, P., Musiał, K., Skibicki, K., 2012. Analysis of Neighbourhoods in Multi-layered Dynamic Social Networks. International Journal of Computational Intelligence Systems , 582–596.

Bródka, P., Skibicki, K., Kazienko, P., Musiał, K., 2011. A Degree Centrality in Multi-layered Social Network, in: International Conference on Computational Aspects of Social Networks, pp. 237–242. doi:10.1109/CASON.2011.6085951.

Brodka, P., Stawiak, P., Kazienko, P., 2011. Shortest Path Discovery in the Multi-layered Social Network, in: 2011 International Conference on Advances in Social Networks Analysis and Mining, IEEE. pp. 497–501. doi:10.1109/ASONAM.2011.67.

Bruneau, M., Chang, S.E., Eguchi, R.T., Lee, G.C., O 'Rourke, T.D., Reinhorn, A.M., Shinozuka, M., Tierney, K., Wallace, W.A., Von Winterfeldt, D., 2003. A Framework to Quantitatively Assess and Enhance the Seismic Resilience of Communities. Earthquake spectra 19, 733–752. doi:10.1193/1.1623497.

Buldyrev, S.V., Parshani, R., Paul, G., Stanley, H.E., Havlin, S., 2010. Catastrophic cascade of failures in interdependent networks. Nature doi:10.1038/nature08932.

Cacchiani, V., Huisman, D., Kidd, M., Kroon, L., Toth, P., Veelenturf, L., Wagenaar, J., 2014. An overview of recovery models and algorithms for real-time railway rescheduling q. Transportation Research Part B doi:10.1016/j.trb.2014.01.009.

Calabrese, F., Pereira, F.C., Di Lorenzo, G., Liu, L., Ratti, C., 2010. The geography of taste: Analyzing cell-phone mobility and social events, in: Lecture Notes in Computer Science (including subseries Lecture Notes in Artificial Intelligence and Lecture Notes in Bioinformatics), pp. 22–37. doi:10.1007/978-3-642-12654-3{_}2.

Calvert, S.C., Snelder, M., 2018. A methodology for road traffic resilience analysis and review of related concepts. Transportmetrica A: Transport Science doi:10.1080/23249935.2017.1363315.

Camahan, J.V., Asce, M., Davis, W.J., Shahin, M.Y., Keane, P.L., Wu, M.I., 1987. Optimal maintenance decisions for pavement management. Journal of Transport Engineering .

Cantillo, V., Macea, L.F., Jaller, M., 2018. Assessing Vulnerability of Transportation Networks for Disaster Response Operations. Networks and Spatial Economics , 1–31doi:10.1007/s11067-017-9382-x.

Capano, G., Woo, J.J., 2017. Resilience and robustness in policy design: a critical appraisal. Policy Science doi:10.1007/s11077-016-9273-x.

Cardillo, A., Zanin, M., Gómez-Gardeñes, J., Romance, M., del Amo, A.J., Boccaletti, S., 2013. Modeling the multi-layer nature of the European Air Transport Network: Resilience and passengers re-scheduling under random failures. European Physical Journal: Special Topics 215, 23–33. doi:10.1140/epjst/e2013-01712-8.

Carrion, C., Levinson, D., 2012. Value of travel time reliability: A review of current evidence. Transportation Research Part A: Policy and Practice 46, 720–741. doi:10.1016/j.tra.2012.01.003.

Cassir, C., 2001. A Flow Model for the Analysis of Transport Network Reliability. Ph.D. thesis. University of Newcastle.

Cats, O., 2016. The robustness value of public transport development plans. Journal of Transport Geography 51, 236–246. doi:10.1016/J.JTRANGEO.2016.01.011.

Cats, O., Jenelius, E., 2014. Dynamic Vulnerability Analysis of Public Transport Networks: Mitigation Effects of Real-Time Information. Networks and Spatial Economics doi:10.1007/s11067-014-9237-7.

Cats, O., Jenelius, E., 2018. Beyond a complete failure: the impact of partial capacity degradation on public transport network vulnerability. Transportmetrica B: Transport Dynamics 6, 77–96. doi:10.1080/21680566.2016.1267596.

Cats, O., Koppenol, G.J., Warnier, M., 2017. Robustness assessment of link capacity reduction for complex networks: Application for public transport systems. Reliability Engineering and System Safety 167, 544–553. doi:10.1016/j.ress.2017.07.009.

Cats, O., Krishnakumari, P., 2020. Metropolitan rail network robustness. Physica A: Statistical Mechanics and its Applications 549, 124317. doi:10.1016/J.PHYSA.2020.124317.

Cats, O., Yap, M., van Oort, N., 2016. Exposing the role of exposure: Public transport network risk analysis. Transportation Research Part A: Policy and Practice 88, 1–14. doi:10.1016/J.TRA.2016.03.015.

Chan, R., Asce, S.M., Schofer, J.L., Asce, M., 2015. Measuring Transportation System Resilience: Response of Rail Transit to Weather Disruptions. Natural Hazards Review 17. doi:10.1061/(ASCE)NH.

Chandramouleeswaran, K.R., Tran, H.T., 2018. Data-driven resilience quantification of the US Air transportation network, in: 2018 Annual IEEE International Systems Conference (SysCon), IEEE. pp. 1–7. doi:10.1109/SYSCON.2018.8369602.

Chang, J.S., Jung, D., Jun, S., Oh, H., 2020. Resilience conceptual framework for assessing the performance of transit service. International Journal of Urban Sciences 24, 339–353. doi:10.1080/12265934.2019.1687319.

Chen, A., Kasikitwiwat, P., Yang, C., 2013. Alternate capacity reliability measures for transportation networks. Journal of Advanced Transportation 47, 79–104. doi:10.1002/atr.216.

Chen, A., Yang, C., Kongsomsaksakul, S., Lee, M., 2007a. Network-based acessibility measures for vulnerability analysis of degradable transportation networks. Networks and Spatial Economics 7, 241–256. doi:10.1007/s11067-006-9012-5.

Chen, A., Yang, H., Lo, H.K., Tang, W.H., 1999. A capacity related reliability for transportation networks. Journal of Advanced Transportation 33, 183–200. doi:10.1002/atr.5670330207.

Chen, A., Yang, H., Lo, H.K., Tang, W.H., 2002. Capacity reliability of a road network: an assessment methodology and numerical results. Transportation Research Part B: Methodological 36, 225–252. doi:10.1016/S0191-2615(00)00048-5.

Chen, C., Skabardonis, A., Varaiya, P., 2003. Travel time reliability as a measure of service, in: Transport Research Board, pp. 74–79.

Chen, P.Y., Hero, A.O., 2013. Node Removal Vulnerability of the Largest Component of a Network. IEEE GlobalSIP .

Chen, S., Tan, J., Claramunt, C., Ray, C., 2011. Multi-scale and multi-modal GIS-T data model. Journal of Transport Geography 19, 147–161. doi:10.1016/J.JTRANGEO.2009.09.006.

Chen, X., Liu, Z., Currie, G., 2016. Optimizing location and capacity of rail-based Park-and-Ride sites to increase public transport usage. Transportation Planning and Technology 39, 507–526. doi:10.1080/03081060.2016.1174366.

Chen, X.Z., Lu, Q.C., Peng, Z.R., Ash, J.E., Chen, X.Z., Lu, Q.C., Peng, Z.R., 2015. Analysis of Transportation Network Vulnerability Under Flooding Disasters. Transportation Research Record: Journal of the Transportation Research 2532, 37–44. doi:10.3141/2532-05.

Chen, Y., Bell, M.G.H., Kaparias, I., 2007b. Reliability analysis of road networks and preplanning of emergency rescue paths, in: Critical Infrastructure. Springer Berlin Heidelberg, Berlin, Heidelberg, pp. 173–196. doi:10.1007/978-3-540-68056-7{_}9.

Chen, Y.W., Tzeng, G.H., 1999. A Fuzzy Multi-objective Model for Reconstructing the Post-quake Road-network by Genetic Algorithm. International Journal of Fuzzy Systems 1, 85–95.

Chen, Y.W., Tzeng, G.H., 2000. Determining the optimal reconstruction priority of a post-quake road-network, in: Proceedings of the 8th International Conference on Computing in Civil and Building Engineering, pp. 686–693. doi:10.1061/40513(279)90.

Cheng, L., Mi, Z., Coffman, D., Meng, J., Liu, D., Chang, D., 2021. The Role of Bike Sharing in Promoting Transport Resilience. Networks and Spatial Economics , 1–19doi:10.1007/s11067-021-09518-9.

Cheng, Y.Y., Ka, R., Lee, W., Lim, E.P., Zhu, F., 2015. Measuring Centralities for Transportation Networks Beyond Structures. Lecture Notes in Social Networks doi:10.1007/978-3-319-19003-7{_}2.

Cheng, Y.Y., Lee, R.K.W., Lim, E.P., Zhu, F., 2013. DelayFlow centrality for identifying critical nodes in transportation networks, in: Proceedings of the 2013 IEEE/ACM International Conference on Advances in Social Networks Analysis and Mining - ASONAM '13, pp. 1462–1463. doi:10.1145/2492517.2492595.

Childress, S., Durango-Cohen, P., 2005. On parallel machine replacement problems with general replacement cost functions and stochastic deterioration. Naval Research Logistics 52, 409–419. doi:10.1002/nav.20088.

Chopra, S.S., Dillon, T., Bilec, M.M., Khanna, V., 2016. A network-based framework for assessing infrastructure resilience: a case study of the London metro system. Royal Society doi:10.1098/rsif.2016.0113.

Chu, J.C., Asce, A.M., Chen, S.C., 2015. Optimization of Transportation-Infrastructure-System Protection Considering Weighted Connectivity Reliability. Journal Infrastructure System doi:10.1061/(ASCE)IS.1943-555X.0000264.

Church, R., Scaparra, M.P., 2007. Analysis of Facility Systems' Reliability When Subject to Attack or a Natural Disaster, in: Critical Infrastructure. Springer, pp. 221–241. doi:10.1007/978-3-540-68056-7{_}11.

Clarke, J., Obrien, E., 2016. A Multi-hazard Risk Assessment Methodology, Stress Test Framework and Decision Support Tool for Transport Infrastructure Networks. Transportation Research Procedia 14, 1355–1363. doi:10.1016/J.TRPRO.2016.05.208.

Cohen, R., Erez, K., ben Avraham, D., Havlin, S., 2000. Resilience of the Internet to Random Breakdowns. Physical Review Letters 85, 4626–4628. doi:10.1103/PhysRevLett.85.4626.

Connolly, L., 2018. Transport Network Risk Analyses, in: 5th Conference on Information Retrieval, Zaragoza. pp. 1–6.

Cooperation Work Programme, 2014. Deliverable 6.1 Stress Test Methodologies. INFRARISK .

Cox, A., Prager, F., Rose, A., 2011. Transportation security and the role of resilience: A foundation for operational metrics. Transport Policy 18, 307–317. doi:10.1016/J.TRANPOL.2010.09.004.

Crescenzi, P., Severini, L., Velaj, Y., 2016. Greedily Improving Our Own Closeness Centrality in a Network. ACM Transactions on Knowledge Discovery from Data 11, 1–32. doi:10.1145/2953882{\"{i}}.

Crucitti, P., Latora, V., Porta, S., 2006. Centrality Measures in Spatial Networks of Urban Streets. Physical Review E 73. arXiv:0504163v2.

Cuadra, L., Salcedo-Sanz, S., Del Ser, J., Jiménez-Fernández, S., Geem, Z., 2015. A Critical Review of Robustness in Power Grids Using Complex Networks Concepts. Energies 8, 9211–9265. doi:10.3390/en8099211.

Da F Costa, L., Rodrigues, F., Travieso, G., Ribeiro Villas Boas, P., 2007. Characterization of complex networks: A survey of measurements. doi:10.1080/00018730601170527.

Daganzo, C.F., Geroliminis, N., 2008. An analytical approximation for the macroscopic fundamental diagram of urban traffic. Transportation Research Part B: Methodological 42, 771–781. doi:10.1016/J.TRB.2008.06.008.

Dall'Asta, L., Barrat, A., Barthélemy, M., Vespignani, A., 2006. Vulnerability of weighted networks. Journal of Statistical Mechanics: Theory and Experiment doi:10.1088/1742-5468/2006/04/P04006.

Danczyk, A., Di, X., Liu, H.X., Levinson, D.M., 2017. Unexpected versus expected network disruption: Effects on travel behavior. Transport Policy 57, 68–78. doi:10.1016/J.TRANPOL.2017.02.002.

D'ariano, A., Pacciarelli, D., Pranzo, M., 2007. Discrete Optimization A branch and bound algorithm for scheduling trains in a railway network. European Journal of Operational Research doi:10.1016/j.ejor.2006.10.034.

De Domenico, M., Solé-Ribalta, A., Cozzo, E., Kivelä, M., Moreno, Y., Porter, M.A., Gómez, S., Arenas, A., 2013. Mathematical formulation of multi-layer networks. Physic Review X 3.

De Domenico, M., Sole-Ribalta, A., Gomez, S., Arenas, A., 2014. Navigability of interconnected networks under random failures. Proceedings of the National Academy of Sciences doi:10.1073/pnas.1318469111.

De Domenico, M., Solé-Ribalta, A., Omodei, E., Gómez, S., Arenas, A., 2015. Centrality in Interconnected Multilayer Networks. Nature communication .

Dekker, S., Hollnagel, E., Woods, D., Cook, R., 2008. Resilience Engineering: New directions for measuring and maintaining safety in complex systems. Technical Report. Lund University School of Aviation.

Delling, D., Pajor, T., Wagner, D., 2009. Accelerating Multi-modal Route Planning by Access-Nodes, in: European Symposium on Algorithms, pp. 587–598.

Derrible, S., 2012. Network Centrality of Metro Systems. PLoS ONE 7, e40575. doi:10.1371/journal.pone.0040575.

Diestel, R., 2000. Graph theory. Electronic edition ed.

Dijkstra, E.W., 1971. A short introduction to the art of programing.

Disney, A., 2020. Social network analysis 101: centrality measures explained.

Dolinayova, A., Zitricky, V., Cerna, L., 2020. Decision-making process in the case of insufficient rail capacity. Sustainability (Switzerland) 12. doi:10.3390/su12125023.

Doll, B., Lyon, M.A., 1998. Risk and resilience: Implications for the delivery of educational and mental health services in schools. School Psychology Review 27, 348–363.

Dong, W., Wang, Y., Yu, H., 2017. An identification model of urban critical links with macroscopic fundamental diagram theory. Frontiers of Computer Science 11, 27–37. doi:10.1007/s11704-016-6080-7.

Donovan, B., Work, D.B., 2017. Empirically quantifying city-scale transportation system resilience to extreme events. Transportation Research Part C: Emerging Technologies doi:10.1016/j.trc.2017.03.002.

Du, L., Peeta, S., 2014. A Stochastic Optimization Model to Reduce Expected Post-Disaster Response Time Through Pre-Disaster Investment Decisions. Networks and Spatial Economics 14, 271–295. doi:10.1007/s11067-013-9219-1.

Du, Q., Kishi, K., Aiura, N., Nakatsuji, T., 2014. Transportation network vulnerability. Transportation Research Record 2410, 96–104. doi:10.3141/2410-11.

Du, W.B., Zhou, X.L., Lordan, O., Wang, Z., Zhao, C., Zhu, Y.B., 2016. Analysis of the Chinese Airline Network as multi-layer networks. Transportation Research Part E: Logistics and Transportation Review doi:10.1016/j.tre.2016.03.009.

Du, Z.P., Nicholson, A., 1991. Degradable transportation systems: Sensitivity and reliability analysis. Transportation Research Part B: Methodological 31, 225–231.

Duan, Y., Lu, F., 2014. Robustness of city road networks at different granularities. Physica A: Statistical Mechanics and its Applications doi:10.1016/j.physa.2014.05.073.

Ducruet, C., Lugo, I., 2013. Structure and dynamics of transportation networks: Models, methods and applications, in: The SAGE Handbook of Transport Studies, pp. 347–364.

Dueñas-Osorio, L.A., 2005. Interdependent Response of Networked Systems to Natural Hazards and Intentional Disruptions. Ph.D. thesis. Georgia Institute of Technology.

Dunn, S., Wilkinson, S.M., 2016. Increasing the resilience of air traffic networks using a network graph theory approach. Transportation Research Part E 90, 39–50. doi:10.1016/j.tre.2015.09.011.

Durango-Cohen, P.L., Sarutipand, P., 2009. Maintenance optimization for transportation systems with demand responsiveness. Transportation Research Part C: Emerging Technologies 17, 337–348. doi:10.1016/J.TRC.2009.01.001.

Duret, A., Leclercq, L., El Faouzi, N.E., 2016. Data Assimilation Using a Mesoscopic Lighthill–Whitham–Richards Model and Loop Detector Data. Transportation Research Record: Journal of the Transportation Research Board doi:10.3141/2560-04.

Edrisi, A., Askari, M., 2019. Probabilistic budget allocation for improving efficiency of transportation networks in pre-and post-disaster phases. International Journal of Disaster Risk Reduction 39, 101113. doi:10.1016/J.IJDRR.2019.101113.

El-Rashidy, R.A., Grant-Muller, S., 2016. The evaluation of redundancy for road traffic networks. TRANSPORT doi:10.3846/16484142.2016.1255913.

Erath, A., Birdsall, J., Axhausen, K.W., Hajdin, R., 2009. Vulnerability Assessment Methodology for Swiss Road Network. Transportation Research Record: Journal of the Transportation Research 2137, 118–126. doi:10.3141/2137-13.

Estrada, E., 2010. Quantifying network heterogeneity. Physical review E., Statistical, non-linear, and soft matter physics doi:10.1103/PhysRevE.82.066102.

Eusgeld, I., Kröger, W., Sansavini, G., Schläpfer, M., Zio, E., 2009. The role of network theory and object-oriented modeling within a framework for the vulnerability analysis of critical infrastructures. Reliability Engineering & System Safety 94, 954–963. doi:10.1016/J.RESS.2008.10.011.

Farhan, B., Murray, A.T., 2008. Siting park-and-ride facilities using a multi-objective spatial optimization model. Computers & Operations Research 35, 445–456. doi:10.1016/J.COR.2006.03.009.

Fawzy Mahrous, R., 2012. Multimodal transportation systems: modelling challenges. Ph.D. thesis. Twente.

FEMA, . Hazus.

Filippidou, I., Kotidis, Y., 2016. IEEE International Conference on Big Data.

Fisher, M.L., 2004. The Lagrangian Relaxation method for solving integer programming problems. Management Science 50, 1861–1871. doi:10.1287/mnsc.1040.0263.

Freckleton, D., Freckleton, D., Heaslip, K., Louisell, W., Collura, J., 2012. Evaluation of Resiliency of Transportation Networks After Disasters. Transportation Research Record: Journal of the Transportation Research 2284, 109–116. doi:10.3141/2284-13.

Freeman, L.C., 1979. Centrality in social networks conceptual clarification. Social Networks .

Freiria, S., Ribeiro, B., Tavares, A.O., 2015. Understanding road network dynamics: Link-based topological patterns. Journal of Transport Geography 46, 55–66. doi:10.1016/J.JTRANGEO.2015.05.002.

Furno, A., El Faouzi, N.E., Sharma, R., Zimeo, E., 2018. Fast Computation of Betweenness Centrality to Locate Vulnerabilities in Very Large Road Networks. Transport Research Board .

Furno, A., El Faouzi, N.E., Sharma, R., Zimeo, E., 2021. Graph-based ahead monitoring of vulnerabilities in large dynamic transportation networks. Plos One .

Galbusera, L., Giannopoulos, G., Ward, D., 2014. Developing stress tests to improve the resilience of critical infrastructures: a feasibility analysis. Technical Report. European Commission. doi:10.2788/954065.

Gallotti, R., Barthelemy, M., 2015. The Multilayer Temporal Network of Public Transport in Great Britain. Scientific Data 2.

Gao, J., Albert-László Barabási, ., 2016. Universal resilience patterns in complex networks. Nature 530. doi:10.1038/nature16948.

Gao, S., Wang, Y., Gao, Y., Liu, Y., 2013. Understanding urban traffic-flow characteristics: A rethinking of betweenness centrality. Environment and Planning B: Planning and Design doi:10.1068/b38141.

Gauthier, P., Furno, A., El Faouzi, N.E., 2018. Road network resilience: how to identify critical linkssubject to day-to-day disruptions? Transport Research Record .

Gecchele, G., Ceccato, R., Gastaldi, M., 2019. Road Network Vulnerability Analysis: Case Study Considering Travel Demand and Accessibility Changes. Journal of Transport Engineering Part A doi:10.1061/JTEPBS.0000252.

GeoSure, . GeoSure Web Page.

Geroliminis, N., Daganzo, C.F., 2007. Existence of urban-scale macroscopic fundamental diagrams: Some experimental findings. ransportation Research Part B: Methodological 42, 759–770.

Ghanem, M., emence Magnien, C., Tarissan, F., 2018. Centrality metrics in dynamic networks: a comparison study, in: IEEE Transactions on Network Science and Engineering, pp. 1–12.

Gibbons, A.A.M., 1985. Algorithmic graph theory. Cambridge University Press.

Gigerenzer, G., Selten, R., 2001. Bounded rationality : the adaptive toolbox. MIT Press.

Goldberg, M.A., 1975. On the Inefficiency of Being Efficient. Environment and Planning A: Economy and Space 7, 921–939. doi:10.1068/a070921.

Goldschlager, N., Selzer, A., Cohn, K., 1976. Treadmill stress tests as indicators of presence and severity of coronary artery disease. Annals of internal medicine 85, 277–86. doi:10.7326/0003-4819-85-3-277.

Goverde, R.M.P., Hansen, I.A., 2013. Performance Indicators for Railway Timetables, in: IEEE International Conference on Intelligent Rail Transportation, pp. 301–306.

Grossi, P., Kunreuther, H., 2005. Catastrophe modeling : A new approach to managing risk. Kluwer Academic Publishers, Boston. doi:10.1007/0-387-23129-3{_}1.

Grossi, P., Kunreuther, H., Windeler, D., 2019. An Introduction to Catastrophe Models and Insurance, in: Springer (Ed.), Catastrophe modeling : A new approach to managing risk, pp. 23–42.

Gu, Y., Fu, X., Liu, Z., Xu, X., Chen, A., 2020. Performance of transportation network under perturbations: Reliability, vulnerability, and resilience. Transportation Research Part E: Logistics and Transportation Review 133. doi:10.1016/j.tre.2019.11.003.

Guo Jingni, Du, Q., He, Z., 2021. A method to improve the resilience of multimodal transport network: Location selection strategy of emergency rescue facilities. Computers & Industrial Engineering doi:https://doi.org/10.1016/j.cie.2021.107678.

Guze, S., 2019. Graph theory approach to the vulnerability of transportation networks. Algorithms 12. doi:10.3390/A12120270.

Hagberg, A.A., Schult, D.A., Swart, P.J., 2008. Exploring Network Structure, Dynamics, and Function using NetworkX, in: Proceedings of the 7th Python in Science Conference (SciPy 2008), pp. 11–15.

Haimes, Y.Y., 2009. On the Definition of Resilience in Systems. Risk Analysis 29, 498–501. doi:10.1111/j.1539-6924.2009.01216.x.

Haldane, A.G., 2009. Why banks failed the stress test ?, in: Bank for International Settlements, Bis, pp. 1–14.

Hansen, W.G., 1959. How Accessibility Shapes Land Use. Journal of the American Institute of Planners 25, 73–76. doi:10.1080/01944365908978307.

Harary, F., Gupta, G., 1997. Dynamic Graph Models. Mathematical and Computer Modelling 25, 79–87.

Hashimoto, T., Loucks, D.P., Stedinger, J.R., 1982. Reliability, resiliency and vulnerability criteria for water ressource system performance evaluation. Water ressources research 18.

Hassan, S.M., Moghaddam, M., Bhouri, N., Scemama, G., 2019. Assessment of System Resilience: Robustness, Reliability and Redundancy of Public Transport Operation .

He, Z., Navneet, K., van Dam, W., Van Mieghem, P., 2021. Robustness assessment of multimodal freight transport networks. Reliability Engineering & System Safety 207, 107315. doi:10.1016/J.RESS.2020.107315.

Heaslip, K., Louisell, W., Collura, J., 2009. A Methodology to Evaluate Transportation Resiliency for Regional Networks, in: 88th Annual Meeting Transport Research Board, pp. 586–592.

Henry, D., Emmanuel Ramirez-Marquez, J., 2012. Generic metrics and quantitative approaches for system resilience as a function of time. Reliability Engineering & System Safety 99, 114–122. doi:10.1016/J.RESS.2011.09.002.

Henry, E., Bonnetain, L., Furno, A., El Faouzi, N.E., Zimeo, E., 2019a. Spatio-temporal Correlations of Betweenness Centrality and Traffic Metrics, in: 6th International Conference on Models and Technologies for Intelligent Transportation Systems, Cracow University of Technology, Kraków, Poland. pp. 1–10.

Henry, E., Furno, A., El Faouzi, N.E., 2019b. A Graph-based Approach with Simulated Traffic Dynamics for the Analysis of Transportation Resilience in Smart Cities, in: Transport Research Board 98th Annual Meeting, Washington DC.

Henry, E., Furno, A., El Faouzi, N.E., 2021a. An Approach to Quantify the Impact of Disruptions on Traffic Conditions Using Dynamic Weighted Resilience Metrics of Transport Networks. Transportation Research Record: Journal of the Transportation Research Board 2675, 61–78. doi:10.1177/ToBeAssigned.

Henry, E., Furno, A., El Faouzi, N.E., 2021b. REINFORCE: Rapid augmentation of large-scale multi-modal transport networks for resilience enhancement-modal transport modelling. Applied Network Science , 1–25.

Henry, E., Furno, A., El Faouzi, N.E., Rey, D., 2021c. Optimal Park-and-ride Facility Location and Fleet Sizing to Enhance the Resilience of Transport Networks, in: 8th International Conference on Transport Network Reliability, pp. 1–9.

Henry, E., Furno, A., El Faouzi, N.E., Rey, D., 2022. Locating park-and-ride facilities for resilient on-demand urban mobility. Transportation report Part E .

Henry, E., Petit, M., Furno, A., Faouzi, N.E.E., 2020. Quick Sub-optimal Augmentation of Large Scale Multi-Modal Transport Networks, in: 9th International Conference on Complex Networks and their Applications, pp. 218–230.

Hitge, G., Vanderschuren, M., 2015. Comparison of travel time between private car and public transport in Cape Town. Journal of the South African Institution of Civil Engineering 57, 35–43. doi:10.17159/2309-8775/2015/v57n3a5.

Holling, C.S., 1973. Resilience of ecological systems. Source: Annual Review of Ecology and Systematics 4, 1–23.

Hollnagel, E., 2008. From protection to resilience: Changing views on how to achieve safety, in: 8th International Symposium of the Australian Aviation Psychology Association, Sydney. pp. 1–7.

Holme, P., Kim, B.J., Yoon, C.N., Han, S.K., 2002. Attack vulnerability of complex networks. Physic Review doi:10.1103/PhysRevE.65.056109.

Hong, J., Tamakloe, R., Lee, S., Park, D., 2019. Exploring the topological characteristics of complex public transportation networks: Focus on variations in both single and integrated systems in the Seoul Metropolitan Area. Sustainability (Switzerland) 11. doi:10.3390/su11195404.

Hongwei, M., Xizhao, Z., 2015. An Evaluation Method for the Connectivity Reliability Based on the Transportation Network of Critical Links. International Journal of Transportation 3, 45–52. doi:10.14257/ijt.2015.3.2.04.

Hoogendoorn, S., Knoop, V., 2012. The Transport System and Transport Policy: Traffic flow theory and modelling.

Hoogendoorn, S.P., Bovy, P.H.L., 2001. State-of-the-art of vehicular traYc cow modelling attention for the subject of macroscopic cow modelling, in: Proceedings of the Institution of Mechanical Engineers, pp. 283–303.

Hoogendoorn, S.P., Knoop, V., 2015. Fundamental diagrams, in: Traffic Flow Theory and Simulation.

Hoogendoorn, S.P., Knoop, V.L., Van Lint, H., Vu, H.L., 2015. Applications of the Generalized Macroscopic Fundamental Diagram. Traffic and Granular Flow doi:10.1007/978-3-319-10629-8{_}65.

Hooper, E., Chapman, L., Quinn, A., 2014. The impact of precipitation on speed–flow relationships along a UK motorway corridor. Theoretical and Applied Climatology 117, 303–316. doi:10.1007/s00704-013-0999-5.

Hu, X., Sun, L., 2012. Knowledge-based modeling for disruption management in urban distribution. Expert Systems with Applications 39, 906–916. doi:10.1016/J.ESWA.2011.07.088.

Hu, Y., Zhu, D., 2009. Empirical analysis of the worldwide maritime transportation network. Physica A 388, 2061–2071. doi:10.1016/j.physa.2008.12.016.

Huang, B., Wu, Q., Zhan, F.B., 2007. A shortest path algorithm with novel heuristics for dynamic transportation networks. International Journal of Geographical Information Science 21, 625–644. doi:10.1080/13658810601079759.

Huang, K., Correia, G.H.d.A., An, K., 2018. Solving the station-based one-way carsharing network planning problem with relocations and non-linear demand. Transportation Research Part C: Emerging Technologies 90, 1–17. doi:10.1016/j.trc.2018.02.020.

Husdal, J., 2004. Reliability and vulnerability versus cost and benefits, in: 2nd International Symposium on Transportation Network Reliability, pp. 1–12.

IAA, 2013. Stress testing and scenario analysis. Technical Report. International Actuarial Association.

Iida, Y., Kurauchi, F., Shimada, H., 2000. Traffic management system against major earthquakes, in: International Association of Traffic and Safety Sciences Research, pp. 6–17. doi:10.1016/S0386-1112(14)60024-8.

Ilbeigi, M., 2019. Statistical process control for analyzing resilience of transportation networks. International Journal of Disaster Risk Reduction doi:10.1016/j.ijdrr.2018.10.002.

Immers, B., Bleukx, A., Stada, J., Tampère, C., Yperman, I., 2004. Robustness And Resilience Of Road Network Structures, in: 9th International Scientific Conference MOBILITA, Bratislava. pp. 1477–1494.

INFRARISK, . Novel indicators for identifying critical INFRAstructure at RISK from Natural Hazards .

INRIX, 2020. Global Traffic Scorecard.

Insee, 2016. Zone Iris definition.

ITF, 2016. Capacity to Grow: Transport Infrastructure Needs for Future Trade Growth. Technical Report. International Transport Forum.

Jacob, R., Harikrishnan, K.P., Misra, R., Ambika, G., 2017. Measure for degree heterogeneity in complex networks and its application to recurrence network analysis. Royal Society open science doi:10.1098/rsos.160757.

Jafino, B.A., Kwakkel, J., Verbraeck, A., 2020. Transport network criticality metrics: a comparative analysis and a guideline for selection. Transport Reviews 40, 241–264. doi:10.1080/01441647.2019.1703843.

Janić, M., 2015. Reprint of "Modelling the resilience, friability and costs of an air transport network affected by a large-scale disruptive event". Transportation Research Part A: Policy and Practice doi:10.1016/j.tra.2015.07.012.

Janić, M., 2021. An approach to analysing and modelling the reliability of transport services. Transportation Planning and Technology 44, 647–678. doi:10.1080/03081060.2021.1943133.

Jaroszweski, D., Hooper, E., Chapman, L., 2014. The impact of climate change on urban transport resilience in a changing world. Progress in Physical Geography: Earth and Environment 38, 448–463. doi:10.1177/0309133314538741.

Jayasinghe, A., Sano, K., Rattanaporn, K., 2017. Application for developing countries: Estimating trip attraction in urban zones based on centrality. Journal of Traffic and Transportation Engineering (English Edition) 4, 464–476. doi:10.1016/j.jtte.2017.05.011.

Jayasinghe, A., TalatMunshi, 2014. 'Centrality Measures' as a tool to identify the Transit Demand at Public Transit Stops; A Case of Ahmedabad City, India. International Journal of Advanced Research 2, 1063–1074.

Jen, E., 2003. Stable or robust? What's the difference? Complexity 8, 12–18. doi:10.1002/cplx.10077.

Jenelius, E., 2010. Redundancy importance: Links as rerouting alternatives during road network disruptions. Procedia Engineering 3, 129–137. doi:10.1016/J.PROENG.2010.07.013.

Jenelius, E., Cats, O., 2015. The value of new public transport links for network robustness and redundancy. Transportmetrica A: Transport Science 11, 819–835. doi:10.1080/23249935.2015.1087232.

Jenelius, E., Mattsson, L.G., 2012. Road network vulnerability analysis of area-covering disruptions: A grid-based approach with case study. Transportation Research Part A: Policy and Practice 46, 746–760. doi:10.1016/j.tra.2012.02.003.

Jenelius, E., Mattsson, L.G., 2015. Road network vulnerability analysis: Conceptualization, implementation and application. Computers, Environment and Urban Systems 49, 136–147. doi:10.1016/j.compenvurbsys.2014.02.003.

Jenelius, E., Petersen, T., Mattsson, L.G., 2006. Importance and exposure in road network vulnerability analysis. Transportation Research Part A , 537–560.

Jian, S., Rey, D., Dixit, V., 2019. An Integrated Supply-Demand Approach to Solving Optimal Relocations in Station-Based Carsharing Systems. Networks and Spatial Economics 19, 611–632. doi:10.1007/s11067-018-9401-6.

Jiao, J., Zhang, F., Liu, J., 2020. A spatiotemporal analysis of the robustness of high-speed rail network in China. Transportation Research Part D: Transport and Environment 89, 102584. doi:10.1016/J.TRD.2020.102584.

Jin, J.G., Tang, L.C., Sun, L., Lee, D.H., 2014. Enhancing metro network resilience via localized integration with bus services. Transportation Research Part E: Logistics and Transportation Review 63, 17–30. doi:10.1016/J.TRE.2014.01.002.

Jones, B.D., 1999. Bounded Rationality. Annual Review Political Science 2, 297–321.

Jones, P., Anciaes, P., 2016. Congestion Reduction in Europe: Advancing Transport Efficiency Urban. Technical Report. CREATE.

Justin Boche, 2019. Pietonnisation de la presqu'ile de Lyon.

Kazerani, A., Winter, S., . Modified Betweenness Centrality for Predicting Traffic Flow. Technical Report.

Kepaptsoglou, K.L., Konstantinidou, M.A., Karlaftis, M.G., Stathopoulos, A., 2014. Planning Postdisaster Operations in a Highway Network Network Design Model with Interdependencies. Transportation Research Record: Journal of the Transportation Research 2459, 1–10. doi:10.3141/2459-01.

Kessels, F., Van Lint, H., Vuik, K., Hoogendoorn, S., 2015. Genealogy of traffic flow models. EURO Journal on Transportation and Logistics 4, 445–473. doi:10.1007/s13676-014-0045-5.

Kim, S., Yeo, H., 2016. A Flow-based Vulnerability Measure for the Resilience of Urban Road Network. Procedia - Social and Behavioral Sciences doi:10.1016/j.sbspro.2016.04.006.

Kini, V., Dayoub, E.J., Hess, P.L., Marzec, L.N., Masoudi, F.A., Ho, P.M., Groeneveld, P.W., 2018. Clinical Outcomes After Cardiac Stress Testing Among US Patients Younger Than 65 Years. Journal of the American Heart Association 7. doi:10.1161/JAHA.117.007854.

Kinsley, A.C., Rossi, G., Silk, M.J., VanderWaal, K., 2020. Multilayer and Multiplex Networks: An Introduction to Their Use in Veterinary Epidemiology. Frontiers in Veterinary Science 7, 596. doi:10.3389/fvets.2020.00596.

Kivelä, M., Barthelemy, M., Gleeson, J.P., Moreno, Y., Porter, M.A., 2014. Multilayer Networks. Journal of Complex Networks 2, 203–271. arXiv:1309.7233v4.

Knoop, V., Snelder, M., Van Zuylen, H., Hoogendoorn, S., 2012. Link-level Vulnerability Indicators for Real-World Networks. Transportation Research Part A Policy and Practice .

Kostakos, V., 2009. Temporal graphs. Physica A: Statistical Mechanics and its Applications 388, 1007–1023. doi:10.1016/J.PHYSA.2008.11.021.

Kramarz, M., Przybylska, E., 2019. Identification of sources of knowledge about disruptions in intermodal transport. Organization and Management 4. doi:10.29119/1899-6116.2019.48.3.

Krug, J., Burianne, A., Bécarie, C., Leclercq, L., 2021. Refining trip starting and ending locations when estimating travel-demand at large urban scale. Journal of Transport Geography 93, 103041. doi:10.1016/J.JTRANGEO.2021.103041.

Kuang, A., Tang, Z., Shan, L., 2013. Road Network Capacity Reliability Considering Travel Time Reliability. Procedia - Social and Behavioral Sciences 96, 1818–1827. doi:10.1016/J.SBSPRO.2013.08.207.

Kurant, M., Thiran, P., 2006. Extraction and analysis of traffic and topologies of transportation networks. Physical Review E - Statistical, Nonlinear, and Soft Matter Physics 74. doi:10.1103/PhysRevE.74.036114.

Kyte, M., Khatib, Z., Shannon, P., Kitchener, F., 2001. Effect of Environmental Factors on Free-Flow Speed. Transport Research Record .

Lam, J.C., Adey, B.T., Heitzler, M., Hackl, J., Gehl, P., van Erp, N., D'Ayala, D., van Gelder, P., Hurni, L., 2018. Stress tests for a road network using fragility functions and functional capacity loss functions. Reliability Engineering & System Safety 173, 78–93. doi:10.1016/J.RESS.2018.01.015.

Latora, V., Marchiori, M., 2001. Efficient Behavior of Small-World Networks. Physic Review 87. doi:10.1103/PhysRevLett.87.198701.

Laval, J.A., Leclercq, L., 2013. The Hamilton-Jacobi partial differential equation and the three representations of traffic flow. Transportation Research Part B: Methodological doi:10.1016/j.trb.2013.02.008.

Leclercq, L., Geroliminis, N., 2013. Estimating MFDs in Simple Networks with Route Choice. Procedia - Social and Behavioral Sciences 80, 99–118. doi:10.1016/j.sbspro.2013.05.008.

Lee, Y.J., Vuchic, V.R., 2005. Transit Network Design with Variable Demand. Journal of transportation engineering doi:10.1061/(ASCE)0733-947X(2005)131:1(1).

Lefauconnier, A., 2005. Le temps de recherche d'une place de stationnement. Technical Report. Ademe.

Leu, G., Curtis, N.J., Abbass, H., Curtis, N., 2010. Resilience of ground transportation networks: A case study on Melbourne, in: 33rd Australasian Transport Research Forum Conference, Canberra. pp. 1–14.

Leung, I.X.Y., Chan, S.Y., Hui, P., Lio', P., 2011. Intra-City Urban Network and Traffic Flow Analysis from GPS Mobility Trace .

Lhomme, S., 2012. Les modèles de graphes théoriques. Technical Report. École des Ingénieurs de la Ville de Paris.

Lhomme, S., Serre, D., Diab, Y., Laganier, R., 2013. Analyzing resilience of urban networks: A preliminary step towards more flood resilient cities. Natural Hazards and Earth System Science doi:10.5194/nhess-13-221-2013.

Li, C., Fang, Q., Ding, L., Cho, Y.K., Chen, K., 2020. Time-dependent resilience analysis of a road network in an extreme environment. Transportation Research Part D: Transport and Environment 85, 102395. doi:10.1016/J.TRD.2020.102395.

Li, M., Han, J., 2017. Complex Network Theory in Urban Traffic Network, in: Proceedings of the 2017 2nd International Conference on Materials Science, Machinery and Energy Engineering (MSMEE 2017), pp. 910–913. doi:10.2991/msmee-17.2017.175.

Li, M., Wang, H., Wang, H., 2019. Resilience Assessment and Optimization for Urban Rail Transit Networks: A Case Study of Beijing Subway Network. IEEE Access 7. doi:10.1109/ACCESS.2019.2919105.

Lighthill, M.J., Whitham, G.B., 1955. On kinematic waves II. A theory of traffic flow on long crowded roads, in: Proceedings of the Royal Society A, London. pp. 317–345.

Litman, T., 2006. Lessons from Katrina and Rita: What major disasters can teach transportation planners. Journal of Transportation Engineering 132, 11–18. doi:10.1061/(ASCE)0733-947X(2006)132:1(11).

Litman, T., 2021. Urban Mobility Report. Technical Report. Victoria Transport Policy.

Litman, T.A., 2008. Evaluating Accessibility for Transport Planning Evaluating Accessibility for Transportation Planning. Technical Report. Victoria Transport Policy.

Liu, C., Fan, Y., Ordóñez, F., 2009. A two-stage stochastic programming model for transportation network protection. Computers & Operations Research 36, 1582–1590. doi:10.1016/J.COR.2008.03.001.

Liu, H., Hu, X.B., Ke Zhang, S.Y., Di Paolo, E., 2011. Application of Complex Network Theory and Genetic Algorithm in Airline Route Networks. Transportation Research Record doi:10.3141/2214-07.

Liu, L., 2011. Data Model and Algorithms for Multimodal Route Planning with Transportation Networks. Ph.D. thesis. Munich.

Liu, Y., Tan, Y., 2013. Complexity Modeling and Stability Analysis of Urban Subway Network: Wuhan City Case Study. Procedia - Social and Behavioral Sciences 96, 1611–1621. doi:10.1016/J.SBSPRO.2013.08.183.

Lomax, T., Schrank, D., Turner, S., Margiotta, R., 2003. Selecting travel reliability measures. Technical Report.

Lu, Q.C., Lin, S., 2019. Vulnerability Analysis of Urban Rail Transit Network within Multi-Modal Public Transport Networks. Sustainability 11, 2109. doi:10.3390/su11072109.

Lu, X., Wrathall, D.J., Sundsøy, P.R., Nadiruzzaman, M., Wetter, E., Iqbal, A., Qureshi, T., Tatem, A.J., Canright, G.S., Engø-Monsen, K., Bengtsson, L., 2016. Detecting climate adaptation with mobile network data in Bangladesh: anomalies in communication, mobility and consumption patterns during cyclone Mahasen. Climatic Change doi:10.1007/s10584-016-1753-7.

Luin, B., Petelin, S., 2020. Coupling models of road tunnel traffic, ventilation and evacuation. Transport 35, 336–346. doi:10.3846/transport.2020.12079.

Lyons, G., 2004. Transport and society. Transport Reviews 24, 485–509. doi:10.1080/0144164042000206079.

Machado, C.A., Hue, N.P.M.d.S., Berssaneti, F.T., Quintanilha, J.A., 2018. An overview of shared mobility. doi:10.3390/su10124342.

Mahdavi, H., Bhouri, N., Scemama, G., 2020. Dynamic Resilience of Public Transport Network: A Case Study for Fleet-Failure in Bus Transport Operation of New Delhi. Transportation Research Procedia 47, 672–679.

Malandri, C., Mantecchini, L., Paganelli, F., Postorino, M.N., 2021. Public Transport Network Vulnerability and Delay Distribution among Travelers. Sustainability 13, 8737. doi:10.3390/su13168737.

Mandloi, D., Thill, J.C., 2010. Object-Oriented Data Modeling of an Indoor/Outdoor Urban Transportation Network and Route Planning Analysis, in: Geospatial Analysis and Modelling of Urban Structure and Dynamics, pp. 197–220. doi:10.1007/978-90-481-8572-6{_}11.

Mannino, C., Mascis, A., 2009. Optimal Real-Time Traffic Control in Metro Stations. Operations Research 57, 1026–1039. doi:10.1287/opre.1080.0642.

Mariotte, G., Leclercq, L., Laval, J.A., 2017. Macroscopic urban dynamics: Analytical and numerical comparisons of existing models. Transportation Research Part B: Methodological 101, 245–267. doi:10.1016/J.TRB.2017.04.002.

Marra, A.D.., Corman, F., Marra, A.D., 2019. From delay to disruption: The impact of service degradation on public transport network ETH Library From delay to disruption: the impact of service degradation on public transport network, in: 8th Symposium of the European Association for Research in Transportation (hEART), Budapest. pp. 886–897. doi:10.3929/ethz-b-000368811.

Martín, B., Ortega, E., Cuevas-Wizner, R., Ledda, A., De Montis, A., 2021. Assessing road network resilience: An accessibility comparative analysis. Transportation Research Part D: Transport and Environment 95, 102851. doi:10.1016/J.TRD.2021.102851.

Martinez-Pastor, B., Nogal, M., O'Connor, A., Caulfield, B., 2016. A sensitivity analysis of a dynamic restricted equilibrium model to evaluate the traffic network resilience, in: Transportation Research Board, pp. 1–10.

Matisziw, T.C., Murray, A.T., 2009. Modeling s–t path availability to support disaster vulnerability assessment of network infrastructure. Computers & Operations Research 36, 16–26. doi:10.1016/J.COR.2007.09.004.

Matisziw, T.C., Murray, A.T., Grubesic, T.H., 2010. Strategic Network Restoration. Network Spatial Economic doi:10.1007/s11067-009-9123-x.

Mattsson, L.G., Jenelius, E., 2015. Vulnerability and resilience of transport systems - A discussion of recent research. Transportation Research Part A: Policy and Practice doi:10.1016/j.tra.2015.06.002.

Melnikov, V.R., Krzhizhanovskaya, V.V., Boukhanovsky, A.V., Sloot, P.M., 2015. Data-driven Modeling of Transportation Systems and Traffic Data Analysis during a Major Power Outage in the Netherlands, in: Procedia Computer Science, Elsevier B.V.. pp. 336–345. doi:10.1016/j.procs.2015.11.039.

Mercier, A., Crozet, Y., Ovtracht, N., Buettner, B., Wulfhorst, G., 2013. Stress tests on urban mobility: lessons for public policies. 13th WCTR .

Merschman, E., Doustmohammadi, M., Salman, A.M., Anderson, M., 2020. Postdisaster Decision Framework for Bridge Repair Prioritization to Improve Road Network Resilience. Transportation Research Record 2674, 81–92. doi:10.1177/0361198120908870.

Miao, Y., Ni, A., 2019. Vulnerability analysis of intercity multimode transportation networks; A case study of the Yangtze River Delta. Sustainability (Switzerland) 11. doi:10.3390/su11082237.

Michaelis, L., Menten, M.L., 2009. Fundamentals of Enzyme Kinetics : Michaelis-Menten and Deviations.

Miller, B.A., Arcolano, N., Bliss, N.T., 2013. Efficient anomaly detection in dynamic, attributed graphs: Emerging phenomena and big data, in: IEEE ISI 2013 - 2013 IEEE International Conference on Intelligence and Security Informatics: Big Data, Emergent Threats, and Decision-Making in Security Informatics, pp. 179–184. doi:10.1109/ISI.2013.6578815.

Mine, H., Kawai, H., 1982. Mathematics for reliability analysis.

Mohring, H., 1972. Optimization and Scale Economies in Urban Bus Transportation. American Economic Review .

Morelli, A.B., Cunha, A.L., 2020. Measuring urban road network resilience to extreme events: an application for urban floods. Physics and Society .

Mouronte-López, M.L., 2021. Analysing the Vulnerability of Public Transport Networks. Journal of Advanced Transportation 2021, 1–22. doi:10.1155/2021/5513311.

Mudigonda, S., Ozbay, K., Bartin, B., 2019. Evaluating the resilience and recovery of public transit system using big data: Case study from New Jersey. Journal of Transportation Safety & Security 11, 491–519. doi:10.1080/19439962.2018.1436105.

Murray, A., Matisziw, T., Systems, T.G.J.o.G., 2007, u., 2007. Critical network infrastructure analysis: interdiction and system flow. Journal of Geographical Systems .

Murray, A.T., Grubesic, T.H., 2007. Overview of reliability and vulnerability in critical infrastructure, in: Critical Infrastructure. Springer Berlin Heidelberg, Berlin, Heidelberg, pp. 1–8. doi:10.1007/978-3-540-68056-7{_}1.

Murray-Tuite, P., 2006. A comparison of transportation network resilience under simulated System Optimum and User Equilibrium conditions. Proceedings of the 2006 Winter Simulation Conference doi:10.1145/1218112.1218367.

Myung, Y.S., Kim, H.J., 2004. A cutting plane algorithm for computing k-edge survivability of a network. European Journal of Operational Research doi:10.1016/S0377-2217(03)00135-8.

Nagurney, A., Qiang, Q., 2008. A network efficiency measure with application to critical infrastructure networks. Journal of Global Optimization 40, 261–275. doi:10.1007/s10898-007-9198-1.

Nakanishi, H., Matsuo, K., Black, J., 2013. Transportation planning methodologies for post-disaster recovery in regional communities: the East Japan Earthquake and tsunami 2011. Journal of Transport Geography 31, 181–191. doi:10.1016/J.JTRANGEO.2013.07.005.

Nawod Kalpana, H., Jayasinghe, A., Abenayake, C., Wijayawardana, N., Kalpana, L., Jayasinghe, A.B., Abenayake, C.C., P Wijayawardana, P.N., 2021. Network Centrality Assessment: Assessing the Transport Network Resilience to Urban Flooding Spatial Analysis. Journal of South Asian Logistics and Transport 1, 99–114. doi:10.4038/jsalt.v1i1.29.

NBC, 2018. Genoa bridge collapse causes traffic jams.

Newell, G.F., 2002. A simplified car-following theory: a lower order model. Transportation Research Part B: Methodological 36, 195–205.

Newman, M.E.J., 2001. Scientific collaboration networks. II. Shortest paths, weighted networks, and centrality. Physical Review E 64, 016132. doi:10.1103/PhysRevE.64.016132.

Newman, M.E.J., 2002. Assortative mixing in networks. Physic Review Letters 89.

Newman, M.E.J., 2004. Analysis of weighted networks. Physical review E doi:10.1103/PhysRevE.70.056131.

Nicholson, A., 2003. Transport network reliability measurement ans analysis. Transportes 11, 49–62.

Nicosia, V., Tang, J., Mascolo, C., Musolesi, M., Russo, G., Latora, V., 2013. Temporal Networks. doi:10.1007/978-3-642-36461-7.

Nielsen, L.K., Kroon, L., Maróti, G., 2012. A rolling horizon approach for disruption management of railway rolling stock. European Journal of Operational Research doi:10.1016/j.ejor.2012.01.037.

Oliveira, E.L.d., Portugal, L.d.S., Junior, W.P., 2014. Determining Critical Links in a Road Network: Vulnerability and Congestion Indicators. Procedia - Social and Behavioral Sciences 162, 158–167. doi:10.1016/J.SBSPRO.2014.12.196.

Opsahl, T., Agneessens, F., Skvoretz, J., 2010. Node Centrality in Weighted Networks: Generalizing Degree and Shortest Paths. Social Networks .

Opsahl, T., Colizza, V., Panzarasa, P., Ramasco, J.J., 2008. Prominence and Control: The Weighted Rich-Club Effect. To PRL 101, 168702. doi:10.1103/PhysRevLett.101.168702.

Özdamar, L., Ekinci, E., Küçükyazici, B., 2004. Emergency Logistics Planning in Natural Disasters. Annals of Operations Research 129, 217–245. doi:10.1023/B:ANOR.0000030690.27939.39.

Pagani, A., Mosquera, G., Alturki, A., Johnson, S., Jarvis, S., Wilson, A., Guo, W., Varga, L., 2019. Resilience or robustness: identifying topological vulnerabilities in rail networks. Royal Society open science 6, 181301. doi:10.1098/rsos.181301.

Pajor, T., 2009. Multi-Modal Route Planning. Ph.D. thesis. Karlsruhe.

Pan, B., Demiryurek, U., Shahabi, C., 2012. Utilizing Real-World Transportation Data for Accurate Traffic Prediction, in: IEE 12th International Conference on Data Mining, pp. 595–604.

Peeta, S., Sibel Salman, F., Gunnec, D., Viswanath, K., 2010. Pre-disaster investment decisions for strengthening a highway network. Computers & Operations Research 37, 1708–1719. doi:10.1016/J.COR.2009.12.006.

Peng, H., Wang, H., Du, B., Bhuiyan, M.Z.A., Ma, H., Liu, J., Wang, L., Yang, Z., Du, L., Wang, S., Yu, P.S., 2020. Spatial temporal incidence dynamic graph neural networks for traffic flow forecasting. Information Sciences 521, 277–290. doi:10.1016/J.INS.2020.01.043.

Perra, N., Fortunato, S., 2008. Spectral centrality measures in complex networks. Physical Review E - Statistical, Nonlinear, and Soft Matter Physics 78. doi:10.1103/PhysRevE.78.036107.

Pitilakis, K., Argyroudis, S., Kakderi, K., Selva, J., 2016. Systemic Vulnerability and Risk Assessment of Transportation Systems Under Natural Hazards Towards More Resilient and Robust Infrastructures. Transportation Research Procedia 14, 1335–1344.

Pokharel, R., Ieda, H., 2016. Road Network Evaluation from a Reliability Perspective: An Accessibility and Network Closure Vulnerability Approach. Asian Transport Studies 4, 37–56.

Porta, S., Crucitti, P., Latora, V., 2006. The network analysis of urban streets : a primal approach. Environment and Planning B: Planning and Design 33, 705–725. doi:10.1068/b32045.

Porta, S., Latora, V., Wang, F., Rueda, S., Strano, E., Scellato, S., Cardillo, A., Belli, E., Càrdenas, F., Cormenzana, B., Latora, L., Strano are, E., 2012. Street Centrality and the Location of Economic Activities in Barcelona. Urban studies 49, 1471–1488. doi:10.1177/0042098011422570.

Porta Sergio, S.E., Latora Vito, C.A., Wang Fahui, Scellato Salvatore, 2009. Street centrality and densities of retail and services in Bologna, Italy. Environment and Planning B: Planning and Design 36, 450–465. doi:10.1068/b34098.

Postance, B., Hillier, J., Dijkstra, T., Dixon, N., 2017. Extending natural hazard impacts: an assessment of landslide disruptions on a national road transportation network. Environmental Research Letters .

Pregnolato, M., Ford, A., Glenis, V., Wilkinson, S., Dawson, R., 2017. Impact of Climate Change on Disruption to Urban Transport Networks from Pluvial Flooding. Journal of Infrastructures Systems 23. doi:10.1061/(ASCE)IS.1943-555X.0000372.

Pregnolato, M., Ford, A., Robson, C., Glenis, V., Barr, S., Dawson, R., 2016. Assessing urban strategies for reducing the impacts of extreme weather on infrastructure networks. Royal Society Open Science doi:10.1098/rsos.160023.

Puzis, R., Altshuler, Y., Elovici, Y., Bekhor, S., Shiftan, Y., Pentland, A., 2013. Augmented betweenness centrality for environmentally aware traffic monitoring in transportation networks. Journal of Intelligent Transportation Systems: Technology, Planning, and Operations doi:10.1080/15472450.2012.716663.

Qian, X., 2009. Application of Macroscopic Fundamental Diagrams to Dynamic Traffic Management. Ph.D. thesis. TU delft.

Qiang, Q., Nagurney, A., 2011. A Bi-Criteria Indicator to Assess Supply Chain Network Performance for Critical Needs Under Capacity and Demand Disruptions. Transportation Research A 46, 801–812.

Raimbault, J., 2015. Models coupling urban growth and transportation network growth: An algorithmic systematic review approach, in: European Colloquium on Theoretical and Quantitative Geography 2015, pp. 45–46.

RAIN Project, . RAIN .

Rana, M.M.P., 2011. Urbanization and sustainability: challenges and strategies for sustainable urban development in Bangladesh. Environment, Development and Sustainability 13, 237–256. doi:10.1007/s10668-010-9258-4.

Ren, Y., Ercsey-Ravasz, M., Wang, P., González, M.C., Toroczkai, Z., 2014. Predicting commuter flows in spatial networks using a radiation model based on temporal ranges. Nature Communications doi:10.1038/ncomms6347.

RESOLUTE consortium, . RESilience management guidelines and Operationalization appLied to Urban Transport Environment.

Rey, D., Bar-Gera, H., 2020. Long-term scheduling for road network disaster recovery. International Journal of Disaster Risk Reduction 42, 101353. doi:10.1016/J.IJDRR.2019.101353.

Richards, P.I., 1956. Shock Waves on the Highway. Operations Research 4, 42–51. doi:10.1287/opre.4.1.42.

Rocha, L.E., 2017. Dynamics of air transport networks: A review from a complex systems perspective. Chinese Journal of Aeronautics 30, 469–478. doi:10.1016/J.CJA.2016.12.029.

Rodríguez-Núñez, E., García-Palomares, J.C., 2014. Measuring the vulnerability of public transport networks. Journal of Transport Geography 35, 50–63. doi:10.1016/J.JTRANGEO.2014.01.008.

Saadat, Y., Ayyub, B.M., Zhang, Y., Zhang, D., Huang, H., 2020. Resilience-Based Strategies for Topology Enhancement and Recovery of Metrorail Transit Networks. ASCE-ASME Journal of Risk and Uncertainty in Engineering Systems, Part A: Civil Engineering 6, 04020017. doi:10.1061/AJRUA6.0001057.

Schäfer, R.P., Thiessenhusen, K.U., Wagner, P., 2002. A traffic information system by means of real-time floating car data, in: ITS world Congress, pp. 1–8.

Scheurer, J., Curtis, C., Porta, S., 2007. Spatial Network Analysis of Public Transport Systems: Developing a Strategic Planning Tool to Assess the Congruence of Movement and Urban Structure in Australian Cities, in: 30th Australasian Transport Research Forum (ATRF, pp. 1–23.

Schmöcker, J.D., Bell, M.G.H., 2002. The PFE as a tool for robust multi-modal network planning. Multi-modal network planning .

Scott, D.M., Novak, D.C., Aultman-Hall, L., Guo, F., 2006. Network Robustness Index: A new method for identifying critical links and evaluating the performance of transportation networks. Journal of Transport Geography doi:10.1016/j.jtrangeo.2005.10.003.

Sevilla, I., Chrobocinski, P., Barmpas, F., Schmidt, F., Kerle, N., Kostaridis, A., Doulamis, A., Russotto, R., 2018. Improving Resilience of Transport Instrastructure to Climate Change and other natural and Manmande events based on the combined use of Terrestrial and Airbone Sensors and Advanced Modelling Tools. Technical Report. CONAMA2018. Madrid.

Sevtsuk, A., Mekonnen, M., 2012. Urban network analysis A new toolbox for ArcGIS. Revue internationale de géomatique , 287–305.

Shalaby, A., Eng, P., King, D., 2016. Performance Metrics and Analysis of Transit Network Resilience in Toronto. Transport Research Board .

Shang, W.L., Chen, Y., Ochieng, W.Y., 2020a. Resilience Analysis of Transport Networks by Combining Variable Message Signs with Agent-Based Day-to-Day Dynamic Learning. IEEE Access 8, 104458–104468. doi:10.1109/ACCESS.2020.2999129.

Shang, W.L., Chen, Y., Song, C., Ochieng, W.Y., 2020b. Robustness Analysis of Urban Road Networks from Topological and Operational Perspectives. Mathematical Problems in Engineering doi:10.1155/2020/5875803.

Shariat-Mohaymany, A., Babaei, M., 2010. An approximate reliability evaluation method for improving transportation network performance. Transport 25. doi:10.3846/transport.2010.24.

Silver, G., Akbarzadeh, M., Estrada, E., 2018. Tuned communicability metrics in networks. The case of alternative routes for urban traffic. Chaos, Solitons & Fractals 116, 402–413. doi:10.1016/j.chaos.2018.09.044.

Sivak, M., 2002. How common sense fails us on the road: contribution of bounded rationality to the annual worldwide toll of one million traffic fatalities. Transportation Research Part F: Traffic Psychology and Behaviour 5, 259–269. doi:10.1016/S1369-8478(03)00003-2.

Soh, H., Lim, S., Zhang, T., Fu, X., Kee, G., Lee, K., Gih, T., Hung, G., Di, P., Prakasam, S., Wong, L., 2010. Weighted complex network analysis of travel routes on the Singapore public transportation system. Physica A 389, 5852–5863. doi:10.1016/j.physa.2010.08.015.

Sohouenou, P.Y., Neves, L.A., 2021. Assessing the effects of link-repair sequences on road network resilience. International Journal of Critical Infrastructure Protection 34, 100448. doi:10.1016/J.IJCIP.2021.100448.

Solé-Ribalta, A., Arenas, A., Gómez, S., 2019. Effect of shortest path multiplicity on congestion of multiplex networks. New J. Phys 21, 35003. doi:10.1088/1367-2630/ab023e.

Soltani-Sobh, A., Heaslip, K., Khoury, J.E., 2015. Estimation of road network reliability on resiliency: An uncertain based model. International journal of disaster risk reduction doi:10.1016/j.ijdrr.2015.10.005.

Song, Z., He, Y., Zhang, L., 2017. Integrated planning of park-and-ride facilities and transit service. Transportation Research Part C: Emerging Technologies 74, 182–195. doi:10.1016/j.trc.2016.11.017.

Sossoe, K., 2017. Modeling of multimodal transportation systems of large networks. Ph.D. thesis. Paris-Est.

Stamos, I., Mitsakis, E., Salanova, M., Aifadopoulou, G., 2015. Impact assessment of extreme weather events on transport networks: A data-driven approach. Transportation Research Part D 34, 168–178. doi:10.1016/j.trd.2014.11.002.

Steen, R., Aven, T., 2011. A risk perspective suitable for resilience engineering. Safety Science 49, 292–297. doi:10.1016/j.ssci.2010.09.003.

Sterbenz, J.P.G., Hutchison, D., Çetinkaya, E.K., Jabbar, A., Rohrer, J.P., Schöller, M., Smith, P., 2010. Resilience and survivability in communication networks: Strategies, principles, and survey of disciplines. Computer Networks 54, 1245–1265. doi:10.1016/j.comnet.2010.03.005.

Strogatz, S.H., 2001. Exploring complex networks. Nature .

Sullivan, J., Novak, D., Aultman-Hall, L., Scott, D., 2010. Identifying critical road segments and measuring system-wide robustness in transportation networks with isolating links: A link-based capacity-reduction approach. Transportation Research Part A: Policy and Practice 44, 323–336. doi:10.1016/J.TRA.2010.02.003.

Sun, S., Wu, Y., Ma, Y., Wang, L., Gao, Z., Xia, C., 2016. Impact of Degree Heterogeneity on Attack Vulnerability of Interdependent Networks. Nature Publishing Group doi:10.1038/srep32983.

Suryani, E., 2019. Modelling Reliability of Transportation Systems to Reduce Traffic Congestion, in: IOP Conference:Journal of Physics, pp. 1–6. doi:10.1088/1742-6596/1196/1/012029.

Sytral, 2015. L'enquete deplacements sur Lyon Villeurbanne 2014-2015 .

Tamvakis, P., Xenidis, Y., 2013. Comparative Evaluation of Resilience Quantification Methods for Infrastructure Systems. Procedia - Social and Behavioral Sciences doi:10.1016/j.sbspro.2013.03.030.

Tang, J., Heinimann, H.R., 2018. A resilience-oriented approach for quantitatively assessing recurrent spatial-temporal congestion on urban roads. Plos One doi:10.1371/journal.pone.0190616.

Tang, J.K., 2011. Temporal network metrics and their application to real world networks. Ph.D. thesis. Cambridge.

Taylor, A., 2020. Deadly Flooding in Southeastern France.

Taylor, M.A., Sekhar, S.V., Glen, M., 2006. Application of Accessibility Based Methods for Vulnerability Analysis of Strategic Road Networks. Network and Spatial Economics , 267–291doi:10.1007/s11067-006-9284-9.

Taylor, M.A.P., D'Este, G.M., 2007. Transport Network Vulnerability: a Method for Diagnosis of Critical Locations in Transport Infrastructure Systems, in: Critical Infrastructure, pp. 9–30. doi:10.1007/978-3-540-68056-7{_}2.

The Associated Press, 2021a. Maritime traffic jam grows outside blocked Suez Canal.

The Associated Press, 2021b. NYC subway breakdown blamed on 'power off' button being hit.

Therrien, A., 2021. Roads in Washington are literally splitting apart from the heat.

Thomson, R.C., Richardson, D.E., 1995. A graph theory approach to road network generalization, in: 17th international cartographic conference, pp. 1871–1880.

Travençolo, B.A.N., Da, L., Costa, F., 2008. Accessibility in complex networks. Physics Letters A 373, 89–95. doi:10.1016/j.physleta.2008.10.069.

Trudeau, R.J., 1993. Introduction to graph theory. Dover Pub.

Tu, Y., Yang, C., Chen, X., 2010. Methodology for Evaluating and Improving Road Network Topology Vulnerability, in: 2010 International Conference on Intelligent Computation Technology and Automation, IEEE. pp. 664–669. doi:10.1109/ICICTA.2010.603.

Tuzun Aksu, D., Ozdamar, L., 2014. A mathematical model for post-disaster road restoration: Enabling accessibility and evacuation. Transportation Research Part E: Logistics and Transportation Review 61, 56–67. doi:10.1016/J.TRE.2013.10.009.

Tympakianaki, A., Koutsopoulos, H.N., Jenelius, E., Cebecauer, M., 2018. Impact analysis of transport network disruptions using multimodal data: A case study for tunnel closures in Stockholm. Case Studies on Transport Policy 6, 179–189. doi:10.1016/j.cstp.2018.05.003.

Ulusan, A., Ergun, O., 2018. Restoration of services in disrupted infrastructure systems: A network science approach. Plos One doi:10.1371/journal.pone.0192272.

United Nations, 2018. World Urbanization Prospects: the 2018 Revision. Technical Report. United Nations.

Vajanapoom K Tipper D, A.S., 2010. A Risk Management Approach to Resilient Network Design. IEEE Communication Magazine .

Van Lint, J.W.C., Van Zuylen, H.J., Tu, H., 2008. Travel time unreliability on freeways: Why measures based on variance tell only half the story. Transportation Research Part A: Policy and Practice 42, 258–277.

Van Nes, R., 2002. Design of multimodal transport networks : a hierarchical approach. Ph.D. thesis. Delft University.

Von Ferber, C., Holovatch, T., Holovatch, Y., Palchykov, V., 2008. Public transport networks: empirical analysis and modeling. European Physical Journal B .

Wakabayashi, H., Iida, Y., 1992. Upper and lower bounds of terminal reliability of road networks: an efficient method with Boolean Algebra. Journal of Natural Disaster Science .

Wang, H., Hernandez, J.M., Van Mieghem, P., 2008. Betweenness centrality in a weighted network. Physical Review E - Statistical, Nonlinear, and Soft Matter Physics 77, 1–10. doi:10.1103/PhysRevE.77.046105.

Wang, J., 2015. Resilience of Self-Organised and Top-Down Planned Cities-A Case Study on London and Beijing Street Networks. Plos one doi:10.1371/journal.pone.0141736.

Wang, J., Mo, H., Wang, F., Jin, F., 2011. Exploring the network structure and nodal centrality of China's air transport network: A complex network approach. Journal of Transport Geography 19, 712–721. doi:10.1016/J.JTRANGEO.2010.08.012.

Wang, X., Miao, S., Tang, J., 2020. Vulnerability and Resilience Analysis of the Air Traffic Control Sector Network in China. Sustainability 12, 3749. doi:10.3390/su12093749.

Watts, D.J., Strogatz, S.H., 1998. Collective dynamics of 'small-world' networks. Nature 393, 440–442. doi:10.1038/30918.

Wei, D., Ya Li, Zhang, Y., Deng, Y., 2012. Degree centrality based on the weighted network, in: 2012 24th Chinese Control and Decision Conference (CCDC), IEEE. pp. 3976–3979. doi:10.1109/CCDC.2012.6244633.

White, H.P., Senior, M.L., 1983. Transport geography. London Longman.

Whyte, A., 2021. Glasgow Subway: Inner and Outer services suspended due to points failure.

Woods, D.D., 2015. Four concepts for resilience and the implications for the future of resilience engineering. Reliability Engineering and System Safety doi:10.1016/j.ress.2015.03.018.

Wu, J., Tan, Y.J., Deng, H.Z., Zhu, D.Z., 2010. A new measure of heterogeneity of complex networks based on degree sequence, in: Unifying Themes in Complex Systems. Springer Berlin Heidelberg, pp. 66–73. doi:10.1007/978-3-540-85081-6{_}9.

Wu, K., Guler, S.I., Guler, W., 2018. Optimizing transit signal priority implementation along an arterial, in: Transport Research Board, pp. 1–21.

Xie, C., Lin, D.Y., Travis Waller, S., 2010. A dynamic evacuation network optimization problem with lane reversal and crossing elimination strategies. Transportation Research Part E: Logistics and Transportation Review 46, 295–316. doi:10.1016/J.TRE.2009.11.004.

Xu, M., Wu, J., Liu, M., Xiao, Y., Wang, H., Hu, D., 2019. Discovery of Critical Nodes in Road Networks Through Mining from Vehicle Trajectories. IEEE Transactions on Intelligent Transportation Systems doi:10.1109/TITS.2018.2817282.

Yamsaengsung, S., Papasratorn, B., 2017. Towards Improving User Interaction with Navigation Apps: an Information Quality Perspective, in: 9th International Conference on Advances in Information Technology, pp. 119–131. doi:10.18502/kss.v3i1.1401.

Yan, Y., Hong, L., He, X., Ouyang, M., Peeta, S., Chen, X., 2017. Pre-disaster investment decisions for strengthening the Chinese railway system under earthquakes. Transportation Research Part E: Logistics and Transportation Review 105, 39–59. doi:10.1016/J.TRE.2017.07.001.

Yang, X.H., Wang, B., Chen, S.Y., Wang, W.L., 2012. Epidemic dynamics behavior in some bus transport networks. Physica A: Statistical Mechanics and its Applications 391, 917–924. doi:10.1016/J.PHYSA.2011.08.070.

Yang, Y., He, Z., Song, Z., Fu, X., Wang, J., 2018. Investigation on structural and spatial characteristics of taxi trip trajectory network in Xi'an, China. Physica A: Statistical Mechanics and its Applications 506, 755–766. doi:10.1016/J.PHYSA.2018.04.096.

Yap, M., Cats, O., Törnquist Krasemann, J., van Oort, N., Hoogendoorn, S., 2021. Quantification and control of disruption propagation in multi-level public transport networks. International Journal of Transportation Science and Technology doi:10.1016/J.IJTST.2021.02.002.

Ye, P., Wu, B., Fan, W., Author, C., 2016. Modified Betweenness-Based Measure For Traffic Flow Prediction Of Urban Road. Transportation Research Record: Journal of the Transportation Research Board 2563, 144–150.

Yi, W., Özdamar, L., 2007. A dynamic logistics coordination model for evacuation and support in disaster response activities. European Journal of Operational Research 179, 1177–1193. doi:10.1016/J.EJOR.2005.03.077.

Yin, C., Liu, Y., Wei, X., Chen, W., 2018. Road Centrality and Urban Landscape Patterns in Wuhan City, China. Journal of Urban Planning and Development 144. doi:10.1061/(ASCE)UP.1943-5444.0000441.

Yin, J., Yu, D., Lin, N., Wilby, R.L., 2017. Evaluating the cascading impacts of sea level rise and coastal flooding on emergency response spatial accessibility in Lower Manhattan, New York City. Journal of Hydrology doi:10.1016/j.jhydrol.2017.10.067.

Yoo, S., Yeo, H., 2016. Evaluation of the resilience of air transportation network with adaptive capacity. International Journal of Urban Sciences doi:10.1080/12265934.2016.1166979.

Yossyafra, Y., Haryana, I.B., Ferdina, Y., 2018. A simulation model in evaluating the resilience of urban public transport service during the flood disaster, in: MATEC Web of Conferences, pp. 1–6. doi:10.1051/matecconf/2018229.

Zhang, Yuanyuan, Wang Xuesong, Zeng Peng, Xiaohong Chen, 2011. Centrality characteristics of road network patterns of traffic analysis zones. Transport Research Record doi:10.3141/2256-03.

Zhang, D.m., Du, F., Huang, H., Zhang, F., Ayyub, B.M., Beer, M., 2018a. Resiliency assessment of urban rail transit networks: Shanghai metro as an example. Safety Science 106, 230–243. doi:10.1016/J.SSCI.2018.03.023.

Zhang, J., Wang, S., Wang, X., 2018b. Comparison analysis on vulnerability of metro networks based on complex network. Physica A: Statistical Mechanics and its Applications 496, 72–78. doi:10.1016/J.PHYSA.2017.12.094.

Zhang, L., Lu, J., Fu, B.b., Li, S.b., 2019. Dynamics analysis for the hour-scale based time-varying characteristic of topology complexity in a weighted urban rail transit network. Physica A: Statistical Mechanics and its Applications 527, 121280. doi:10.1016/J.PHYSA.2019.121280.

Zhang, M., Lomax, T., 2008. Estimating Congestion Index at the Link Level with TransCAD GIS, in: Plan, Build, and Manage Transportation Infrastructure in China, American Society of Civil Engineers, Reston, VA. pp. 7–17. doi:10.1061/40952(317)2.

Zhang, W., Wang, N., 2016. Resilience-based risk mitigation for road networks. Structural Safety 62, 57–65. doi:10.1016/J.STRUSAFE.2016.06.003.

Zhang, X., Miller-Hooks, E., Denny, K., 2015. Assessing the role of network topology in transportation network resilience. Journal of Transport Geography 46, 35–45. doi:10.1016/J.JTRANGEO.2015.05.006.

Zhang, Y., Ng, S.T., 2021. A hypothesis-driven framework for resilience analysis of public transport network under compound failure scenarios. International Journal of Critical Infrastructure Protection 35, 100455. doi:10.1016/J.IJCIP.2021.100455.

Zhao, S., Zhao, P., Cui, Y., 2017. A network centrality measure framework for analyzing urban traffic flow: A case study of Wuhan, China. Physica A: Statistical Mechanics and its Applications 478, 143–157. doi:10.1016/j.physa.2017.02.069.

Zhou, J., Coit, D.W., Felder, F.A., Wang, D., 2021. Resiliency-based restoration optimization for dependent network systems against cascading failures. Reliability Engineering & System Safety 207, 107383. doi:10.1016/j.ress.2020.107383.

Zhou, Y., Fang, Z., Thill, J.C., Li, Q., Li, Y., 2015. Functionally critical locations in an urban transportation network: Identification and space–time analysis using taxi trajectories. Computers, Environment and Urban Systems 52, 34–47. doi:10.1016/J.COMPENVURBSYS.2015.03.001.

Zhou, Y., Jiang, Q., Qin, J., 2019. Pre-disaster retrofit decisions for sustainable transportation systems in urban areas. Sustainability (Switzerland) 11. doi:10.3390/su11154044.

Zhou, Y., Wang, J., 2018. Critical Link Analysis for Urban Transportation Systems. IEEE Transactions on Intelligent Transportation Systems 19, 402–415. doi:10.1109/TITS.2017.2700080.

Zhu, S., Levinson, D., 2011. Disruptions to Transportation Networks: A Review. Springer.

Zhu, Y., Ozbay, K., Xie, K., Yang, H., 2016. Using Big Data to Study Resilience of Taxi and Subway Trips for Hurricanes Sandy and Irene. Transportation Research Record: Journal of the Transportation Research Board , 70–80doi:10.3141/2599-09.

Zhu, Y., Xie, K., Ozbay, K., Zuo, F., Yang, H., 2017. Data-Driven Spatial Modeling for Quantifying Networkwide Resilience in the Aftermath of Hurricanes Irene and Sandy. Transportation Research Record: Journal of the Transportation Research Board , 9–18doi:10.3141/2604-02.